

FLUORESCENCE SPECTROSCOPY OF EXOGENOUS, EXOGENOUSLY-INDUCED AND ENDOGENOUS FLUOROPHORES FOR THE PHOTODETECTION AND PHOTODYNAMIC THERAPY OF CANCER.

Thèse présentée au Département de Génie Rural

Ecole Polytechnique Fédérale de Lausanne

par

Matthieu Zellweger

Jury:

Dr Georges Wagnières, rapporteur
Prof. Hubert van den Bergh, corapporteur
Dr Christian Depeursinge, corapporteur
Prof. René Salathé, corapporteur
Prof. Philippe Monnier, corapporteur
Prof. Stanley Brown, corapporteur

Lausanne, Février 2000

Foreword

This work is the final report about my research activity as a Ph.D. student in the LPAS laboratory of Prof. Hubert van den Bergh, at the Swiss Federal Institute of Technology - Lausanne (EPFL). Some parts of this report have been published or submitted during the course of my Ph.D. thesis. I therefore included the text of the publications instead of an original chapter whenever relevant. In such a case, the reference is clearly stated. A brief introduction always precedes the resulting 'chapters'.

Due to this inclusion, the reader might find some redundant information within this report. On the other hand, it should be emphasized that each chapter can be read as a stand-alone text and need not be linked to any other part of the whole work. However, I tried to avoid the unnecessary repetition of information and this is especially true for the references. Whenever the reader feels that a reference should have been included to support an information in the introduction, they should check the introduction of the following published chapter for a more detailed reference list. The same criticism applies to the introduction and, again, the reader should check the published section of a chapter if they feel that it lacks some information.

As will be seen in the authors' list of the published chapters of this work, a lot has been done in close collaboration with other people. Whenever relevant (i.e. whenever I don't appear as the first author of a paper that has been included in my report), I stated in the introduction what my exact contribution was. It should be understood that those papers have been included in my report with full knowledge and agreement from my co-authors and Ph.D. supervisors.

Finally, I would like to apologize to the native English speaking reader for my less than perfect command of their language.

Lausanne, December 1999

To my parents, for their care and support.

To Elena, my companion during these years as a Ph.D. student.

Thesis
A giant leap for a man
A small step for mankind

Lausanne, November 1999

Abbreviations

List of abbreviations used throughout the text in alphabetical order:

2I-EtNBS	2-iodo-5-ethylamino-9-diethylaminobenzo[a]phenothiazinium chloride
AF	Autofluorescence
ALA	5-Aminolaevulinic acid, δ -Aminolaevulinic Acid
AMD	Age-related macular degeneracy
BCC	Basal cell carcinoma
BPDMA	Benzoporphyrin derivative monoacid ring A
BSA	Bovine serum albumin
CCD	Charge-coupled device
CFDA	Carboxyfluorescein diacetate
CIS	Carcinoma in situ
CNV	Choroidal neovascularization
CT	Computerized tomography
ENT	Ear, nose, throat
EtNBA	5-ethylamino-9-diethylaminobenzo[a]phenoxazinium chloride
EtNBS	5-ethylamino-9-diethylaminobenzo[a]phenothiazinium chloride
FAD	Flavin adenine dinucleotide (oxidized form)
FDA	Food and Drug Administration
FMN	Flavin mononucleotide
FP	Fluorophore
FWHM	Full width at half-maximum
GI	Gastro-intestinal (tract)
h-ALA	5-Aminolaevulinic acid hexylester
HPD	Hematoporphyrin Derivative
HPLC	High performance liquid chromatography
LIF	Light-Induced fluorescence
Lu-TeX	Lutetium Texaphyrin
MP	Molecular Probes
mTHPC	5,10,15,20-tetra(<i>m</i> -hydroxyphenyl)chlorin, Foscan [®]
MRI	Magnetic resonance imaging
NADH	Nicotinamide adenine dinucleotide (reduced form)
NADPH	Nicotinamide adenine dinucleotide phosphate (reduced form)
PBS	Phosphate buffered saline
PDT	Photodynamic therapy
PET	Positron emission tomography

Phe	Phenylalanine
PK	Pharmacokinetics
PPIX	Protoporphyrin IX
PPV	Positive Predictive Value
PS	Photosensitizer
RPE	Retinal pigmented epithelium
RuDPP	Ruthenium-(4,7-diphenyl-1,10-phenanthroline)
SCC	Squamous cell carcinoma
SNR	Signal to noise ratio
SPECT	Single photon emission computed tomography
Trp	Tryptophane
Tyr	Tyrosine
UADT	Upper aerodigestive tract

Abstract

The purpose of this thesis is to study different applications of fluorescence spectroscopy and imaging to detect early cancerous lesions in two organs: the bronchi and the urinary bladder. Early diagnosis of epithelial carcinomas is of major importance because the risk of the tumor infiltrating the underlying tissues and eventually spreading throughout the host increases as the lesion develops. Endoscopy is a central tool in achieving this goal as it facilitates access to hollow organs. The additional use of fluorescence spectroscopy provides otherwise unavailable information about the histopathological status of the tissue.

Fluorescence spectroscopy requires a fluorophore. The fluorophores can be of three types, the exogenous (synthesized out of the patient's body), the exogenously induced (synthesized in the patient's body from exogenous precursors) and the endogenous fluorophores (synthesized in the patient's body). This work has consequently been divided in three parts according to the types of fluorophore.

The exogenous fluorophore mTHPC was used in clinical routine in Lausanne as a photosensitizer for the photodynamic therapy of early carcinomas in the esophagus and the bronchi. Strong interpatient fluctuations in therapeutic response have been observed in patients treated with similar doses of mTHPC and light. This is thought to be due to metabolic differences between patients leading to various concentrations of mTHPC in the target organ. To some extent, this can be compensated by adjusting the light dose for each patient, according to the tissular mTHPC concentration. Several methods can provide this information, among them fluorescence spectroscopy. The usual method in Lausanne is to measure the mTHPC fluorescence level with an optical fiber on the target organ. This can be a difficult measurement, because the operator has limited control upon the fiber. We propose a simplified way of measuring this concentration in the oral cavity instead of on the target organ. This location is relevant because it is easily accessible and because there is a significant correlation between the mTHPC fluorescence signal in the bronchi or in the esophagus, and in the oral cavity. Five patients undergoing PDT were included in this study. The mTHPC fluorescence signal was measured in their oral cavity in the two hours preceding PDT. It was found that this signal is fairly reproducible and little sensitive to the exact location in the oral mucosa. It is not very sensitive to the pressure applied to the fiber either. This measurement location is easier to access than the bronchi or the esophagus, yields more reproducible results and yet does not result in any loss of useful information.

The exogenous fluorophores Lu-Tex, EtNBS and 2I-EtNBS (the last two being Nile Blue derivatives) have been tested as potential tumor detection agents in a hamster animal model bearing an early cancerous lesion similar to those encountered in the human upper aero-digestive tract. The Lu-Tex and the Nile Blue derivatives were expected to localize in greater quantity in the lesion than in the surrounding healthy tissue. The fluorescence spectroscopy allowed us to measure a pharmacokinetics curve in both types of tissue and to evaluate the selectivity of these molecules for early lesions of the hamster. Twenty-six animals received a 12 mg/kg intracardiac injection of a Lu-Tex solution. The pharmacokinetics curve showed that Lu-Tex displays some selectivity (1.5:1) in this model. Moreover, it seems not to be detectable in the skin of the animals after 24 hours and this observation was confirmed by skin irradiation tests. This is a clear advantage of Lu-Tex over fluorophores such as mTHPC or HPD. A similar study was conducted with EtNBS and 2I-EtNBS on 30 hamsters. Despite promising preliminary results (3:1 selectivity 100-200 min after the injection of 2.5 mg/kg of 2I-EtNBS), this selectivity could not be reproduced.

Sytox[®] Green is an impermeant metachromatic dye. This category of fluorophore represents a different type of approach to cancer detection as it does not rely on the accumulation of different quantities of fluorophore in the healthy or cancerous cells at a given point in time. Instead, it is sensitive to local environmental factors (in this case, the permeability of the membrane) that differ between the two types of cell. The fluorescence quantum yield of Sytox[®] Green increases 1000-fold when bound to DNA, an event likely to occur in cancer cells with damaged membranes.

Since Sytox[®] Green does not cross intact membranes, it will not bind to DNA in healthy cells. This fluorophore was injected intracardiacally into 9 hamsters (0.3 mg/kg). No pharmacokinetics curve could be measured, but images have been taken. They display contrasts (up to 10:1) between healthy and early cancerous cells. Moreover, it seems that there is a correlation between the histopathological status of the tissue and the position of the emission maximum of Sytox[®] Green.

The exogenously induced fluorophore Protoporphyrin IX (PPIX) is synthesized in mammals from 5-aminolevulinic acid (ALA) among others. This highly fluorescent fluorophore is the immediate metabolic precursor of heme in its biosynthetic pathway. When in contact with an aqueous solution of ALA, cancer cells tend to temporarily accumulate more PPIX than their healthy counterparts, thus becoming visible under appropriate fluorescence excitation light. This detection method has been successfully used in recent years for the detection of early cancerous lesions in the urinary bladder. The use of ALA as a precursor has one drawback, however. Its properties as a zwitterion at physiological pH reduce its bioavailability because it crosses cell membranes with difficulty. To circumvent this limitation, we tested more lipophilic precursors, the ALA-esters, in cultured cells and the best of them, ALA-hexylester in patients. In cultured cells, it was found that the concentration of long-chained esters at which the PPIX production is maximal decreases as the chain-length increases (up to two orders of magnitude for C6-C8 side chains). Above this optimal concentration, the PPIX production decreases again. This production was also maximal at or around physiological pH. The ALA hexylester was then applied topically, in solution at concentrations ranging from 4 to 16 mM, in the urinary bladder of 25 patients undergoing a cystoscopy to detect bladder malignancies. The PPIX fluorescence intensity underwent a twofold increase using the best conditions (8 mM), a 20-fold lower concentration as compared to ALA.

The endogenous fluorophores are numerous. They occur naturally and are collectively responsible for the fluorescence properties of biological tissues. This native fluorescence of tissues is sometimes called autofluorescence. Evidence exists that the autofluorescence of bronchial tissues changes when they turn dysplastic and to carcinoma in situ. Imaging devices rely on this principle to detect early cancerous lesions in the bronchi. In the third part of this thesis, we propose a spectroscopic study conducted on 50 patients known or suspected to bear such lesions to optimize their detection by autofluorescence. Several autofluorescence excitation wavelengths have been tested, from 350 nm to 495 nm. It was observed that early lesions undergo a general decrease of autofluorescence with respect to healthy tissues. In the 550 nm region, this decrease is of up to one order of magnitude, whereas it is less marked in the 650 nm region, thus inducing a modification of the spectral shape of the autofluorescence emission. Whereas they also undergo a decrease in autofluorescence, metaplastic and inflammatory tissues seem to retain their autofluorescence spectral shape. The violet-blue wavelengths (400-465 nm) give the largest contrast (up to 6 at an excitation wavelength of 405 nm) whereas the UV wavelengths and those above 480 nm appear not to be very helpful. The contrast is maximized when the autofluorescence emission spectra are divided into two regions, a 'green' (500-590 nm) and a 'red' (600+ nm) region. These results have been implemented in an imaging device to detect early cancerous lesions. It has been tested in the clinical context on 16 patients between September and December 1999. Although preliminary, this study shows that the autofluorescence can help detect lesions that would otherwise have remained invisible under white-light illumination. Positive predictive values are improved by the concomitant use of autofluorescence bronchoscopy with respect to white-light bronchoscopy alone. A systematic analysis of the green and red images showed that a threshold could be defined to have an objective criterion for lesions' positivity and limit the number of false-positive results.

Résumé

Le but de cette thèse est d'étudier la spectroscopie et l'imagerie de fluorescence appliquées à la détection de cancers précoces dans deux organes, les bronches et la vessie. En effet, il est très important de diagnostiquer les carcinomes à un stade précoce de leur développement car le risque de les voir infiltrer les tissus sous-jacents et métastatiser à travers le corps augmente au fur et à mesure de leur progression. Pour ce faire, l'endoscopie est une méthode de choix car elle permet d'accéder facilement aux organes creux. Complétée par la spectroscopie de fluorescence, elle livre des informations supplémentaires sur le status histopathologique du tissu.

Pour qu'il y ait spectroscopie de fluorescence, il faut un fluorophore. On peut classer les fluorophores en trois groupes. Les fluorophores exogènes sont synthétisés hors de l'organisme du patient, les fluorophores induits sont synthétisés dans l'organisme du patient à partir de précurseurs exogènes et les fluorophores endogènes sont synthétisés dans l'organisme du patient. Le présent travail est par conséquent séparé en trois parties.

La mTHPC est un fluorophore exogène. A Lausanne, elle est utilisée en thérapie photodynamique de cancers précoces des bronches et de l'oesophage car c'est un photosensibilisateur. Cependant, pour une dose de mTHPC et de lumière données, on observe des réponses thérapeutiques très variables d'un patient à un autre. Cela est probablement dû au métabolisme respectif des patients, qui fait que la concentration de mTHPC sur le site du traitement peut varier. Il faut par conséquent ajuster la dose de lumière appliquée pour compenser, dans une certaine mesure, ces fluctuations, mais cela implique que l'on connaisse la quantité de mTHPC présente dans le tissu. La spectroscopie de fluorescence, entre autres, permet d'estimer cette concentration. A Lausanne, la méthode de choix est de mesurer l'intensité de la fluorescence de la mTHPC en posant une fibre optique sur l'organe à traiter. Cette mesure peut s'avérer difficile car l'opérateur n'a de la fibre qu'un contrôle limité. Nous proposons ici une méthode visant à simplifier cette mesure. Au lieu de la faire directement sur le site du traitement, il est en effet possible de la faire dans la cavité buccale. Cet organe est facile d'accès et son signal de fluorescence de la mTHPC est corrélé avec celui des bronches ou de l'oesophage. Cinq patients, qui devaient subir une thérapie photodynamique, ont été inclus dans cette étude. Le signal de fluorescence de la mTHPC a été mesuré dans leur cavité buccale dans les heures précédant le traitement. Ce signal est bien reproductible et peu sensible à l'emplacement exact de la mesure ou à la pression appliquée à la fibre de mesure. Les résultats des mesures dans la cavité buccale sont plus reproductibles que ceux acquis dans les bronches ou l'oesophage, cet organe est plus facilement accessible et aucune information utile n'est perdue.

Le Lu-Tex, le EtNBS et le 2I-EtNBS sont aussi des fluorophores exogènes (les deux derniers nommés sont des dérivés du Nile Blue). Ils ont été testés dans un modèle animal, le hamster. Dans ce modèle, une tumeur précoce qui ressemble aux tumeurs des voies aérodigestives supérieures humaines peut être induite. Nous nous attendions à ce que le Lu-Tex et les dérivés du Nile Blue se localisent en plus grandes quantités dans les lésions précoces que dans le tissu sain environnant, faisant ainsi preuve d'une certaine sélectivité pour ces lésions. Nous avons mesuré leur pharmacocinétique dans les deux types de tissus par spectroscopie de fluorescence. Vingt-six hamsters ont reçu une injection intracardiaque d'une solution de Lu-Tex (12 mg/kg). La pharmacocinétique montre que le Lu-Tex est un peu sélectif (1.5:1) pour les lésions précoces dans ce modèle. De plus, il n'est plus détectable dans la peau après 24 heures (une observation confirmée par des tests d'irradiation), un net avantage par rapport à des molécules comme la mTHPC ou le HPD. Une étude similaire a été menée avec le EtNBS et le 2I-EtNBS sur 30 animaux. Malgré des résultats préliminaires prometteurs (nous avons observé une sélectivité de 3:1 100 à 200 minutes après l'injection de 2.5 mg/kg de 2I-EtNBS), cette sélectivité n'a pas pu être reproduite.

Le Sytox[®] Green est un fluorophore imperméant métachromatique. Cette catégorie de molécules représente une approche différente de la détection de cancers car elle ne se base pas sur une accumulation du fluorophore qui serait différente dans les cellules saines et les cellules de cancers

précoces à un moment donné, mais sur des molécules qui soient sensibles à leur environnement différent dans les deux types de cellules (en l'occurrence la perméabilité de la membrane). Le rendement quantique de fluorescence du Sytox[®] Green augmente d'un facteur 1000 quand il est lié à l'ADN. Cette association est probable dans les cellules cancéreuses car leurs membranes peuvent être abîmées, ce qui n'est pas le cas dans les cellules saines. Ce fluorophore a été injecté intracardiaquement à 9 hamsters (0.3 mg/kg). Nous n'avons pas pu mesurer de pharmacocinétique mais des images ont été enregistrées. Un contraste a effectivement été observé entre les cellules saines et les cellules cancéreuses (jusqu'à 10:1) avec cette molécule dans ce modèle. De plus, il semblerait que le status histopathologique du tissu soit corrélé avec la position du maximum d'émission de fluorescence du Sytox[®] Green.

La protoporphyrine IX (PPIX) est un fluorophore induit très fluorescent. Chez les mammifères, elle est synthétisée entre autres à partir d'acide 5-aminolévulinique (ALA). Elle est le prédécesseur immédiat de l'hème dans sa biosynthèse. Lorsqu'elles sont en contact avec une solution aqueuse d'ALA, les cellules cancéreuses accumulent temporairement plus de PPIX que les cellules saines et cela les rend visibles sous une lumière d'excitation de fluorescence. Ce phénomène a été utilisé avec succès depuis plusieurs années pour détecter des cancers précoces dans la vessie. Le principal désavantage de l'ALA est qu'il traverse difficilement les membranes cellulaires car c'est un zwitterion à pH physiologique. Il se trouve donc en faibles concentrations à l'intérieur des cellules, là où la biosynthèse de la PPIX a lieu. Pour contourner cette difficulté, nous avons testé des précurseurs de la PPIX plus lipophiles, les esters d'ALA, sur des cellules en culture. Le meilleur d'entre ces esters, l'hexylester d'ALA a aussi été testé in vivo, sur des patients. Sur les cellules en culture, nous avons constaté que la concentration d'ester d'ALA avec laquelle la production de PPIX est maximale diminue avec l'augmentation de la longueur de la chaîne aliphatique (jusqu'à deux ordres de grandeur pour les esters C6-C8). Au delà de cette concentration optimale, la production de PPIX diminue de nouveau. Cette production est aussi maximale autour du pH physiologique. L'hexylester d'ALA a ensuite été appliqué topiquement, en solution à des concentrations allant de 4 à 16 mM, dans la vessie de 25 patients qui subissaient une cystoscopie pour détecter des lésions cancéreuses. Dans les meilleures conditions (8 mM), l'intensité de fluorescence de la PPIX a été doublée, et cela alors que ces conditions représentent une diminution de la concentration d'un facteur 20 par rapport à l'ALA.

Les fluorophores endogènes sont nombreux. Ils sont naturellement présents dans les tissus et sont responsables de la fluorescence de tous les tissus biologiques, un phénomène parfois appelé autofluorescence. Il est rapporté que l'autofluorescence des bronches change lors du processus de cancérisation, lorsque de normal le tissu devient dysplasique puis carcinomateux. Il existe des appareillages d'imagerie basés sur ce principe pour détecter les cancers précoces des bronches. Dans la troisième partie de ce travail, nous présentons une étude de spectroscopie de fluorescence menée sur 50 patients portant ou à risque de porter une telle lésion et visant à optimiser leur détection par autofluorescence. Plusieurs longueurs d'onde d'excitation ont été testées, allant de 350 à 495 nm. En général, les lésions précoces voient leur autofluorescence baisser par rapport à celle des tissus sains. Autour de 550 nm, cette baisse est d'environ un ordre de grandeur et elle est moins importante autour de 650 nm, ce qui signifie que la forme des spectres d'autofluorescence change. Les tissus métaplasiques et inflammatoires voient aussi l'intensité de leur autofluorescence baisser mais conservent toutefois leur forme. Les longueurs d'onde dans le violet et le bleu (400 à 465 nm) donnent les meilleurs contrastes (jusqu'à un facteur 6 pour une excitation à 405 nm) alors que les longueurs d'onde dans l'UV ou au-dessus de 480 nm sont peu efficaces. Pour maximiser le contraste, il faut séparer le spectre d'émission d'autofluorescence en deux zones, une zone 'verte' (500-590 nm) et une zone 'rouge' (600+ nm). Ces résultats ont été implémentés dans un système d'imagerie d'autofluorescence. Il a été testé avec succès en clinique sur 16 patients entre septembre et décembre 1999. Bien que cette étude soit préliminaire, elle montre que l'autofluorescence peut aider à détecter des lésions invisibles en lumière blanche. Les valeurs prédictives positives sont améliorées par l'usage de la bronchoscopie par autofluorescence en complément à la bronchoscopie en lumière blanche par rapport à la lumière blanche seulement. Une analyse systématique des images rouges et vertes ainsi obtenues a montré que l'on peut définir un seuil objectif comme critère de positivité pour une lésion. Ce faisant, il est possible de limiter le nombre de faux-positifs.

Contents (*Published work*)

Introduction	12
Chapter 1: Some facts about cancer and its management	15
1.1 Facts about cancer	15
1.2 Cancer detection	16
1.3 Cancer treatment	17
Chapter 2: Fluorescence photodetection and photodynamic therapy: basic concepts	20
2.1 Fluorescence photodetection	20
2.2 Photodynamic therapy (PDT)	22
Part I: Exogenous Fluorophores	29
Chapter 3: mTHPC in the clinical context.	31
3.1 The photosensitizer	31
3.2 Clinical work with mTHPC by other groups	32
3.3 Pre- and clinical work with mTHPC in Lausanne	34
3.4 <i>Stability of the fluorescence measurement of Foscan[®]...</i>	38
Chapter 4: Lutetium Texaphyrin (Lu-TeX, PCI-0123).	47
4.1 The photosensitizer	47
4.2 Preclinical and clinical uses of the Lu-TeX	48
4.3 <i>Fluorescence Pharmacokinetics of Lutetium Texaphyrin...</i>	54
Chapter 5: Sytox [®] Green.	63
5.1 Sytox [®] Green: the fluorophore	64
5.2 Sytox [®] Green: the study	65
Part II: Exogenously-Induced Fluorophores	76
Chapter 6: PPIX in cultured cells	78
6.1 The model	81
6.2 <i>5-aminolevulinic acid and its derivatives: physical...</i>	83

Chapter 7: PPIX in the clinical context	95
7.1 Protoporphyrin IX in the clinical context	95
7.2 Fluorescence spectroscopy of the PPIX in the bladder	97
7.3 <i>Photodetection of early human bladder cancer based...</i>	102
Part III: Endogenous Fluorophores	115
Chapter 8: Autofluorescence of the human bronchial tissue	117
8.1 The endogenous fluorophores	117
8.2 The autofluorescence of healthy tissues and of early cancerous lesions	122
8.3 <i>In vivo autofluorescence spectroscopy of human bronchial...</i>	128
8.4 <i>Absolute autofluorescence spectra of human healthy...</i>	143
Chapter 9: Cancer photodetection in the tracheo-bronchial tree by autofluorescence imaging	154
9.1 Commercial systems	155
9.2 The Wolf-EPFL system	157
9.3 Clinical results: examples	164
9.4 Future prospects	184
Conclusion	187
Acknowledgments	189
Appendixes	191
A1. The optical fiber-based spectrofluorometer	192
A2. Some additional exogenous fluorophores	194
A3. Additional autofluorescence measurements	203
A4. Publications and patents	220
A5. Curriculum Vitae	223

調 和

Harmony

Introduction

This work is the result of a multidisciplinary research approach intended to contribute to improved management of a major health problem: cancer. Although several dozens of diseases are included in this term, they all share some common features that distinguish them from non-cancerous ailments. One of these features is their ability, past a certain stage of development, to spread and invade distant sites of the body. These secondary tumors are known as metastases and are a typical feature of advanced invasive cancers. However, this ability to spread appears in the late stages of the disease only. The pre- or early malignant lesions that precede many invasive cancers are localized lesions. Whereas invasive cancers and metastases are difficult to eradicate completely, the early localized lesions are manageable with a higher rate of success. In this report, we will focus on the lesions of the tracheo-bronchial tree and the urinary bladder. They are frequent cancers but, unfortunately, they are still difficult to diagnose in the early stages of development with existing detection methods. Consequently, there is a need for improvement to overcome this difficulty. In fact, most of the techniques used nowadays to detect cancers are moving towards earlier recognition. In parallel, the treatments of the disease need less invasive options because the mere removal of an early cancer-bearing but otherwise functional organ might not be the optimal solution to a very early lesion, barely a few cell layers thick. This report describes our work in a multidisciplinary team towards both goals, the improvement of the detection techniques of early cancerous lesions and their therapy by minimally invasive methods.

It is focused on endoscopically reachable tumors and especially the tumors of the tracheo-bronchial tree and of the urinary bladder.

Chapter 1 deals with the issue of cancer. It is a brief summary of some facts about cancer, the current methods of detection and their limits as well as the usual methods of management of the disease. It is intended as a brief survey of the tools available to clinicians and should not be regarded as an exhaustive review. Nevertheless, we tried to state the facts that are of importance for the reader to know as a background for this work.

The fluorescence photodetection and the photodynamic therapy of early cancers of hollow organs are relatively new tools in the hand of clinicians. **Chapter 2** briefly summarizes the principles of fluorescence photodetection and photodynamic therapy along with some of their uses. It also presents their advantages as well as their limitations. Still, these methods show promising results and are currently under constant development. In this work, each of the subsequent chapters presents the results of our efforts to contribute to a particular side of this development. It is based on a decade-long collaboration between clinicians and scientists and a wide range of competencies that work in synergy. There is hope for even more successes in the future in the battle against cancer. Fluorescence photodetection and photodynamic therapy will certainly bring some contribution of their own.

Fluorescence photodetection and photodynamic therapy share a common feature in this work: they rely on the use of spectrofluorometric techniques to investigate fluorescing substances. We chose to distinguish three categories of such substances, hereafter called fluorophores (FPs). **Exogenous fluorophores** are foreign to the human body (this means that they are synthesized outside of the organism) and will be dealt with in **Part I (Chapters 3, 4 and 5)**. In Lausanne, they are essentially used in the clinics as photosensitizers (PS) for the photodynamic therapy of early cancers of the esophagus or the bronchi and for the photodynamic therapy of the age-related macular degeneracy (AMD). **Chapter 3** presents some developments in the routine application of the PS mTHPC in the clinical environment of the CHUV Hospital at Lausanne for the photodynamic therapy of early cancers of the esophagus and of the tracheo-bronchial tree. Indeed, a major difficulty encountered by the pioneers of the mTHPC-mediated PDT is the interpatient fluctuations of the tissular level of PS for a constant injected dose which can potentially lead to under- or overtreatments if the light dose is not adjusted accordingly. This has been overcome by the setting up of individual dosimetry by means of fluorescence spectroscopy. Our contribution is a further development of this individual dosimetry.

Some other exogenous fluorophores are also injected in Lausanne. **Chapter 4** reports the results of a pre-clinical study of a more recent photosensitizer, the Lutetium Texaphyrin (Lu-Tex), in an animal model. The pharmacokinetics and the tumor vs. healthy tissue localization properties of this fluorophore are examined. In fact, the poor selectivity of most fluorophores for early cancerous lesions make them of little help to localize and delineate the pathological cells. In our animal model, the Lu-Tex displays a reproducible selectivity for early cancers. **Chapter 5** deals with experiments carried out on the same animal model as in Chapter 4 with further exogenous fluorophores. Due to some of their physical chemical properties, it is hoped that some of these substances could be interesting photodetection candidates. In particular, EtNBS, 2I-EtNBS and Sytox[®] Green have been investigated in more details and show promising results.

Part II (Chapter 5 and 6) of this work deals with **exogenously-induced fluorophores**. Whereas exogenous fluorophores were foreign substances injected to the human body, exogenously-induced fluorophores are fluorophores that are synthesized within the body following the application of an exogenous substance. In this work, we have studied the action of 5-aminolaevulinic acid (ALA) and some of its ester-derivatives. When in contact with these substances, living cells start to produce a fluorophore, the protoporphyrin IX (PPIX). Moreover, it seems that cells with a higher metabolic activity produce more of it than cells with a lower metabolic activity. It appears that this is the case with early cancer cells. In **Chapter 6**, we present the results of a preclinical study with cells in culture. A series of ester derivatives has been tested and our results show that long-chained esters can induce more PPIX than ALA itself. This is probably due to the poor penetration of ALA through the biological membrane because of

its electrical charge, a difficulty that is reduced with less polar esters. This study is to be linked to another preclinical study carried out in Lausanne on the same substances and their interaction with *ex vivo* mucosae. **Chapter 7** describes the subsequent step of our investigations on this series of substances, namely the clinical application of these results. The ALA-hexylester (hALA) has been tested in the urology clinic of the CHUV Hospital to detect early cancers of the urinary bladder. A topical application of hALA leads to the production of PPIX in cancer cells and less in healthy cells, hence yielding a contrast that allows the clinician to better delineate and notice the lesions. This is, in fact, used as a routine clinical procedure with ALA but, for the aforementioned reasons of the polarity of ALA, it requires solutions of high concentration and long instillation times. Our results with hALA suggest that the concentration of the solution could be diminished by a factor of close to 50 and the instillation time by a factor 3 for this application.

The **endogenous fluorophores** are the central subject of **Part III (Chapter 8 and 9)** of this work. As stated by their name, these fluorophores are not foreign substances, but rather naturally occurring fluorophores. They encompass several categories of fluorescing substances within biological tissue and they are described in detail in **Chapter 8**, where we also report a study on the fluorescence of these endogenous fluorophores (thereafter autofluorescence) in the tracheo-bronchial tree. We carried out this study to optimize the spectroscopic design of an autofluorescence imaging photodetection system for the tracheo-bronchial tree. In fact, the currently available autofluorescence photodetection devices lack a wide optimization study and this could be detrimental to their efficiency. To improve their performance, we studied a range of fluorescence excitation wavelengths. We analyzed the resulting autofluorescence spectra and propose a way to discriminate healthy from pre-/early cancerous tissue. This is of crucial importance for the development of future autofluorescence imaging devices. Moreover, the use of a calibrated lamp allowed us to express some of our spectra in physical units rather than in the usual 'arbitrary units'. This work is also presented in this chapter. In **Chapter 9**, we discuss the result of a collaboration with the firm *Richard Wolf GmbH* (Germany). A novel photodetection device has been developed that takes into account the spectroscopic measurements presented in chapter 8 and also presents several advantages over the previous generation of similar systems (one of them having been developed in Lausanne). Its performances are evaluated in terms of detection of early cancerous lesions in the tracheobronchial tree. The first clinical results of this system are presented in this section.

As stated above, the common thread of all these studies is the use of spectrofluorometry. An optical fiber-based spectrofluorometer has been developed in our group to allow us to perform all the endoscopical measurements. It has consequently been the central tool in the course of this work. Its versatility allowed us to probe the same sample with several excitation wavelengths in real-time, its sensitivity allowed us to detect very faint signals (such as the autofluorescence of biological tissue) and the fact that it was fabricated in-house allowed us to adapt it and modify it when necessary to each of our experiments. The exact design and set-up are presented in each chapter and will therefore not be described here.



Cancer

Chapter 1

Some facts about cancer and its management

1.1 Facts about cancer

The term 'cancer' is a generic denomination (equivalent to *malignant* tumor) for the diseases associated with the uncontrolled proliferation of cells and the production of other cancerous foci at distant sites of the body. These secondary tumors are called metastases. *Benign* tumors, also associated with the uncontrolled proliferation of cells, do not metastasize. As time elapses, these metastases become more and more invasive, eventually disrupting the organs which ensure the survival of the whole organism [1,2]. The metastases may cause the same symptoms as the primary tumor and further damage the host.

In the western world, cancer is the second cause of mortality after cardiovascular diseases. It is projected that about 25% of males and 20% of females born in 1985 in the United States will eventually die of cancer. Due to demographic patterns, these figures are unlikely to go down since a major proportion of the population lives to an age when the risk of developing cancer becomes high [2].

The causes of cancer are numerous. While it is impossible to point out the origin of every tumor, two thirds of all cancer deaths in the industrialized world can be attributed to two causes: tobacco consumption and diet. In particular, tobacco smoke accounts for 30 percent of cancer deaths,

making it the major known carcinogen. Among others, it is related to cancer of the lung (the most frequent cancer in the western world [3]), upper respiratory tract, esophagus and bladder [4,5]. Other causes include solar irradiation (UV rays), ionizing radiation (from radon, for example), chemicals (asbestos, benz[a]pyrene, aflatoxin) and some viruses [6].

The development of cancer is usually a long-term process. Many factors may act together to set off the initial cellular malfunction (initiation) and stimulate the growth of initiated cells (promotion). One or two decades may elapse before the initiated cells grow into clinically detectable tumors [2]. During this time interval, the cells undergo several modifications. Since the majority of cancers stems from the cells lining the body cavities (epithelia), we will limit our description here to the changes occurring in epithelial cells along the cancerization process. The cancers arising from this type of cell are called carcinoma. Metaplasia is the first modification undergone by the cell. It is characterized by a change in which one adult cell type is replaced by another, less-differentiated adult cell type [7]. This change is a defense mechanism for the cells and it can happen following any type of injury including nutritional ones, like the deficiency in certain vitamins. Assuming that the injurious agent or the adverse environment is removed and that the cells have not been initiated by a carcinogen, these lesions are at least potentially reversible [7]. However, in case it is not removed and it is a carcinogen, the epithelia are then further modified and are eventually characterized by an increasing degree of cellular and/or nuclear atypia. This is called dysplasia (mild, moderate and severe) and this step is no longer reversible [7]. The following step is the carcinoma in situ (CIS). At this stage, the whole epithelial layer is replaced by atypical cells. It is not known which fraction of CIS evolve towards invasive lesions, but it is believed that all invasive lesions have evolved from an earlier CIS.

The outcome of most cancers is poor in terms of survival. The reason is that the tumors are often detected only after symptoms appear [8], which means in a late stage. By that time, many tumors have already grown large and/or invasive and their management may be difficult. On the other hand, small early tumors are less likely to have metastasized and are hence easier to treat. However, these early cancerous lesions are asymptomatic for the patients who do not notice any alarming symptom. Their small size also makes them difficult for the clinician to localize. This fact is the main reason for the research carried out in the field that we are dealing with in this work: fluorescence photodetection of early cancers. It should be noted that, for asymptomatic people, large-scale screening procedures such as chest x-rays, routine proctoscopies or widespread mammographies are better undertaken for specific high-risk patients rather than on a wide basis for the whole population [6]. For the sake of public health costs and on a pure cost-benefit analysis, the latter are better advised to perform simple inexpensive measures such as self-examination of the breast, routine cytology or stool examination for blood traces [6].

1.2 Cancer detection

As stated above, a main feature of cancers is that an earlier detection is likely to yield a better outcome. The very first suspicion of a malignant disease relies on subtle clues (such as fatigue, weakness, weight loss, headache, pain, and so on) or the awareness of risk factors from the patient's history (family medical history, occupational exposure, personal habits) [6]. Most detection methods then involve either radiological examination or, in the case of hollow organs, an endoscopy and the histopathological analysis of cells. Endoscopy is of particular significance since most cancers (about 90% [9]) arise from the epithelia (maybe due to the fact that epithelial cells are the most exposed to the various carcinogens). Often, a combination of these methods is useful and it increases both the sensitivity (the percentage of positive tests in abnormal tissues) and the specificity (the percentage of negative tests in normal tissues) of the detection.

Two-dimensional x-ray imaging has benefited from the developments of computational power over the past three decades. Nowadays, x-ray computerized tomographic scanners (CT) are widely used to produce 3D images of the inside of the body by measuring the x-ray absorption coefficient of all the volume elements (voxels) that make up the anatomical structure [10]. Contrast agents can also be used to enhance a normally weak contrast to make, for example, blood vessels or lymph nodes stand out. As a matter of fact, in oncology, an iodinated contrast

enhancement agent (generally a derivative of iodinated benzoic acid) is of much help [10]. Methods like magnetic resonance imaging (MRI) produce a soft tissue contrast between healthy and pathologic tissue, sometimes also through a contrast enhancement agent - in this case a paramagnetic substance [10]. Positron emission tomography (PET) and single-photon emission computed tomography (SPECT) can produce 3D images of physiological functions such as blood flow, oxygen consumption or glucose metabolism [11]. Ultrasonography, being cheap, non-invasive and repeatable, is an interesting method for a start, but it may overlook small lesions and its reliability is very operator-dependent [10]. However, all these methods still suffer from a limited spatial resolution. This is their main drawback and it suggests that the development of different detection approaches to find smaller hence earlier lesions. They may, however, help localize lesions for further sampling techniques like fine needle biopsy.

If a tumor is suspected in a hollow organ, for example through a cytological analysis, an endoscopy can be performed to detect it. This examination will often also allow the physician to clearly delineate the lesion and to learn more about the type of lesion involved. The limitation of the endoscopy, though, is that the tumor has to be visible under white-light examination to be actually localized. Indeed, it is unfortunate that many early cancers closely resemble their healthy surrounding areas, thus making their detection at an early stage a difficult task. However, when a tumor is suspected under endoscopic examination, a biopsy is taken and a histopathological analysis of the cells is performed. This will confirm or exclude the findings and produce valuable information about the exact type and staging of the lesion. It should be noted, though, that the endoscopy is unable to clearly delineate invisible lesions. Some other methods like cytology or tumor marker (p53, telomerase, etc.) have proven fairly sensitive and specific but they do not produce any information about the exact localization of the diseased area.

A modality of cancer detection that will be investigated in more detail in this work is the fluorescence photodetection of pre-/early cancerous lesions. Because light needs to be brought to the site to be inspected, this method is limited to the hollow organs, to the skin or to the interstitial treatment of lesions close to the skin's surface. It has been thoroughly studied and is likely to undergo more developments in the near future. Fluorescence photodetection uses excitation light to excite a fluorophore and detect alterations in the tissue. It is well-tolerated and simple, when compared to methods like the MRI or the CT. Moreover, it seems promising as a method to detect pre-/early cancerous lesions. Despite its relative novelty, this feature could provide photodetection with wide acceptance as a way to find cancerous lesions at an earlier stage and consequently improve the current poor prognosis associated with the large, invasive lesions.

An ideal method of cancer detection should be quick, cheap and reliable. In such a case, one could imagine screening the entire population for certain cancers. This goal is within reach in the case of the pap-smear for cervical cancer or cytology for urinary bladder cancers. However, it is hard to imagine that such a screening would be easy for bronchial cancer. Sputum cytology is efficient but it does not provide any information about the localization of the lesion. Moreover, any further investigation requires a bronchoscopy, a difficult and time-consuming examination that does not even allow the operator to examine the entire organ (unlike a cystoscopy in the spherical bladder). Considering that, it is not surprising that the systematic screening of the whole population for bronchial cancer is considered overly demanding on the public health system. It should also be noted that it is relevant in a very small fraction of the population only, namely the people who either already have a bronchial lesion or are very likely to have one due to their personal habits of tobacco consumption. In the particular case of bronchial cancer, a sensible choice of patients to be screened thus seems the best way to keep the cost/benefit of the detection of lesions within reasonable limits.

1.3 Cancer treatment

Of all the modalities of treating cancers, surgery is probably the oldest and the commonest [4]. Despite its limitations (traumatic experience of a major operation, need to remove large parts of healthy tissue to ensure a complete removal of the tumor, not applicable to tumors that have metastasized throughout the body), it is still the most widely used [12]. Recent developments in

imaging technology and in the computational power available to physicians allowed the improvement in real-time image-guided surgery as a method of treating cancer [13]. It should be remembered that it is the sole initial treatment for over 50% of all patients with a localized malignant disease, for 40% of the patients with a regional malignant disease and less than 10% of patients when there is a distant spread [6].

Radiation therapy relies on the emission of powerful ionizing radiation (gamma rays or x-rays) by a radioactive source or of particle streams (protons, neutrons, electrons, argon or neon ions) generated by particle accelerators [14]. This radiation destroys the cells directly (genetic damage) or indirectly (induction of apoptosis). Since the healthy cells recover from the radiation exposure more easily than the cancer cells, the functionality of the organ is usually retained [12]. However, like surgery, radiotherapy is inefficient against tumors that have metastasized widely throughout the body. Sometimes, it also fails to completely eradicate the tumor cells [12]. Attempts are reported to identify drugs to enhance the radiation effects (radiosensitizers) or selectively protect normal tissues (radioprotectors) but are still in an experimental stage [14].

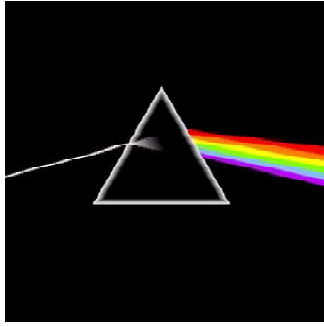
Chemotherapy is the name given to the systemic administration of anticancer drugs. Although this method successfully treats some forms of cancer (leukemias, lymphomas and testicular cancers), it fails to cure the most common cancers alone. This is the reason why it is sometimes used as a complement to either surgery or radiotherapy. The drugs also damage the rapidly growing cells of the body (bone marrow, hair cells) thus sometimes damaging important body functions [12]. Moreover, some tumors develop a resistance to the anticancer drugs during the course of treatment. Some forms of breast and prostate cancers are sensitive to the administration of hormones [4,12]. This sensitivity can be exploited although it is effective on those cancers only.

Most of the treatment modalities mentioned above are well adapted to managing large invasive tumors. However, the current trend of moving towards improved earlier detection has urged the clinicians to find less invasive treatments for less invasive lesions. Over the past decades, photodynamic therapy (PDT, Chapter 2) has proven a valuable alternative to manage them. This method relies on the combination of light, a non-toxic drug, the photosensitizer (PS), and oxygen. When the drug is activated by the light, it becomes highly toxic (hence its description as phototoxic). As long as the irradiation takes place at the very location of the lesion or as long as the drug has been accumulated selectively in the lesion (or both), the destruction of the lesion can be selective enough to completely retain the functionality of the target organ. This is even true if the PS has not been accumulated selectively in the lesion. The use of this method is limited to the early lesions of the hollow organs and/or the skin, since it requires the diffusion of visible light to the target organ and this can only be done through an endoscope, externally for skin cancers or interstitially in some cases. Some experience has been gained in our group about photodynamic therapy for cancers of the upper aero-digestive tract, the esophagus and the bronchi [15] and the bladder [16]. By now, PDT is accepted as a valuable therapeutic choice for suitable cancers as well as for some non-cancerous diseases [17].

References

1. Weinberg, R.A., 'How Cancer Arises', Scientific American, 275(3), 62-70, September 1996.
2. 'Cancer Biology', R.W. Ruddon, editor, Oxford University Press, 1995.
3. Bolliger, C.T., K. Haeussinger, 'Early detection of lung cancer', in 'European respiratory monograph, Pulmonary endoscopy and biopsy techniques', Vol. 3, Monograph 9, Chapter 2, J. Strausz, editor, 1998.
4. 'Cancer and its management', R. Souhami, J. Tobias, 2nd edition, Blackwell Science, Oxford, UK, 1995.
5. Trichopoulos, D., Li, F.P., Hunter, D.J., 'What Causes Cancer?', Scientific American, 275(3), 80-87, September 1996.
6. Laszlo, J., in 'Textbook of Medicine', J.B. Wyngaarden and L.H. Smith Jr, Editors, 16th edition, W.B. Saunders Company, Philadelphia, USA, 1982.

7. 'Biopsy Pathology of the Bronchi', E. McDowell, Th. Beals, Chapman and Hall, London, 1986.
8. Sidransky, D., 'Advances in Cancer Detection', *Scientific American*, 275(3), 104-109, September 1996.
9. 'Molecular Biology of the Cell', B. Alberts, D. Bray, J. Lewis, M. Raff, K. Roberts, J.D. Watson, 3rd edition, Garland Publishing, New York, USA, 1994.
10. 'CT and MRI in Oncology', Buthiau, Khayat, editors, Springer-Verlag, 1998.
11. Giger, M.L., Ch.A. Pelizzari, 'Advances in Tumor Imaging', *Scientific American*, 275(3), 110-112, September 1996.
12. Hellman, S., E.E. Vokes, 'Advancing Current Treatments for Cancer', *Scientific American*, 275(3), 118-123, September 1996.
13. Eric, W., L. Grimson, R. Kikinis, F. Jolesz, P. Black, 'Image-Guided Surgery', *Scientific American*, 280(6), 62-69, June 1999.
14. Chabner, B.A., in 'Textbook of Medicine', J.B. Wyngaarden and L.H. Smith Jr, Editors, 16th edition, W.B. Saunders Company, Philadelphia, USA, 1982.
15. Radu, A., P. Grosjean, Ch. Fontollet, G. Wagnières, A. Woodtli, H. van den Bergh, Ph. Monnier, 'Photodynamic Therapy for 101 Early Cancers of the Upper Aerodigestive Tract, the Esophagus, and the Bronchi: A Single-Institution Experience', *Diagnostic and Therapeutic Endoscopy*, Vol. 5, 145-154, 1999.
16. Jichlinski, P., A. Marti, C.-A. Porret, N. Lange, G. Wagnières, H. van den Bergh, H.-J. Leisinger, 'Photothérapie focale basée sur la protoporphyrine IX induite par l'hexyl ester d'acide aminolévulinique (h-ALA). Une étude de faisabilité sur de petits papillomes à bas degré de malignité', *Communication libre, 55e Assemblée annuelle de la Société Suisse d'Urologie*, Fribourg, Suisse, 2-4 septembre 1999.
17. Lipson, R.L., 'Historical perspective', in 'Photodynamic therapy, basic principles and clinical applications', Henderson and Dougherty, editors, Marcel Dekker Inc., New York, USA, 1992.



Light

Chapter 2

Fluorescence photodetection and photodynamic therapy: basic concepts

2.1 Fluorescence photodetection

Fluorescence photodetection of cancers is the method of cancer detection based on light-induced fluorescence (LIF) to characterize tissues. The use of LIF to characterize cancers has been reported since the first half of this century and has undergone many developments recently thanks to the progress made in optical fibers and instrumentation [1]. The core of the method is the ability of light to induce fluorescence and to generate a contrast, be it that of an exogenous or exogenously-induced fluorophore or that of the naturally-occurring fluorophores (native tissue fluorescence or autofluorescence). In this work, we will not consider the non-oncological applications of LIF. Additionally, we will only discuss the cancerous lesions arising in the hollow organs, thus leaving detection and treatment of cancers of the skin, the liver, the pancreas, etc. and affections of the eye aside.

The reliable detection of cancers in their early stages is positively correlated with the prospects of cure. However, in order to efficiently detect early cancerous lesions in hollow organs (by means of an endoscopy), the clinician needs to visualize a contrast between the lesion itself and the surrounding healthy tissues. As the lesions often do not stand out under white-light examination, an additional method that would produce a better contrast is desirable. In the case of fluorescence

photodetection, it implies either a selective accumulation of an exogenously-applied fluorophore or a detectable change in the tissue autofluorescence. It is to be noted that many invasive cancerous lesions are preceded by premalignant changes such as dysplasias and carcinoma in situ (CIS) and that an efficient method to detect early cancers would also need to be sensitive to and specific for such changes. Indeed, the method would be of tremendous help to the clinician if it were to delineate and detect pre- or early malignant tumors that are difficult to spot with the unaided eye while not generating any contrast on normal epithelia.

Many exogenous fluorophores (most of them being primarily tested as PDT photosensitizers [1]) have been tested in clinical (HPD [2-5], mTHPC [6,7], Lu-Tex [8,9], BPDMA [10]) or pre-clinical (EtNBA, EtNBS and 2I-EtNBS [11-14] and Sytox[®] Green) contexts in Lausanne. Unfortunately, although it has been reported that some of these fluorophores may induce a contrast between invasive tumors and the surrounding healthy tissue (HPD, mTHPC, in patients; Lu-Tex and EtNBS in tumors implanted in animal models), none of them displayed a very useful contrast for the detection of early-stage lesions. Moreover, substances like HPD induce a notable skin photosensitivity that can last for up to a couple of months. This is the major drawback of exogenous photosensitizers when they are used as photodetection agents. For this reason, such substances are hardly injected to patients for the sole purpose of detection anymore.

In the search for a useful contrast between early lesions and the healthy mucosa, the method of exogenous induction of an endogenous fluorophore is more promising. This method relies on the exogenous supply of a substance that is not a fluorophore itself but a pro-fluorophore. The pro-fluorophore will be included in the biosynthetic pathways of the cells and turned into a fluorescent molecule (the actual fluorophore) on the spot, in the target organ. By far the most widely used pro-fluorophore is the 5-aminolaevulinic acid (ALA) which is an intermediate product in the biosynthetic pathway of heme (see introduction of Chapter 6). The relative rates of the biochemical processes involved in this biosynthesis lead to the temporary accumulation of an intermediary product, the highly fluorescent Protoporphyrin IX (PPIX). This method has shown that it provides a good contrast between early lesions and the surrounding healthy mucosa because even *early* cancer cells have a different metabolic turnover than healthy cells. Moreover, it is reported that some enzymes have a different activity in early cancer cells than in normal cells, thus inducing a different rate of the processes involved in the heme biosynthetic pathway. These cells therefore accumulate more fluorescent PPIX than healthy cells, making them easy to spot as bright red fluorescent patches against a non-fluorescent background. This method has been successfully used for the detection of tumor cells in the urinary bladder [15-17] or the skin [18,19]. Some work has also been done in the bronchi [20]. Recently, the ALA-PPIX fluorescence photodetection of early cancers in the urinary bladder has won worldwide acceptance as a routine clinical practice.

The main drawback of the ALA-mediated fluorescence photodetection is the limited extent to which ALA can enter the target cells. This disadvantage can be linked to the physical chemical properties of the molecule as ALA is a zwitterion under physiological conditions. The lipid bilayer of biological membranes is relatively impermeable to charged molecules, hence the cellular uptake of ALA is small. Consequently, in order to increase the transport of ALA across the cellular membranes, high drug doses and long administration times are necessary. These drawbacks are unwanted for several reasons: firstly, ALA is an expensive drug. Secondly, in urology for example, long intravesical instillation times require the costly hospitalization of patients and finally, they are a source of discomfort to the patients. A possible way to overcome these difficulties is to use more lipophilic ALA derivatives, provided they have the same PPIX generation properties. The transformation of ALA into a series of its ester derivatives has been conducted in our group. These new substances have been tested *in vitro* on cells in culture. This work is presented in Chapter 6. The ALA esters have also been involved in an *ex vivo* study in Lausanne [21]. Based on these preclinical works, a clinical pilot study has been undertaken. It is presented in Chapter 7. The results of this study indicate that the use of ALA-hexylester (hALA) could be associated with a significant decrease in the cost of this technique with respect to ALA and an increase in the comfort of the patient, thanks to shorter instillation times and lower drug concentration.

Methods relying on tissue autofluorescence to detect early cancerous lesions have been widely studied. In principle, they provide information about the biochemical state of the tissue, as most endogenous fluorophores are metabolism-related [22,23]. Generally, a decrease in autofluorescence is observed in pre-/early cancerous lesions along with modifications of the spectral shape of the autofluorescence emission spectrum. The results of these studies have been implemented in several commercial and laboratory imaging devices [5, 24-26]. Despite their varying approaches in the treatment of the light detected, all of them take advantage of a difference in the emitted steady-state fluorescence by healthy and cancerous tissues to produce a contrast. The point spectroscopic [1,23] or autofluorescence imaging [1,27] studies about a given organ are numerous (larynx [28], bronchi [29-33], UADT [34-36], colon [37-39], skin [40], oral cavity [41,42], breast [43], esophagus [44,45], bladder [46], cervix [47,48]) and report interesting selectivities and specificities for the point spectroscopic approaches. The implementation of the findings of these point spectroscopic approaches into imaging systems allows the investigation of large areas of the tissue at once instead of probing several discrete locations. Unfortunately, the imaging systems do not enjoy the unequivocal acceptance they are aiming at [30,33,49,50]. This might be due to the fact that the process of imaging the autofluorescence of a whole zone of an organ through an endoscope is much more difficult than point-recording an autofluorescence spectrum with an optical fiber (edge effects, faintness of the detected signals, geometry of the organ, etc.). This might also be due to the lack of optimization of most commercial devices. Two principles seem to emerge in the conception of these devices, namely the pure autofluorescence (Xillix, Pentax) that relies on the fluorescence emitted by the tissue only and the 'autofluorescence + retrodiffusion' (Storz) that uses both the fluorescence emitted by the tissue and some of the excitation light that is backscattered by the tissue. However, in both cases, the devices rely on sub-optimal evidence and there is room for improvement. We carried out a study of the autofluorescence of bronchial tissues *in vivo*. This study was intended to optimize the spectral features of a future autofluorescence imaging photodetection device and its results are presented in Chapter 8. In the frame of a collaboration with the company Wolf Endoskope GmbH (Knittlingen, Germany), we implemented these results into the development of a novel photodetection device. It is briefly described in Chapter 9, along with early clinical results.

It has been proposed that time-resolved autofluorescence could produce more information about the mechanisms underlying the modifications of the autofluorescence spectra along the cancerization process. These results have been presented in some recent systems for time-resolved autofluorescence point-measurements [51] and imaging applications [52] to detect pre- or early cancerous lesions.

2.2 Photodynamic therapy (PDT)

Photodynamic therapy (PDT) is a method of treatment of cancer (as well as some non-cancerous diseases) based on the interaction of a photosensitizer (PS), light and molecular oxygen. None of them are, by themselves, toxic and only their interaction leads to cellular/tissular damage. Two mechanisms have been proposed [53] for the phototoxic effects: in both cases, a photon excites the PS from its singlet ground state to an electronically-excited singlet state and then, via an inter-system crossing, the PS is sometimes transformed into an excited triplet state. This triplet state can undergo two types of reactions: it can react either directly with the surrounding molecules to form radical or radical ions which will eventually form cytotoxic species after subsequent interaction with oxygen (Type I reaction) or it can react with molecular (triplet) oxygen and generate singlet oxygen, a highly cytotoxic molecule (Type II reaction) [54]. In both cases, all three elements, namely a PS, light and oxygen are necessary for successful PDT [53].

The ideal PS has the following characteristics: it is selectively accumulated by tumor tissues (very seldomly achieved by current PSs [53]); it is a pure compound to avoid the complex pharmacokinetics and localization properties of PSs made up of mixtures of different compounds; it is rapidly excreted from the body (hence it avoids the lasting skin photosensitization which is the main secondary effect of HPD/Photofrin[®]-PDT). The ideal PS should also be non-toxic and water-soluble to facilitate its administration to the patient. It should absorb light in the 600+ nm

region of the spectrum because photons of a longer wavelength will penetrate better in the biological tissue, and finally it should have a good singlet oxygen generation quantum yield to shorten the irradiation times.

There are numerous PSs on the market and many are used in a clinical context. The most commonly used [55,56] and best-known PS used for the PDT of tumors is probably the Hematoporphyrin Derivative (HPD) and its purified form Photofrin[®] which is the only PS to have been granted FDA approval as well as approval in other countries (France, the Netherlands, Canada, Japan, etc.) for clinical use. It has, however, some major drawbacks: it is a mixture of compounds, its absorption coefficient in the red part of the spectrum is small, its injection into patients invariably results in an extended skin photosensitivity (lasting for up to two months) that can be not only uncomfortable but also potentially life-threatening and it displays no selectivity for early cancerous lesions. All these drawbacks emphasize the need for the development of new PSs.

Among the so-called second-generation PSs currently under clinical evaluation, 5,10,15,20-tetra(*m*-hydroxyphenyl) chlorin (mTHPC, Foscan[®]) has been extensively studied in clinical practice in our group for the photodynamic treatment of early cancers of the bronchi and the esophagus. One part of this work focuses on the clinical use of this PS. Its advantages are clear compared to Photofrin[®], namely its purity, its strong absorption properties at 652 nm, its strong phototoxicity and limited skin photosensitization [57]. Its therapeutic efficiency has been demonstrated in numerous publications although its selectivity for early tumors has not been clearly established.

Further second-generation PSs include the Benzoporphyrin Derivative Monoacid Ring A (BPDMA), under current clinical assessment for the photodynamic treatment of Barrett's esophagus, an ailment resulting from the contact of stomachal acid with the esophagus epithelium, eventually resulting in general metaplasia of the esophagus surface and an increased risk of developing cancerous foci. The BPDMA is also under clinical assessment for the photodynamic treatment of age-related macular degeneracy (AMD), a non-cancerous condition affecting some 28% of the population above 75 years in the USA and leading to severe and rapidly progressing vision loss and eventually to blindness. This condition is thought to be due to a progressive accumulation of photoreceptors' waste products between the retinal pigmented epithelium (RPE) and the choroid. The growth of novel blood vessels, termed 'neovascularization', from the choroidal layer towards the RPE causes damage to the photoreceptors and consequent vision loss. In this case, PDT could be an effective treatment as the effect of the PS in such a treatment is to close the neovascularisation. Clinical trials in phases I, II and III have been completed for the BPDMA mediated PDT of AMD. BPDMA is also under investigation for the treatment of skin cancer and, at a preclinical stage, for the treatment of rheumatoid arthritis in animal models.

Lutetium Texaphyrin (Lu-Tex) has several very interesting features. It also seems to display some selectivity for the neovascularization, and has been involved in large-scale phase I and II clinical studies in Lausanne as a treatment for AMD. It has undergone trials in patients with atherosclerosis [58] and in animal models bearing transplanted tumors (human mammary sarcoma in mice [8], human colon carcinoma in mice [9], SMT-F tumors in mice [59,60]) with good selectivity properties. This might be due to the fact that tumors also have the ability to induce the growth of neo-vessels when they grow past a certain stage. In the frame of this work, we only studied Lu-Tex at a preclinical stage for early cancer detection in an animal model.

New PSs with interesting properties are being regularly reported on in the literature for different types of tumors in an animal model or in the first phases of clinical trials. All these PSs bear some advantages compared to HPD or mTHPC, be it their solubility in water, their quick excretion after an injection or their selectivity itself.

There are also reports about PPIX-mediated PDTs. The same properties that made it an interesting photodetection molecule make it an interesting PS. Its generation (topical application

of a precursor), its selectivity for malignant lesions and its rapid elimination from the site have several advantages over other PSs (no skin photosensitization, no stress on the immune system of the patient, no systemic effects). In this work, though, we only used it as a photodetection molecule.

As a treatment modality for early cancers, PDT has several advantages over methods like chemotherapy, radiotherapy or surgery. First of all, it is less invasive: the treatments require one injection of PS only and the light is brought to the target organ via an endoscope through the natural openings of the body. This minimal invasiveness is beneficial to the patient as it only requires short anesthesia, it keeps the healing process to the location of treatment only (no external scar) and it does not bring about severe side-effects like nausea or hair loss associated with other methods of treatment. It is also beneficial to the health system in general as it requires a short stay in hospital - sometimes only one day. Secondly, PDT is designed to locally treat early lesions with as little as possible damage to the surrounding or deeper layers of tissue. This feature, together with the healing faculties of the tissues, allows it to retain total functionality of the target organ, a characteristic of much importance to the patient who would otherwise undergo an esophagectomy or a cystectomy, for example. In principle, the PDT could benefit from a double selectivity - that of the PS and that of the excitation light. Still, the method is efficient with one selectivity only (usually that of the applied light). The third advantage of PDT is its repeatability. Whereas some methods involving systemic application of exogenous substances can induce resistance phenomena, the PDT can be repeated as many times as necessary without any kind of diminishing efficiency. These features may well explain the low mortality associated with careful PDT and its outstanding results in terms of cosmetics and quality of life of patients after treatment.

The major drawbacks of PDT are, in the first place, the skin photosensitization associated with certain PSs. Whereas the first generation PSs could induce a sensitivity that could last for up to two months, mTHPC, for example, requires patients to stay in the shade for a couple of weeks only [60]. This is a significant improvement but it is also questionable as an ethical problem as some of these patients may undergo PDT for palliative and not for curative reasons. It is therefore necessary to ask whether the deal is fair. Moreover, whereas some side-effects of the other methods may be more uncomfortable than dangerous (hair loss), skin photosensitization is potentially life-threatening depending on the surface of skin that has been exposed, the length of the exposure and the general condition of the patient. Another drawback of PDT is its limited range of application as far as the size of tumors goes. Since it is difficult for visible light to reach layers of tissue deeper than typically 2 cm, this sets the maximal depth of the manageable tumors. This unavoidably limits the range of application of PDT to early localized lesions on the surface of the target organ. Although it is in phase with the current trends in detection methods, it also means that some tumors may be beyond the capabilities of PDT. As well, with the notable exception of interstitial PDT (in which case, the advantage of low invasiveness is lost), PDT is inefficient against tumors that are not reachable through an endoscope or at least an optical fiber.

In summary, PDT has imposed itself as a valuable alternative in the hands of the clinicians over the past two decades for the treatment of early cancers. Like other methods, it has advantages and limitations, it can manage certain types of tumors and not other ones. Still, it has the potential to improve the curative and the palliative treatments of some cancers, along with a demonstrated ability to reduce the cost of such treatments with respect to other methods. The careful use of this method for the management of selected patients suffering from relevant lesions will certainly make it a more frequently used treatment in the future.

References

1. Wagnières, G., W. Star, B. Wilson, 'In vivo fluorescence spectroscopy and imaging for oncological applications', *Photochemistry and Photobiology*, 68(5), 603-632, 1998.
2. Profio, A., O. Balchum, 'Fluorescence diagnosis of cancer', in 'Methods in porphyrin photosensitization', David Kessel, editor, Plenum Publishing Corporation, 43-50, 1985.

3. Anthony, D., A. Profio, O. Balchum, 'Fluorescence spectra in lung with porphyrin injection', *Photochemistry and Photobiology*, Vol. 49, No. 5, 583-586, 1989.
4. Kessel, D., 'Tumor localization and photosensitization by derivatives of hematoporphyrin: a review', *IEEE Journal of Quantum Electronics*, Vol. QE-23, No. 10, 1718-1720, 1987.
5. Wagnières, G., A. Studzinski, D. Braichotte, Ph. Monnier, Ch. Depeursinge, A. Châtelain, H. van den Bergh, 'Clinical imaging fluorescence apparatus for the endoscopic photodetection of early cancers by use of Photofrin II', *Applied Optics*, 36(22), 5608-5620, 1997.
6. Braichotte, D., J.-F. Savary, Th. Glanzmann, P. Westermann, S. Folli, G. Wagnières, Ph. Monnier, H. van den Bergh, 'Clinical pharmacokinetic studies of tetra(meta-hydroxyphenyl)chlorin in squamous cell carcinoma by fluorescence spectroscopy at 2 wavelengths', *International Journal of Cancer*, 63, 198-204, 1995.
7. Fan, K., C. Hopper, P. Speight, G. Buonaccorsi, S. Bown, 'Photodynamic therapy using mTHPC for malignant disease in the oral cavity', *International Journal of Cancer*, 73(1), 25-32, 1997.
8. Woodburn, K., Q. Fan, D. Miles, D. Kessel, Y. Luo, S. Young, 'Localization and Efficacy Analysis of the Phototherapeutic Lutetium Texaphyrin (PCI-0123) in the Murine EMT6 Sarcoma Model', *Photochemistry and Photobiology*, 65(3), 410-415, 1997.
9. Kostenich, G., A. Orenstein, L. Roitman, Z. Malik, B. Ehrenberg, 'In vivo photodynamic therapy with the new near-IR absorbing water soluble photosensitizer lutetium texaphyrin and a high intensity pulsed light delivery system', *Journal of Photochemistry and Photobiology B: Biology*, 63, 36-42, 1997.
10. Kollias, N., H. Lui, J. Wimberly, R. Anderson, 'Monitoring of benzoporphyrin derivative monoacid ring A (BPD-MA) in skin tumors by fluorescence during photodynamic therapy. Preliminary observations', *Proceedings SPIE*, 1881, 41-47, 1993.
11. Cincotta, L., D. Szeto, E. Lampros, T. Hasan, A. Cincotta, 'Benzophenothiazine and benzoporphyrin derivative combination phototherapy effectively eradicates large murine sarcomas', *Photochemistry and Photobiology*, 63(2), 229-237, 1996.
12. Cincotta, L., J. Foley, T. MacEachern, E. Lampros, A. Cincotta, 'Novel photodynamic effect of a benzophenothiazine on two different murine sarcomas', *Cancer Research*, 54, 1249-1258, March 1, 1994.
13. Cincotta, L., J. Foley, A. Cincotta, 'Phototoxicity, redox behavior and pharmacokinetics of benzophenoxazine analogues in EMT-6 murine sarcoma cells', *Cancer Research*, 53, 2571-2580, June 1, 1993.
14. Dr Louis Cincotta, Ergoscience, Charlestown, MA, USA, personal communication.
15. Jichlinski, P., M. Forrer, J. Mizeret, Th. Glanzmann, D. Braichotte, G. Wagnières, G. Zimmer, L. Guillou, F. Schmidlin, P. Graber, H. van den Bergh, H.-J. Leisinger, 'Clinical Evaluation of a Method for Detecting Superficial Transitional Cell Carcinoma of the Bladder by Light-Induced Fluorescence of Protoporphyrin IX Following Topical Application of 5-Aminolevulinic Acid', *Lasers in Surgery and Medicine* 20:402-408, 1997.
16. Kriegmair, M., R. Baumgartner, W. Lumper, R. Waidelich, A. Hofstetter, 'Early clinical experience with 5-aminolevulinic acid for the photodynamic therapy of superficial cancer', *British Journal of Urology*, 77, 667-671, 1996.
17. Kennedy, J., R. Pottier, D. Pross, 'Photodynamic therapy with endogenous portoporphyrin IX: basic principles and present clinical experience', *Journal of Photochemistry and Photobiology, B: Biology*, 6, 143-148, 1990.
18. Peng, Q., T. Warloe, J. Moan, H. Heyerdahl, H. Steen, J. Nesland, K. Giercksky, 'Distribution of 5-aminolaevulinic acid-induced porphyrins in noduloulcerative basal cell carcinoma', *Photochemistry and Photobiology*, 62, 906-913, 1995.
19. Svanberg, K., T. Andersson, D. Killander, I. Wang, U. Stenram, S. Andersson-Engels, R. Berg, J. Johansson, S. Svanberg, 'Photodynamic therapy of non-melanoma malignant tumors of the skin using topical 5-aminolaevulinic acid sensitization and laser irradiation', *British Journal of Dermatology*, 130, 743-751, 1994.

20. Baumgartner, R., R. Huber, H. Schulz, H. Stepp, K. Rick, F. Gamarra, A. Leberig, C. Roth, 'Inhalation of 5-aminolevulinic acid: a new technique for fluorescence detection of early stage lung cancer', *Journal of Photochemistry and Photobiology, B: Biology*, 36, 169-174, 1996.
21. Marti, A., N. Lange, H. van den Bergh, D. Sedmera, P. Jichlinski, P. Kucera, 'Optimalisation of the formation and distribution of protoporphyrin IX in the urothelium: An in vitro approach', *Journal of Urology*, 162, 546-552, 1999.
22. Richards-Kortum, R., E. Sevick-Muraca, 'Quantitative optical spectroscopy for tissue diagnosis', *Annual Review of Physical Chemistry*, 47, 555-606, 1996.
23. Bigio, I., J. Mourant, 'Ultraviolet and visible spectroscopies for tissue diagnostics: fluorescence spectroscopy and elastic scattering spectroscopy', *Physics in Medicine and Biology*, 42, 803-814, 1997.
24. Lam, S., T. Kennedy, M. Unger, Y. Miller, D. Gelmont, V. Rusch, B. Gipe, D. Howard, J. LeRiche, A. Coldman, A. Gazdar, 'Localization of bronchial intraepithelial neoplastic lesions by fluorescence bronchoscopy', *Chest*, 113(3), 696-702, 1998.
25. Leonhard, M., 'New incoherent autofluorescence/fluorescence system for early detection of lung cancer', *Diagnostic and therapeutic endoscopy*, 5, 71-75, 1999.
26. Adachi, R., T. Utsui, K. Furusawa, 'Development of the autofluorescence endoscope imaging system', *Diagnostic and therapeutic endoscopy*, 5, 65-70, 1999.
27. Andersson-Engels, S., C. af Klinteberg, K. Svanberg, S. Svanberg, 'In vivo fluorescence imaging for tissue diagnostics', *Physics in Medicine and Biology*, 42, 815-824, 1997.
28. Harries, M., S. Lam, C. MacAulay, J. Qu, B. Palcic, 'Diagnostic Imaging of the larynx: autofluorescence of laryngeal tumours using the helium-cadmium laser', *The Journal of Laryngology and Otology*, Vol.109, 108-110, February 1995.
29. Hung, J., S. Lam, J. LeRiche, B. Palcic, 'Autofluorescence of Normal and Malignant Bronchial Tissue', *Lasers in Surgery and Medicine*, 11:99-105, 1991.
30. Kurie, J., J. Lee, R. Morice, G. Walsh, F. Khuri, A. Broxson, J. Ro, W. Franklin, R. Yu, W. Hong, 'Autofluorescence Bronchoscopy in the Detection of Squamous Metaplasia and Dysplasia in Current and Former Smokers', *Journal of the National Cancer Institute*, 90(13), 991-995, 1998.
31. Kakihana, M., K. Il, T. Okunaka, K. Furukawa, T. Hirano, C. Konaka, H. Kato, Y. Ebihara, 'Early detection of bronchial lesions using system of autofluorescence endoscopy (SAFE) 1000', *Diagnostic and therapeutic endoscopy*, Vol.5, 99-104, 1999.
32. Häussinger, K., F. Stanzel, R.M. Huber, J. Pichler, H. Stepp, 'Autofluorescence detection of bronchial tumors with the D-Light/AF', *Diagnostic and therapeutic endoscopy*, Vol.5, 105-112, 1999.
33. George, P., 'Fluorescence Bronchoscopy for the Early Detection of Lung-Cancer', *Thorax*, 54(2), 180-183, 1999.
34. Dhingra, J., D. Perrault, K. McMillan, E. Rebeiz, S. Kabani, R. Manoharan, I. Itzkan, M. Feld, S. Shapshay, 'Early Diagnosis of Upper Aerodigestive Tract Cancer by Autofluorescence', *Arch Otolaryngol Head Neck Surg*, Vol 122, November 1996.
35. Fryen, A., H. Glanz, W. Lohmann, T. Dreyer, R.M. Bohle, 'Significance of autofluorescence for the optical demarcation of field cancerisation in the upper aerodigestive tract', *Acta Otolaryngol (Stockh)*, 117, 316-319, 1997.
36. Gillenwater, A., R. Jacob, R. Richards-Kortum, 'Fluorescence spectroscopy: a technique with potential to improve the early detection of aerodigestive tract neoplasia', *Head & Neck*, 556-562, 1998.
37. Fiarman, G., M. Nathanson, A. West, L. Deckelbaum, L. Kelly, C. Kapadia, 'Differences in Laser-Induced Autofluorescence Between Adenomatous and Hyperplastic Polyps and Normal Colonic Mucosa by Confocal Microscopy', *Digestive Diseases and Sciences*, Vol. 40, No. 6, 1261-1268, June 1995.

38. Cothren, R., M. Sivak, J. Van Dam, R. Petras, M. Fitzmaurice, J. Crawford, J. Wu, J. Brennan, R. Rava, R. Manoharan, M. Feld, 'Detection of dysplasia at colonoscopy using laser-induced fluorescence: a blinded study', *Gastrointestinal Endoscopy*, 44, 168-176, 1996.
39. Schomacker, K., J. Frisoli, C. Compton, Th. Flotte, J. Richter, N. Nishioka, Th. Deutsch, 'Ultraviolet laser-induced fluorescence of colonic tissue: basic biology and diagnostic potential', *Lasers in Surgery and Medicine*, 12, 63-78, 1992.
40. Zeng, H., C. MacAulay, D. McLean, B. Palcic, 'Spectroscopic and Microscopic Characteristics of Human Skin Autofluorescence Emission', *Photochemistry and Photobiology*, Vol. 61, No 6, 639-645, 1995.
41. Gillenwater, A., R. Jacob, R. Ganeshappa, B. Kemp, A. El-Naggar, L. Palmer, G. Clayman, M. Mitchell, R. Richards-Kortum, 'Noninvasive diagnosis of oral neoplasia based on fluorescence spectroscopy and native tissue autofluorescence', *Arch Otolaryngol Head Neck Surg*, Vol. 124, 1251-1258, Nov 1998.
42. Ingrams, D., J. Dhingra, K. Roy, D. Perrault, I. Bottrill, S. Kabani, E. Rebeiz, M. Pankratov, S. Shapshay, R. Manoharan, I. Itzkan, M. Feld, 'Autofluorescence characteristics of oral mucosa', *Head & Neck*, 27-32, January 1997.
43. Gupta, P., S. Majumder, A. Uppal, 'Breast cancer diagnosis using N₂ laser excited autofluorescence spectroscopy', *Lasers in Surgery and Medicine*, 21: 417-422, 1997.
44. Vo-Dinh, T., M. Panjehpour, B. Overholt, 'Laser-induced fluorescence for esophageal cancer and dysplasia diagnosis', *Annals New York Academy of Science*, 116-122, 1997.
45. Vo-Dinh, T., M. Panjehpour, B. Overholt, C. Farris, P. Buckley III, R. Sneed, 'In vivo cancer diagnosis of the esophagus using differential normalized fluorescence (DNF) indices', *Lasers in Surgery and Medicine*, 16, 41-47, 1995.
46. Koenig, F., F. McGovern, H. Enquist, R. Larne, Th. Deutsch, K. Schomaker, 'Autofluorescence guided biopsy for the early diagnosis of bladder carcinoma', *The Journal of Urology*, Vol. 159, 1871-1875, 1998.
47. Ramanujam, N., M. Mitchell, A. Mahadevan, S. Thomsen, A. Malpica, Th. Wright, N. Atkinson, R. Richards-Kortum, 'Development of a multivariate statistical algorithm to analyze human cervical tissue fluorescence spectra acquired in vivo', *Lasers in Surgery and Medicine*, 19, 46-62, 1996.
48. Ramanujam, N., M. Mitchell, A. Mahadevan-Jansen, S. Thomsen, G. Staerckel, A. Malpica, Th. Wright, N. Atkinson, R. Richards-Kortum, 'Cervical precancer detection using a multivariate statistical algorithm based on laser-induced fluorescence spectra at multiple excitation wavelengths', *Photochemistry and Photobiology*, 64(4), 720-735, 1996.
49. Zargi, M., L. Smid, I. Fajdiga, B. Bubnic, J. Lenarcic, P. Oblak, 'Laser-induced fluorescence in diagnostics of laryngeal cancer' *Acta Otolaryngol. (Stockh)*, S527, 125-127, 1997.
50. Dal Fante, M., 'Diagnostica endoscopica in fluorescenza della displasia e del CIS bronchiale', <http://www.villaggiodelsalute.com/&Na/sem-2/dalfante.htm>, 1999.
51. Thomas Glanzmann, 'Steady-state and time-resolved fluorescence spectroscopy for photodynamic therapy and photodetection of cancer', PhD thesis #1920, EPFL, 1998.
52. Jérôme Mizeret, 'Cancer detection by endoscopic frequency-domain fluorescence lifetime imaging', PhD thesis #1839, EPFL, 1998.
53. Henderson, B., T. Dougherty, 'How does photodynamic therapy work?', *Photochemistry and Photobiology*, Vol. 55, No 1, 145-157, 1992.
54. Moan, J., K. Berg, H. Steen, T. Warloe, K. Madslie, 'Fluorescence and photodynamic effects of phthalocyanines and porphyrins in cells', in 'Photodynamic therapy, basic principles and clinical applications', Henderson and Dougherty, editors, Marcel Dekker Inc., 1992.
55. Schwartz, S. 'Historical perspective', in 'Photodynamic therapy, basic principles and clinical applications', Henderson and Dougherty, editors, 1992.

56. Lipson, R., E. Baldes, A. Olsen, 'The use of a derivative of hematoporphyrin in tumor detection', *The Journal of the National Cancer Institute*, 26:1, 1961.
57. Wagnières, G., Ch. Hadjur, P. Grosjean, D. Braichotte, J.-F. Savary, Ph. Monnier, H. van den Bergh, 'Clinical evaluation of the cutaneous phototoxicity of 5,10,15,20-Tetra (m-hydroxyphenyl)chlorin', *Photochemistry and Photobiology*, 68(3), 382-387, 1998.
58. Rockson, S., P. Kramer, M. Razavi, A. Szuba, S. Filardo, J. Cooke, D. Adelman, 'Photoangioplasty of human atherosclerosis with Lutetium Texaphyrin (Antrin™)', *Photochemistry and Photobiology*, 69, Special Issue, TPM-B3, p. 49S, June 1999.
59. Young, S., K. Woodburn, M. Wright, T. Mody, Q. Fan, J. Sessler, W. Dow, R. Miller, 'Lutetium Texaphyrin (PCI-0123): a near-infrared, water-soluble photosensitizer', *Photochemistry and Photobiology*, 63(6), 892-897, 1996.
60. Hammer-Wilson, M., M. Ghahramanlou, M. Berns, 'Photodynamic activity of Lutetium-Texaphyrin in a mouse tumor system', *Lasers in Surgery and Medicine*, 24, 276-284, 1999.

Part I

***EXOGENOUS
FLUOROPHORES***

The first part of this thesis reports the uses of fluorescence spectroscopy for the investigations of exogenous fluorophores in vivo (for a definition of exogenous fluorophores, see p. 13).

We separated this first part in three chapters: the first chapter deals with the clinical applications of mTHPC, a second generation PS. In Lausanne, it is now mainly used for the photodynamic therapy of early cancers of the bronchi, the esophagus or the UADT [1,2]. Although now accepted in routine practice in Lausanne, the mTHPC mediated PDTs require some care in order to be successful and we present the limitations as well as a possible improvement for this modality of treatment. A brief summary of some of the work done by other groups with this PS precedes the description of the clinical applications of mTHPC in Lausanne.

The second chapter presents pre-clinical results obtained on an animal model with another second-generation PS, the Lutetium Texaphyrin (Lu-TeX). Although we used it as a photodetection substance on early cancerous lesions in this model, it should be noted that it has also been used in Lausanne as a photodynamic therapy molecule for the treatment of AMD, a non-cancerous ocular affection. The selectivity and skin photosensitization properties of Lu-TeX are the core of the study presented here.

The third chapter of this first part reports on more trials we carried out on the same animal model with the Sytox[®] Green. Most fluorophores used nowadays (Photofrin[®], mTHPC or Lu-TeX) are localized in early lesions at a different extent than in normal tissue. The Sytox[®] Green is sensitive to its physical chemical environment and changes its spectroscopical or fluorescence properties according to its localization.

Some additional fluorophores have been tested in the hamster animal model. This work is described in the Appendix A2.



*Getting ready for a PDT in the esophagus
(Medlight SA, CH-1024 Ecublens)*

Chapter 3 mTHPC in the clinical context

This chapter deals with the clinical uses of the PS 5,10,15,20-tetra(*m*-hydroxyphenyl)chlorin (systematic name, also abbreviated as mTHPC) or Foscan[®] (commercial name). The first section briefly summarizes the physical chemical properties of this substance. The structure of the mTHPC, its excitation and emission spectra are presented. In the following section (3.2), we give a summary of the clinical work reported by other groups with the mTHPC as well as their observations and difficulties encountered when dealing with this molecule. Section 3.3 surveys the pre- and early clinical work carried out in Lausanne on mTHPC. Animal studies and clinical optimization studies have been conducted, thus generating wide experience in the use of this PS. Particular attention is paid to the inherent characteristics of the mTHPC mediated PDTs and to the behavior of this PS when injected into the human body. Finally, in section 3.4, we include the results of a study that we carried out to ease the necessary measurements implied by the mTHPC mediated PDTs.

3.1 The photosensitizer

The photosensitizer (PS) 5,10,15,20-tetra(*m*-hydroxyphenyl)chlorin (Foscan[®], mTHPC) is one of the so-called second generation PSs. It is an amphiphilic molecule that hardly dissolves in water. As a matter of fact, for i.v. injection, it has to be dissolved in a mixture of water,

polyethylene glycol 400 and ethanol (5:3:2 vol/vol/vol). Its chemical structure is given in Fig. 3.1.

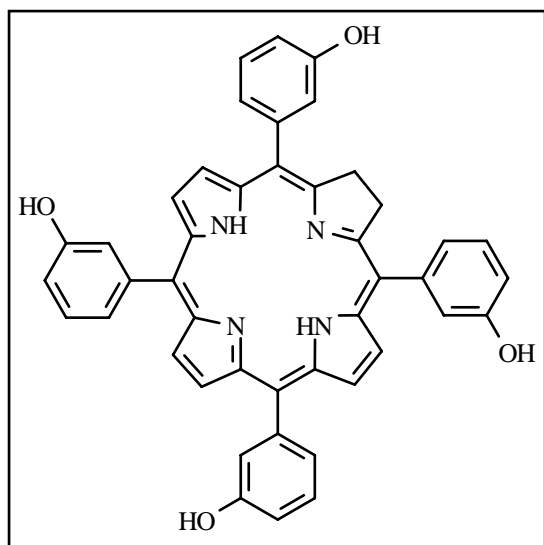


Figure 3.1: mTHPC.

mTHPC is a pure compound ($\geq 98\%$) and has an absorption coefficient of $38'000 \text{ M}^{-1}\text{cm}^{-1}$ at 652 nm, which is about one order of magnitude greater than that of HPD [3]. mTHPC is also more phototoxic than HPD and it has a fluorescence quantum yield of about 20% in tissue [4]. These features make it a very potent PS. Its excitation spectrum is given in Fig. 3.2a (detection wavelength: 690 nm) and emission spectrum in lung tissue is given in Fig. 3.2b (excitation wavelength: 420 nm). As a PS for PDT, mTHPC displays clear advantages over Photofrin[®]. It has therefore been tested in both preclinical and clinical studies.

3.2 Clinical work with mTHPC by other groups

Following preclinical studies on nude mice bearing mesothelioma xenografts [5,6], Ris et al presented a first clinical study about the PDT of chest malignancies with mTHPC [7]. In this study, the authors describe how they applied mTHPC PDT to the tumor bed of malignant mesotheliomas after the surgical resection of the tumor. They injected 0.3 mg/kg of mTHPC i.v. and, after a drug-light interval of 48 hours or 72 hours, applied laser light at 650 nm for the phototherapy. The authors report a tumor vessel necrosis and thrombosis as the cause for the tumor necrosis. They also report first-order kinetics of the mTHPC in the organism (half-life of about 12 hours) and a selectivity of the PS for the tumor of up to 6:1 (tumor vs bronchi) at 48 hours. Their measurements of the PS tissue level was done by HPLC. In the case of

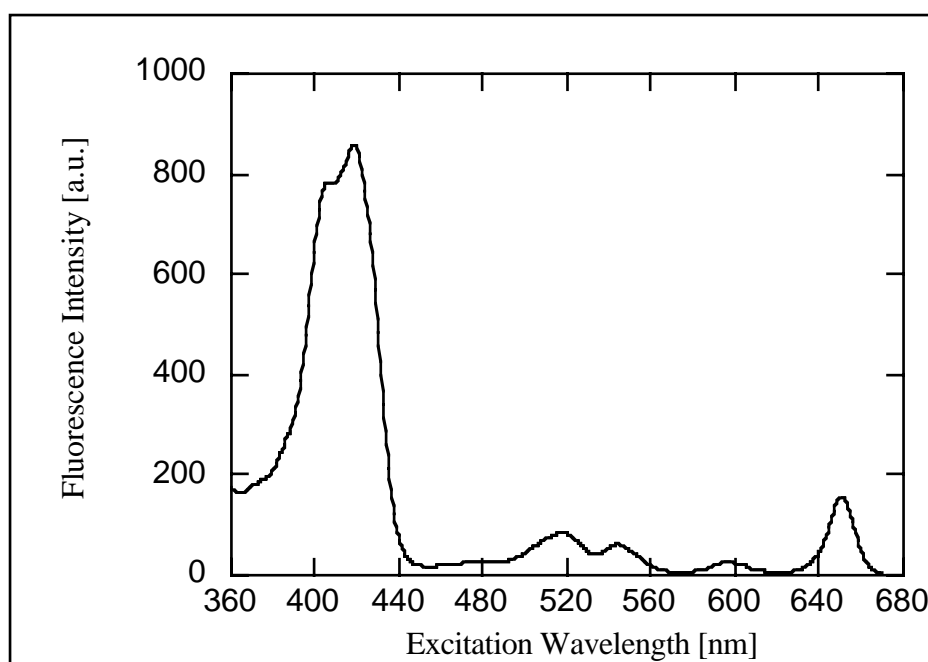


Figure 3.2a: Excitation spectrum of mTHPC in the injection solution ($c = 1.87 \mu\text{M}$, in accordance with the protocol described in section 3.4, Materials and Methods). The detection wavelength is 690 nm.

mesothelioma, PDT seems to be an attractive modality of treatment. Indeed, surgery is the only option that produces some results [7] and the use of PDT on the tumor bed after the gross resection of the malignancy might improve the survival of patients through better control of tumor regrowth. The authors report skin photosensitization as the only side-effect of the mTHPC, an observation that

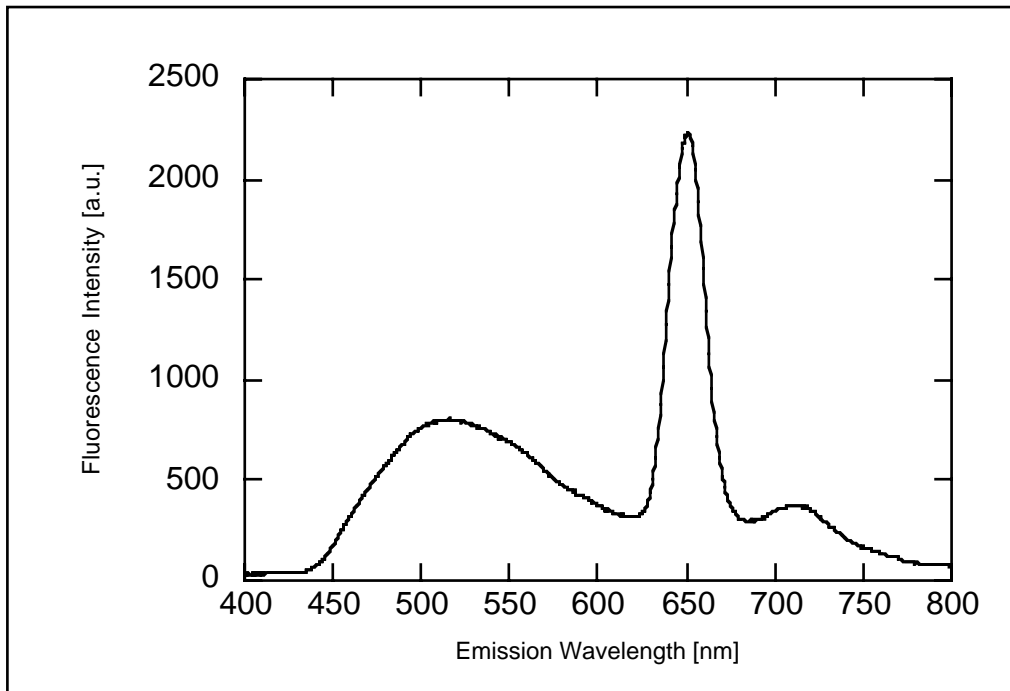


Figure 3.2b: Autofluorescence of the bronchial tissue and fluorescence emission spectrum of mTHPC 96 hours after an i.v. injection (measured in vivo in accordance with the protocol described in section 3.4, Materials and Methods). The excitation wavelength is 420 nm.

has also been reported by other authors [3]. However, because of the aggressiveness of mesothelioma, all patients involved in their study eventually died from the disease during the follow-up. No recurrence was observed on the sites of combined treatments. The authors conclude that the intraoperative PDT is feasible, although associated with additional morbidity if large areas are treated.

The mTHPC has been used to treat oral cancers by Fan et al [8]. This modality of managing oral cancer has been successful, with most of the localized single early lesions cleared after a non-thermal irradiation at 652 nm 72 to 96 hours after the i.v. administration of the PS. The authors also report treatments of patients with field cancerization but with less success. In the stomach, Ell et al [9] report promising results. They evaluated the mTHPC-mediated PDT as an alternative to radical surgical treatment for early cancers on 22 patients. Again, they used red light at 652 nm to irradiate the spots to be treated and they administered the PS i.v. at a dose of 0.075 mg/kg. They also used a drug-light interval of 96 hours. The authors report that the PDT was successful in 73% of the patients for a follow up period of 12 months. They also report skin photosensitivity and some local pain as the major side effects.

In a study about several types of tumors in patients (prostate, larynx, nasopharynx and bronchi), Ronn et al [10] detect a peak of mTHPC plasma level within the first 24 hours after the i.v. injection. Their main finding is that this peak does not occur immediately after the injection. The authors do not recover any mTHPC nor any of its metabolites in the urine of patients (in agreement with Ris et al). They also postulate that the interaction of mTHPC with the metabolism of patients is not a simple function of weight or body surface and caution that subsequent decisions about PDT dosing parameters should not be made without further study of some metabolic functions. In a later study by the same group [11], the authors injected a dose of mTHPC in the range of 0.0375 mg/kg to 0.15 mg/kg into animal models and 16 patients six days before PDT. When comparing the plasma levels of PS between the different species, they found that the plasma levels in humans were not only markedly higher than in animal models, but also that within one species, the interindividual plasma levels of mTHPC varied by up to threefold for a given injected dose. An interesting conclusion of their work is therefore that no matter whether animal or human, there is a significant variability from one individual to another after the

Location	In situ SCC	Micro-invasive SCC	Total
UADT	3/4	2/2	5/6
Esophagus	9/10	12/18	21/28
Bronchi	11/12	2/4	13/16
Total	23/26	16/24	39/50

Table 3.1: Results of photodynamic therapy with Foscan® for 50 early squamous cell carcinomas (SCC) in the upper aerodigestive tract (UADT), the esophagus and the bronchi: complete responses with no recurrence as a function of the tumor staging and site [1].

formal light dosimetry but whereas in the former the authors use exactly the same irradiation parameters for all the patients, in the latter, the authors vary the light doses according to the tumor depth and histology. They also sometimes report different tumor and normal tissue reactions for patients treated with the same light and drug dosages.

More has been done with mTHPC. It is beyond the scope of this work to go into too much detail about it. A good reference list can be found in a short summary edited by the producer of the PS [14].

3.3 Pre- and clinical work with mTHPC in Lausanne

One of the early clinical studies is that of Braichotte et al [15] that presents the pharmacokinetics of mTHPC in patients. These authors observe that mTHPC fluorescence reaches a maximum after some 30 to 90 hours following injection, depending on the site of the measurement (lesion or healthy tissue) and the patient. They also observe a slower clearance of mTHPC from healthy tissue than from the lesion. As well, these authors report a significant interpatient variation of the fluorescence signal of mTHPC for the same injected dose of 0.15 mg/kg. They warn that these disparities could lead to over- or undertreatments if not taken into account at the time of PDT. Another observation they present is the fact that the serum level of mTHPC is low just after the injection. They suggest that the PS might be taken up in the liver first and then slowly released again, a mechanism also suggested by Ronn et al [10]. These authors finally report a selectivity of mTHPC for advanced carcinoma as high as 16:1 but did not observe the same selectivity on early lesions. In two subsequent works, Braichotte et al [16,17] devise a way to overcome the interindividual variations of the tissular mTHPC level. They propose a simple approach based on a large database: the product of the mTHPC fluorescence level measured in the target tissue and the light dose should be constant for a given PDT result. This approach allows clinicians, provided they know the fluorescence level of mTHPC, to easily calculate the light dose to be applied, thus individualizing the PDT. The light dose monitoring method has been used ever since in Lausanne and has proven successful (Tables 3.1 and 3.2) [1,18]. Several methods have been compared [19] and the light-induced fluorescence (LIF) method of light-dose monitoring has been chosen in Lausanne.

The principle of LIF monitoring is the following: the fluorescence intensity of mTHPC is measured on the target organ just before the PDT with an optical fiber. The light dose is then calculated using this fluorescence intensity and adjusted to the patient undergoing treatment.

The method of monitoring the light dose by LIF on the target organ suffers from one drawback, though. It has to be performed endoscopically. This fact is associated with some difficulties and might be subject to some simplifications, provided another testing location could be found that

injection. Moreover, the authors suggest that some individual tailoring of the light dose be applied, based on the patient's plasma level of PS to compensate for its variability.

The use of mTHPC as a PS for PDT has also been reported for the treatment of carcinoma of the head and neck [12] and for nonmelanomatous skin tumors [13]. In both cases, the authors observe a 96-hour drug-light interval and use 652 nm light. Neither of these studies involves

would produce the same information about the fluorescence level. This has been studied in our group and the results of this study can be found in Section 3.4. They also have been published in:

Matthieu Zellweger, Pierre Grosjean, Philippe Monnier, Hubert van den Bergh, Georges Wagnières, 'Stability of the fluorescence measurement of Foscan[®] in the normal human oral cavity as an indicator of its content in early cancers of the esophagus and the bronchi', Photochemistry and Photobiology, 69(5), 605-610, 1999.

The drug-light interval has also been studied in Lausanne for mTHPC-mediated PDTs [20]. In this study, the authors used an animal model, the Syrian hamster, to find the best delay between the injection of the PS and irradiation in terms of PDT efficiency. The authors report that the PDT-induced tissue damage is strongly dependent on the drug-light interval. They observe an optimal interval on SCCs if the irradiation takes place between 3 and 8 days after the injection and they also observe that it diminishes significantly on the healthy mucosa between these two points in time. Some light is also shed upon the mechanism of mTHPC PDTs in this model as the authors observe a different type of tissue reaction depending on the drug-light interval. Indeed, the PDT damage is massive and non-selective if irradiation takes place between 6 and 48 hours after the injection, which seems to hint at a vascular localization of the PS. On the other hand, if the PDT takes place between 4 and 8 days after the injection, the damage seems to be more like a direct effect on cells. These observations are in agreement with the authors' additional experiments of fluorescence microscopy that shows an epithelial localization of the PS at these drug-light intervals. In Lausanne, we chose to perform the mTHPC PDTs 96 hours after the injection of the PS into the patient.

Esophagotracheal fistula	3
Occult esophageal perforation	2
Esophageal stenosis	2
Bronchial stenosis	3
Skin photosensitization	12

Table 3.2: Complications following photodynamic therapy with Foscan[®] for early cancers of the UADT, the esophagus and the bronchi [1].

Other factors have also been studied in Lausanne such as the effect of the fluence rate on the PDT outcome in an animal model [21], the dependence of the PDT outcome on the irradiation wavelength in an animal model [22] and the extent of skin photosensitization following the injection of the PS into patients [3].

Finally, a lot of work about mTHPC has been done in Lausanne by Glanzmann [23]. In a work about the pharmacokinetics of mTHPC in human plasma [19], this author and his coauthors propose a detailed pharmacokinetics curve of the PS in the plasma of 20 patients. It is very interesting to note that the curve actually shows that the level of mTHPC first diminishes after injection and then increases again to reach a maximum after about 10 hours. This is not only in agreement with other studies but also with the devised mechanism that the liver might trap the PS first and release it slowly afterwards. These authors also show that there is good correlation between the fluorescence signal of the tissular mTHPC measured in the bronchi and the oral cavity and very good correlation between the fluorescence signal of the tissular mTHPC measured in the esophagus and the oral cavity. This can be considered as a starting point of the study presented in Section 3.4. Glanzmann et al [24] also studied the correlation between the pharmacokinetics and the pharmacodynamics of mTHPC in an animal model, namely the Syrian hamster, and its clinical counterpart in patients. They find a similar pharmacokinetics curve but a factor 3 in the fluorescence signal of the PS for the same injected drug dose, in agreement with previously reported inter-species fluctuations [11]. The authors demonstrate that the mTHPC pharmacokinetics in early SCCs of the human UADT, the esophagus and the bronchi are better correlated to that of the chemically-induced early SCC of the hamster cheek pouch mucosa than to that of implanted advanced carcinoma in other rodent tumor models. They also demonstrate that this model is therefore useful to gather startup values for first clinical trials with new PSs, to a multiplicative scaling factor, although it should be used with some caution when investigating the PS uptake or the PDT response. Their final conclusion is that '*... the usefulness of this animal model is rather to be found in preclinical screening studies of new PS than in optimization of PDT parameters of PS already in clinical use*'.

References

1. Radu, A., P. Grosjean, Ch. Fontolliet, G. Wagnières, A. Woodtli, H. van den Bergh, Ph. Monnier, 'Photodynamic Therapy for 101 Early Cancers of the Upper Aerodigestive Tract, the Esophagus, and the Bronchi: A Single-Institution Experience', *Diagnostic and Therapeutic Endoscopy*, Vol. 5, 145-154, 1999.
2. Grosjean, P., J.-F. Savary, G. Wagnières, J. Mizeret, A. Woodtli, J.-F. Theumann, Ch. Fontolliet, H. van den Bergh, Ph. Monnier, 'Tetra(m-hydroxyphenyl)chlorin clinical photodynamic therapy of early bronchial and oesophageal cancers', *Lasers in Medical Science*, 11, 227-235, 1996.
3. Wagnières, G., Ch. Hadjur, P. Grosjean, D. Braichotte, J.-F. Savary, Ph. Monnier, H. van den Bergh, 'Clinical evaluation of the cutaneous phototoxicity of 5,10,15,20-Tetra (m-hydroxyphenyl)chlorin', *Photochemistry and Photobiology*, 68(3), 382-387, 1998.
4. Dr Georges Wagnières, EPFL, personal communication.
5. Ris, H.-B., H. Altermatt, B. Nachbur, Ch. Stewart, Q. Wang, C. Lim, R. Bonnett, U. Althaus, 'Effect of drug-light interval on photodynamic therapy with meta-tetrahydroxyphenylchlorin in malignant mesothelioma', *International Journal of Cancer*, 53, 141-146, 1993.
6. Ris, H.-B., H. Altermatt, Ch. Stewart, Th. Schaffner, Q. Wang, C. Lim, R. Bonnett, U. Althaus, 'Photodynamic therapy with m-tetrahydroxyphenylchlorin in vivo: optimization of the therapeutic index', *International Journal of Cancer*, 55, 245-249, 1993.
7. Ris, H.-B., H. Altermatt, B. Nachbur, Ch. Stewart, Q. Wang, C. Lim, R. Bonnett, U. Althaus, 'Intraoperative photodynamic therapy with m-tetrahydroxyphenylchlorin for chest malignancies', *Lasers in Surgery and Medicine*, 18(1), 39-45, 1996.
8. Fan, K., C. Hopper, P. Speight, G. Buonaccorsi, S. Bown, 'Photodynamic therapy using mTHPC for malignant disease in the oral cavity', *International Journal of Cancer*, 73(1), 25-32, 1997.
9. Ell, C., L. Gossner, A. May, H. Schneider, E. Hahn, M. Stolte, R. Sroka, 'Photodynamic ablation of early cancers of the stomach by means of mTHPC and laser irradiation - Preliminary clinical experience', *Gut*, 43(3), 345-349, 1998.
10. Ronn, A., M. Nouri, L. Lofgren, B. Steinberg, A. Westerborn, T. Windhal, M. Shikowitz, A. Abramson, 'Human tissue levels and plasma pharmacokinetics of Temoporfin (Foscan®, mTHPC)', *Lasers in Medical Science*, 11(4), 267-272, 1996.
11. Ronn, A., J. Batti, C. Lee, D. Yoo, M. Siegel, M. Nouri, L. Lofgren, B. Steinberg, 'Comparative biodistribution of meta-tetra(hydroxyphenyl)chlorin in multiple species: clinical implications for photodynamic therapy', *Lasers in Surgery and Medicine*, 20(4), 437-442, 1997.
12. Dilkes, M., M. de Jode, A. Rowntree-Taylor, J. McGilligan, G. Kenyon, P. McKelvie, 'm-THPC photodynamic therapy for head and neck cancer', *Lasers in Medical Science*, 11(1), 23-29, 1996.
13. Kübler, A., Th. Haase, Ch. Staff, B. Kahle, M. Rheinwald, J. Mühling, 'Photodynamic therapy of primary nonmelanomatous skin tumours of the head and neck', *Lasers in Surgery and Medicine*, 25, 60-68, 1999.
14. 'mTHPC Foscan® and Photodynamic Therapy Bibliography', Scotia Pharmaceuticals Ltd Editors, Publications, c/o SRI Library, Kentville, Nova Scotia, Canada, 1998.
15. Braichotte, D., J.-F. Savary, Th. Glanzmann, P. Westermann, S. Folli, G. Wagnières, Ph. Monnier, H. van den Bergh, 'Clinical pharmacokinetic studies of tetra(meta-hydroxyphenyl)chlorin in squamous cell carcinoma by fluorescence spectroscopy at 2 wavelengths', *International Journal of Cancer*, 63, 198-204, 1995.
16. Braichotte, D., J.-F. Savary, Ph. Monnier and H. van den Bergh, 'Optimizing Light Dosimetry in Photodynamic Therapy of Early Stage Carcinomas of the Esophagus Using Fluorescence Spectroscopy', *Lasers in Surgery and Medicine*, 19, 340-346, 1996.
17. Braichotte, D., J.-F. Savary, Th. Glanzmann, Ph. Monnier, G. Wagnières and H. van den Bergh, 'Optimizing Light Dosimetry in Photodynamic Therapy of the Bronchi by Fluorescence Spectroscopy', *Lasers in Medical Science*, 11, 247-254, 1996.

18. Grosjean, P., G. Wagnières, Ch. Fontollet, H. van den Bergh, Ph. Monnier, 'Treatment failures after PDT with Foscan[®] and 514 nm light for early SCC in the esophagus', RC6, 7th Biennial Congress of the International Photodynamic Association, Nantes, France, July 1998.
19. Glanzmann, Th., Ch. Hadjur, M. Zellweger, P. Grosjean, M. Forrer, J.-P. Ballini, Ph. Monnier, H. van den Bergh, K.L. Chang and G. Wagnières, 'Pharmacokinetics of Tetra(*m*-hydroxyphenyl)chlorin in Human Plasma and Individualized Light Dosimetry in Photodynamic Therapy', *Photochemistry and Photobiology*, 67(5), 596-602, 1998.
20. Andrejevic-Blant, S., Ch. Hadjur, J.-P. Ballini, G. Wagnières, Ch. Fontollet, H. van den Bergh and Ph. Monnier, 'Photodynamic therapy of early squamous cell carcinoma with tetra(*m*-hydroxyphenyl)chlorin: optimal drug-light interval', *British Journal of Cancer*, 76(8), 1021-1028, 1997.
21. Andrejevic Blant, S., A. Woodtli, G. Wagnières, Ch. Fontollet, H. van den Bergh, Ph. Monnier, 'In vivo fluence rate effect in photodynamic therapy of early cancers with tetra(*m*-hydroxyphenyl)chlorin', *Photochemistry and Photobiology*, 64(6), 963-968, 1996.
22. Andrejevic Blant, S., J.-F. Theumann, M. Forrer, G. Wagnières, H. van den Bergh, Ph. Monnier, 'Wavelength-dependent effect of tetra(*m*-hydroxyphenyl)chlorin for photodynamic therapy in an 'early' squamous cell carcinoma model', *Lasers in Medical Science*, 12, 269-273, 1997.
23. Thomas Glanzmann, 'Steady-state and time-resolved fluorescence spectroscopy for photodynamic therapy and photodetection of cancer', PhD thesis #1920, EPFL, 1998.
24. Glanzmann, Th., M. Forrer, S. Andrejevic Blant, A. Woodtli, P. Grosjean, D. Braichotte, H. van den Bergh, Ph. Monnier, G. Wagnières, 'Pharmacokinetics and pharmacodynamics of tetra(*m*-hydroxyphenyl)chlorin in the hamster cheek pouch tumor model in comparison with its clinical counterpart', submitted to the *Journal of Photochemistry and Photobiology, B: Biology*.

3.4

Stability of the fluorescence measurement of Foscan[®] in the normal human oral cavity as an indicator of its content in early cancers of the esophagus and the bronchi.

Matthieu Zellweger¹, Pierre Grosjean², Philippe Monnier², Hubert van den Bergh¹ and Georges Wagnières¹

¹Institute of Environmental Engineering, Swiss Federal Institute of Technology, EPFL, CH-1015 Lausanne; ²Department of Otolaryngology, Head and Neck Surgery, CHUV Hospital, CH-1011 Lausanne, Switzerland.

Keywords: mTHPC, photosensitizer, light-induced fluorescence.

Abbreviations: PDT, photodynamic therapy; Foscan[®] (mTHPC): 5, 10, 15, 20-tetra(m-hydroxyphenyl)chlorin; PS: photosensitizer; LIF: light-induced fluorescence; HPR: half-peak range; FWHM: full width at half maximum; SD: standard deviation; ASD: adimensional standard deviation; SNR: Signal to Noise Ratio.

ABSTRACT

Photodynamic therapy (PDT) with Foscan[®] (mTHPC) is used to cure early cancers of the esophagus or the tracheo-bronchial tree. However, fixed PDT parameters (drug dose, light dose, etc) do not permit an accurate prediction of the tissue damage. Large interpatient fluctuations in tissue drug level, at the time of light application, suggest that the light dose must be adjusted to the drug dose shortly before the PDT. This drug dose can be measured endoscopically by Light-Induced Fluorescence spectroscopy, but this measurement is inconvenient and somewhat difficult. A better test site, yet yielding comparable information, is needed. The oral cavity seems ideal. However it first had to be established to what extent the estimation of the drug dose was dependent upon the location of the measurement and the pressure applied to the probe. These measurements prove not only correlated to similar measurements in the esophagus or the bronchi, but also more consistent and less sensitive to the location and the applied pressure. The buccal mucosa is therefore recommended as a test site for measuring the Foscan[®] fluorescence signal at the time of PDT in the esophagus or the bronchi. This measurement is accurate enough for use in light dose adjustment.

Photochemistry and Photobiology, 69(5), 605-610, 1999.

INTRODUCTION

Photodynamic therapy (PDT) with Foscan[®] (mTHPC) has been used among others for the curative treatment of early stage cancer of the head and neck, the esophagus and the tracheo-bronchial tree (1-7). In these studies, the following therapeutic parameters have been thoroughly investigated: dose of Foscan[®], drug-light interval, illumination wavelength and light dose (3-7). However, it has been reported that for identical treatment parameters there was an important interindividual fluctuation in the degree of tissue damage after PDT (4,5,8). Whereas some patients exhibited only little tissue destruction sometimes leading to tumor recurrence, others showed massive necrosis and in a few cases severe complications such as fistulae or stenosis occurred (8). Interpatient variability in drug metabolism, leading to as much as an order of magnitude difference in drug concentration 4 days after injection, may well account for this fact (9, 10). The bottom line of this observation is that one cannot control the photosensitizer (PS) level in the tissue of interest from the injected dose only.

These fluctuations can, to some extent, be overcome by adapting the light dose to the tissular PS level, i.e. compensating for low drug levels by giving a higher light dose and vice versa. Light-induced fluorescence (LIF), among others (11, 12), has been shown to be a valuable method to estimate this PS level (4, 5, 10, 13). The actual measuring of the LIF spectra can be performed endoscopically with a previously described (14) optical fiber-based spectrofluorometer. However, in vivo spectrofluorometry in the esophagus or the bronchi is not very convenient in routine clinical practice. The measurement itself may be sensitive to several factors such as, among others, the positioning of the optical fiber, the heterogeneity of the tissue or the experience of the physician. The major consequence is a large amount of fluctuations in the observed fluorescence signal even when measured over a small and apparently homogeneous tissue surface. As we want as accurate an estimation of the fluorescence signal, and consequently as accurate an estimation of the tissular Foscan[®] as possible, it is best to keep the fluctuations of the fluorescence signals to a minimum. Performing such clinical LIF

measurements in the oral cavity seemed ideal, because the oral cavity is very accessible. Moreover, since there is little or no contrast in the Foscan[®] uptake between normal and early stage malignant tissues (4, 5, 10), the LIF signals can be obtained on normal tissues. Furthermore, a highly significant correlation between the LIF signals in the bronchi or the esophagus on the one hand and the LIF signals in the oral cavity on the other hand has been demonstrated (10). Last but not least, shifting the monitoring measurements from the busy operating room during anesthesia to another location just prior to the intervention is also highly advantageous.

Hence, the aim of this study is to assess the sensitivity of the LIF measurement in the oral cavity to the above-mentioned factors like pressure and location, and to confirm whether or not the endoscopical LIF measurements can be replaced by faster, simpler and more reproducible measurements in the oral cavity without loss of relevant information.

MATERIALS AND METHODS

Patients. Five patients (4 male and 1 female) were involved in this study. The mean age was 68.1 years (range 63-75). The patients were scheduled for PDT of an early cancer in the bronchi (1 case) or the esophagus (4 cases). They received an i.v. injection of 0.15 mg of Foscan[®] per kg of body weight according to the protocol accepted by the Ethics Committee of the CHUV Hospital in Lausanne, Switzerland. The LIF measurements took place just before PDT, 96h after the drug injection, and within 2 hours prior to anesthesia. All the patients gave their written informed consent and none of them reported any pain or discomfort due to the measurements in the oral cavity.

Foscan[®]. Foscan[®] was kindly supplied by Scotia Pharmaceutical Ltd., Guildford, UK as a lyophilized dark purple crystalline powder and was stored in the dark at 4° C. Immediately prior to use, twenty milligrams of Foscan[®] were dissolved in a 5 ml solution of 30% polyethylene glycol 400, 20% ethanol and 50% water. The solution was then i.v. injected over 5 to 10 min through a bacterial filter within 30 min of preparation at a dose of 0.15 mg/kg.

Foscan[®] (solution in methanol) has a strong absorption band centered at 416 nm (Soret band, half peak range (HPR): 394 to 427 nm, $\epsilon = 189,000$) and four minor absorption bands centered at 516 nm (HPR: 498 to 530 nm, $\epsilon = 14,800$), 542 nm (HPR: 554, no lower value because of overlap, $\epsilon = 9,600$), 594 nm (HPR: 587 to 606 nm, $\epsilon = 5,100$) and 650 nm (HPR: 642 to 656 nm, $\epsilon = 33,500$) respectively (15).

Fluorescence spectroscopy. Our optical fiber-based spectrofluorometer (Fig. 1) consists of an excitation source (UXL-75 XE, 75W high pressure Xenon lamp, Ushio Inc., Japan) whose light is diverted into a spectrograph (Chromex 250, Chromex, Albuquerque NM 87107, USA), filtered (BG3, Schott Glaswerke, D-55116 Mainz, Germany, blue band pass, center wavelength: 372 nm, Full Width at Half-Maximum (FWHM): 184 nm) and injected into an optical fiber (PUV600T, CeramOptec GmbH, D-53121 Bonn, Germany, NA=0.4, 4.2m, 600 μm core diameter). The excitation wavelength is 420 ± 7.5 nm and the typical power at the end of the fiber is 60 μW . The detection range is between 450 nm and 800 nm and the resolution of the apparatus is 11 nm (FWHM). The fiber can be inserted into a metallic cylindrical handpiece (diameter 5.6 mm, length: 60 mm) in such a way that an application of the handpiece on the tissue results in a direct contact of the fiber tip with the organ. The fluorescence is collected in the same fiber and separated from the excitation light by a dichroic mirror (DC450, Reynard, San Clemente CA 92673-6227, USA, dichroic mirror, cut-off wavelength: 440 nm). It is then filtered by a long-pass filter (FG455, Andover Corporation, Salem NH 03079-2800, USA, long-pass filter, cut-on wavelength: 450 nm) and dispersed in a spectrograph (Chromex 250, Chromex, Albuquerque NM 87107, USA) to be detected by a Peltier cooled CCD (TE/CCD-256, UV coated, Spectroscopy Instruments GmbH, D-82205 Gilching, Germany). The whole setup is controlled by a 486 PC (Fast 486/50, Spectroscopy Instruments GmbH, D-82205 Gilching, Germany) with CSMA software (Spectroscopy Instruments GmbH, D-82205 Gilching, Germany) and mounted on a trolley that allows transport to the

medical facility. The acquisition time of the spectra is 1 second.

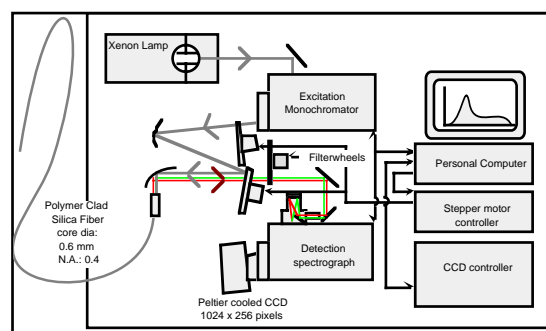


Figure 1: Experimental setup for point fluorescence measurements.

Before clinical measurements, the fluorescence spectrum of an aqueous solution of Rhodamine B ($c = 1 \cdot 10^{-6}$ M) in a 10mm quartz cuvette is measured. The magnitude of the peak at 575 nm allows for a certain degree of instability of the spectrofluorometer setup to be taken into account and corrected for. Fluorescence excitation is also at 420 nm and detection between 450 and 800 nm.

Procedure. The fluorescence spectrum of the oral mucosa was measured at several locations in the oral cavity of the patient: upper right cheek, middle right cheek, lower right cheek, dorsal tongue, ventral tongue, upper lip, lower lip, upper left cheek, middle left cheek and lower left cheek. Then the LIF spectra were measured again on the middle right cheek applying a range of increasing pressures: gentle touch, light pressure, high pressure and pressure applied with one finger from the outside of the cheek (for a description of our estimation of these pressures, see below and in Table 1). The probe was held perpendicular to the tissue in every measurement. Six spectra were measured at each location and at each pressure. No photobleaching was observed during the measurements.

The pressure applied to the fiber tip was subjectively assessed by the physician. An estimate of the pressure was obtained in the following manner: a small piece of chicken muscle was laid on an analytical balance. The balance was set to zero. The handpiece was applied ten times in a row onto the piece of meat with approximately the same force as when measuring in the oral cavity: gentle touch, light pressure, high pressure and very high pressure (simulating the highest

pressure obtained when applying a force from the outside of the cheek). The value was recorded each time. The mean value and the standard deviation were calculated; the range of pressures as given by the smallest and the largest values were also observed. This yielded the following values:

	Mean value	Range
Gentle touch	0.03 ± 0.01 N	< 0.04 N
Light pressure	0.19 ± 0.03 N	0.12-0.25 N
High pressure	0.97 ± 0.3 N	0.7-1.2 N
Very high pressure	3.5 ± 0.6 N	> 2.5 N

Table 1: Estimated pressures applied to the fiber tip. The values represent the average of ten measurements of the force applied together with the corresponding standard deviation.

Table 1 indicates that, although estimates, the values are reproducible enough and well separated. It is possible that the actual value applied to the patient's mucosa is somewhat different. Nevertheless, it was assumed here that the pressures actually applied to the patient's mucosa were of the same order of magnitude as our estimation. Moreover, as will be seen later, one should note that the LIF spectra proved quite insensitive to the pressure applied to the fiber tip. This reduces the importance of the estimation of the applied pressure.

Endoscopic measurements (esophagus and bronchi). After the routine endoscopic observation of the site, the optical fiber of our spectrofluorometer was passed through the biopsy channel of the endoscope. It was then placed onto the site to be measured and the endoscopic illumination was switched off. Four spectra were recorded on the same location and the endoscopic light was then switched on again. The site was checked for the absence of blood prior to proceeding to further measurements. Again, no photobleaching was observed during the measurements.

Analysis of results. The magnitude of the Foscan[®] fluorescence peak at 652 nm was obtained by subtracting the autofluorescence background. The autofluorescence was measured on the healthy oral mucosa of

three patients without PS and applying a scaling factor in the 610-620 nm window. Hence four values (esophagus, bronchi) or six values (oral cavity) were obtained for each location and each applied pressure. From these values, the mean and the standard deviation were calculated. They are plotted in Fig. 2 through 4. For visual comfort, they are plotted relatively to the largest, hence described as 'relative units' [r.u.].

The fluctuations of the mean values in each figure give a measure of the interpatient fluctuations. To quantify the intra-patient fluctuations, the adimensional standard deviation (ASD = SD divided by the mean) has been calculated and expressed as a percentage of the mean. The ASDs are plotted in Fig. 5.

Statistical Analysis. The statistical significance of our results has been tested with the two-sided Wilcoxon Mann-Whitney Test (16). It is indicated in the figure caption.

RESULTS

Bronchi

The LIF data from the bronchi are shown in Fig. 2a. Each bar represents the mean value for one patient of the measurements taken at several sites in the bronchi (3 to 7 sites depending on the patient). The standard deviation of the mean is also indicated. The mean values quantify the inter-patient fluctuations of the Foscan[®] fluorescence signal. These inter-patient fluctuations are up to a factor higher than 5. The intra-patient fluctuations are quantified by the ASDs and plotted in Fig. 5 Br1-Br4. They range between 27% and 59% (41% in average, plotted as a straight line).

Esophagus

Figure 2b is a set of similar data measured in the esophagus. The mean values represent the mean of the measurements taken in one given patient at several sites (4 to 6 sites depending on the patient). The inter-patient fluctuations are up to a factor higher than 4. The intra-patient fluctuations are quantified by the ASDs and plotted in Fig. 5 Es1-Es5. They range between 15% and 49% (30% in average, plotted as a straight line).

Oral cavity

The values of the LIF signals from the oral cavity are shown in Fig. 3 (dependance

upon the location) and Fig. 4 (dependance upon the applied pressure).

In the Fig. 3, the mean values represent the mean of the measurements taken in one given patient at several sites in the oral cavity (upper right cheek, middle right cheek, lower right cheek, dorsal tongue, ventral tongue, upper lip, lower lip, upper left cheek, middle left cheek, and lower left cheek). The inter-patient fluctuations are up to a factor higher than 4. The intra-patient fluctuations are quantified by the ASDs and plotted in Fig. 5 Loc1-Loc5. They range between 8% and 22% (14% in average, plotted as a straight line).

In the Fig. 4, the mean values represent the mean of the measurements taken in one given patient at several pressures on the middle right cheek mucosa (gentle touch, light pressure, high pressure and pressure applied with a finger from the outside of the cheek). The inter-patient fluctuations are up to a factor higher than 5. The intra-patient fluctuations are quantified by the ASDs and plotted in Fig. 5 Pr1-Pr5. They range between 7% and 29% (16% in average, plotted as a straight line).

At this stage, it is already clear that the intra-patient fluctuation is smaller (by a factor 2 to 3, $p < 0.01$) when the Foscan[®] fluorescence signal is measured in the oral cavity instead of the bronchi or the esophagus. A better reproducibility is precisely what was intended with the assessment of the oral cavity as a test site for the measurement of the Foscan[®] fluorescence signal.

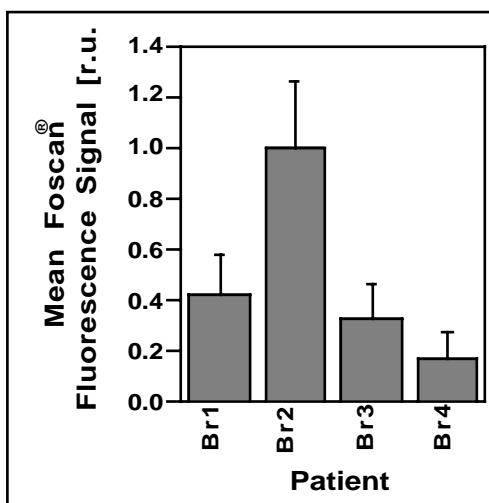


Figure 2a: Mean fluorescence signals of Foscan[®] (measured 96h after i.v. injection of 0.15 mg/kg) in the bronchi of four patients on normal mucosa. Each bar

represents the average of 3 to 7 sites measured from a given patient. The uncertainties given correspond to the 67% confidence interval.

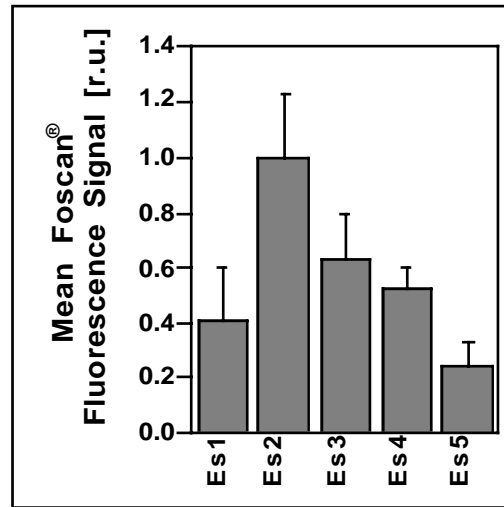


Figure 2b: Mean fluorescence signals of Foscan[®] (measured 96h after i.v. injection of 0.15 mg/kg) in the esophagus of five patients on normal mucosa. Each bar represents the average of 3 to 7 sites measured from a given patient. The uncertainties given correspond to the 67% confidence interval.

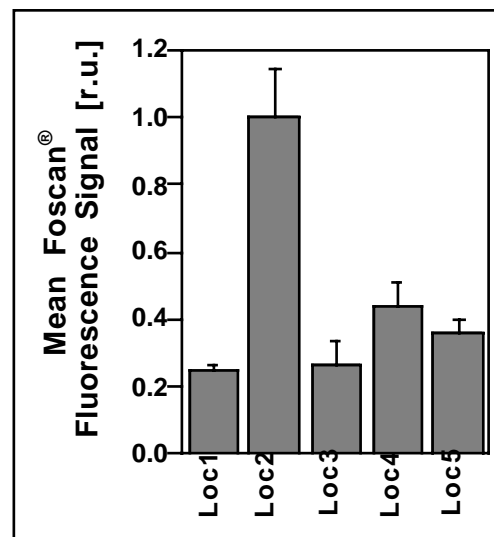


Figure 3: Mean fluorescence signals of Foscan[®] (measured 96h after i.v. injection of 0.15 mg/kg) in the oral cavity of five patients as a function of the location. Each bar represents the average of 10 different sites in the oral cavity (6 measurements on each site). The uncertainties given correspond to the 67% confidence interval.

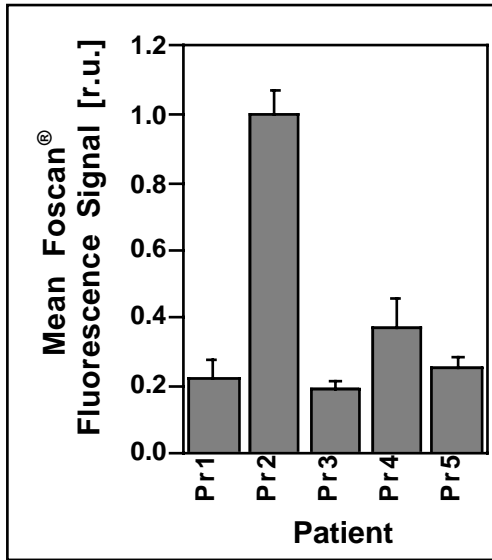


Figure 4: Mean fluorescence signals of Foscan[®] (measured 96h after i.v. injection of 0.15 mg/kg) in the oral cavity of five patients as a function of the pressure. Each bar represents the average of 4 different pressures in the oral cavity (6 measurements at each pressure). The uncertainties given correspond to the 67% confidence interval.

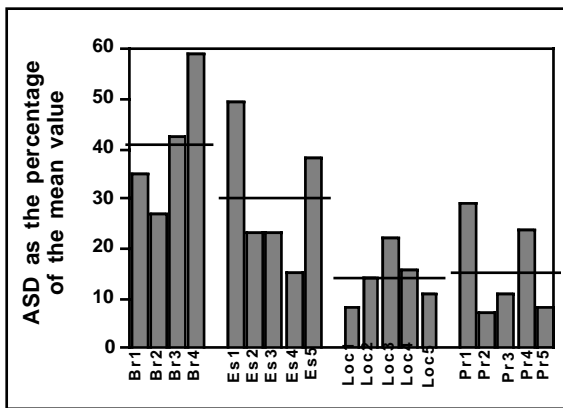


Figure 5: Adimensional Standard Deviation (ASD) of the mean values of the fluorescence signals of Foscan[®] (measured 96h after i.v. injection of 0.15 mg/kg) measured in the bronchi (Br1-Br4), the esophagus (Es1-Es5) and the oral cavity (Loc1-Loc5 and Pr1-Pr5) expressed as a percentage of the mean. The ASDs are grouped by type of measurement. For each group, the average is plotted as a straight line.

DISCUSSION

A successful PDT depends on several parameters, among which the tissular PS

level at the time of light application and the light dose itself. Only a good combination of both will ensure a positive outcome of the treatment. The fluorescence signal of Foscan[®] measured in vivo in different patients at the same time after PS injection is known to fluctuate from one patient to another, even when all patients receive the same dose of PS (3-5, 10). Braichotte et al. suggested (4, 5) that a small tissue concentration of PS could, up to a certain extent, be compensated by a large dose of light and vice-versa. At the time of light application, it is therefore of major importance to the clinician to evaluate the tissular level of Foscan[®]. This will allow them to calculate the appropriate light dose to be applied.

Endoscopic LIF measurements

In the study presented here, we measured the fluorescence signal of Foscan[®] (shown to be correlated with the tissular level of this PS (10)) endoscopically on the site of the subsequent PDTs, hence in the bronchi and the esophagus (Fig. 2a and 2b respectively). Several sources of fluctuations were likely to influence the LIF measurements, among which the instrumental fluctuations, the physiological fluctuations within one patient, the metabolic fluctuations from one patient to another or the positioning fluctuations. In our setup, the instrumental fluctuations were taken into account and corrected for (see 'Materials and Methods' section) and the typical Signal to Noise Ratio (SNR) was of about 250. It was therefore assumed that the instrumental fluctuations were of a negligible impact upon the results of the LIF measurements. We found, as it has also been described by Braichotte et al. (4, 5) and Glanzmann et al. (10) that an inter-patient fluctuation of the fluorescence signal of Foscan[®] of up to one order of magnitude occurs. In our study, these fluctuations were quantified by the fluctuations of the mean values ranging from 1 to 5.8. It is likely that these fluctuations reflect metabolic differences (9) between the patients and are therefore unavoidable with the present formulation of Foscan[®]. Nevertheless, as these fluctuations can be corrected for using the abovementioned method, they are not a major drawback either. It is interesting, though, to note that these inter-patient fluctuations were similar in all the Fig. 2 through 4.

A more critical issue is the intra-patient fluctuations. Both the physiological fluctuations and the positioning fluctuations contribute to them. The physiological fluctuations are true inhomogeneities in the amount of PS in a given organ. There are therefore to be observed in our measurements. The positioning fluctuations are due to the difficulties encountered by the clinician when probing a target organ through the working channel of the endoscope. This is a clear limit of the endoscopical measurements since the clinician only has a remote influence upon the placing optical fiber probe onto the tissue. Moreover, due to the geometry and the mechanical properties of both the bronchi and the esophagus, the control of the location and the pressure applied to the probe during the measurements is difficult. As well, since the illumination light of the endoscope is switched off during the measurements, some unavoidable movements (be it from the clinician or the patient) can displace the probe without the operator noticing. All these reasons account for the observed intra-patient fluctuations. In our study, we quantified the intra-patient fluctuations with the ASDs. We found that the ASDs were consistently smaller (2 to 3 times in average) when the fluorescence signal was measured in the oral cavity than when it was measured endoscopically ($p < 0.01$). This was the primary goal of our study and it implies that the pre-PDT monitoring measurements can advantageously take place in the oral cavity rather than through an endoscope on the site of the treatment. These intra-patient fluctuations seem to be smaller in the esophagus than in the bronchi. This is at first surprising since one would think that due to its geometry and mechanical properties, and the subsequent difficulties to place the probe, the values would fluctuate more in the esophagus than in the bronchi. One possible explanation is that the difference between the best measurements and the worst ones might be larger in the bronchi than in the esophagus because all the measurements in the esophagus are slightly inconvenient. In the bronchi, some measurements are relatively comfortable whereas other ones are difficult. The comparison between the inter- and the intra-patient fluctuations is possible and necessary. A monitoring method would be useless if the intra-patient fluctuations were

to be larger than the inter-patient fluctuations. In our study, the inter-patient fluctuations range from 1 up to 5.8 whereas the intra-patient fluctuations reach up to 59% of the mean value. It is therefore necessary to take the inter-patient fluctuations into account and to monitor the light dose for each PDT.

Measurements in the oral cavity

The aim of our study was to assess the relevance of the use of the oral cavity as a test site for the LIF measurements. A better test site for the evaluation of the PS tissular level is such that it would allow the clinician to decrease the intra-patient fluctuations while yielding the desired information, the PS fluorescence signal in the target organ. It has been reported by Glanzmann et al. (10) that a highly significant correlation exists between the Foscan[®] fluorescence signal measured in the bronchi or the esophagus and the Foscan[®] fluorescence signal measured in the oral cavity. Our observation is that the intra-patient fluctuations are 2 to 3 times smaller when the Foscan[®] fluorescence signal is measured in the oral cavity. Although some of the fluctuations that are observed in the bronchi or the esophagus are certainly due to the experimental difficulty of the measurement itself (positioning fluctuations), some fluctuations (observed in all organs) are also certainly due to real differences in the amount of Foscan[®] present in the tissue at this particular time and location or to changes in the tissue optics or architecture etc (physiological fluctuations). This is reflected in the measurements done in the oral cavity. It is possible to keep the contribution of the positioning fluctuations to the total fluctuations to a minimum when measuring in the oral cavity. It is however impossible to avoid slight fluctuations of the Foscan[®] fluorescence signal due to physiological fluctuations. The oral cavity can be used as a test site and the exact location within the oral cavity where the measurements take place is not of crucial importance. Moreover, the LIF measurements in the oral cavity prove little sensitive to the pressure. Although the ASD values themselves would not be relevant for the pressure measurements (Fig. 4) since all the measurements took place at the same location, their value gives a measure of the reproducibility of the measurements. For the

pressure measurements (Fig. 4), the ASD range from 7% to 29%, hence are even smaller than the ASDs for the measurements as a function of the location (Fig. 3). This means that the measurements as a function of the pressure (Fig. 4) are even more reproducible than the ones as a function of the location (Fig. 3). Consequently, we can assume that the pressure is not a crucially important issue either. In one patient, though, there is a linear correlation between the pressure and the fluorescence signal: the increasing pressure yielded a monotonically decreasing fluorescence signal. Even in this case, the standard deviation of the individual pressure measurements was rather small (data not shown). One possible explanation for this could be that this patient was particularly slim (185 cm, 57 kg, Body Mass Index (BMI) = 16.7, whereas the other four patients had the following features: 164 cm, 59.3 kg, BMI = 22.04; 170 cm, 84 kg, BMI = 29.07; 178 cm, 93 kg, BMI = 29.35; 173 cm, 74 kg, BMI = 24.73 (17)) and therefore probably had thinner, and hence more pressure sensitive, mucosae.

An interesting feature of Fig. 2-4 is that the ranges of the mean values for the four figures are quite similar. It is no surprise as it is likely that the inter-patient fluctuations are due to their metabolism (metabolic fluctuations) and should therefore be observed whatever the measurements.

Most of the mentioned drawbacks of the endoscopical measurements are easily avoided if the measurement session is to take place in the oral cavity: this location is of easy access, hence the clinician can have direct control of the probe, the movements of the patient due to respiration and heartbeat are much less critical, etc.

Our measurements took place before the PDT itself. This is of great importance. The LIF measurements can be performed in any quiet room in the medical facility instead of a busy operating room. Moreover, shifting these measurements from the operating time to the preceding hours also shortens the anesthesia duration, which is certainly beneficial for the patient.

CONCLUSION

The monitoring of the tissular Foscan[®] fluorescence signal in the oral cavity instead of on the PDT target site (bronchi or esophagus) has been shown to be feasible. This measurement location is more accessible and well tolerated. The previously reported inter-patient LIF signal intensity fluctuations are confirmed here in the bronchi and the esophagus. The correlation between the LIF signals for the oral mucosa on the one hand, and the esophagus and the bronchi respectively on the other hand implies a significant clinical simplification of the pre-PDT LIF measurement, while yielding comparable information.

Acknowledgments- We gratefully acknowledge support from the Swiss National Fund for Scientific Research, Grants #21-43507.95 and 20-50691.97, the Swiss Priority Program in Optics, the 'CHUV-EPFL-UNIL' Fund for collaboration in the area of biomedical technology, the 'Fonds de Service' and 'Fonds de Perfectionnement' of the ENT, Head and Neck Surgery Department of the CHUV Hospital. The authors are also grateful to Scotia QuantaNova, Guildford, UK, for providing the Foscan[®].

REFERENCES

1. Grosjean, P., G. Wagnières, Ch. Fontolliet, H. van den Bergh and Ph. Monnier (1998) Clinical photodynamic therapy for superficial cancer in the esophagus and the bronchi: 514 nm compared with 630 nm light irradiation after sensitization with Photofrin II. *Br. J. Cancer*, **77**(11), 1989-1995.
2. Monnier, Ph., M. Savary, Ch. Fontolliet, G. Wagnières, A. Châtelain, Ph. Cornaz, C. Depeursinge and H. van den Bergh (1990) Photodetection and photodynamic therapy of 'early' squamous cell carcinomas of the pharynx, esophagus and tracheo-bronchial tree. *Lasers Med. Sci.* **5**, 149-169.
3. Grosjean, P., J.-F. Savary, J. Mizeret, G. Wagnières, A. Woodtli, J.-F. Theumann, Ch. Fontolliet, H. van den Bergh and Ph. Monnier (1996) Photodynamic therapy for cancer of the upper aerodigestive tract using tetra(m-hydroxyphenyl)chlorin. *J. Clin. Laser Med. Surg.*, **14**(5), 281-287.
4. Braichotte, D.R., J.-F. Savary, Ph. Monnier and H. van den Bergh (1996) Optimizing Light Dosimetry in Photodynamic Therapy of Early Stage Carcinomas of the Esophagus Using Fluorescence Spectroscopy. *Lasers Surg. Med.*, **19**, 340-346.

5. Braichotte, D., J.-F. Savary, Th. Glanzmann, Ph. Monnier, G. Wagnières and H. van den Bergh (1996) Optimizing Light Dosimetry in Photodynamic Therapy of the Bronchi by Fluorescence Spectroscopy. *Lasers Med. Sci.*, **11**, 247-254.
6. Savary, J.-F., Ph. Monnier, Ch. Fontolliet, J. Mizeret, G. Wagnières, D. Braichotte and H. van den Bergh (1997) Photodynamic therapy for early squamous cell carcinomas of the esophagus, bronchi and mouth with m-Tetra(Hydroxyphenyl) Chlorin. *Arch. Otolaryngol. Head & Neck Surg.*, **123**, 162-168.
7. Andrejevic-Blant, S., Ch. Hadjur, J.-P. Ballini, G. Wagnières, Ch. Fontolliet, H. van den Bergh and Ph. Monnier (1997) Photodynamic therapy of early squamous cell carcinoma with tetra(m-hydroxyphenyl)chlorin: optimal drug-light interval. *Br. J. Cancer*, **76**(8), 1021-1028.
8. Grosjean, P., J.-F. Savary, G. Wagnières, J. Mizeret, A. Woodtli, J.-F. Theumann, Ch. Fontolliet, H. van den Bergh and Ph. Monnier (1996) Tetra(m-hydroxyphenyl)chlorin Clinical Photodynamic Therapy of Early Bronchial and Esophageal Cancers. *Lasers Med. Sci.*, **11**, 227-235.
9. Belitchenko, I., V. Melnikova, L. Bezdetsnaya, H. Rezzoug, J.-L. Merlin, A. Potapenko and F. Guillemin (1998) Characterization of Photodegradation of Meta-tetra(Hydroxyphenyl) chlorin (mTHPC) in Solution: Biological Consequences in Human Tumor Cells. *Photochem. Photobiol.*, **67**(5), 584-590.
10. Glanzmann, Th., Ch. Hadjur, M. Zellweger, P. Grosjean, M. Forrer, J.-P. Ballini, Ph. Monnier, H. van den Bergh, K.L. Chang and G. Wagnières (1998) Pharmacokinetics of Tetra(m-hydroxyphenyl)chlorin in Human Plasma and Individualized Light Dosimetry in Photodynamic Therapy. *Photochem. Photobiol.*, **67**(5), 596-602.
11. Weersink, R.A., J.E. Hayward, K.R. Diamond and M.S. Patterson (1997) Accuracy of Noninvasive in vivo Measurements of Photosensitizer Uptake Based on a Diffusion Model of Reflectance Spectroscopy. *Photochem. Photobiol.*, **66**(5), 326-335.
12. Wilson, B.C., M.S. Patterson and L. Lilge (1997) Implicit and Explicit Dosimetry in Photodynamic Therapy: a New Paradigm. *Lasers Med. Sci.*, **12**, 182-199.
13. Wang, K., K. Gutta and J. Densmore (1995) The Use of Laser Induced Fluorescence (LIF) in the Determination of Photosensitizer Concentration during Photodynamic Therapy (PDT) of Barrett's Esophagus. *Lasers Med. Sci.*, **S7**, 42-42.
14. Forrer, M., Th. Glanzmann, J. Mizeret, D. Braichotte, G. Wagnières, H. van den Bergh, P. Jichlinski and H.-J. Leisinger (1994) Fluorescence Excitation and Emission Spectra of ALA Induced Protoporphyrin IX in Normal and Tumoral Tissue of the Human Bladder. Proceedings of Optical Biopsy and Fluorescence Spectroscopy and Imaging, Lille, France, September 9-10th 1994, **2324**, p.84-88.
15. meta-Tetrahydroxyphenylchlorin (mTHPC) Temoporfin Foscan - a photosensitizer in the photodynamic therapy of cancer, Notes on Nomenclature and Physico-Chemical Properties, Scotia QuantaNova Pharmaceuticals Ltd, Guildford, Surrey, GU1 1BA, UK, (1998).
16. Rice, J.A. (1995), in *Mathematical Statistics and Data Analysis*, ch. 11, Duxbury Press, Belmont, California, USA.
17. Bender, A.E. and L.J. Brookes (1987), in *Body Weight Control*, p.40, Churchill Livingstone, Edinburgh, UK.



Animal studies

(<http://www.angelfire.com/tn/allabouthamsters/story.html>)

Chapter 4

Lutetium Texaphyrin

In this chapter, we report about the use of a novel second generation PS Lutetium Texaphyrin, also called Lu-TeX, Lutrin™ or Antrin™ [1]. The Lu-TeX is supplied by *Pharmacyclics* in Sunnyvale, CA, USA. Section 4.1 first briefly surveys the physical chemical properties of this substance in terms of chemical structure and absorption and emission spectra. In section 4.2, we present an overview of the preclinical and clinical uses of Lu-TeX as well as its properties as a photodetection or photodynamic agent. This also includes some generalities about the work done in Lausanne with Lu-TeX as a PS to treat AMD. Finally, in section 4.3, we give the text of a study about the selectivity properties of Lu-TeX in our hamster cheek pouch animal model. In this paper, we report on the localization behavior of this molecule with respect to early squamous cell carcinoma and we present the pharmacokinetics of this behavior measured by LIF.

4.1 The photosensitizer

The PS Lutetium Texaphyrin (thereafter Lu-TeX) is a member of the Texaphyrin family. The texaphyrins are tripyrrolic pentaaza expanded porphyrins. The structure of Lu-TeX is given in Fig. 4.1. It is a pure synthetic compound that is soluble in water. The incorporation of the paramagnetic ion gadolinium into the texaphyrin moiety yields a substance that can be used as a radiation sensitizer and MRI contrast agent [2].

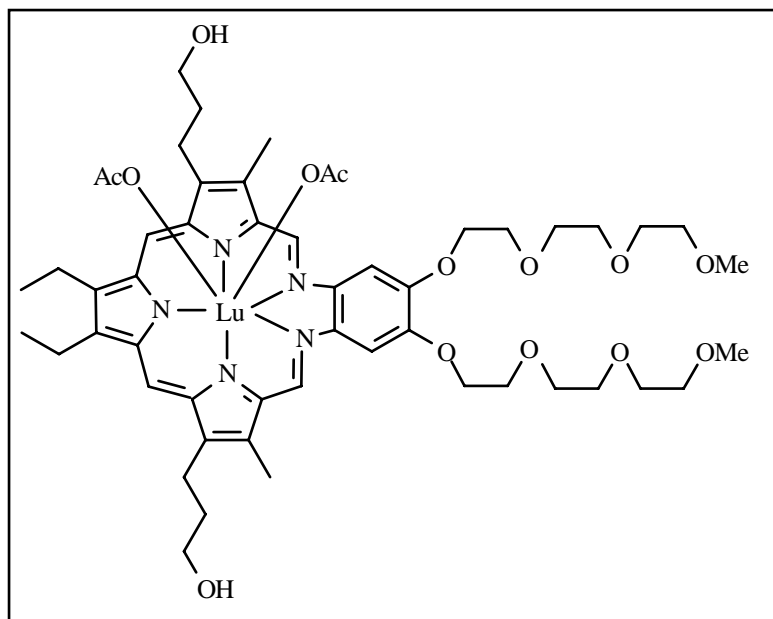


Figure 4.1: Lutetium Texaphyrin (Lu-Tex).

Lu-Tex has an absorption coefficient of 126,000 at 474 nm (Soret) and of 42,000 at 732 nm in MeOH [2]. Its fluorescence quantum yield has been evaluated at 0.15% against fluorescein in PBS supplemented with 10% BSA [3]. It is a shiny green crystalline solid. Its absorption spectrum is given in Fig. 4.2a and emission spectrum in hamster tumor-bearing cheek pouch tissue is given in Fig. 4.2b (excitation wavelength: 460 nm).

It is consistently reported that the major limitations of the available PSs include a poor solubility in water or a low absorption coefficient in the 650+ nm range. Lu-Tex has the potential to overcome both these limitations and is therefore involved in an increasing number of trials.

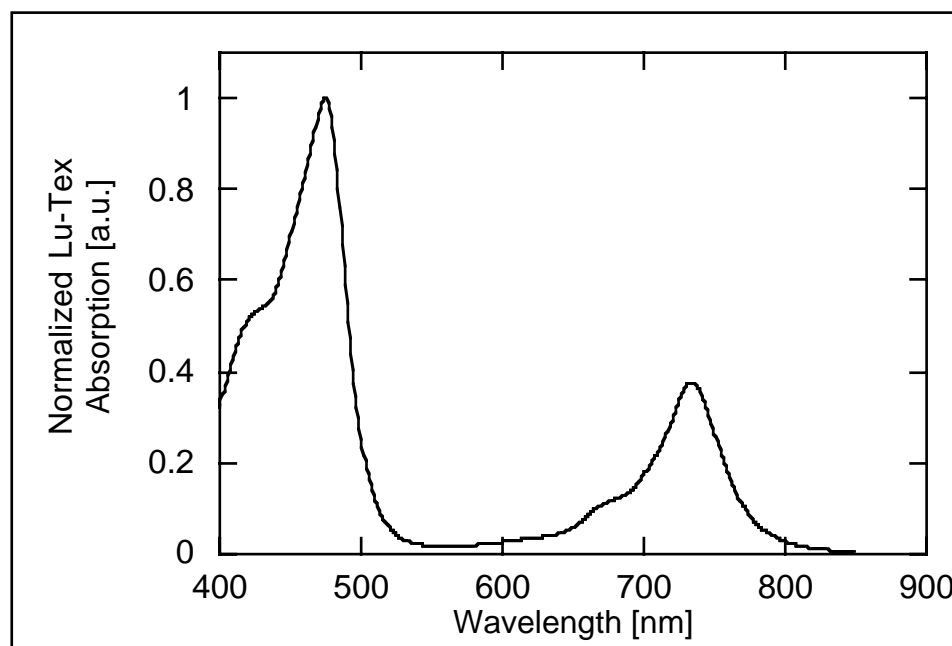


Figure 4.2a: Normalized absorption spectrum of Lu-Tex in water [3].

4.2 Preclinical and clinical uses of Lu-Tex

In a preclinical study on mice, Young et al [2] test the localization properties of Lu-Tex in a mouse mammary tumor. These authors implant the tumor model in the animals and then inject Lu-Tex intravenously. They measure the quantity of Lu-Tex in different tissues of the mice by means of radio-labeled Lu-Tex. The authors report good selectivity properties of this PS. Indeed, they observe tumor-to-muscle ratios of up to 10.55 5 hours after the injection of the PS. Moreover, they succeed in curing 100% of the tumors by PDT (irradiation at 732 nm) when irradiation takes place 3 hours after the injection. This cure rate is down at 75% when the drug-

light interval is 5 hours. The authors link this difference to modifications of the plasma concentration of the PS. However, their experiments with larger tumors in the same model produced less promising results, with a cure rate of 43% for cancers of larger size (thickness: 3-7 mm and surface diameter: 6-15 mm). It should be mentioned that the authors do not observe any skin photosensitivity in any of the treated animals.

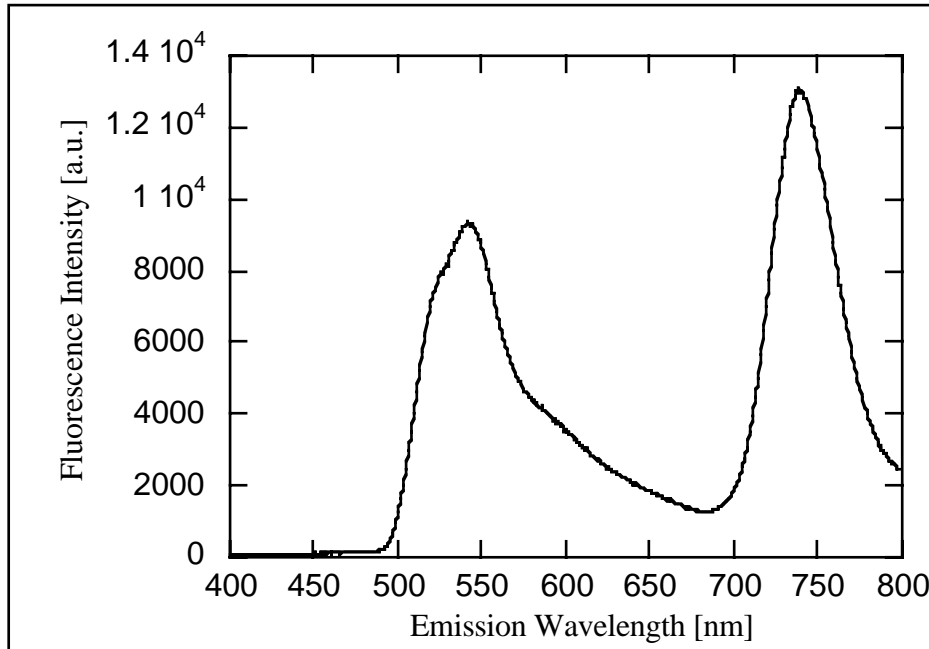


Figure 4.2b: Autofluorescence of the hamster cheek pouch tissue and fluorescence emission spectrum of Lu-Tex in the hamster tumor-bearing cheek pouch tissue (measured *in vivo* in accordance with the protocol described in section 4.3, Materials and Methods). The excitation wavelength is 460 nm.

ratio and tumor responses in breast cancers, Kaposi's sarcoma and basal cell carcinoma. All in all, the authors observe that the treatments are well tolerated with the exception of some local pain at the treatment site for patients receiving a dose of Lu-Tex $\geq 1.7 \mu\text{mol/kg}$. The fact that this PS induces few side effects is also reported by Sickenberg et al [5]. These authors only mention temporary tinglings in the fingers of some patients following the intravenous injection of Lu-Tex (2-4 mg/kg).

Another preclinical study in an animal model is presented by Kostenich et al [6]. In this paper, these authors use *in vivo* LIF to non-invasively measure the distribution kinetics of Lu-Tex in the tissue, their aim being to find the optimal drug-light interval to achieve the highest possible ratio between the tumor and the healthy tissue at the time of irradiation. To carry out their study, they use mice bearing a human colon tumor. The authors present a kinetics curve displaying a maximum 3 to 4 hours after injection in both the healthy and the tumor-bearing foot of the mice. Interestingly, the fluorescence signal of Lu-Tex is higher in the normal foot than in the tumor-bearing one at the time of this maximum but then it decreases faster in the normal foot than in the tumor-bearing one and, as a result, the PS's fluorescence is higher in the tumor-bearing foot than in the normal one after 24 hours. This seems to last for at least another 24 hours as the fluorescence signal in the normal foot goes down to zero whereas it does not decrease anymore in the tumor-bearing foot in this interval. Consequently, these authors chose to perform the PDTs 24 hours after the injection of Lu-Tex. Their explanation about the pharmacokinetics of this in both feet is that the fluorescence signal was collected from the skin and the underlying tissues such as the tumor and muscle. Still, these authors used light at 488 nm to excite the fluorescence of the Lu-Tex and it is likely that the effective penetration of this light in the tissue would be < 1 mm. They therefore probably only probed the skin of the mice. This is consistent with the mention by the authors of another work that shows that the Photofrin II concentration in the skin overlying small tumors can be significantly different from its concentration in the contralateral

A clinical Phase I study with Lu-Tex is reported by Wieman et al [4] for patients with malignancies accessible to light. The patients in this study underwent a Lu-Tex mediated PDT with light at 732 nm and with varying doses of Lu-Tex (from 0.5 $\mu\text{mol/kg}$ to 2.5 $\mu\text{mol/kg}$). The authors report neither any significant drug-related systemic toxicity nor significant skin photosensitization. Moreover, they report a 15:1 tumor vs healthy skin

skin [7]. If it were the case, it could be seen as a limitation of the model chosen by the authors, as human tumors implanted in mice probably model the human tumors up to a certain extent only. The PDTs performed by the authors on these model tumors demonstrate however that Lu-TeX has a good antitumor efficiency when excited at 730 nm.

In another study with implanted murine tumor in mice, Woodburn et al [8] report a selectivity of Lu-TeX for the tumor over the normal leg of the mice of 2:1 15 hours after the injection when excited at 450 nm. These authors also perform PDTs on the legs of the mice. Irradiations at 3 hours after the injection of Lu-TeX give 100% cures whereas irradiations at 5 hours give only 50% cure rates. These authors do not observe any cure when the irradiations take place at 12 or 24 hours after the injection of the PS. This is in disagreement with the findings of Kostenich et al [6], although both studies were conducted with the same animal model.

Hammer-Wilson et al recently compared the photodynamic activity of Lu-TeX with that of Photofrin [9]. By means of a study about the toxicity of Lu-TeX for their animal model (mice), the authors first report that all the mice excrete colored urine beginning one hour after the injection and returning to normal by 24 hours after the injection. The authors also present the results of their irradiating the tumors at 740 nm 5 hours after the injection of the PS. They also show that this drug-light interval produces the best PDT effects (up to 67% of the animals remain tumor-free during the whole follow-up period) as shorter intervals lead to significant mortality (1 hour) or difficult healing, extensive tissue damage and impaired movements (3 hours). On the other hand, longer drug-light intervals lead to little reaction (12 hours) or no reaction at all (24 hours). These authors conclude that Lu-TeX is a better PS than Photofrin as 100% of the tumors respond to the PDT (67% with Photofrin) and 40% of the mice remain tumor-free during the observation period (16%). They also propose the vasculature as the primary target of the Lu-TeX mediated photodynamic effect.

The selective accumulation of Lu-TeX in the atheromatous plaque is reported by Woodburn et al [10-12] in a rabbit model. The subsequent PDTs show promising results as a way to selectively destroy the plaque without damaging the surrounding normal arterial wall. A phase I clinical study for the same disease in humans is reported by Rockson et al [13]. The PDTs seem to be not only efficient against the disease, but also well tolerated and apparently do not lead to any adverse effect.

Past a certain stage of their development, tumors induce the growth of new blood vessels, a process called neovascularization. Under the conditions applied, the uptake and removal processes of Lu-TeX can make it selective for such tumors [14]. In our group, Lu-TeX has been involved in a large-scale study as a PS for the treatment of CNV in AMD by PDT [3,5]. Although this affection is a non-cancerous disease, it is also characterized by neovascularization. In this case, the PS is injected into the patient intravenously and is then activated by laser radiation. In principle, this leads to the selective thrombosis of the new vessels through a photodynamic effect.

Since Lu-TeX is a relatively new PS as compared to HPD or mTHPC, much remains to be studied about it. One question is its selectivity in a non-grafted tumor. As a matter of fact, most studies that involve Lu-TeX [2,6,8,9] have been carried out on immuno-deficient animals bearing a human tumor or a grafted tumor from a donor animal. Although this is a valuable model for various reasons, it does not give much information about the behavior of a given substance in an early tumor from the animal itself. This is the reason behind our investigations in the hamster cheek pouch model. The results of this study are given below in section 4.3 and can be found in:

Matthieu Zellweger, Alexandre Radu, Philippe Monnier, Hubert van den Bergh, Georges Wagnières, 'Fluorescence Pharmacokinetics of Lutetium Texaphyrin (PCI-0123, Lu-TeX) in the skin and in the healthy and tumoral hamster cheek pouch mucosa.', Journal of Photochemistry and Photobiology B: Biology, 55(1), 56-62, 2000.

The measurement of the PK of Lu-TeX in the hamster model is similar to the measurement by Glanzmann [15] of the PK of mTHPC in the same model. In both cases, the hamsters bore chemically-induced early cancerous lesions of the cheek pouch mucosa and, in both cases, the

PK of the FP was measured by LIF. The results of both studies are therefore comparable. In his study, Glanzmann also compares the PK of mTHPC in hamsters to that in humans and finds similar shapes, albeit with a factor 3 of intensity difference. This inter-species comparison is beyond our scope here, but we can compare these two FPs in the same animal model.

The PK of Lu-TeX in the hamster cheek pouch model is very different from that of mTHPC in the same model. Lu-TeX reaches a fluorescence intensity maximum after about 100 min following injection and is down to undetectable levels after 24 hours in all cases. On the other hand, mTHPC reaches its fluorescence intensity maximum in the hamster cheek pouch mucosa after 4 to 6 days and has a half-life after the maximum of about 12 (± 3) days. Assuming that five half-life periods bring the fluorescence to undetectable levels, it means that in the most conservative estimations, mTHPC is down to undetectable levels after 45 days. Thus, it can be seen that the PK of mTHPC is much slower than that of Lu-TeX in the hamster model.

Much is not known at the present time about the behavior of FPs in organisms. Consequently, the linking of such differences to specific properties of the molecules is difficult. However, the first striking difference between Lu-TeX and mTHPC is their solubility in water. Whereas Lu-TeX is a fairly soluble species (the injection solution is aqueous), mTHPC is rather lipophilic and has to be injected in a half-aqueous half-organic solvent mixture. It is possible that the aqueous environment of the hamster vascular system induces the precipitation or the aggregation of mTHPC at the time of injection, whereas it does not have such an effect on Lu-TeX. This is one of the reasons invoked by Glanzmann et al to explain the PK of mTHPC in another study, this time in the human plasma [16]. The other one, in agreement with other studies in animal models [17], is thought to be the trapping of mTHPC by the liver, a very likely event in the case of a lipophilic drug. Neither of these reasons can apply to Lu-TeX however, as it is a hydrophilic drug. In this sense, its rapid PK is probably much closer to that of fluorescein, another hydrophilic drug whose PK in all models shows a very quick excretion of the dye following injection. For instance, Hammer-Wilson et al state [9] that the mice they use excrete green-colored urine during the first 24 hours after the Lu-TeX injection, a fact that we also observed in all our animals.

In the hamster model, mTHPC has been found to be little selective for the induced early lesions. Indeed, Glanzmann [15] reports that the differences in the fluorescence level measured on different mucosae are likelier to be of statistical nature rather than reflecting a true selectivity. In humans, Glanzmann reports some selectivity of mTHPC for early SCCs in the bronchi 4 days after the injection of the solution (1.5:1) [15]. This discrepancy shows that it is difficult to extrapolate any conclusions about the selectivity of a FP in humans based on its selectivity in animal models. It should be noted however, that unlike mTHPC, Lu-TeX has been found to be slightly selective for the chemically-induced early cancerous lesions of the hamster cheek pouch (see below, Section 4.3). Again, it is difficult to link this property to any molecular feature of the species. It should be noted, however, that Fingar et al [14] observed (but do not provide any explanation for this observation) that Lu-TeX can selectively induce the closure of neo-vessels without damaging the surrounding blood vessels. If found to be true, such an observation could suggest properties such as a selectivity for neovessels. This could be one of the reasons behind the selectivity of Lu-TeX for early cancerous lesions.

Fluorescence microscopy studies with tissue samples of hamster cheek pouches have been performed with mTHPC-injected animals. They have been reported by Andrejevic et al [18]. The authors observe what hints at a vascular localization of mTHPC shortly after injection and a cellular localization afterwards. Although such studies produce crucial information about the exact localization of the FP in the tissue, they were impossible to perform with Lu-TeX due to its very low fluorescence quantum yield. Consequently, not much is known about its localization in the tissue. It can be estimated, however, that the excitation wavelength of 460 nm used to probe the Lu-TeX penetrates to a depth similar to that of 420 nm (reported by Glanzmann to be around 200 μm [15 and references 35-39 therein, p. 39]). It therefore probes the epithelium (50 to 100 μm thick in the hamster [15]) and some of the underlying layers of the hamster tissues. This information does not, however, produce much useful information and it is likely that the low

fluorescence quantum yield of Lu-*Tex* will prove a major limitation to further investigations of this kind.

The PK of BPDMA was also measured by LIF in the hamster animal model [19]. As it is a lipophilic molecule, it was injected to the hamsters (2 mg/kg) in a liposomal formulation. This formulation is fairly soluble in water and was therefore injected after dissolution in standard saline. In the case of liposomal BPDMA, the PK looks similar to that of Lu-*Tex* with a rapid uptake of the FP in the cheek pouch mucosa [19], followed by a maximum at around 100 minutes after the injection and a plateau afterwards. It seems that there could be another increase in the fluorescence signal after the plateau, starting at around 200 minutes, but this is beyond the scope of preclinical tests involving this FP as it has been approved for human use between 60 and 120 minutes after the injection only. It should also be noted that this FP does not show any selectivity for early lesions in humans.

Similar measurements on the same animal model with the FP Zinc-phthalocyanine (ZnPC) demonstrated that this lipophilic FP might be a little selective for the painted cheek pouch of the hamster (2.5:1) [20]. The PK of this FP shows greater similarity to that of mTHPC than to that of Lu-*Tex* as the increase in the fluorescence signal is rather slow, reaching a local maximum after 25 hours, followed by a plateau and a possible further increase of the signal. The measurements were performed up to 55 hours after the injection but, at that time, the signal showed no sign of decreasing and it cannot be excluded that it would increase even more after a longer interval.

References

1. <http://www.pharmacyclics.com/>
2. Young, S, K. Woodburn, M. Wright, T. Mody, Q. Fan, J. Sessler, W. Dow, R. Miller, 'Lutetium Texaphyrin (PCI-0123): a Near-Infrared, Water-Soluble Photosensitizer', *Photochemistry and Photobiology*, 63(6), 892-897, 1996.
3. Jean-Pierre Ballini, EPFL, personal communication.
4. Wieman, T., V. Fingar, S. Taber, M. Panjehpour, C. Julius, T. Panella, A. Yuen, S. Horning, K. Woodburn, J. Engel, R. Miller, M. Renschler, S. Young, 'Phase I photodynamic therapy trial with Lutetium-Texaphyrin (PCI-0123) in patients with metastatic cancer, 24th Annual Meeting of the American Society for Photobiology, Atlanta, GA, USA, June 1996.
5. Sickenberg, M., J.-P. Ballini, L. Zografos, B. Piguet, H. van den Bergh, P. Zilliox, S.M. Robertson, 'Preliminary clinical results of Lu-*Tex* fluorescence pharmacokinetic and photodynamic therapy to treat choroidal neovascularization', XIIth Congress of the European Society of Ophthalmology, SOE 1999, Stockholm, Sweden, June 1999.
6. Kostenich, G., A. Orenstein, L. Roitman, Z. Malik, B. Ehrenberg, 'In vivo photodynamic therapy with the new near-IR absorbing water soluble photosensitizer lutetium texaphyrin and a high intensity pulsed light delivery system', *Journal of Photochemistry and Photobiology B: Biology*, 63, 36-42, 1997.
7. Bellnier, D., Y. Ho, R. Pandey, J. Missert, T. Dougherty, 'Distribution and elimination of photofrin II in mice', *Photochemistry and Photobiology*, 50, 221-228, 1989.
8. Woodburn, K., Q. Fan, D. Miles, D. Kessel, Y. Luo, S. Young, 'Localization and Efficacy Analysis of the Phototherapeutic Lutetium Texaphyrin (PCI-0123) in the Murine EMT6 Sarcoma Model', *Photochemistry and Photobiology*, 65(3), 410-415 1997.
9. Hammer-Wilson, M., M. Ghahramanlou, M. Berns, 'Photodynamic activity of Lutetium-Texaphyrin in a mouse tumor system', *Lasers in Surgery and Medicine*, 24, 276-284, 1999.
10. Woodburn, K., Q. Fan, D. Kessel, M. Wright, T. Mody, G. Hemmi, D. Magda, J. Sessler, W. Dow, R. Miller, S. Young, 'Phototherapy of cancer and atheromatous plaque with texaphyrins', *Journal of Clinical Laser Medicine and Surgery*, 14(5), 343-348, Oct. 1996.

11. Woodburn, K., Q. Fan, R. Miller, 'Reduction of atheromatous plaque with Antrin™ photoangioplasty', *Photochemistry and Photobiology*, 69, Special Issue, SPM-E4, p. 19S, June 1999.
12. Woodburn, K., P. Thiemann, D. Kessel, F. Qing, 'Photoangioplasty with Antrin™ injection', Regular Communication, RC120, 7th Biennial Congress of the International Photodynamic Association, Nantes, France, July 1998.
13. Rockson, S., P. Kramer, M. Razavi, A. Szuba, S. Filardo, J. Cooke, D. Adelman, 'Photoangioplasty of human atherosclerosis with Lutetium Texaphyrin (Antrin™)', *Photochemistry and Photobiology*, 69, Special Issue, TPM-B3, p. 49S, June 1999.
14. Fingar, V., P. Haydon, S. Taber, T. Wieman, 'Selective destruction of tumor blood vessels after PDT using Lutetium Texaphyrin', RC117, 7th Biennial Congress of the International Photodynamic Association, Nantes, France, July 1998.
15. Thomas Glanzmann, 'Steady-state and time-resolved fluorescence spectroscopy for photodynamic therapy and photodetection of cancer', PhD thesis #1920, EPFL, 1998.
16. Glanzmann, Th., Ch. Hadjur, M. Zellweger, P. Grosjean, M. Forrer, J.-P. Ballini, Ph. Monnier, H. van den Bergh, K.L. Chang and G. Wagnières, 'Pharmacokinetics of Tetra(*m*-hydroxyphenyl)chlorin in Human Plasma and Individualized Light Dosimetry in Photodynamic Therapy', *Photochemistry and Photobiology*, 67(5), 596-602, 1998.
17. Ronn, A., J. Batti, C. Lee, D. Yoo, M. Siegel, M. Nouri, L. Lofgren, B. Steinberg, 'Comparative biodistribution of meta-tetra(hydroxyphenyl)chlorin in multiple species: clinical implications for photodynamic therapy', *Lasers in Surgery and Medicine*, 20(4), 437-442, 1997.
18. Andrejevic-Blant, S., Ch. Hadjur, J.-P. Ballini, G. Wagnières, Ch. Fontolliet, H. van den Bergh and Ph. Monnier, 'Photodynamic therapy of early squamous cell carcinoma with tetra(*m*-hydroxyphenyl)chlorin: optimal drug-light interval', *British Journal of Cancer*, 76(8), 1021-1028, 1997.
19. Dr Ramiro Conde, EPFL, personal communication.
20. Dr Thomas Glanzmann, Dublin City University, personal communication.

4.3

Fluorescence Pharmacokinetics of Lutetium Texaphyrin (PCI-0123, Lu-Tex) in the skin and in the healthy and tumoral hamster cheek pouch mucosa.

Matthieu Zellweger¹, Alexandre Radu², Philippe Monnier², Hubert van den Bergh¹ and Georges Wagnières¹

¹Institute of Environmental Engineering, Swiss Federal Institute of Technology, EPFL, CH-1015 Lausanne; ²Department of Otolaryngology, Head and Neck Surgery, CHUV Hospital, CH-1011 Lausanne, Switzerland.

Keywords: Lutetium Texaphyrin (Lu-Tex, PCI-0123), fluorescence spectroscopy, hamster cheek pouch mucosa.

Abbreviations: PK: pharmacokinetics; Lu-Tex: Lutetium Texaphyrin; PDT: photodynamic therapy; PS: photosensitizer; HPD: hematoporphyrin derivative; mTHPC: 5, 10, 15, 20-Tetra(m-hydroxyphenyl)chlorin, Foscan[®]; LIF: light-induced fluorescence; DMBA: 7, 12-dimethylbenzanthracene; SNR: signal to noise ratio.

ABSTRACT

We investigated the pharmacokinetics (PK) of Lutetium Texaphyrin (Lu-Tex), a second generation photosensitizer, in the Syrian hamster cheek pouch early cancer model.

Ten male hamsters, five with chemically induced early squamous cell cancer of the left cheek pouch, received an intracardiac injection of a 10 mg/ml Lu-Tex solution resulting in a dose of 12 mg Lu-Tex per kg of bodyweight. The pharmacokinetics of the dye was measured during the 24 hours following the injection with an optical fiber-based spectrofluorometer on the ventral skin, the healthy and the tumoral cheek pouch mucosa. The Lu-Tex fluorescence was excited at 460 nm and detected around 740 nm.

All the measurements yield very similar pharmacokinetic curves. The fluorescence intensity reaches a maximum between two and three hours after the injection and, at its maximum, it is consistently higher (up to 1.5 times) on the tumor than on the healthy mucosa. It remains smaller on the skin than on cheek pouch mucosa. After 24 hours, the Lu-Tex fluorescence is no longer detectable either on the skin, on the lesion or on the healthy mucosa. Moreover, Lu-Tex clearly displays a significant fluorescence selectivity between early carcinoma and healthy mucosa in this model. Furthermore, the inter-animal fluctuations of the fluorescence signal are small ($\pm 16\%$ on the tumor-bearing mucosa). Eight minute-long skin irradiation tests have been performed 24 hours after the injection of the Lu-Tex on the ventral skin of sixteen additional animals with a solar simulator. No reaction was observed, neither macroscopically nor microscopically, which further demonstrates, as suggested by the fluorescence measurements, that this photosensitizer is significantly cleared from the skin after 24 hours.

Journal of Photochemistry and Photobiology B: Biology, 55(1), 56-62, 2000.

INTRODUCTION

Photodynamic therapy (PDT) [1-5] is a treatment for cancer as well as non-cancerous diseases. It is based on the combined effects of a photosensitizer (PS) and light [6]. This method has been successfully used to treat early tumoral lesions in organs such as the esophagus, the bronchi, and the skin among others [7-14]. Hematoporphyrin Derivative (HPD) and its somewhat purified form Photofrin[®] are the first PSs to have been used on a large scale and the latter was eventually granted FDA approval in the USA as well as approval in other countries for the treatment of various cancers by PDT. However, despite good clinical efficacy, this first generation PS suffers from some major drawbacks: lack of clearly defined chemical composition, relatively low phototoxicity, small if any selectivity for early carcinomas, and relatively long retention in the skin after intravenous administration. This initiated the search for new PSs. Among the second generation PSs, Foscan[®] (mTHPC) has been widely studied [15-21]. Despite the fact that Foscan[®] represents an improvement over Photofrin[®] in terms of chemical purity, phototoxicity and duration of skin photosensitization [22], it still has some drawbacks such as low solubility in water, slow clearance from the body (4-6 weeks) and lack of clear selectivity for early cancers. The situation is similar for some of the other second generation PSs [23]. Hence, the search for better PSs is still on. Of the many molecules tested, Lutetium Texaphyrin (Lu-Tex, PCI-0123) displays interesting properties. It is a pure compound, it is water soluble, it absorbs in the near-IR range (732 nm) and it shows minor toxicity [24]. Studies conducted by Young et al [25], Woodburn et al [26], and Kostenich et al. [27] in mice with implanted tumors reveal a high selectivity of Lu-Tex for the lesions with a good anti-tumoral response after PDT. However, little is known about its behaviour in animals bearing an early non-grafted tumor. Both the photodetection and the PDT of early cancers will improve with enhanced uptake and better contrast of the PS between neoplastic and normal tissue. We therefore investigated the pharmacokinetics (PK) of Lu-Tex, by means of Light Induced Fluorescence (LIF), in a chemically induced early squamous cell carcinoma of the hamster cheek pouch, in

the normal cheek pouch and on the ventral skin. We also irradiated the skin of the hamsters with a solar simulator 24 hours following the injection of the Lu-Tex to support the observations that were made through the LIF that the PS is in negligible quantity in the skin at that time. The hamster cheek pouch is an interesting model for the superficial squamous cell cancers of the upper aero-digestive tract and esophagus in humans [28, 29].

MATERIALS AND METHODS

Animal Model

Twenty-six pathogen-free, male, 5-6 weeks old golden Syrian hamsters weighing 110-140 grams, were used in our experiments (BRL, Fuellinsdorf, Switzerland), ten for the LIF measurements and sixteen for the skin photosensitization tests. Chemically induced early squamous cell carcinomas (carcinoma in situ and microinvasive carcinoma) of the left cheek pouch were produced in five of these animals by topical application of a 0.5% 7,12-dimethylbenzanthracene (DMBA, Sigma Chemicals, Buchs, Switzerland) in paraffin solution three times weekly for ten weeks following a previously described protocol [28]. The malignant changes occurring during the carcinogenesis are highly reproducible between different groups of animals and resemble both macroscopically and microscopically those encountered in humans with carcinomas of the upper aerodigestive tract and the esophagus [28]. The right cheek pouch, which was not painted with DMBA, served as a control. The animals were housed at room temperature with a 12 hour light/dark cycle. Food and drinking water were given ad libitum. All experiments were performed under intraperitoneal anaesthesia (Ketalar 150 mg/kg and Xylesine 15 mg/kg) and in accordance with protocols approved by the Experimental Animal Ethics Committee of the CHUV Hospital in Lausanne.

Photosensitizer

A drug product formulation of Lu-Tex (PCI-0123) was kindly supplied by Pharmacyclics, Inc. (Sunnyvale, CA, USA). Bacterial contamination was avoided by filtering the solution into presterilized containers inside a laminar flow hood. The Lu-Tex solution was then stored in the dark at 4°C. Lu-Tex has a strong Soret-type absorption band at 474 nm ($\epsilon = 126'000$)

and a Q-type absorption band at 732 nm ($\epsilon = 42'000$) in methanol [25].

Fluorescence Spectroscopy

Our optical fiber-based spectrofluorometer has been described elsewhere [30]. In brief, it consists of an excitation source (UXL-75 XE, 75W high pressure Xenon lamp, Ushio Inc., Japan) whose light is passed through a spectrograph (Chromex 250, Chromex, Albuquerque NM 87107, USA), filtered (DC550, Reynard USA, blue-green band pass, center wavelength: 475 nm, Full Width at Half-Maximum (FWHM): 110 nm) and injected into a quartz optical fiber (PUV600T, CeramOptec GmbH, D-53121 Bonn, Germany, NA=0.4, 4.2m, 600 μ m core diameter). The excitation wavelength is 460 nm and the typical power at the end of the fiber is 75 μ W. The fiber can be inserted into a metallic cylindrical handpiece (diameter 5.6 mm, length: 60 mm) in such a way that an application of the handpiece on the tissue results in contact of the fiber tip with the organ [30]. The fluorescence is collected in the same fiber and separated from the excitation light by a dichroic mirror (DC475, Reynard, San Clemente CA 92673-6227, USA, dichroic mirror, cut-off wavelength: 480 nm). It is then filtered by a long pass filter (FG495, Andover Corporation, Salem NH 03079-2800, USA, long-pass filter, cut-on wavelength: 500 nm) and dispersed in a spectrograph (Chromex 250, Chromex, Albuquerque NM 87107, USA) to be detected by a Peltier cooled CCD (TE/CCD-256, UV coated, Spectroscopy Instruments GmbH, D-82205 Gilching, Germany). LIF is observed in the range between 500 nm and 800 nm with a resolution of 11 nm (FWHM). The whole setup is controlled by a 486 PC (Fast 486/50, Spectroscopy Instruments GmbH, D-82205 Gilching, Germany) with CSMA software (Spectroscopy Instruments GmbH, D-82205 Gilching, Germany) and mounted on a trolley for transport to the medical facility. The acquisition time of one spectrum is 1 second.

Procedure

Pharmacokinetics studies were carried out in the following way. The animals were first anaesthetized. A background (autofluorescence) spectrum was then measured on the skin of the belly, the tumor-bearing and the healthy cheek pouch mucosa. The cheek pouches were turned

inside out for the acquisition of the spectra. The hamsters were then injected intracardially with the relevant quantity of Lu-TeX, according to their weight, in order to achieve the dose of 12 mg PS per kg of bodyweight (the control animals did not receive this injection). The fluorescence spectra of the belly, the healthy and the tumoral cheek pouch mucosae were then measured at several time intervals between 10 minutes and 24 hours after the injection. The anaesthesia was not extended and the animals therefore woke up during the measurement sessions. At each time interval, four different spectra were recorded after a slight displacement of the fiber on each of the three abovementioned locations. The animals were sacrificed with an overdose of ether at the end of the measurement session. The entire tumoral and healthy cheek pouch mucosae were resected and fixed in 5% buffered formalin (pH=7.0), paraffin embedded, sectioned in 5 μ m thick slices and stained with haematoxylin and eosin for standard histological examination in order to check the accuracy of the induced lesions.

Analysis of results

The spectra of each hamster were first normalized at 525 nm (since the autofluorescence of any one hamster is expected to be constant over time, as has been observed during the measurement sessions, this allows for a certain degree of instability of the spectrofluorometer setup to be taken into account and corrected for). The magnitude of the Lu-TeX fluorescence peak at 740 nm was then obtained by subtracting the autofluorescence background (the autofluorescence was measured on the cheek pouch mucosa of each hamster before the injection), thus yielding a relative measure of the fluorescence intensity of the Lu-TeX in the tissue. The fluorescence units obtained in this way are termed "relative units" (r.u.) in the figures. Four independent measurements were made at each site and time interval on each animal. From these data, the mean value and the standard deviation were calculated. Inter-animal variations of the fluorescence signal were expected and observed as the values of LIF signals varied. A graph representing all these measurements is shown in Fig. 2 and 3 (scattered dots) and a curve has been drawn through the data points for visual interpretation only.

Skin irradiation tests

The skin photosensitization was evaluated with a solar simulator (81192 Solar Simulator, Oriel, Stratford, CT 06497, USA) designed to simulate the solar spectrum from 200 nm to 2500 nm at noon on a clear summer day at sea level at our latitude (45° N). The light intensity was 100 mW/cm². Sixteen hamsters, separated in 4 groups of 4 animals, were irradiated under a protective mask bearing four circular holes of 15 mm diameter. All the animals had their belly shaved beforehand. The first 4 animals received no injection of Lu-Tex and served as control. They received an anaesthesia and an irradiation of 5 min, 10 min, 20 min and 30 min respectively to assess the damage to their skin due to the light itself. They were sacrificed at 5 days after the irradiation, the samples of the skin were resected and fixed in 5% buffered formalin (pH=7.0), paraffin embedded, sectioned in 5 µm thick slices and stained with haematoxylin and eosin for standard histological examination in order to check the extent of the damage. The 12 remaining animals received an intracardiac injection of the relevant quantity of Lu-Tex, according to their weight, in order to achieve the dose of 12 mg PS per kg of bodyweight. Twenty-four hours after the injection, which is the time at which we did not detect any fluorescence from the Lu-Tex in the skin of the animals, the animals were anaesthetized and irradiated under the solar simulator for 8 minutes, a light dose that proved to be just under the threshold of light-induced skin damage. The animals were sacrificed with an overdose of ether at 1 day, 2 days and 4 days after the irradiation. The irradiation spots of the ventral skin were resected and fixed in 5% buffered formalin (pH=7.0), paraffin embedded, sectioned in 5 µm thick slices and stained with haematoxylin and eosin for standard histological examination in order to check for the presence or the absence of necrosis.

RESULTS

Lu-Tex pharmacokinetics

Figure 1 represents the pharmacokinetics curves measured on a tumoral and a healthy cheek pouch mucosa (5 hamsters). They show a simultaneous maximum for the tumoral and the healthy tissue after about 100 min. A rapid decay then follows that reaches 50% of the maximum after 300 to 500 min. Each dot represents the mean value of four measurements on a given site in one

animal as a function of the time interval after the injection. The standard deviations have been omitted in all but a few dots for the sake of clarity. At the time of maximal intensity, the Lu-Tex fluorescence is consistently (up to 1.5 times) higher in the tumor than in the healthy cheek pouch. Similarly, Fig. 2 represents the data from the healthy cheek pouch mucosa and the skin of the belly (5 animals). The maximum for the healthy cheek pouch mucosa is around 100 min, as in Fig. 1, and the maximum for the ventral skin is around 200 min. In all three cases (tumor-bearing cheek pouch, healthy cheek pouch and ventral skin), the fluorescence of the Lu-Tex returns to the detection limit after 1440 min (24 hours).

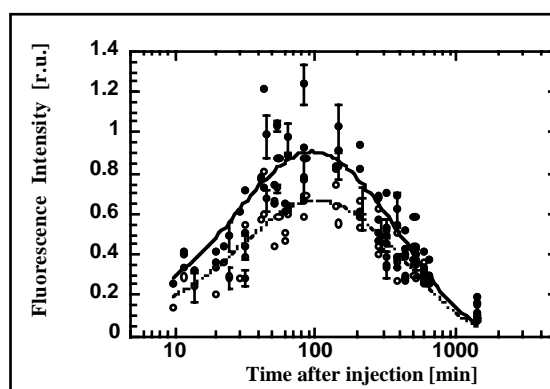


Figure 1: Normalized fluorescence signals due to the Lutetium Texaphyrin (Lu-Tex, PCI-0123) injected at 12 mg/kg measured on the healthy (dotted line and white circles) and tumor bearing (plain line and black circles) cheek pouch mucosa of five hamsters. Each dot represents the average of 4 measurements on a given animal. The uncertainties given correspond to the 67% confidence interval. The curve has been drawn for visual support.

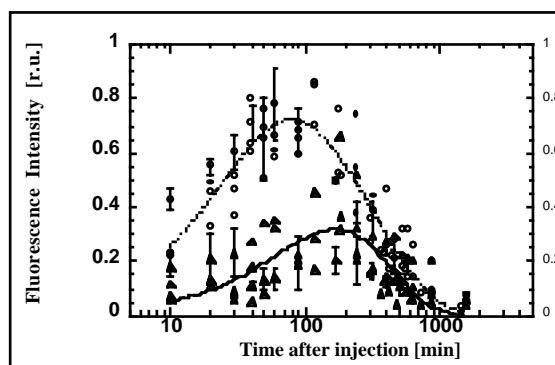


Figure 2: Normalized fluorescence signals due to the Lutetium Texaphyrin (Lu-Tex, PCI-0123) injected at 12 mg/kg measured on the healthy cheek pouch mucosa (dotted line and white circles) and the

ventral skin (plain line and black triangles) of five hamsters. Each dot represents the average of 4 measurements on a given animal. The uncertainties given correspond to the 67% confidence interval. The curve has been drawn for visual support.

Skin photosensitization

The 4 control animals were observed daily after the irradiation they received. The animal that received 5 minutes of irradiation did not display any erythema. At no point in time was there any visible spot on its belly. A very light erythema was observed on the first day but it might have been due to the shaving. The animal that received 10 minutes of irradiation displayed a very mild erythema. The shape of the irradiation spots was slightly visible after four days but this mark receded on the fifth day. The animal that received 20 minutes of irradiation had a marked erythema on the second day after the irradiation. The shape of the spots was clearly visible and there was a clear desquamation of the skin. On the fourth day, the skin was still dry with marked spots, a small coagulation crust and on the fifth day, the skin was recovering albeit still dry and desquamating. The animal that received 30 minutes of irradiation had a marked erythema on the second day after the irradiation. The erythema was clearly visible, as well as the exact shape of the irradiation spots. On the fourth day, blisters were observed as well as an important desquamation and significant marks. On the fifth day, scars were observed at the location where blisters previously lied.

For the subsequent irradiations, it was decided to use an irradiation time of 8 minutes as it is below the observed threshold (10 minutes) of an erythematous reaction induced by the light alone. It should be noted that this irradiation time has also been used to assess the skin damage due to the presence of Foscan[®] in the skin [22]. The hamsters underwent the same procedure, except that they had previously received an injection of Lu-TeX. The irradiation took place 24 hours after the injection to investigate the presence or absence of photosensitizer in the skin of the belly. The animals were observed daily and sacrificed after 1, 2 and 4 days. After one day, no reaction was visible on any of the four irradiated animals. No reaction was

observed either on any of the animals after 2 days or after 4 days. To assess the microscopical damage, the sections of the skin of the hamsters were observed in a transmission microscope and no trace of necrosis or damage to the mucosa or the underlying tissues was observed either. This suggests that the PS was in negligible quantities in the skin of the animals at the time of irradiation, 24 hours after the injection. This seems to corroborate our observation that the fluorescence signal of the Lu-TeX was below the detection limits when measured by LIF.

DISCUSSION

Our study focussed on the PK of Lu-TeX in early superficial squamous cell cancer of the cheek pouch, healthy cheek pouch mucosa and skin of the Syrian golden hamster. This model was thought to be particularly appropriate because a standard procedure, namely a regular painting of the cheek pouch with a carcinogenic agent, yields reproducible early tumoral lesions [28]. These tumors have not only proven an appropriate model for the human aerodigestive lesions [29], but they actually are early tumors of the hamster itself and not xenografts. Indeed, many animal models used for the assessment of PSs and similar studies rely on implanted or transplanted tumors. They are usually much more invasive tumors than the early lesions we are dealing with in this paper. For this reason, the PK of the PS obtained on such invasive grafted tumors can be significantly different from that obtained on early lesions.

Our results show a rapid fluorescence intensity maximum after the injection of the PS (after 100 minutes for the cheek pouch and after 200 minutes for the skin of the belly) and a clearly higher fluorescence signal of the Lu-TeX on the tumor-bearing cheek pouch mucosa. This maximum is well reproducible. This kind of behavior has not been demonstrated for Foscan[®] in early cancers neither in the same animal model [29, 31] nor in patients [32]. One also observes a rapid decay of the PS fluorescence intensity (that becomes undetectable after 24 hours) from the measured locations (Fig. 1). It also appears that little Lu-TeX is detectable in the skin of the animals (Fig. 2). Such an observation, if transposable to human beings, could signify a drastic improvement over previously used

PSs as extended skin photosensitivity is a major drawback [22]. Moreover, since the overall fluorescence signal of Lu-Tex in the skin is kept to a small value, it could be expected that the skin photosensitivity should be small. This is confirmed by our results. Indeed, the irradiation during eight minutes, a light-dose that is below the threshold of light-induced damage to the skin, of the skin of the hamsters with a solar simulator 24 hours after the injection of the Lu-Tex leads to no detectable damage. This is a procedure which has been used in humans to assess the skin photosensitivity following the injection of Foscan[®] [22]. This study has indeed shown that the Foscan[®], unlike the Lu-Tex, induces a skin photosensitization lasting for up to 6 weeks. This observation has also been confirmed as one of the major side effects following the Foscan[®] injection in humans [22]. Clearly, our results show that there is a negligible quantity of PS in the skin of the animals or in the underlying layers and this is consistent with the LIF measurements. This is in contrast with Foscan[®] in the same model [31], where it is observed that this PS accumulates non-negligibly in the skin of the animal. Care should be exercised, though, as the skin of a rodent is not necessarily a good model for the human skin. Nevertheless, the observation of no skin photosensitivity is consistent with previously reported results in a study conducted on mice with Lu-Tex by Young et al [25]. It is also in agreement with results presented by Woodburn et al [26] about photodynamic therapies taking place with the Lu-Tex in tumors implanted in a rodent model. As a matter of fact, these authors report that the normal tissues surrounding the treatment sites do not undergo significant damage. They also report that the therapies taking place after 24 hours lead to no cure of the tumor [26], but rather demonstrate that short time periods after the injection lead to better cure rates than longer intervals, an observation that is consistent with the idea of a rapid elimination of the PS from the body of the mice and in agreement with the findings of Young et al [25]. Hammer-Wilson et al also recently compared the photodynamic activity of the Lu-Tex with that of Photofrin in a mouse model [33]. By means of a study about the toxicity of the Lu-Tex for their model, the authors first report that all the mice excrete colored urine

beginning one hour after the injection and returning to normal by 24 hours after the injection. The authors also present the results of their irradiating the tumors at 740 nm, 5 hours after the intravenous injection of the PS. They also show, in agreement with Young et al [25] and Woodburn et al [26] that this drug-light interval yields the best PDT effects (up to 67% of the animals remain tumor-free during the whole follow-up period) as shorter intervals lead to significant mortality (1 hour) or difficult healing, extensive tissue damage and impaired movements (3 hours). On the other hand, longer drug-light intervals lead to little reaction (12 hours) or no reaction at all (24 hours). Another preclinical study in an animal model is presented by Kostenich et al [27]. In this paper, these authors use *in vivo* LIF to non-invasively measure the distribution kinetics of the Lu-Tex in the tissue of mice bearing a human colon tumor, their aim being to find the optimal drug-light interval to achieve the highest possible ratio between the tumor and the healthy tissue at the time of irradiation. The authors present a kinetics curve displaying a maximum 3 to 4 hours after the intraperitoneal injection in both the healthy and the tumor-bearing foot of the mice. Unexpectedly, the fluorescence signal of the Lu-Tex is higher in the normal foot than in the tumor-bearing one at the time of this maximum but then it decreases faster in the normal foot than in the tumor-bearing one and, as a result, the PS's fluorescence is higher in the tumor-bearing foot than in the normal one after 24 hours. This seems to last for at least another 24 hours as the fluorescence signal in the normal foot goes down to zero whereas it does not decrease anymore in the tumor-bearing foot in this interval. Consequently, these authors chose to perform the PDTs 24 hours after the intraperitoneal injection of the Lu-Tex. Their explanation about the pharmacokinetics of this PS in both feet is that the fluorescence signal was collected from the skin and the underlying tissues such as the tumor and muscle. However, the contribution to the fluorescence signal of these tissues is measured collectively and with little control over the exact contribution of each of them. The administration mode of the Lu-Tex might also explain why these authors find a lasting presence of the Lu-Tex in the body of their animal model and a higher Lu-Tex fluorescence in the normal foot than in the tumor-bearing one, especially since these

findings seem to contradict those of Woodburn et al [26] who used the same animal model, albeit not the same tumor model. Indeed, whereas Woodburn et al [26] and Young et al [25] injected the Lu-Tex intravenously, Kostenich et al [27] administer it intraperitoneally and this type of administration may potentially affect the biodistribution, the uptake and the clearance rate of the PS. This is maybe also a limitation of this model as human tumors implanted in mice probably model the early human tumors up to a certain extent only. Other authors also report the absence of skin phototoxicity in humans following the injection of the Lu-Tex [34].

The inter-animal fluctuations in PK are a major issue when dealing with PSs. In clinical conditions, it is observed that a given injected dose of PS does not necessarily mean that the tissular dose will remain constant from patient to patient. It is likely that this is a consequence of their individual metabolism [30, 35]. In our study, we quantified the inter-animal fluctuations using the maxima of the pharmacokinetics curves. For the tumor-bearing mucosae, we found a fluctuation of $\pm 16\%$ (range 0.76-1.08) in the fluorescence intensity (5 hamsters). Similarly, we found a fluctuation of $\pm 12\%$ (range 0.6-0.8) (10 animals) on the healthy cheek pouch mucosa. Finally, we found fluctuations of $\pm 48\%$ (range 0.14-0.44) on the ventral skin (5 animals). These values are small as compared to what is observed with others PSs, like Foscan[®] in animal models [29] or in patients [35] where they can reach one order of magnitude. However, they indicate that a certain injected dose of PS can lead to tissular fluorescence levels which vary in intensity from one animal to another. The exact reason why the fluctuations are larger on the ventral skin than on the cheek pouch mucosa is unknown. However, several factors may account for this variability. The fluorescence signal of Lu-Tex is small on the skin. The SNR is therefore smaller than on the cheek pouch mucosa. In addition, it is more difficult to perfectly clean the ventral skin than the cheek pouch mucosa due to the presence of hair. It may well be that some fluorescent species (traces of Lu-Tex containing urine, food leftovers) remained despite our thorough cleaning of the skin.

The fluorescence spectra were normalized to compensate for the fluctuations of the spectrofluorometer within one measurement session; these spectra were normalized to the maximum of the autofluorescence. It is to be noted that this procedure was applied for the spectra of one hamster at a time. This is consistent with the idea that the autofluorescence of one animal should not dramatically change during 24 hours, hence it has been used as an internal standard for the normalization. Consequently, the scale of Fig. 2 and Fig. 3 has to be seen as the relative fluorescence intensity of the Lu-Tex as compared to an autofluorescence level of unity. It should be added that the autofluorescence measurements themselves (the background spectra acquired on each animal before the injection) were very close in both shape and intensity from one animal to another and showed very little (less than 5%) fluctuation in intensity during the measurements sessions (data not shown).

It has been demonstrated by Glanzmann et al. [35] that there is a good correlation between the fluorescence contrast and the PS content in the tissue with the Foscan[®] dye. Due to a much smaller fluorescence quantum yield of the Lu-Tex as compared to that of the Foscan[®], the detection threshold for Lu-Tex will be higher, and hence such a correlation more difficult to demonstrate. Nevertheless, our results seem to indicate that the Lu-Tex fluorescence signal is consistently lower in the healthy than in the early lesion bearing mucosa and that this PS does not accumulate significantly in the skin 24 hours after the injection. Both these observations are improvements over the existing PSs.

CONCLUSION

Of the many novel PSs available, Lu-Tex (PCI-0123) appears promising. Its fluorescence signal is clearly higher on the early lesions than on the normal mucosa, it shows a rapid clearance from the body and from the skin in this animal model and it displays smaller inter-animal fluctuations as compared to Foscan[®]. These properties make it a very interesting photodetection candidate. Moreover, Lu-Tex has some major advantages over the other known dyes in terms of ease of use and administration, physical chemical properties and behaviour in an animal model.

ACKNOWLEDGEMENTS

We gratefully acknowledge support from the Swiss Fonds National for Scientific Research Grant # 21-43507.95 and 20-50691.97, the Swiss Priority Program in Optics, the 'Fonds de Service' and 'Fonds de Perfectionnement' of the ENT, Head and Neck Surgery Department of the CHUV Hospital. The authors are also grateful to Pharmacyclics, Inc. (Sunnyvale, CA, USA), for providing the Lutetium Texaphyrin (Lu-*Tex*, PCI-0123).

REFERENCES

- G. Jori, C. Perria, Photodiagnosis and phototherapeutic techniques in medicine, Documento Editoriale, Milano, Italy, 1995.
- J.J. Schuitmaker, P. Baas, H.L.L.M. van Leengoed, F.W. van den Muelen, W. Star, N. van Zandwijk, Photodynamic therapy: a promising new modality for the treatment of cancer, *J. Photochem. Photobiol. B: Biol.*, 34 (1996), 3-12.
- T.J. Dougherty, C.J. Gomer, B.W. Henderson, G. Jori, D. Kessel, M. Korbelik, J. Moan, Q. Peng, Photodynamic therapy, *J. Natl. Cancer Inst.*, 90(12) (1998), 889-905.
- G.I. Stables, D.V. Ash, Photodynamic therapy, *Cancer Treatment Reviews*, 21(4) (1995), 311-323.
- E.S. Edell, D.A. Cortese, Photodynamic Therapy: Its use in the management of Bronchogenic Carcinoma, *Clin. in Chest Med.*, 16(3) (1995), 455-463.
- B.W. Henderson, T.J. Dougherty, How does photodynamic therapy work, *Photochem. Photobiol.*, 55 (1992), 145-157.
- P. Grosjean, G. Wagnières, C. Fontolliet, H. van den Bergh, Ph. Monnier, Clinical photodynamic therapy for superficial cancer in the esophagus and the bronchi: 514 nm compared with 630 nm light irradiation after sensitization with Photofrin II, *Br. J. Cancer*, 77(11) (1998), 1989-1995.
- Ph. Monnier, M. Savary, C. Fontolliet, G. Wagnières, A. Châtelain, P. Cornaz, C. Depeursinge, H. van den Bergh, Photodetection and photodynamic therapy of 'early' squamous cell carcinomas of the pharynx, esophagus and tracheo-bronchial tree, *Lasers Med. Sci.*, 5 (1990), 149-169.
- T. Sutedja, P. Postmus, Photodynamic therapy in lung cancer. A review, *J. Photochem. Photobiol. B: Biol.*, 36 (1996), 199-204.
- Y. Hayata, H. Kato, K. Furuse, Y. Kusunoki, S. Suzuki, S. Mimura, Photodynamic Therapy of 168 Early Stage Cancers of the Lung and Oesophagus: a Japanese Multi-centre Study, *Lasers Med. Sci.*, 11 (1996), 255-259.
- H. Kato, Photodynamic therapy for lung cancer - A review of 19 years' experience, *J. Photochem. Photobiol. B: Biol.*, 42 (1998), 96-99.
- A. Radu, P. Grosjean, Ch. Fontolliet, G. Wagnières, A. Woodtli, H. Van den Bergh, Ph. Monnier, Photodynamic Therapy for 101 Early Cancers of the Upper Aerodigestive Tract, the Esophagus and the Bronchi: A Single-Institution Experience, Diagnostic and Therapeutic Endoscopy, in press.
- G. Koderhold, R. Jindra, H. Koren, G. Alth, G. Schenk, Experiences of photodynamic therapy in dermatology, *J. Photochem. Photobiol. B: Biol.*, 36 (1996), 221-223.
- R.-M. Szeimies, P. Calzavara-Pinton, S. Karrer, B. Ortel, M. Landthaler, Topical photodynamic therapy in dermatology, *J. Photochem. Photobiol. B: Biol.*, 36 (1996), 213-219.
- P. Grosjean, J.-F. Savary, J. Mizeret, G. Wagnières, A. Woodtli, J.-F. Theumann, C. Fontolliet, H. van den Bergh, Ph. Monnier, Photodynamic therapy for cancer of the upper aerodigestive tract using tetra(m-hydroxyphenyl)chlorin, *J. Clin. Laser Med. Surg.*, 14(5) (1996), 281-287.
- P. Grosjean, J.-F. Savary, G. Wagnières, J. Mizeret, A. Woodtli, J.-F. Theumann, C. Fontolliet, H. van den Bergh, Ph. Monnier, Tetra(m-hydroxyphenyl)chlorin clinical photodynamic therapy of early bronchial and oesophageal cancers, *Lasers Med. Sci.*, 11 (1996), 227-235.
- M.G. Dilkes, M.L. DeJode, A. Rowntree-Taylor, J.A. McGilligan, G.S. Kenyon, P. McKelvie, m-THPC photodynamic therapy for head and neck cancer, *Lasers Med. Sci.*, 11 (1996), 23-29.
- L. Ma, J. Moan, K. Berg, Evaluation of a new photosensitizer, meso-tetra-hydroxyphenyl-chlorin, for use in photodynamic therapy: a comparison of its photobiological properties with those of two other photosensitizers, *Int. J. Cancer*, 57 (1994), 883-888.
- K. Fan, C. Hopper, P. Speight, S. Bown, Photodynamic therapy using a new photosensitizer, mTHPC, in the treatment of oral cancer, *Journal of Dental Research*, 75(5) (1996), 1164-1164.
- K.F.M. Fan, C. Hopper, P.M. Speight, G.A. Buonaccorsi, S.G. Bown, Photodynamic therapy using mTHPC for malignant disease in the oral cavity, *Int. J. Cancer*, 73(1) (1997), 25-32.

21. H.B. Ris, H.J. Altermatt, B. Nachbur, C.M. Stewart, Q. Wang, C.K. Lim, R. Bonnett, U. Althaus, Intraoperative Photodynamic Therapy with m-Tetrahydroxyphenylchlorin for Chest Malignancies, *Lasers Surg. Med.*, 18(1) (1996), 39-45.
22. G. Wagnières, Ch. Hadjur, P. Grosjean, D. Braichotte, J.-F. Savary, Ph. Monnier, H. van den Bergh, Clinical Evaluation of the Cutaneous Phototoxicity of 5, 10, 15, 20-Tetra(m-hydroxyphenyl)chlorin, *Photochem. Photobiol.*, 68(3) (1998), 382-387.
23. R. Bonnett, New photosensitisers for the photodynamic therapy of tumours, *Proc. SPIE*, Vol. 2078 (1994), 74-90.
24. T.D. Mody, M. Wright, V. Linquist, S.W. Young, J.L. Sessler, A. Harriman, M. Berns, R.A. Miller, Lutetium (III) texaphyrin: a novel photodynamic therapy agent, *Photochem. Photobiol.*, 59S (1994), 37S.
25. S.W. Young, K.W. Woodburn, M. Wright, T.D. Mody, Q. Fan, J.L. Sessler, W.C. Dow, R.A. Miller, Lutetium Texaphyrin (PCI-0123): a Near-Infrared, Water-Soluble Photosensitizer, *Photochem. Photobiol.*, 63(6) (1996), 892-897.
26. K.W. Woodburn, Q. Fan, D.R. Miles, D. Kessel, Y. Luo, S.W. Young, Localization and Efficacy Analysis of the Phototherapeutic Lutetium Texaphyrin (PCI-0123) in the Murine EMT6 Sarcoma Model, *Photochem. Photobiol.*, 65(3) (1997), 410-415.
27. G. Kostenich, A. Orenstein, L. Roitman, Z. Malik, B. Ehrenberg, In vivo photodynamic therapy with the new near-IR absorbing water soluble photosensitizer lutetium texaphyrin and a high intensity pulsed light delivery system, *J. Photochem. Photobiol. B: Biol.*, 63 (1997), 36-42.
28. S. Andrejevic, J.-F. Savary, Ch. Fontolliet, Ph. Monnier, H. van den Bergh, 7,12-Dimethylbenz[a]anthracene-induced 'early' squamous cell carcinoma in the Golden Syrian hamster: evaluation of an animal model and comparison with 'early' forms of human squamous cell carcinoma in the upper aero-digestive tract, *Int. J. Exp. Pathol.*, 77 (1996), 7-14.
29. Th. Glanzmann, M. Forrer, S. Andrejevic-Blant, A. Woodtli, P. Grosjean, D. Braichotte, H. van den Bergh, Ph. Monnier, G. Wagnières, Pharmacokinetics and pharmacodynamics of tetra(m-hydroxyphenyl)chlorin in the hamster cheek pouch tumor model in comparison with its clinical counterpart, in preparation.
30. M. Zellweger, P. Grosjean, Ph. Monnier, H. van den Bergh, G. Wagnières, Fluorescence measurement of Foscan[®] in the human oral cavity to predict tissue damage induced by photodynamic therapy in the esophagus and the bronchi, *Photochem. Photobiol.*, 69(5) (1999), 605-610.
31. S. Andrejevic, J.-F. Savary, Ph. Monnier, C. Fontolliet, D. Braichotte, G. Wagnières, H. van den Bergh, Measurements by fluorescence microscopy of the time-dependent distribution of meso-tetrahydroxyphenylchlorin in healthy tissues and chemically induced 'early' squamous cell carcinoma of the Syrian hamster cheek pouch, *J. Photochem. Photobiol. B: Biol.*, 36 (1996), 143-151.
32. D. Braichotte, J.-F. Savary, Th. Glanzmann, P. Westermann, S. Folli, G. Wagnières, Ph. Monnier, H. van den Bergh, Clinical Pharmacokinetic Studies of Tetra(meta-hydroxyphenyl)chlorin in Squamous Cell Carcinoma by Fluorescence Spectroscopy at 2 Wavelengths, *Int. J. Cancer*, 63 (1995), 198-204.
33. M. Hammer-Wilson, M. Ghahramanlou, M. Berns, 'Photodynamic activity of Lutetium-Texaphyrin in a mouse tumor system', *Lasers Surg. Med.*, 24 (1999), 276-284.
34. T. Wieman, V. Fingar, S. Taber, M. Panjehpour, C. Julius, T. Panella, A. Yuen, S. Horning, K. Woodburn, J. Engel, R. Miller, M. Renschler, S. Young, 'Phase I photodynamic therapy trial with Lutetium-Texaphyrin (PCI-0123) in patients with metastatic cancer, 24th Annual Meeting of the American Society for Photobiology, Atlanta, GA, USA, June 1996.
35. Th. Glanzmann, Ch. Hadjur, M. Zellweger, P. Grosjean, M. Forrer, J.-P. Ballini, Ph. Monnier, H. van den Bergh, K.L. Chang, G. Wagnières, Pharmacokinetics of Tetra(m-hydroxyphenyl)chlorin in Human Plasma and Individualized Light Dosimetry in Photodynamic Therapy, *Photochem. Photobiol.*, 67(5) (1998), 596-602.



The Quest for Color

(<http://www.nationalgeographic.com/ngm/9907/highlights.html#d>
The National Geographic Magazine, July 1999)

Chapter 5

Sytox[®] Green

There are countless substances that are potential photodetection agents or PSs. In this chapter, we deal with a possible novel photodetection agent, Sytox[®] Green (the work that we conducted on additional substances is reported in Appendix A2). Most photodetection candidates are molecules which are expected to localize preferentially in the tumors in comparison with healthy tissue or whose retention will be longer in the former than in the latter. This amounts to relying on different quantities of photodetection agent at a given moment. Here, we present a different approach. The spectroscopic properties of Sytox[®] Green are modified by its physical chemical environment. This behavior is called metachromasia. The ideal metachromatic photodetection agent will undergo dramatic spectroscopic changes when in contact with a cancer cell, be it a shift of its emission maximum, a change of its fluorescence quantum yield or any other change that will clearly distinguish it from its counterparts in contact with healthy cells only.

Wagnières et al [1] have proposed some work on in vivo animal models using metachromatic dyes. They studied the behavior of a DNA-staining fluorescent dye, TOTO-1, in a rat bladder tumor model. This is an impermeant dye that undergoes a 1000-fold increase in its fluorescence quantum yield when bound to DNA. We therefore chose not to use this molecule.

The administration of the substance (solvent, concentration) was adjusted in healthy untreated animals first. Then, a basic pharmacokinetics curve was measured on their cheek pouch by LIF. The same pharmacokinetics curve was then measured on the cheek pouches of treated hamsters to

determine the maximal intensity of fluorescence of both the healthy and the treated cheek pouch and hence the maximal contrast as a function of the elapsed time. Images were also recorded.

The protocol of regular painting of the hamster cheek pouch with a carcinogenic agent is described in section 4.3, Materials and Methods as well as in a paper by Andrejevic et al. [2]. The healthy untreated animals were kept following the same rules as the painted animals.

This chapter closes the first part of this work. Exogenous dyes are numerous and novel substances are reported regularly. Next to the substances that are in routine clinical practice, it is important to keep looking for new and improved photodetection agents or PSs. With this prospect, a relevant animal model can be of tremendous help. However, when testing new fluorophores, it should always be kept in mind that the ultimate goal of such research is the clinical application of the molecule. Consequently, questions like the applicability of the dye in clinical practice, its toxicity, its side-effects and so on should be assessed very early in the investigations, no matter how interesting it might look. This is the challenge, and maybe sometimes the frustration, of clinically-oriented applied research.

5.1 Sytox[®] Green: the fluorophore

The fluorophore (FP) Sytox[®] Green is a nucleic acid stain. It is a member of the cyanine family [3]. Its structure is proprietary information and its molecular weight is around 600 g/mol (approximate value, not including counterions) [4]. The interesting feature of this FP is its ability to mark the cells with compromised membrane and not the healthy cells (impermeant FP). Upon binding to nucleic acids, its fluorescence is enhanced by a factor of 1000 (excitation: 450-500 nm and emission: 500+ nm) [4,5]. It is essentially non-fluorescent except when bound to DNA or RNA. Figure 5.1 gives the normalized absorption and emission spectra of DNA-bound Sytox [5].

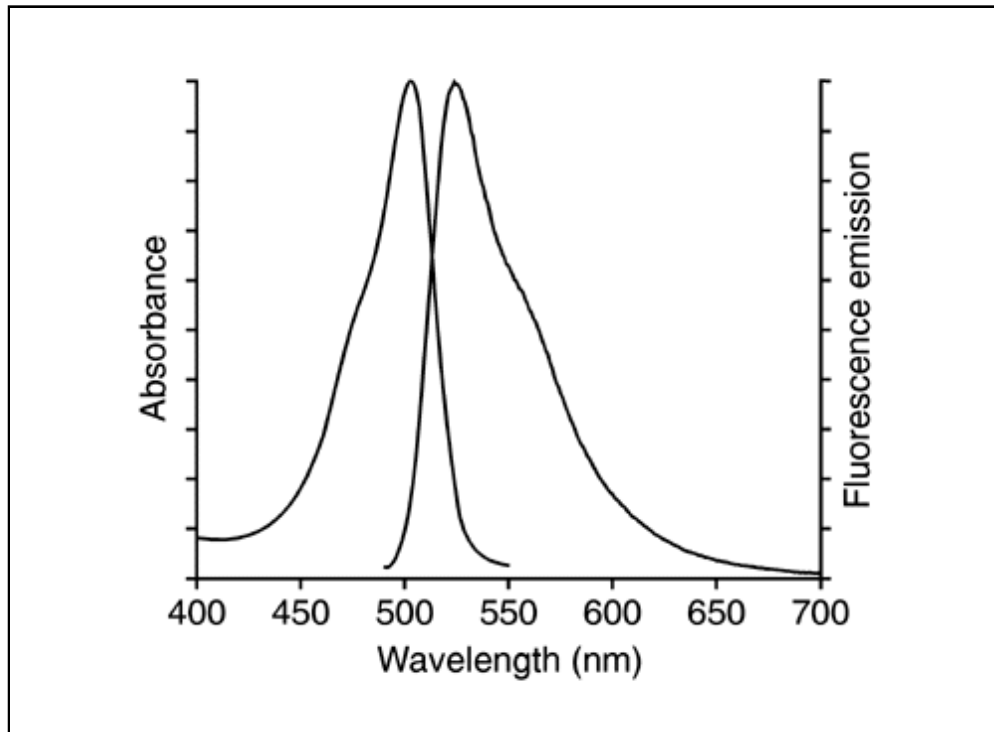
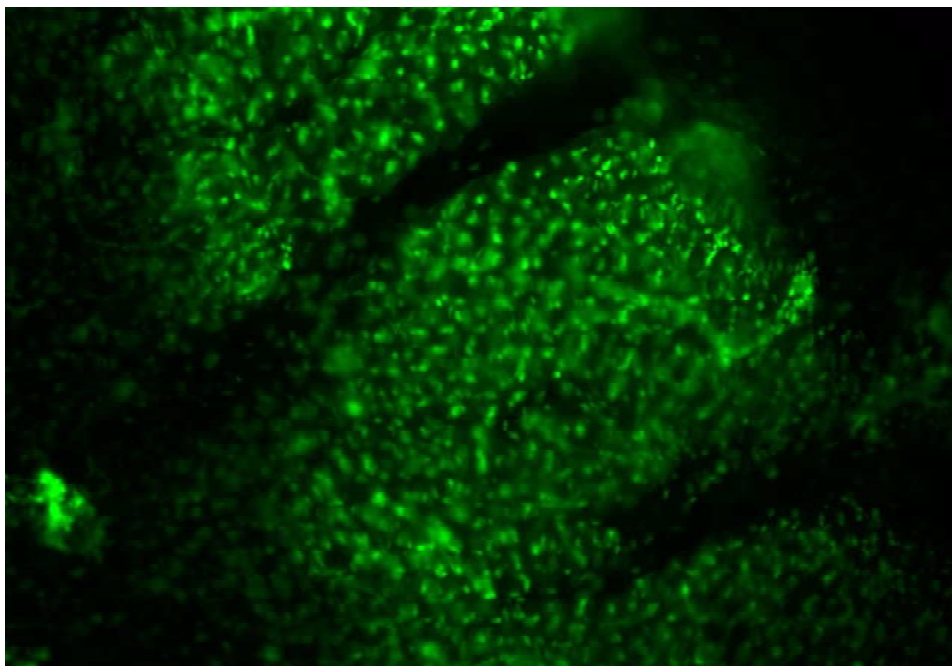


Figure 5.1: Normalized absorption and emission spectra of the DNA-bound Sytox[®] Green. The spectra are normalized to an arbitrary value of 100 and hence expressed in relative units. The detection wavelength is 530 nm and the excitation wavelength is 488 nm [5].

Sytox[®] Green is a typical metachromatic dye. Moreover, its inability to cross the uncompromised cell membranes should prevent it from marking the normal cells. The changes undergone by the dye upon nucleic acid binding should also avoid possible mistakes in the assignment of the cells in the wrong category.

Sytox[®] Green staining is reported to be quite selective for nuclear DNA [4,6]. Indeed, some pictures taken in our group (Fig. 5.2 [7]) on cell cultures show a clear difference between non-marked (dark dull green) and marked (bright green) cells.



The cells undergo many transformations along the cancerization process. Some of these involve modifications of the membrane, its structure and its function. Among many others, we should mention the alteration of the composition of the cell surface and the increased uptake of amino acids and several other exogenous molecules [8]. Generally, we

Figure 5.2: Cells marked with Sytox[®] Green [7].

can consider that both the changes in the membrane that have been inferred and the changes that have been observed alter the functionality of the cell membrane. Some of these changes are summarized in Fig. 5.3 [8].

As given in Fig. 5.3, the permeability of the cell membrane might be altered during the cancerization process [1,8,9]. If so, Sytox[®] Green should mark the cancer cells and not the healthy ones - their membrane function is to exclude such big organic molecules [9]. This is the reason behind our trying to test this dye in our animal model.

5.2 Sytox[®] Green: the study

Preparation and administration

Sytox[®] Green was obtained from Molecular Probes, Eugene, OR, USA as a 5 mM solution in DMSO. The stock solution was diluted with sterile PBS by a factor of 20. This resulted in no precipitation nor any kind of formation of a cloudy residue or any change in the solution color.

Each hamster was first anaesthetized. A background spectrum was then measured on both cheek pouches before the injection, along with a reference spectrum acquired on a Rhodamine B cuvette before the measurement session (this was intended to correct the actual value later measured on the peak of the dyes for the slight variations of excitation power delivered by the lamp). Then, the hamster received an intracardiac injection of 0.2 ml/100 g of the dye solution to achieve a dose of 0.3 mg/kg. Shortly after the injection, we started to measure the pharmacokinetics of the fluorophore by Light-Induced Fluorescence (LIF) in both the untreated cheek pouch (thereafter labeled 'healthy') and the treated cheek pouch ('cancerous').

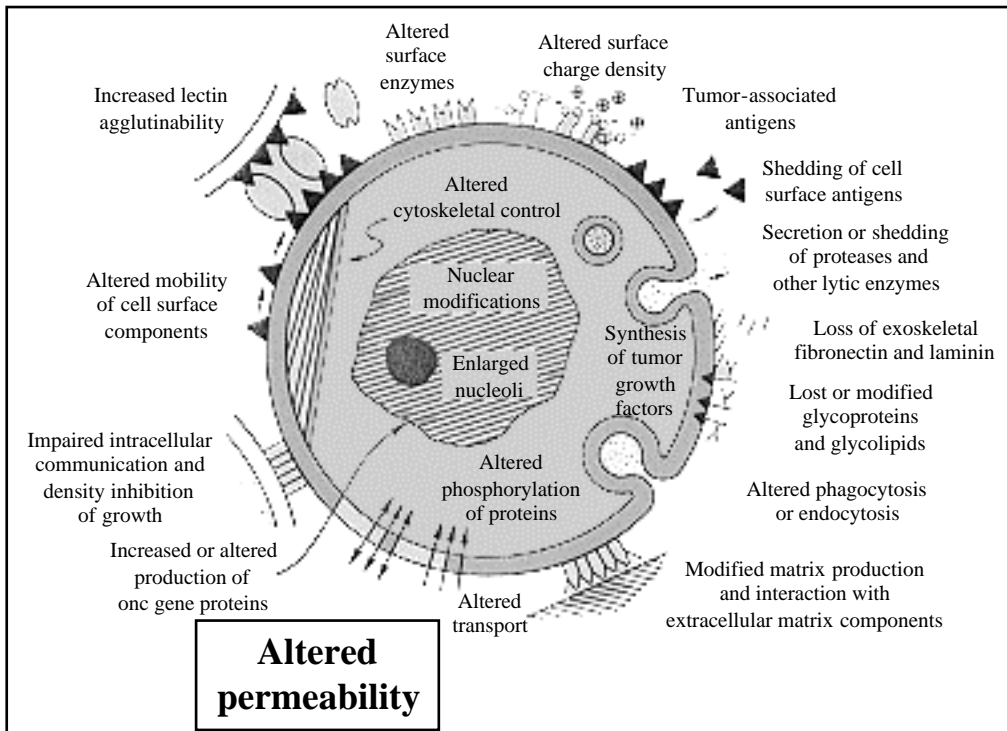


Figure 5.3: Some cellular alterations observed after neoplastic transformation [8].

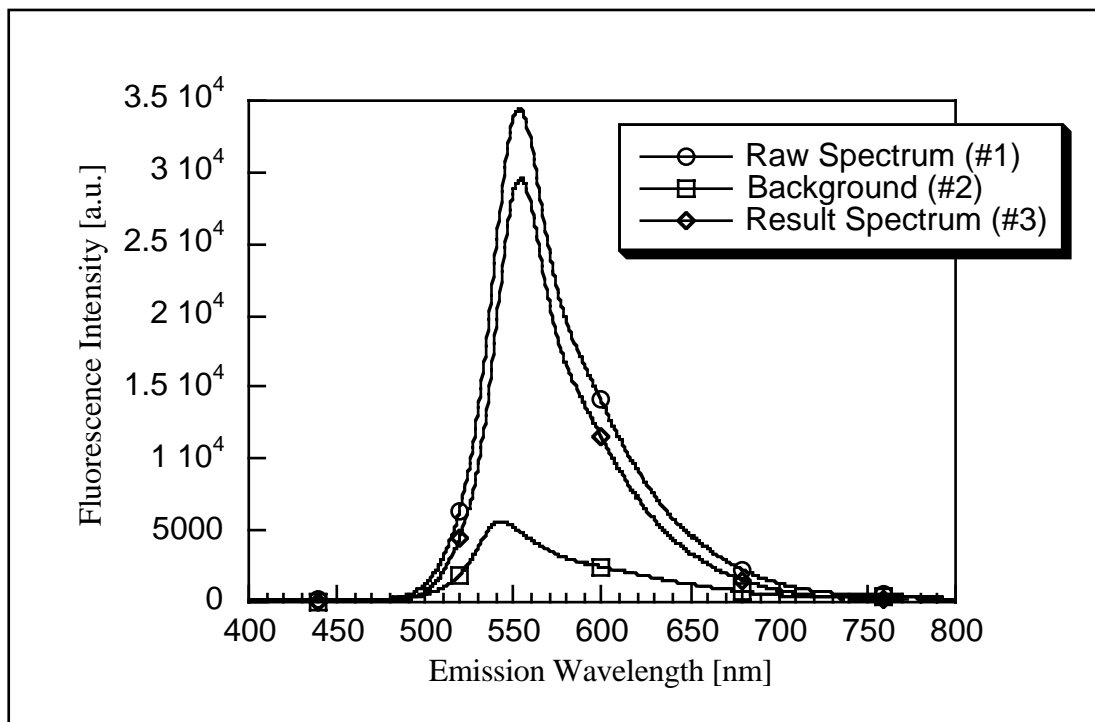


Figure 5.4: Fluorescence emission spectrum of Sytox[®] Green on the cancerous cheek pouch of one hamster 120 min after the injection of 0.3 mg/kg. The excitation wavelength is 465 nm. The result spectrum is obtained after the procedure described above.

The measurements were done by spectrofluorometry, using our optical fiber-based spectrofluorometer described in Appendix A1. The excitation wavelength was 465 nm and detection took place above 525 nm (Filters: Short Pass 550 nm; Dichroic 550 nm; Long Pass 495

nm). The background curve was subtracted and the value of the fluorescence intensity was calculated at the maximum of the peak (in the 550-555 nm window) with no further correction.

The spectra were acquired at different time intervals after the injection (4 spectra for each point in time), thus allowing us to calculate a mean value and a standard deviation, both plotted on the graphs (see Fig. 5.4 for an example). Twelve treated hamsters were involved in this study. During the first part of the study (November 1998), two animals received an injection of Sytox[®] Green. Some of the results are plotted in the form of pharmacokinetics curves in Fig. 5.5. The second part of the study (February 1999) involved 10 more animals. These results are displayed in Fig. 5.7 and the following figures.

Results and discussion

Figure 5.4 shows the spectra obtained in vivo. The three curves are the raw measured spectrum (#1), the background spectrum (#2) and the resulting spectrum (raw spectrum - background, #3).

Figures 5.5a and 5.5b are the pharmacokinetics curves obtained on the first two animals. Each curve represents the measurements for one animal. The vertical scales are comparable. For each graph, not only the mean value and the standard deviation of the mean have been plotted, but also the maximal value observed on both the healthy and the cancer bearing mucosa.

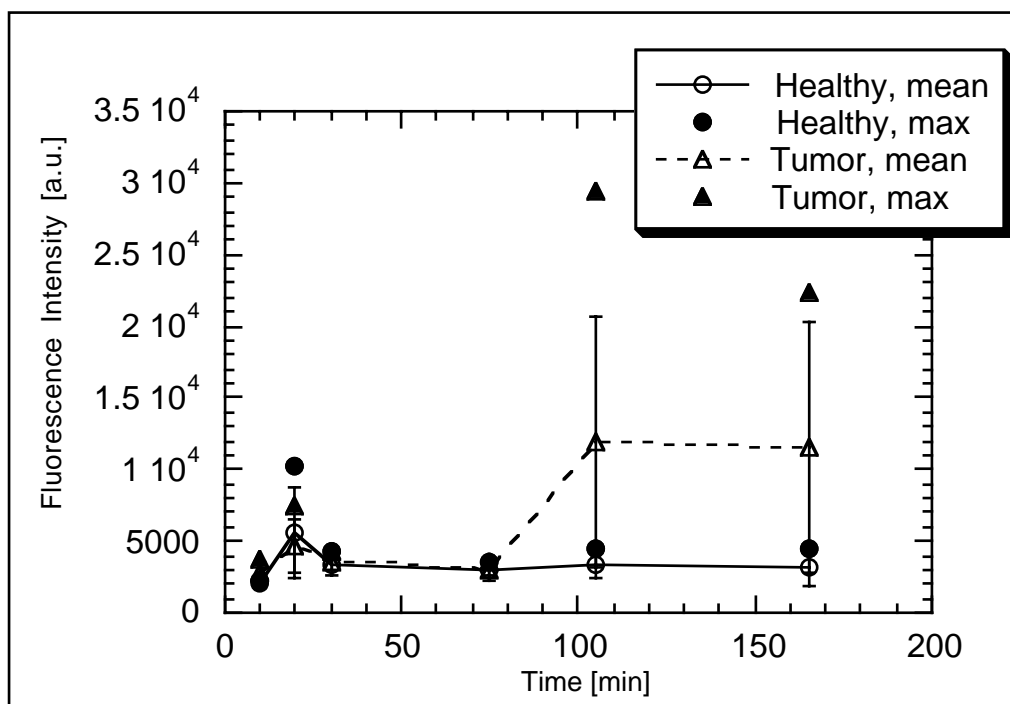


Figure 5.5a: Fluorescence emission signal of Sytox[®] Green on the healthy and cancerous cheek pouch of one hamster as a function of the time interval after the injection of 0.3 mg/kg. The excitation wavelength is 465 nm and detection is above 495 nm. For each point, the mean of four measurements together with the standard deviation are displayed (white markers). As well, the maximum value for that time interval is plotted (black markers).

It should be noted that the point measurements have been carried out on two animals only. Additional animals were included in an imaging study.

As can be seen on Fig. 5.5a and 5.5b, it is unclear what the exact pharmacokinetics curve looks like. The most puzzling information is not the non-reproducibility of the curves but the maximal value of the fluorescence on both the healthy and the cancerous mucosa. On the healthy mucosa, the maximal values are kept small, relatively constant and the standard deviations of the means are also small.

This means that the fluorescence signal is, as expected, small and quite consistently so. As a matter of fact, the Sytox[®] Green should not be bound to DNA in the healthy mucosa since the cells have an intact membrane. On cancerous mucosa, it was observed that the means are not reproducible and that the standard deviations are large. This means that some measurements produce a very large fluorescent signal (which one would expect if the dye binds to the DNA) and some do not. This could mean that our slight displacement of the

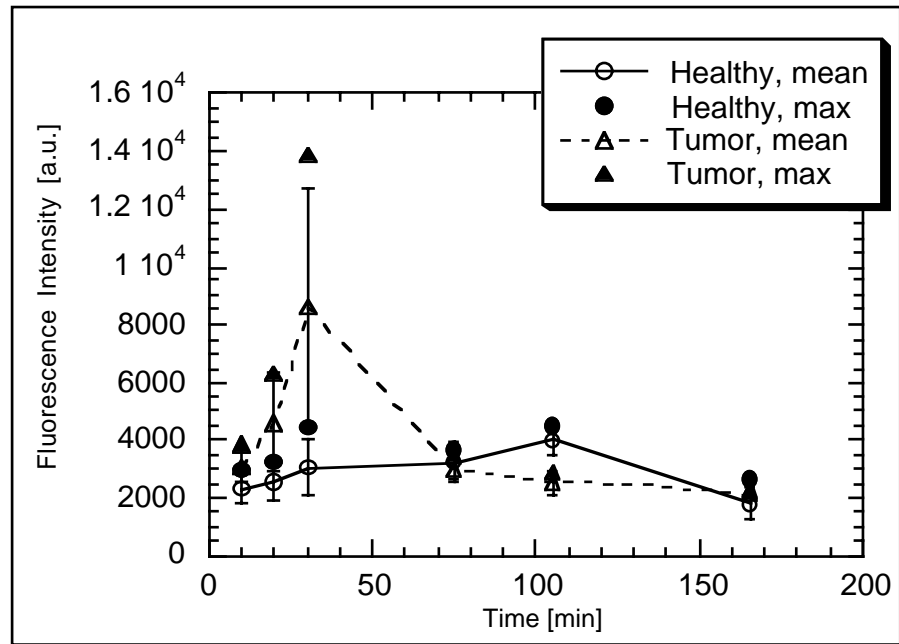


Figure 5.5b: Fluorescence emission signal of Sytox[®] Green on the healthy and cancerous cheek pouch of one hamster as a function of the time interval after the injection of 0.3 mg/kg. The excitation wavelength is 465 nm and detection is above 495 nm. For each point, the mean of four measurements together with the standard deviation are displayed (white markers). As well, the maximum value for that time interval is plotted (black markers).

fiber between two measurements on one site was sufficient to go from a fluorescent spot (like a small patch of early cancerous cells) to a non-fluorescent spot (like the healthier surrounding mucosa), as one would be likely to observe on a field cancerized mucosa. This is the reason why we also plotted the maximal values for each time point. There is no doubt that, at these points in time, a highly fluorescent signal was measured. However, this seemed to happen randomly (it is not correlated to the time) and it seemed to be very limited as far as actual geometrical range goes. To overcome this difficulty, we decided to take images together with spectroscopical measurements on the following series of animals.

During anaesthesia, the cheek pouch to be observed was exposed by means of a homemade device (Fig. 5.6) [10]. The whole site was illuminated by means of an argon ion laser at 457 nm. The pictures were then recorded with a color CCD camera and taped on a standard VHS VCR. They were printed and are given in Fig. 5.11-5.13, along with the relevant fluorescence emission spectrum (Fig. 5.7-5.8, measured after the procedure described above) and the histopathological analysis of the spot (a surgical thread was used to mark the measurement spot and a biopsy was taken after the sacrifice of the animal). It should be noted, though, that the taking of a biopsy is a difficult operation and that, consequently, the accuracy of this biopsy may be limited.

The biopsies were analyzed in a routine fashion and the results of the histopathological analysis are given below in Fig. 5.7 and 5.8, along with the fluorescence spectra of the corresponding location.

As can be seen in Fig. 5.7 and 5.8, a certain correlation can be found between the fluorescence intensity of Sytox[®] Green in the mucosa and the histopathological status of the location. It is clear that the inaccuracy inherent to our biopsy-taking procedure may induce a discrepancy between the spot that has been measured and the spot that has been observed by the histopathologist. All that is certain is that every measurement on a non-healthy spot has been done on a site bearing some kind of pre-/early cancerous lesion. This indicates that the histopathological status of the non-healthy mucosa should be treated with some caution. However, the healthy spots (or in Fig. 5.7, the light dysplasia) come from the contralateral cheek

pouch that has not been painted with the carcinogen. It is therefore certain that these spectra are those of relatively spared mucosa. It is interesting to note that, in both figures, the contralateral spot produces a spectra whose intensity at 550 nm is significantly smaller than that of the non-healthy mucosae. This may be regarded as an encouraging result in our investigations of Sytox[®] Green.



Figure 5.6: The homemade device to open the mouth of an anaesthetized hamster.

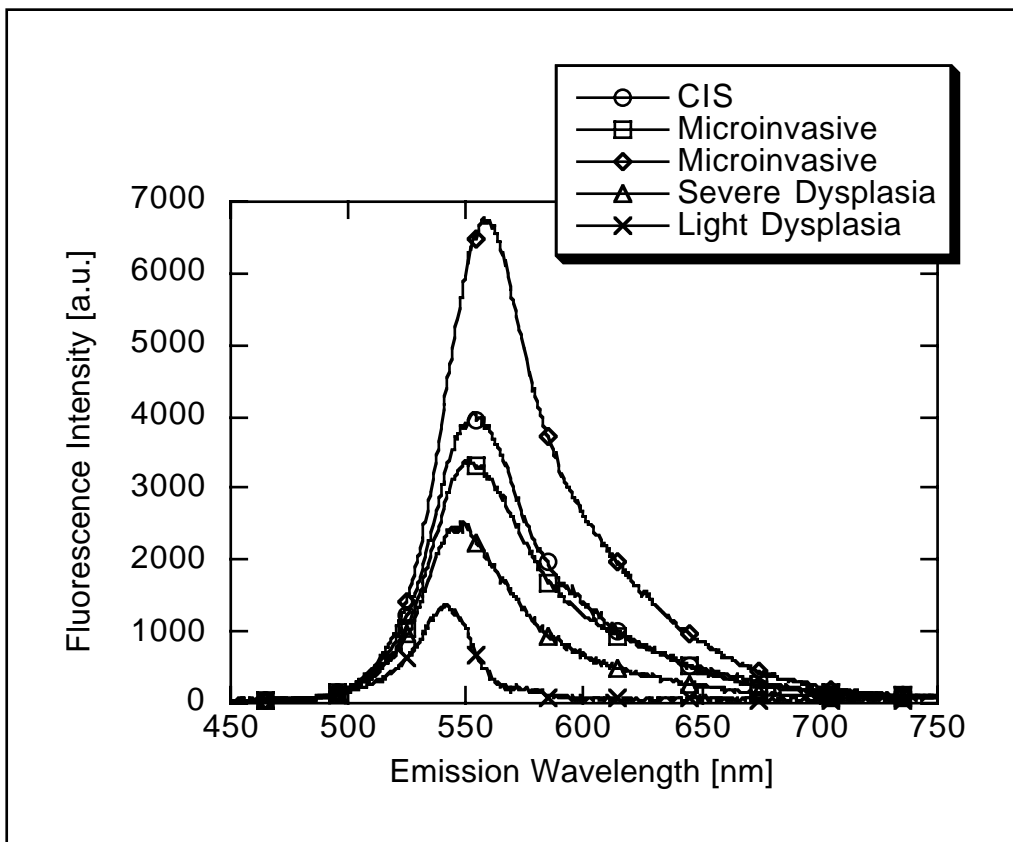


Figure 5.7: Fluorescence spectra of the Sytox[®] Green in the cheek pouch mucosa of one hamster as a function of the histopathological status. The excitation wavelength is 465 nm and the injection-measurement interval is 30 minutes.

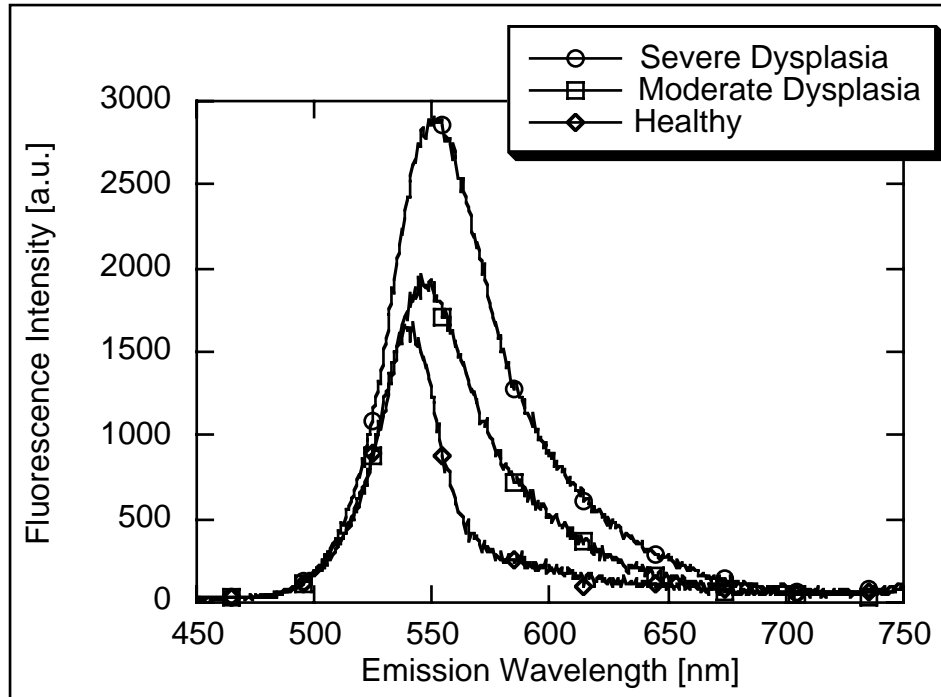


Figure 5.8: Fluorescence spectra of the Sytox[®] Green in the cheek pouch mucosa of one hamster as a function of the histopathological status. The excitation wavelength is 465 nm and the injection-measurement interval is 30 minutes.

displacement of the peak from below 550 nm for the light dysplasia to above 560 nm for microinvasive carcinomas. This would also be accompanied by a concomitant increased absorption at 575 nm (second absorption peak of hemoglobin). This does not seem to be observed in our results. It is likely that this displacement is due to more complex modifications of the tissue. The large standard deviations also indicate that, with the notable exception of the healthy tissue and the invasive carcinoma, there is a non-negligible overlap in the position of the maximum, and this is likely to be detrimental to a clear-cut explanation of the phenomenon. It should also be mentioned that there is an uncertainty on the horizontal axis (histopathological analysis) as this result is known to be operator-dependent.

It cannot be overlooked that this effect could be due to modifications of the optical or architectural properties of the tissue (blood amount, thickening and subsequent shielding by the epithelium). An increased presence of blood in the tissue would be reflected by an increased absorption of the photons at 540 nm (first absorption peak of hemoglobin), which could account for the

Histopathological status	Corresponding number
Healthy	1
Light Dysplasia	2
Moderate Dysplasia	3
Severe Dysplasia	4
Carcinoma in situ	5
Microinvasive Carcinoma	6
Invasive Carcinoma	7

Table 5.1: Histopathological status of the lesions of the hamster cheek pouch mucosae and their corresponding number.

It can be observed in Fig. 5.7 and 5.8 that a shift of the fluorescence emission maximum occurs as the normal tissue turns dysplastic and to carcinoma in situ. Figure 5.9 gives the position of the maximum fluorescence emission as a function of the histopathological status of the tissue (given as a number, see Table 5.1). The fluorescence emission maximum shifts towards longer wavelengths as the histopathological status of the tissue proceeds from healthy to cancer.

A similar plot is given in Fig. 5.10. In this graph, the fluorescence intensity is plotted as a function of the histopathological status of the site of the measurement. It should be noted that the correlation observed in Fig. 5.9 is less marked in Fig. 5.10. In particular, the invasive lesions do not display a higher fluorescence on average than the microinvasive carcinoma or the carcinoma in situ. Part of this could be due to the fact that invasive lesions might be necrotic on their outer side and poorly vascularized, thus keeping large amounts of the dye away from these cells. On the other hand, the correlation is interesting for the dysplasias and the carcinoma in situ and the microinvasive carcinoma, all of them early localized lesions.

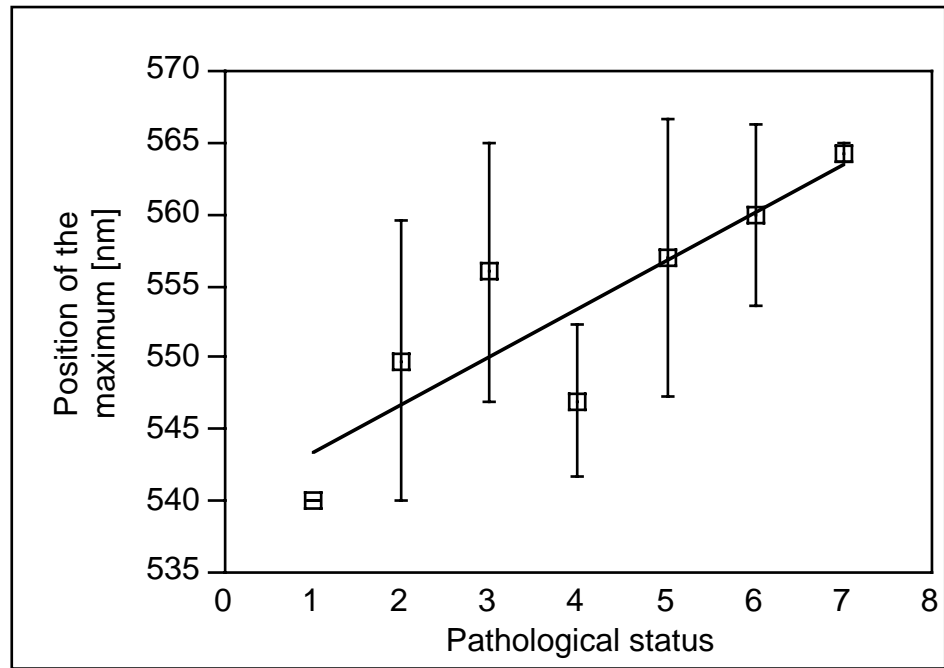


Figure 5.9: Position of the maximum fluorescence emission as a function of the histopathological status of the site of the measurement (average position of the maximum in 7 hamsters).

that invasive lesions might be necrotic on their outer side and poorly vascularized, thus keeping large amounts of the dye away from these cells. On the other hand, the correlation is interesting for the dysplasias and the carcinoma in situ and the microinvasive carcinoma, all of them early localized lesions.

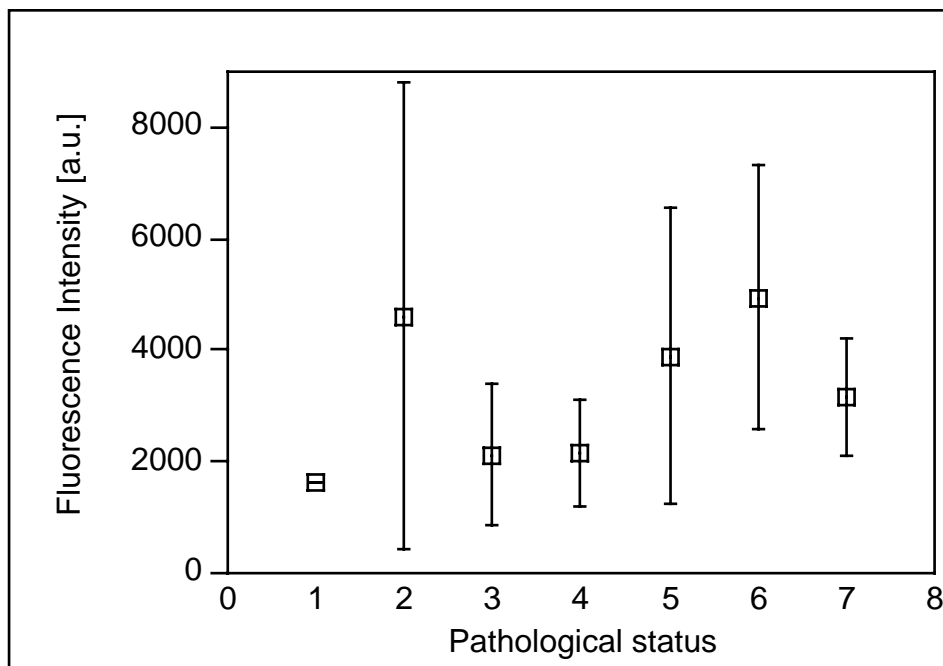


Figure 5.10: intensity of the maximum fluorescence emission as a function of the histopathological status of the site of the measurement (average intensity of the maximum in 7 hamsters).

Images

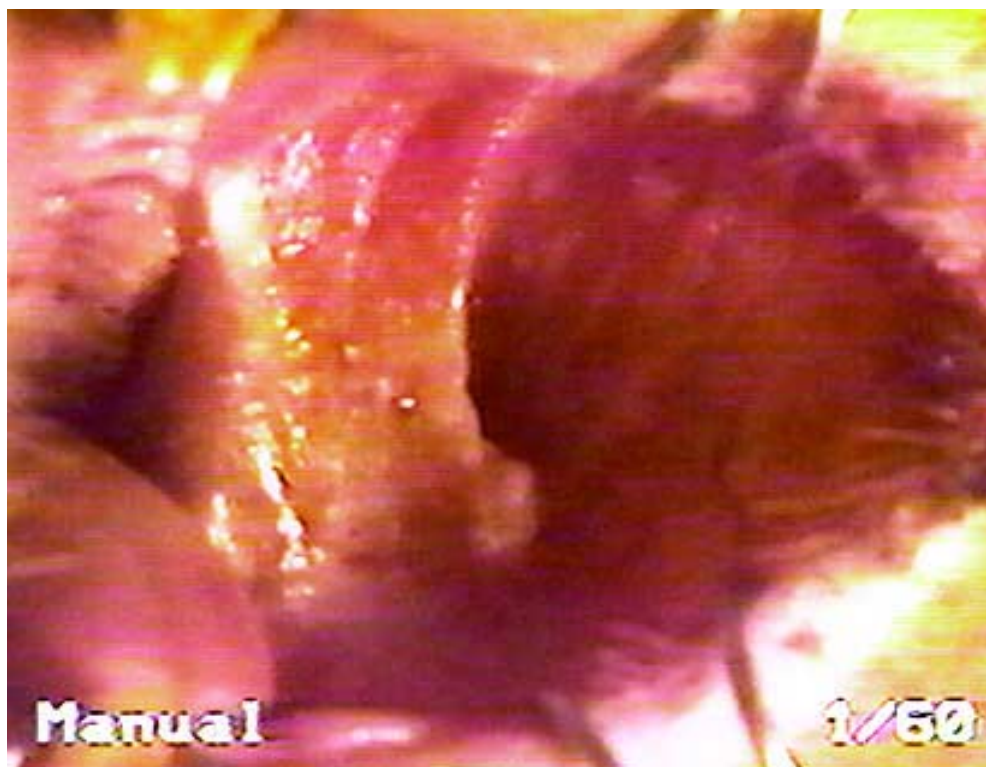


Figure 5.11a: White-light image of the cheek pouch of a hamster following an injection of Sytox[®] Green.

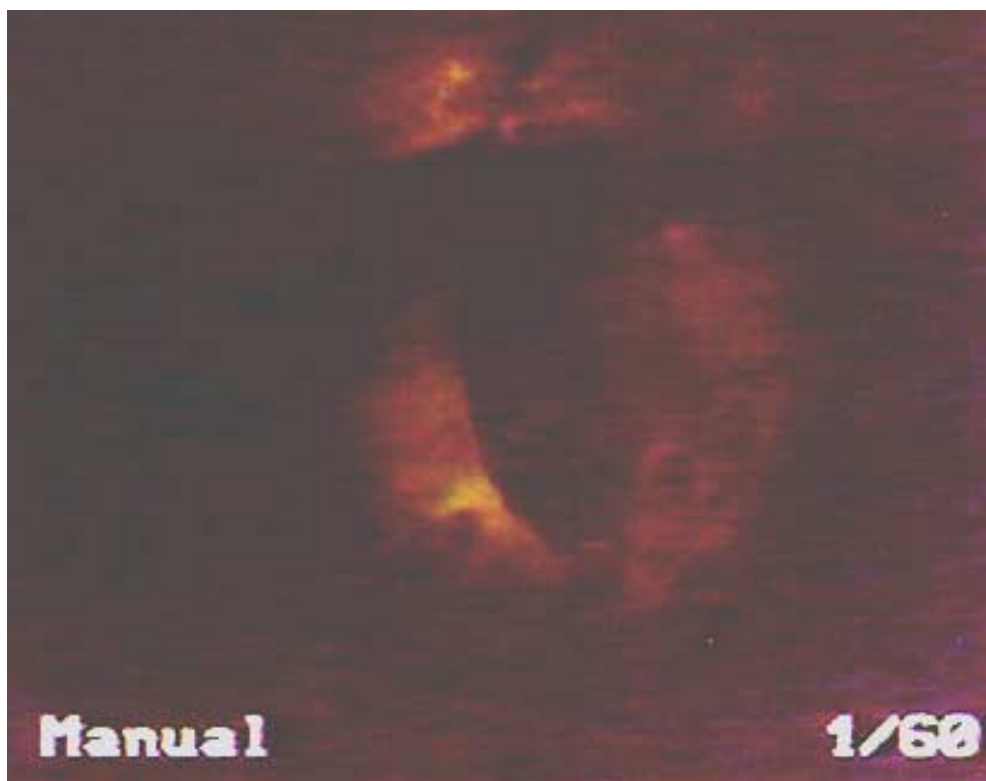


Figure 5.11b: Fluorescence image of the cheek pouch of a hamster following an injection of Sytox[®] Green. The green fluorescent spots are clearly visible whereas the surrounding healthy mucosa is dark. The excitation took place at 457 nm.

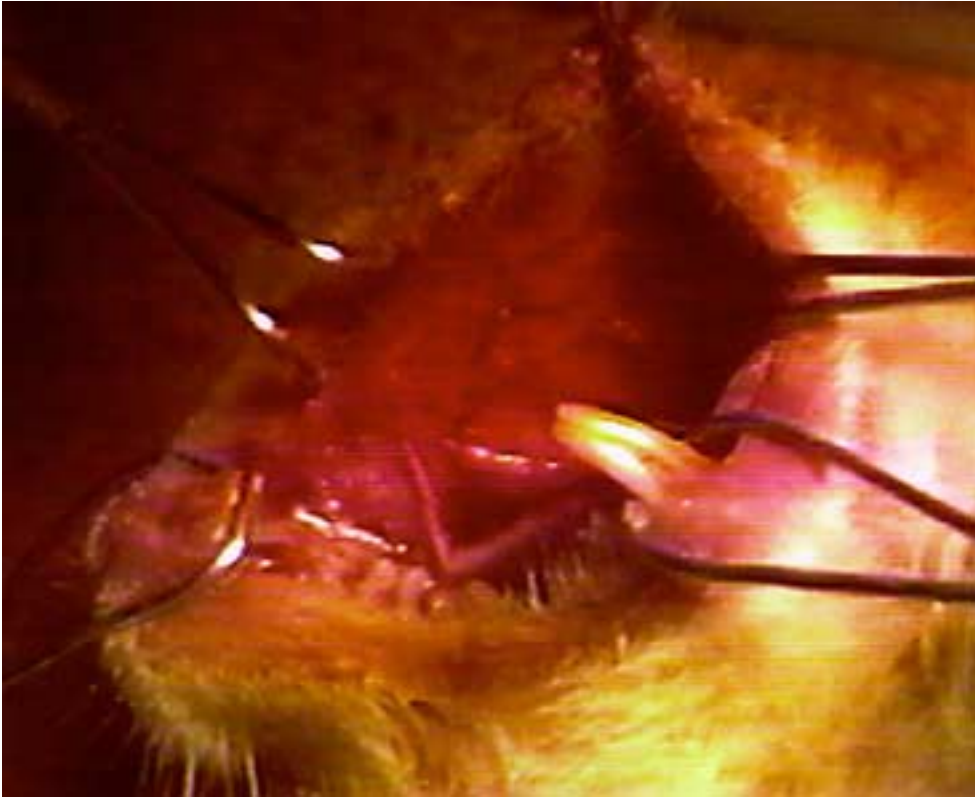


Figure 5.12a: White-light image of the cheek pouch of a hamster following an injection of Sytox[®] Green.

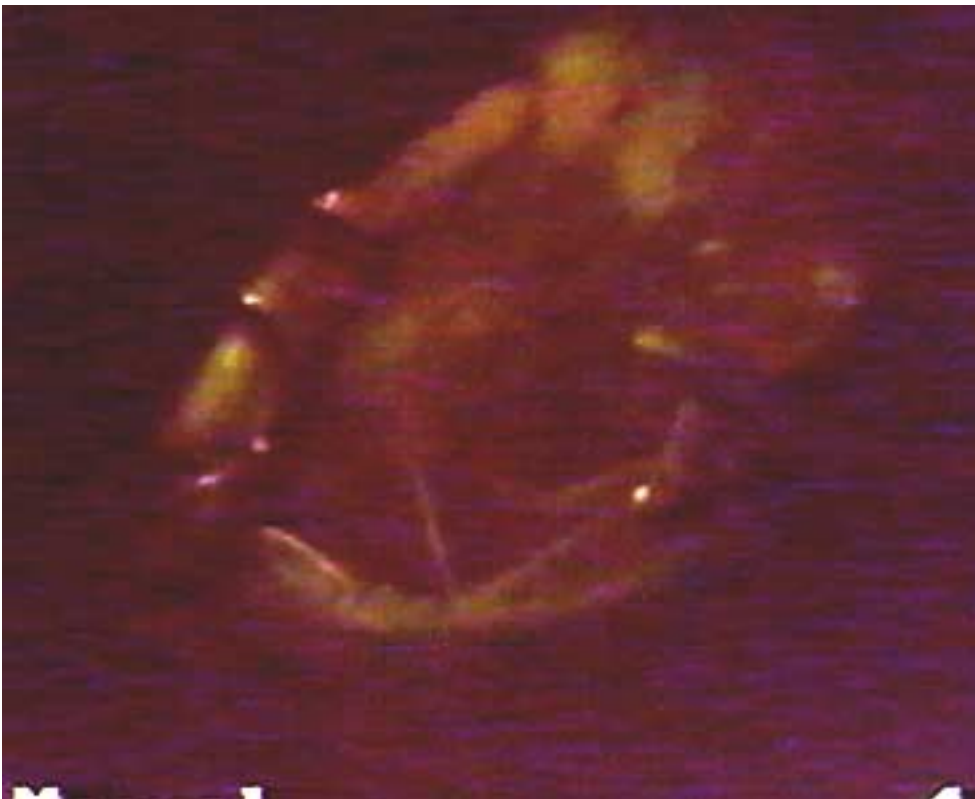


Figure 5.12b: Fluorescence image of the cheek pouch of a hamster following an injection of Sytox[®] Green. The green fluorescent spots are clearly visible whereas the surrounding healthy mucosa is dark. The excitation took place at 457 nm.



Figure 5.13a: White-light image of the cheek pouch of a hamster following an injection of Sytox[®] Green.

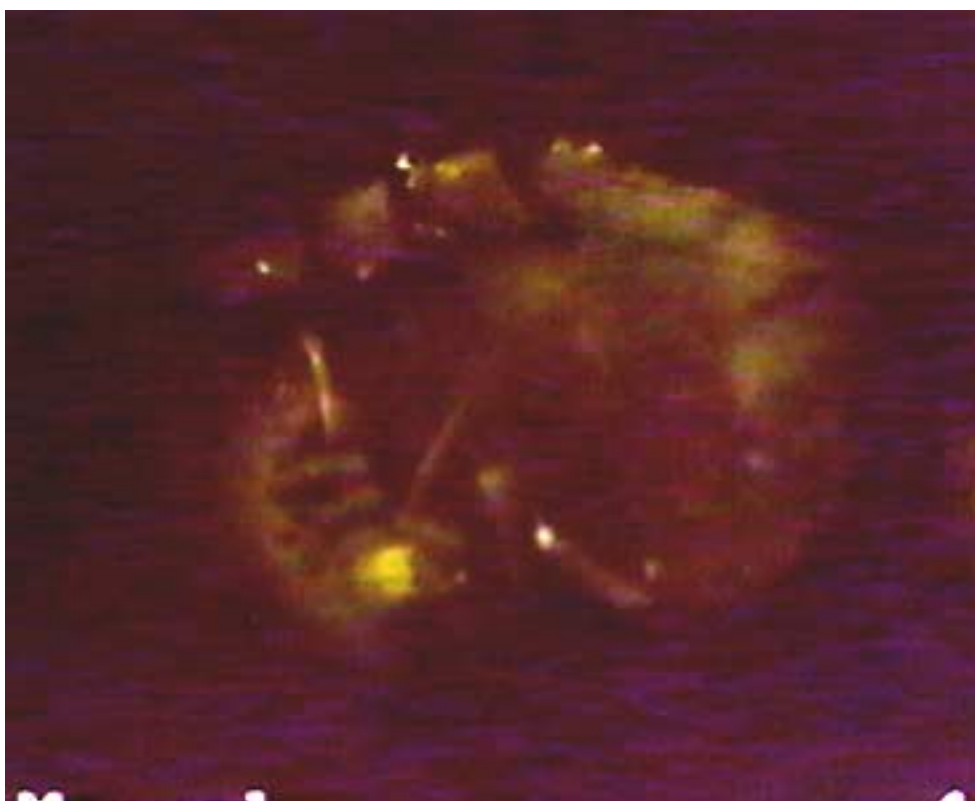


Figure 5.13b: Fluorescence image of the cheek pouch of a hamster following an injection of Sytox[®] Green. The green fluorescent spots are clearly visible whereas the surrounding healthy mucosa is dark. The excitation took place at 457 nm.

Much remains to be done in the race for the perfect photodetection agent. Most of the work is carried out to find more selective dyes or dyes that will be retained longer in the early lesions. The approach of finding dyes that are sensitive to their microenvironment and thus undergo spectroscopic changes rather than temporarily accumulating in different quantities might be a promising one.

Sytox[®] Green appears to have a potential selectivity for early lesions that has not been found in previously used exogenous fluorophores. Its exclusion from healthy cells and its very specific binding to DNA participate to its interesting properties. The limitations of this molecule are elsewhere, however. It has never been injected to humans and our tests are among the earliest ones on living animals. Very little is known about its systemic or topical toxicity, but its mechanism of action - the nucleic acid binding - is linked to the carcinogenic properties of other well-known DNA-marking molecules (ethidium or propidium halides). If similar cancer-induction properties are found in the Sytox[®] Green, it is highly unlikely that it will ever be used in patients. Still, similarly selective molecules should be tested because the primary goal of these investigations is to mark early lesions and Sytox[®] Green achieves this goal better than most substances that are currently used. As well, its very high fluorescence quantum yield makes it easy to detect (a major drawback of Lu-Tex) even in low concentrations, when bound to DNA.

Exogenous fluorophores can be helpful to detect early cancerous lesions. Because most of them remain for a long time within the body of the patients, however, they are usually used for the photodynamic treatment of such lesions only. In this respect, a fluorophore like Lu-Tex could represent an improvement over previous ones because it seems that it is indeed excreted rapidly after injection. It is likely that this property is linked to its water-solubility and this could be a hint as to the properties to be searched for in novel exogenous fluorophores to come.

The use of exogenous fluorophores for the photodetection is also a bit difficult in terms of administration because it requires an injection which increases the risks of allergic reaction. In some cases, it contributes to the detection of early lesions but these substances will only be accepted as good detection alternatives when this contribution will be more marked and more reproducible as well as carrying fewer side-effects.

References

1. Wagnières, G., S. Iinuma, K. Schomacker, T. Deutsch, T. Hasan, 'In vivo tissue characterization using environmentally sensitive fluorochromes', in 'Fluorescence Microscopy and Fluorescent Probes', 203-209, Edited by J. Slavík, Plenum Press, New York, 1996.
2. Andrejevic, S., J.-F. Savary, Ch. Fontollet, Ph. Monnier, H. van den Bergh, '7,12-Dimethylbenz[a]anthracene-induced 'early' squamous cell carcinoma in the Golden Syrian hamster: evaluation of an animal model and comparison with 'early' forms of human squamous cell carcinoma in the upper aero-digestive tract', *International Journal of Experimental Pathology*, 77, 7-14, 1996.
3. 'Color Chemistry', H. Zollinger, VCH Verlagsgesellschaft, Weinheim, Germany, 1987.
4. Haugland, 'Handbook of Fluorescent Probes and Research Chemicals, Molecular probes', sixth edition, 1996.
5. <http://www.probes.com/>
6. Matsuzaki, Suzuki, Fujikura, Takata, 'Nuclear staining for laser confocal microscopy', *Acta Histochem. Cytochem.*, Vol. 30, No. 3, 309-314, 1997.
7. Pascal Uehlinger, EPFL, personal communication.
8. 'Cancer Biology', R.W. Ruddon, editor, Oxford University Press, 1995.
9. 'Physics and the architecture of cell membranes', R. Warren, IOP Publishing, Bristol, UK, 1987.
10. Dr Joël Gagnebin, CHUV Hospital, personal communication.

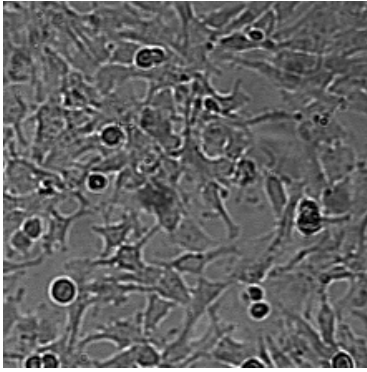
Part II

***EXOGENOUSLY-
INDUCED
FLUOROPHORES***

The second part of this thesis deals with the uses of fluorescence spectroscopy and imaging to investigate exogenously-induced fluorophores (for a definition of exogenously-induced fluorophores, see p. 13). The fluorophore is Protoporphyrin IX (PPIX).

We separated this second part in two chapters, both of them published in peer-reviewed journals. The first chapter deals with a preclinical study in cultured cells. We used this model to test a series of ALA ester derivatives. The ALA ester derivatives are increasingly lipophilic with the increasing length of the aliphatic chain and this might overcome the difficult internalization of ALA by cells in culture. After an intracellular de-esterification, these molecules enter, as ALA, the biosynthetic pathway leading to heme via PPIX. As expected, our results show that the concentration of ALA-esters solution required for a given fluorescence level of PPIX decreases with the increasing length of the aliphatic chain.

Following this preclinical study on cells in culture and a concomitant preclinical ex vivo study on urothelium, we tested our best ALA ester, the hexylester (hALA), in the urology clinics of the CHUV Hospital. The use of ALA hexylester as a profluorophore allows the clinician to reduce the instillation times by a factor of 3 and the concentration of the drug by a factor of 20. We present here the first results of a pilot clinical study.



Cells in culture

Chapter 6

PPIX in cultured cells

In mammals, the biosynthesis of porphyrins is found in almost all types of cells, with the exception of mature red blood cells. This process starts with the condensation of glycine and succinyl Coenzyme A (CoA) to form the aminolaevulinate, the zwitterion form of the 5-aminolaevulinic acid [1]. This step is catalyzed by the 5-aminolaevulinate synthase. This biosynthesis eventually gives the non-fluorescent heme through chelation of an iron ion into the porphyrin ring (see Fig. 6.1), a step that is catalyzed by the ferrochelatase. Heme is found in proteins such as the myoglobin, the hemoglobin, the cytochrome c, among others. The presence of heme inhibits the 5-aminolaevulinate synthase, thus stopping the production of ALA. In this biosynthesis, the immediate precursor of heme is the highly fluorescent and phototoxic protoporphyrin IX (PPIX) and the chelation of the iron ion is the rate-limiting step of the whole process. Exogenously administered ALA bypasses the feed-back mechanism. Thus, when in the presence of a solution of ALA, cells include it into the normal biosynthetic pathway. This can lead to the temporary accumulation of PPIX. The importance of the PPIX accumulation can vary according to the cell type [2] or according to the pathological status of the cells within one type of cells or one organ. In vivo, the exogenous administration of ALA leads to a higher accumulation of PPIX in cancerous cells. This might be due to the fact that the activity of the ferrochelatase is lower in cancer cells, thus leading to a lower chelation of an iron ion and a higher accumulation of

PPIX or to the higher activity of the porphobilinogen deaminase in some tumor cells, thus leading to a higher production of PPIX [3,4]. This whole process also applies to ALA derivatives if they are turned into ALA after their internalization by the cells.

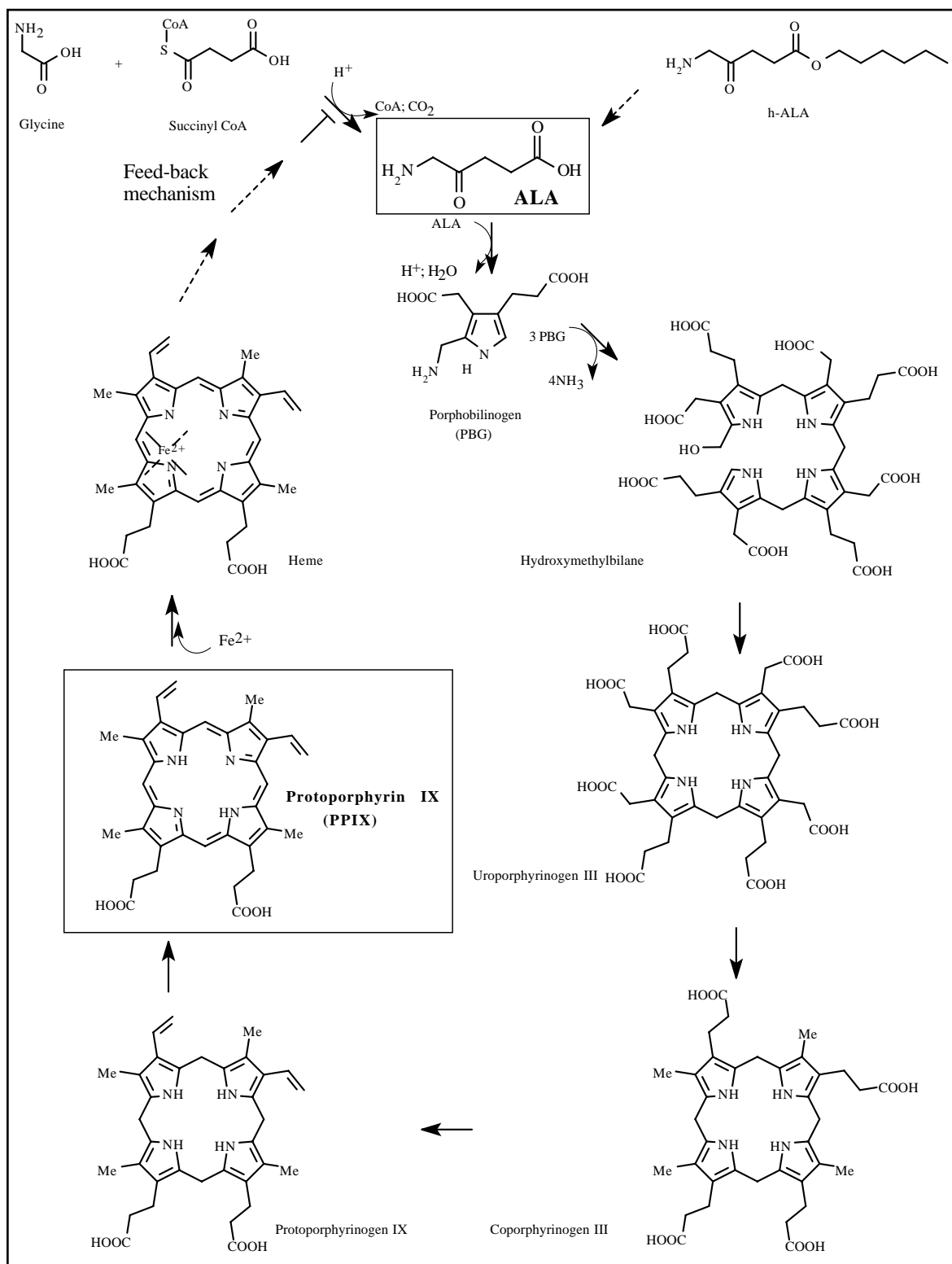


Figure 6.1: The biosynthesis of heme.

There are a number of studies about the exogenous administration of ALA to detect or treat early cancers. This modality has been successfully used in dermatology [5] and urology [6,7]. Several studies about the interaction between ALA or its ester derivatives and cells in culture have also

been reported. In this chapter, we will focus on the preclinical studies on cells in culture as it is the core of the work that we present. The clinical applications will be dealt with in more detail in Chapter 7.

The first step of the whole process is the internalization of ALA. Gaullier et al propose a study [8] about human and hamster cells treated with ALA and ALA aliphatic esters. In human cell lines, these authors find that the long-chained esters (C₆-C₈ in their study) induce the production of PPIX 30 to 150 times more efficiently than ALA, whereas short-chained esters (C₁-C₃) are less efficient than ALA. They mention that the ester yielding the highest production of PPIX *in vitro* is the hexylester. They also find that the PPIX formed by ALA-esters is the same as the species formed by ALA, thus indicating that the mechanism of ALA-esters mediated formation of PPIX probably goes through the initial de-esterification of the molecule by intracellular esterases. As will be seen, our results are fully consistent with those reported by these authors.

Kloek et al [9] also present a study about the *in vitro* behavior of ALA ester derivatives and the subsequent tests of the most promising ALA derivatives in an animal model. Whereas the study by Gaullier et al [8] and our study (section 6.2) only consider ALA monoesters and aliphatic esters (with the only exception of cyclohexylester in our study), these authors synthesized diesters as well as heterocyclic esters. All of the ALA derivatives are reported to induce the formation of PPIX more efficiently than ALA, including the short-chained esters, although this difference is not quite as marked for the methylester. Moreover, these authors report that smaller concentrations of ALA esters induce more PPIX than higher concentrations of ALA, thus demonstrating what we report - that the optimal concentration for the induction of PPIX is smaller for the ALA esters than for ALA. The authors also show that diesters do not induce the formation of PPIX in the cultured cells. This might be due to the fact that these molecules are too lipophilic and are trapped in the cellular membrane. Indeed, to efficiently cross the cellular membranes, a molecule should have both lipophilic and hydrophilic properties, a characteristic which might be lost in diesters.

In a study comparing the PPIX synthesized by normal and malignant urothelial cells when exposed to ALA, Steinbach et al [10] present the result that cancerous cells display fluorescence intensities 9 to 16 times higher than normal cells. For their experiments, these authors use the malignant cell line J82 that we also chose because of its relevance as a model for the transitional cell carcinomas of the urinary bladder. The authors also demonstrate a correlation between the concentration of ALA and the intensity of the fluorescence as well as a further correlation between the duration of exposure and the intensity of the fluorescence. Interestingly, whereas the latter is linear, the former reaches a plateau after a certain concentration (which appears to be cell-type dependent) of ALA, a result that we also observe *in vitro*. The authors did not, however, observe a decrease in the fluorescence intensity for even higher concentrations of ALA. This dependence on higher than optimal concentrations for the production of PPIX has been studied on a human dermal microvascular endothelial cell line (HMEC-1) by He et al [11]. The authors find a monotonic increase of the PPIX accumulation by the cells up to a certain concentration (optimal concentration) and then a decline for higher concentrations. In agreement with Steinbach et al [10], they find a time dependence of the PPIX accumulation. Similar results are also reported by Krammer et al [4]. Again, the authors show that the fluorescence intensity of the PPIX increases up to a certain concentration of ALA and then decreases for higher concentrations. These authors also investigate the pH dependence of the PPIX formation but do not give much detail about the preparation of the solutions at various pH. They find that below a pH of around 6, they do not detect the fluorescence of the PPIX. They also find that this fluorescence increases exponentially between pH 6 and 8. Our results, as will be seen, are in agreement with the observation that an acidic pH is detrimental to the fluorescence of PPIX, either because of a pH dependent precursor uptake or because the pH influences the formation of the PPIX or any other step in the biosynthetic process.

The field of ALA-related PD/PDT has undergone a huge expansion within the past years [3] and the results reported in the literature attest that it is likely to continue. Thus, more and more studies are necessary on *in vitro* and *in vivo* models or in the clinical practice. This also reflects the fact that there is room for improvement in the use of this method. Indeed, ALA is a highly hydrophilic

molecule and hence its penetration through cell membranes is relatively low. The production of the required PPIX is induced after the topical application of high concentrations of aqueous solutions and long exposure times. This is a problem for cells in culture since high concentrations of ALA damage the cells and reduce their viability. It is also a problem *in vivo*, in urological practice, for the patient undergoes a urological investigation after a relatively long instillation duration (4-6 hours in standard procedure). In the case of the clinical application of ALA solutions, it is also a problem of public health cost since a concentrated solution of ALA is of non-negligible cost. It was therefore necessary to test new substances with more lipophilic features than ALA while hopefully retaining its properties as a precursor of PPIX. A series of ALA-esters have therefore been synthesized by Dr. Norbert Lange and tested in our group.

The first step of the preclinical tests of these substances was to investigate their behavior on cells in culture. This study is reported in this chapter (section 6.2). It is in press and will be published in 2000 under the reference:

Pascal Uehlinger, Matthieu Zellweger, Georges Wagnières, Lucienne Juillerat, Hubert van den Bergh and Norbert Lange, '5-aminolevulinic acid and its derivatives: physical chemical properties and protoporphyrin IX formation in cultured cells', Journal of Photochemistry and Photobiology, B: Biology, 54(1), 72-80, 2000.

This study was the core subject of the final graduation work of Pascal Uehlinger to obtain the MSc in Biological Science at the University of Geneva, Switzerland. His work took place in the laboratory of Dr. Lucienne Juillerat and in the laboratory of Prof. Dr. Hubert van den Bergh between April 1998 and January 1999 under the supervision of Dr. Norbert Lange and Matthieu Zellweger. It has been summarized in Pascal Uehlinger's Master's Degree Thesis [12] following extensive preliminary work by Dr. Norbert Lange (synthesis of ALA ester derivatives, design of the study) and Matthieu Zellweger (setting-up of the cultured cells model, setting-up of the experimental protocol of ALA-derivatives-cell interaction).

6.1 The model

To systematically investigate the features of the ALA-esters we set up a cell culture model. The cell lines were chosen for their relevance as models for the tumors we investigate and for their availability. The cell lines were the following (all obtained from ATCC, Rockville, MD, USA):

a549	human lung carcinoma
t24	human urinary bladder transitional cell carcinoma
j82	human urinary bladder transitional cell carcinoma
BEAS-2B	immortalized human normal bronchial epithelium cells

The cells were grown following standard procedures for cell culture [13, see section 6.2, 'Materials and Methods' for details]. Upon reaching reproducible results of colonization in 48-well plates, we studied the interaction of these cell lines and the available ALA-esters.

In this part of our work, fluorescence was used to detect the formation of PPIX in the cell cultures. The 48-well dishes were placed into a warm (37°C) fluorescence multiwell plate reader and the fluorescence of the PPIX was excited at 409 ± 10 nm. It was then detected in the region of the maximal fluorescence emission (640 ± 20 nm). Strictly speaking, this was not the use of fluorescence *spectroscopy* as no actual spectrum was measured. However, the spectral characteristics of the PPIX have been utilized in this chapter (band detection of the PPIX). In Chapter 7, the emission spectrum of the PPIX in the human bladder tissue is presented.

References

1. 'Biochemistry', L. Stryer, Fourth Edition, W.H. Freeman and Company, New York, USA, 1995.
2. Kennedy, J., S. Marcus, R. Pottier, 'Photodynamic therapy (PDT) and photodiagnosis (PD) using endogenous photosensitization induced by 5-aminolevulinic acid (ALA): mechanisms and clinical results', *Journal of Clinical Laser Medicine and Surgery*, 14(5), 289-304, 1996.
3. Peng, Q., K. Berg, J. Moan, M. Kongshaug, J. Nesland, '5-aminolevulinic acid-based photodynamic therapy: principles and experimental research', *Photochemistry and Photobiology*, 65, 235-251, 1997.
4. Krammer, B., K. Uberriegler, 'In-vitro investigation of ALA-induced protoporphyrin IX', *Journal of Photochemistry and Photobiology, B: Biology*, 36, 121-126, 1996.
5. Cairnduff, F., M. Stringer, E. Hudson, D. Ash, S. Brown, 'Superficial photodynamic therapy with topical 5-aminolevulinic acid for superficial primary and secondary skin cancer', *British Journal of Cancer*, 69, 605-608, 1994.
6. Jichlinski, P., M. Forrer, J. Mizeret, Th. Glanzmann, D. Braichotte, G. Wagnières, G. Zimmer, L. Guillou, F. Schmidlin, P. Graber, H. van den Bergh, H.-J. Leisinger, 'Clinical evaluation of a method for detecting superficial transitional cell carcinoma of the bladder by light-induced fluorescence of protoporphyrin IX following topical application of 5-aminolevulinic acid: preliminary results', *Lasers in Surgery and Medicine*, 20, 402-408, 1997.
7. Kriegmair, A., R. Baumgartner, R. Knuechel, P. Steinbach, A. Ehsan, W. Lumper, F. Hofstädter, A. Hofstetter, 'Fluorescence photodetection of neoplastic urothelial lesions following intravesical instillation of 5-aminolevulinic acid', *Urology*, 44, 836-841, 1994.
8. Gaullier, J.-M., K. Berg, Q. Peng, H. Anholt, P. K. Selbo, L.-W. Ma, J. Moan, 'Use of 5-aminolevulinic acid esters to improve photodynamic therapy on cells in culture', *Cancer Research*, 57, 1481-1486, April 15th, 1997.
9. Kloek, J., G. Beijersbergen van Henegouwen, 'Prodrugs of 5-aminolevulinic acid for photodynamic therapy', *Photochemistry and Photobiology*, 64(6), 994-1000, 1996.
10. Steinbach, P., H. Weingandt, R. Baumgartner, M. Kriegmair, F. Hofstädter, R. Knüchel, 'Cellular fluorescence of the endogenous photosensitizer Protoporphyrin IX following exposure to 5-aminolevulinic acid', *Photochemistry and Photobiology*, 62(5), 887-895, 1995.
11. He, D., S. Behar, N. Nomura, S. Sassa, H. Lim, 'The effect of ALA and radiation on porphyrin/heme biosynthesis in endothelial cells', *Photochemistry and Photobiology*, 61(6), 656-661, 1995.
12. Pascal Uehlinger, 'Optimalisation de la production de PPIX par des cellules tumorales humaines en culture à partir de l'acide 5-aminolévulinique et de ses esters', Travail de diplôme, EPFL, Janvier 1999.
13. Dr Lucienne Juillerat, CHUV, personal communication.

5-Aminolevulinic acid and its derivatives: physical chemical properties and protoporphyrin IX formation in cultured cells.

Pascal Uehlinger¹, Matthieu Zellweger¹, Georges Wagnières¹, Lucienne Juillerat², Hubert van den Bergh¹ and Norbert Lange¹

¹Institute of Environmental Engineering, Swiss Federal Institute of Technology, EPFL, CH-1015 Lausanne; ²Institute of Pathology, CHUV Hospital, CH-1011 Lausanne, Switzerland.

Keywords: 5-aminolevulinic acid, 5-aminolevulinic acid esters, photodynamic therapy, fluorescence, protoporphyrin IX, ALA esters, lipophilicity, PDT.

ABSTRACT

Protoporphyrin IX (PpIX) is used as a fluorescence marker and photosensitizing agent in photodynamic therapy (PDT). A temporary increase of PpIX in tissues can be obtained by administration of 5-aminolevulinic acid (ALA). Lipophilicity is one of the key parameters defining the bioavailability of a topically applied drug. In the present work, octanol-water partition coefficients of 5-aminolevulinic acid (ALA) and several of its esters were determined to obtain a parameter related to their lipophilicity. The influence of parameters such as lipophilicity, concentration, time, and pH value on PpIX formation induced by ALA and its esters was then investigated in human cell lines of lung and bladder origins.

ALA esters were found to be more lipophilic as compared to the free acid. The optimal concentration (c_{opt} : precursor concentration, at which maximal PpIX accumulation was observed) was then measured for each precursor. Long-chained ALA esters were found to decrease the value of c_{opt} by up to two orders of magnitude as compared to ALA. The reduction of PpIX formation observed at higher concentration than c_{opt} was correlated to reduced cell viability as determined by measuring mitochondrial activity. Under optimal conditions, the PpIX formation rate induced by the longer chained esters was higher than that of ALA or the shorter chained esters. A biphasic pH dependence on PpIX generation was observed for ALA and its derivatives. Maximal PpIX formation was measured under physiological conditions (pH 7.0 – pH 7.6), indicating that further enhancement of intracellular PpIX content may be achieved by adjusting the pharmaceutical formulation of ALA or its derivatives to these pH levels.

Journal of Photochemistry and Photobiology, B: Biology, 54(1), 72-80, 2000

INTRODUCTION

The exogenously stimulated formation of intracellularly generated protoporphyrin IX (PpIX), a precursor of heme, is becoming one of the fastest developing areas in the field of photodynamic therapy and fluorescence photodetection (PD) of malignant and non-malignant diseases (see [1] and references therein). In most clinical and pre-clinical studies, systemic or topical application of 5-aminolevulinic acid (ALA) is used to temporarily increase the concentration of PpIX in the target tissues. Administration of ALA, a metabolic precursor in the biosynthetic pathway of heme, bypasses the negative feedback control exerted by heme on the enzymatic step in ALA synthesis. Although PpIX formation is present in nearly every nucleated cell, preferential formation and accumulation of this photosensitizer have been demonstrated in tissues known for a high cellular turnover. The main reason for a somewhat selective PpIX accumulation in the latter cell types is still not completely understood. Experimental evidence has been found that, in some tumors, the ferrochelatase activity is reduced, while the activity of the porphobilinogen deaminase is enhanced [2,3]. For historical reasons [4] and due to the ease of administration to the skin of both drug and light, the main applications of ALA mediated PpIX therapy are in dermatology. This modality is now in Phase III trials for the treatment of actinic keratosis and has also been employed clinically for the treatment of basal cell carcinoma. Recently, other medical fields namely Pulmonology [5], Urology [6-9], Gastroenterology [10], ENT [11], Gynecology [12], and Neurosurgery [13] have implemented this technique for the improved management of cancer. In addition to its tumor selectivity, the administration of ALA prevents prolonged cutaneous photosensitivity, one of the major drawbacks of some of the earlier photosensitizers [14].

Despite promising results, it appears that this methodology is open to quite significant improvement, in particular in the case of topically applied ALA. Since ALA is a hydrophilic molecule, its penetration through cellular membranes and into the interstitial space of tissues is low. Hence, ALA-induced PpIX formation is often limited to superficial tissue layers. Furthermore, PpIX formation shows considerable heterogeneity,

when ALA is applied topically. Both, inhomogeneous and limited tissue distribution results in non-efficient treatment of deeper lying or nodular lesions, even if light in the red region of the PpIX absorption spectrum is used [15,16]. Since deeper lying lesions are often not accessible by PDT, they are missed after topical application of ALA. Consequently, relatively high doses of ALA have to be applied over long periods of time, increasing the risk of complications [17,18].

Due to these drawbacks, PpIX-mediated PDT and diagnosis has recently been started with more lipophilic derivatives of ALA in order to enhance ALA's poor bioavailability. Several groups have shown that using such ALA prodrugs may enhance the PpIX concentration by up to two orders of magnitude as compared to the parent molecule [19-23].

Since lipophilicity is one of the key parameters, in the present study the octanol/water partition coefficient *P* of some alkyl esters has been determined as a measure related to this property. With the final goal to define clinical protocols with improved bioavailability of ALA, we investigated the impact of lipophilicity, pH value, concentration and duration of exposure of ALA and its derivatives on PpIX formation and cell viability. This was performed by means of fluorescence spectroscopy of PpIX using four different human cell lines. It was demonstrated that long-chained ALA derivatives and physiological pH values resulted in the highest relative fluorescence values. Using ALA derivatives, the choice of the optimal concentration of the PpIX precursor was shown to be of major importance for cell viability and maximal PpIX formation.

MATERIALS AND METHODS

Chemicals

ALA hydrochloride, ALA-methylester hydrochloride (*m*-ALA), (3-4,5-dimethylthiazol-yl)-2,5-diphenyl tetrazolium bromide (MTT), and *n*-octanol were purchased from Sigma (Fluka, Buchs, Switzerland). 0.1N NaOH was obtained from Merck (Darmstadt, Germany). Other ALA esters (Table 1) were synthesized in our laboratories following the procedure described recently by Kloek et al. [20].

Compound	R ¹	R ²	Mol. Mass [g/mol]	Abbreviation
ALA	H	H	167.6	ALA
ALA-methylester	CH ₃	H	181.6	m-ALA
ALA-ethylester	CH ₂ CH ₃	H	195.6	e-ALA
ALA-butylester	(CH ₂) ₃ CH ₃	H	223.8	b-ALA
ALA-hexylester	(CH ₂) ₅ CH ₃	H	251.8	h-ALA
ALA-octylester	(CH ₂) ₇ CH ₃	H	279.6	o-ALA
ALA-cyclohexylester	C ₆ H ₁₁	H	249.8	ch-ALA

Table 1: List of hydrochlorides of ALA and esters used for *in vitro* experiments (HCl • R²N-CH₂-CO-CH₂-CH₂CO-OR¹ = general structure).

Determination of physical chemical properties

The apparent partition coefficients (P) of ALA and its esters were determined in an octanol/buffer system at 21 °C. The aqueous phase was a 0.1 M phosphate buffered saline solution (PBS) of pH 7.4. The PBS solution and the octanol were mutually saturated before use. Twenty milligrams of the compound to be investigated were dissolved in 10 ml of the aqueous phase and an equal quantity of octanol was added. The mixtures were shaken for about 30 minutes and left for phase separation overnight at 4 °C. Absorption of both phases was measured with an UV-VIS absorption spectrometer (Cary 5, Varian, Australia) at 269 nm (see Figure 1a). The partition coefficients P were calculated according to:

$$P = C_{\text{oct}}/C_{\text{PBS}} = \text{abs}_{\text{oct}}/\text{abs}_{\text{PBS}} \quad (\text{I})$$

Where c_{oct} and c_{PBS} represent the solute concentration in the organic and the aqueous phase respectively, and abs_{oct} the absorption of the compound measured in the octanol and abs_{PBS} the absorption in the PBS solution (see Figure 1b). The use of low concentrations and storage at low temperatures impaired the formation of dimerization products. The absence of these products was confirmed by the absence of characteristic absorption bands in the absorption spectrum of the measured solutions.

Values of acidity constants of ALA and its esters were measured by means of potentiometric titration with a standard pH electrode (Bioblock, Frenkendorf, Switzerland). In brief, 20 mg of the corresponding drug was dissolved in 10 ml

of demineralized water and titrated with 0.1 N NaOH solution. The pH of the solution was plotted against the total volume added.

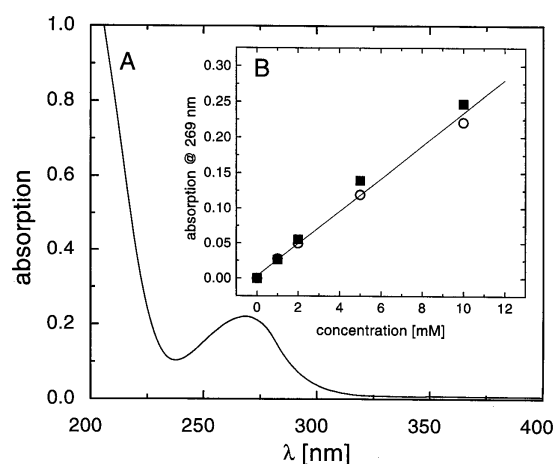


Figure 1: A) Absorption spectra of b-ALA (10 mM) in PBS B) Absorption at 269 nm dependent on b-ALA concentration (• b-ALA in octanol; ○ b-ALA in aqueous phase).

PpIX Fluorescence Measurements

For fluorescence measurements, cells, subcultured in 48-well dishes, were exposed to various concentrations of the corresponding PpIX precursor and transferred into a thermostated fluorescence multiwell plate reader (CytoFluor Series 4000, PerSeptive Biosystems, Framingham, MA, USA, excitation wavelength $\lambda = 409 \pm 10$ nm, detection wavelength $\lambda = 640 \pm 20$ nm). Correction for cell autofluorescence and other offset parameters was provided by five wells not exposed to the PpIX precursors. Reference was provided by 200 ml of a Rhodamine 6G (0.1 g/l) (Lambda Physik, Göttingen, Germany) solution

always present in one of the dishes. The absolute amount of PpIX produced per mg of protein content was estimated from a standard curve.

Cell Cultivation

All cell lines were from ATCC (Rockville, MD, USA) and grown as described. J82 and T24 cells were derived from human transitional cell carcinoma of the bladder, A549 cells from human lung carcinoma, and BEAS-2B cells were immortalized from normal human bronchial epithelium. Culture was performed in the presence of 10% fetal calf serum (FCS) and penicillin/streptomycin at 37°C and 6% CO₂ in a humid environment. For measurement purposes, the cells were subcultured in 48-well dishes (Costar 3548, Integra Biosciences, Cambridge, MA, USA) to give 10⁵ cells/well 72 hours prior to incubation with the ALA or one of its derivatives.

Determination of cell viability

The cell viability was tested by means of an MTT assay. This technique allows quantification of cell survival after cytotoxic insult by testing the enzymatic activity of the mitochondria. It is based on the reduction of the water-soluble tetrazonium salt to a purple, insoluble formazan derivative by the mitochondrial enzyme dehydrogenase. This enzymatic function is only present in living, metabolically active cells. The optical density of the product was quantified by its absorption at 540 nm using a 96-well ELISA plate reader (iEMS Reader MF, Labsystems, USA). MTT, 0.5 mg/ml, was added to each well five hours after exposure to ALA or its derivatives and incubated for 2 hours at 37°C. The medium was then removed and the cells were washed with PBS. For cell lysis and dissolution of the formazan crystals formed, 250 µl of isopropanol containing 1% 4N HCl was added, and the absorption of each residue was determined by using the plate reader at 540 nm. Absorbance of the solution from cells incubated with ALA or its derivatives was divided by the absorption of the solution from the control cell plates to calculate the fraction of surviving cells.

Concentration and Time Dependence of PpIX Formation

The influence of precursor concentration on the total PpIX amount formed was measured

by permanent incubation of the different cell lines with a given ALA derivative dissolved in PBS at pH 7.4. PpIX was measured three and six hours after drug exposure. Concentration dependent saturation of PpIX biosynthesis in A549 cell cultures was determined using different concentrations (0.1-2 mM) of h-ALA. Cells were incubated with a medium containing 5% FCS and fluorescence measurements were carried out every 30 minutes during 24 hours. The influence of the presence of FCS on the PpIX formation was examined by incubation of A549 cells with 0.8 mM solution of h-ALA containing no, 1%, and 5% FCS, respectively. In order to correct all data for background autofluorescence in each experiment six wells were incubated without any PpIX precursor.

Pharmacokinetic studies

PpIX formation in cells incubated with different derivatives of ALA was followed over a period of 5 hours. For this purpose, the cells were incubated with the corresponding PpIX precursor at its optimal concentration (as determined according to the above-mentioned procedure). Measurements of fluorescence intensity were taken every 15 minutes.

pH Dependence of PpIX Formation

The impact of initial extracellular pH was determined using solutions of ALA, h-ALA, and ch-ALA in sterile, isotonic NaCl (aq., 0.9%). The initial pH values, ranging between 5.5 and 8.5, were adjusted with 1N NaOH for ALA and 0.1N HCl for ALA derivatives. ALA and its derivatives were applied using concentrations inferior to their optimal concentration, typically one half of C_{opt}. Fluorescence intensity was measured immediately after incubation and again after 3 hours. Cell viability was tested as described in section 3.5.

RESULTS AND DISCUSSION

Physical Chemical Properties

Lipophilicity of ALA and its derivatives was assessed by measuring the apparent partition coefficient (P) of the compounds between octanol and a PBS solution of pH 7.4. Table 2 summarizes the obtained log P values. The results plotted in figure 2 show that it is possible to vary the lipophilicity of ALA by more than three orders of magnitude when

using ALA esters. The log P values of ALA and m-ALA are negative, representing the hydrophilic feature of these substances. Relative to ALA and m-ALA, all other esters are more lipophilic with positive log P values. Both ALA and its esters are highly protonated at pH 7.4 due to the 5-amino group. Therefore, the apparent partition coefficient may be dependent on the relative amount of uncharged molecules in the aqueous phase. The percentage of molecules with an unprotonated amino group can be calculated using the measured pK_a values (see Table 2). For the different derivatives, this percentage varies between 6 and 12%. The pK_{a1} and pK_{a2} values for ALA given in Table 2 are in good agreement with Novo et al. [24]. The deprotonation of the amino group in o-ALA results in a reversible precipitation of the product in aqueous solution at pH \sim 8 and at a concentration around 20 mM. Furthermore, cleavage of some esters occurs in basic (pH > 9) solutions (data not shown).

Systematic studies of Bridges et al. [25] with a series of homologue carbamates has shown a relative constant absorption rate for compounds with log P values ranging between 0.8 and 2.8. However, carbamates with log P values inferior to 0.8 have shown reduced bladder wall absorption. This suggests a higher tissue uptake for ALA esters containing two or more carbon atoms in their ester function.

Besides higher solubility of compounds with higher lipophilicity in creams and ointments, the data presented in Table 2 has additional impact for the use of ALA esters in dermatology. One of the principal functions of the skin, in particular the stratum corneum (SC), is to avoid the absorption of compounds which come in contact with the skin's surface. Using an approximation based on the analysis of 90 compounds [18], one can estimate the steady state permeability coefficient K_p of ALA

derivatives. It can be calculated that b-ALA will be transported about 50 times more efficiently into the skin than ALA while, using m-ALA, this uptake rate will only be doubled. However, the magnitude of P is important in terms of drug bioavailability. Too lipophilic substances may be accumulated in the SC, which consists primarily of free fatty acids, cholesterol, and ceramides. In order to obtain maximal flux across the entire skin, a balanced partition coefficient and good water and lipid solubility are required. Furthermore, the intrinsic solubility may be modified by co-diffusing formulation components.

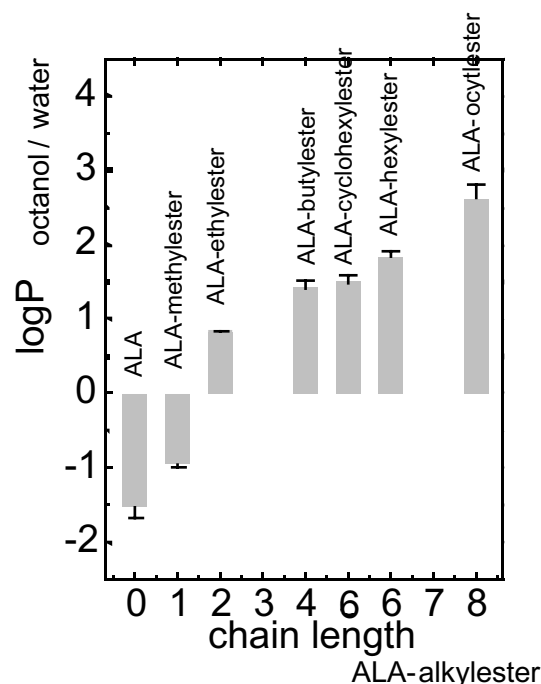


Figure 2: Derived log P values for ALA and its derivatives.

Additionally, one should bear in mind that facilitated drug uptake does not automatically mean higher PpIX formation. Esters of ALA must be cleaved by esterases before entering the ordinary biosynthetic pathway of heme. These enzymes may have a more or less

Compound	Log P	pKa ₁	pKa ₂
ALA	-1.51692	4.1 ± 0.1	8.7 ± 0.2
m-ALA	-0.94233	-	8.4 ± 0.3
e-ALA	0.84113	-	8.4 ± 0.2
b-ALA	1.42315	-	8.3 ± 0.1
h-ALA	1.83883	-	8.3 ± 0.3
o-ALA ^{a)}	2.6199	-	-
ch-ALA	1.49392	-	8.3 ± 0.2

Table 2: Log P and pKa values for ALA and its derivatives. P is the partition coefficient between octanol and aqueous buffer solution (pH 7.4, 21 °C) a) pKa₂ not measurable because of precipitation.

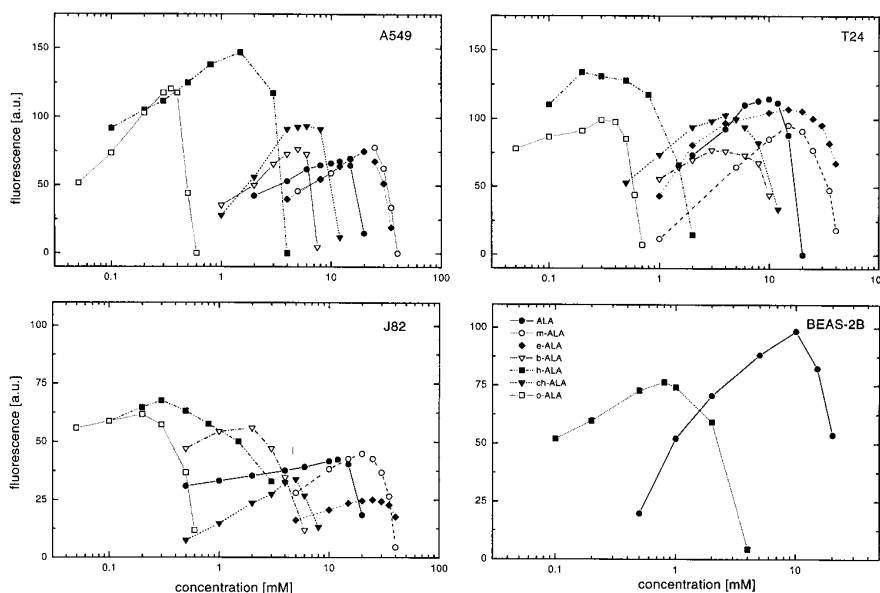


Figure 3: Concentration dependence of PpIX accumulation for four different human cell lines after 3 hours of incubation with ALA(-1-), m-ALA (-j-), e-ALA (-u-), b-ALA (-V-), h-ALA (-n-), ch-ALA (-t-), and o-ALA (-p-). (standard deviations (SD) have been omitted for the sake of clarity, see Fig. 6 for exemplary SD).

marked affinity to certain ester functions [21].

Influence of concentration on the PpIX Accumulation

The amount of porphyrin biosynthesis resulting from incubation of cells with ALA or its derivatives was determined by measuring the intensity of PpIX fluorescence.

All cell lines displayed the capability to produce PpIX when exposed to ALA or a

prodrug given in Table 1. Since, FCS has been shown to provoke efflux of PpIX in several cell lines [26], we incubated A549 cells with h-ALA during 5 hours. Under our experimental conditions no influence of FCS to the total PpIX amount generated has been found (see Table 3). The effect of concentration was assessed using ALA or ALA prodrug concentrations varying over two orders of magnitude.

As shown in Figure 3, there was a dose-dependent PpIX accumulation for each cell line and for each PpIX precursor used. The shape of the dose response curves was similar in each case. While PpIX generation is positively correlated up to an optimal prodrug concentration (c_{opt}), where the highest PpIX fluorescence levels occurred, PpIX generation decreases when exceeding this threshold concentration. The absolute value of the optimal concentration varies with the type of prodrug and cell line. Except for the BEAS-2B cell line, incubation with h-ALA resulted in the highest fluorescence levels.

In general, the c_{opt} for m-ALA and e-ALA was higher when compared to ALA. ALA esters with alkyl groups consisting of four carbon atoms or more (b-ALA, h-ALA, and o-ALA), showed their optimal PpIX formation at significantly lower c_{opt} values (Fig. 4).

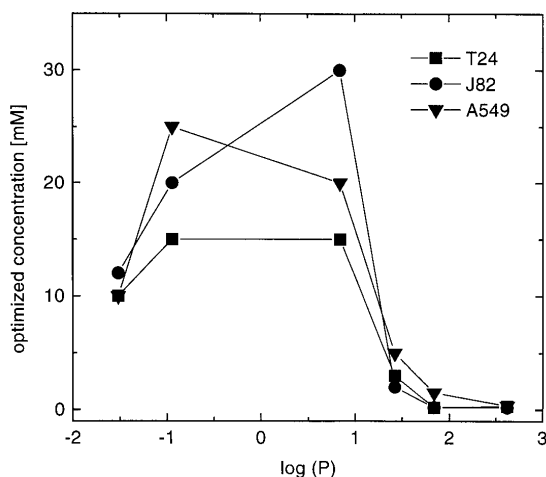


Figure 4: Concentration of ALA and its derivatives needed to induce maximal PpIX accumulation after three hours of incubation on A549 (-t-), T24 (-n-), and J82 (-l-) cell lines.

Furthermore, the bandwidth of the dose-response curves for these esters was always smaller as compared to ALA, m-ALA, or e-ALA (Fig.3), indicating that the choice of the optimal concentration is crucial in order to guarantee an optimal PpIX generation. Similar fluorescence intensity-concentration profiles were measured after 300 minutes of incubation (data not shown). Both, the position of c_{opt} as well as the bandwidth of the dose-response curves remained unchanged. The long-term influence of permanent drug exposure on the PpIX biosynthesis was tested by incubation

of A549 cells with h-ALA, which has shown the most promising results under our conditions with respect to its dose-response behavior (see Fig. 5).

FCS	PpIX fluorescence [a.u.]
0 %	680 ± 150
1 %	670 ± 170
5 %	680 ± 140

Table 3: Influence of FCS on the PpIX formation in A549 cells after 5 hours of incubation with 0.8 mM of h-ALA.

For concentrations smaller than c_{opt} PpIX formation increases in a moderate sigmoidal way with incubation time (Fig 5a). Under optimal conditions, continuously-increasing PpIX accumulation can be observed for 24 hours. Depending on the concentration the linear part of this curves ends between four and 15 hours and proceeds into a moderate plateau. For small concentrations the height of this plateau depends linearly on the concentration of h-ALA, whereas higher concentrations show a saturation of the PpIX biosynthesis (Fig 5b). This might indicate a saturation of the enzymatic functions. However, higher concentrations than c_{opt} end with less PpIX formed, although no reduced cell viability has been determined under these conditions (see below).

No direct correlation between $\log P$ and c_{opt} or the amount of PpIX produced can be noted from the data in the present work (Fig. 4). Excluding ch-ALA, however, a decrease of c_{opt} with increasing chain length for lipophilic ALA derivatives (starting from e-ALA) can be established.

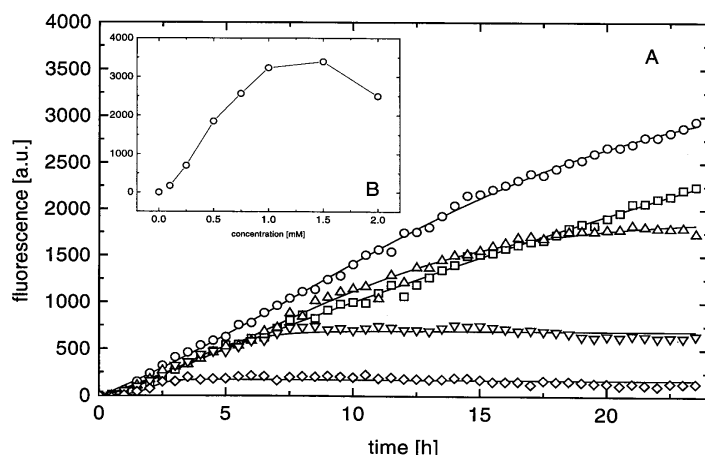


Figure 5: a) Pharmacokinetics of PpIX synthesis in A549 cells treated with different concentrations of h-ALA during 24 hours of permanent drug exposure. Concentrations: 2mM (-□-), 1.5 mM (-△-), 0.5 mM (-▽-), 0.25 mM (-◇-), 0.1 mM (-○-); b) PpIX formation after 24 hours as a function of concentration of h-ALA solutions (Description see materials and methods).

While long-chained derivatives ($C \geq 4$) showed lower c_{opt} values as compared to ALA, m-ALA as well as e-ALA seemed to be less efficient, although more lipophilic than ALA. The combination of two distinct processes may explain this behavior. While lipophilicity defines the transport of a drug across cell membranes, ALA esters must be cleaved by non-specific esterases prior to entering the biosynthetic pathway of heme. Kloek et al. [21] have shown with cell lysates that enzymatic hydrolysis is faster for long-chained esters than for short-chained esters. This information might have an impact for further synthesis of derivatives of ALA. Such new prodrugs should have a similar lipophilicity to h-ALA or o-ALA and the enzymatic cleavage of the ester function should also be optimized. Derivatives of ALA can be adapted to specific esterases of tumor cells for further improvement of the selectivity of ALA-induced PpIX.

Similar dose dependence characteristics have also been observed by other groups with ALA [27-31]. These groups found either a saturation of PpIX or a slight decrease of the resulting PpIX fluorescence with increasing ALA concentration. Gaullier et al. [22] observed an optimal concentration on different human and animal cell lines for long-chained ALA esters in the same order of magnitude as presented in this work. The more than twofold increase of the PpIX

formation rate with ALA esters as compared to ALA is in good agreement with the results we recently obtained from measurements on an organ culture model [19]. Recently, Kloek et al. [21] compared the performance of different ALA derivatives on human T-cell lymphoma cell lines. They found that ALA pentyl ester induced the highest PpIX levels in intact cells, while h-ALA and b-ALA have shown similar fluorescence intensities after 6 hours of incubation. However, in the course of their experiments, incubation was performed using equimolar concentrations for all derivatives. Hence, it might be possible that for long-chained alkyl esters the concentration was too high to produce large amounts of PpIX.

The relative rate of PpIX generation increases with increasing lipophilicity of the corresponding ALA ester from m-ALA to h-ALA, whereas comparable rates of h-ALA and o-ALA suggest a saturation of some enzymatic functions in the biosynthetic pathway within these time ranges. Taking into account c_{opt} , which was 10-100 times lower for long-chained ALA esters compared to ALA, it can be concluded that, using such compounds, the PpIX formation efficiency was enhanced by almost two orders of magnitude by simple chemical derivatization.

Since ALA is known to induce cytotoxic effects in cell culture [32-34], the PpIX accumulation observed was evaluated with respect to the cell viability after incubation with different concentrations of each PpIX precursor. It can be seen from figure 6 that the reduction of PpIX formation after incubation with drug doses higher than c_{opt} coincides with a reduced cell survival. This correlation was observed for all cell lines and prodrugs. Incubation with lower doses of ALA or its derivatives did not affect cell viability, as confirmed by the MTT test. From these experiments, it is obvious that only well-defined drug doses will improve the PpIX formation in clinical applications when using ALA esters instead of ALA.

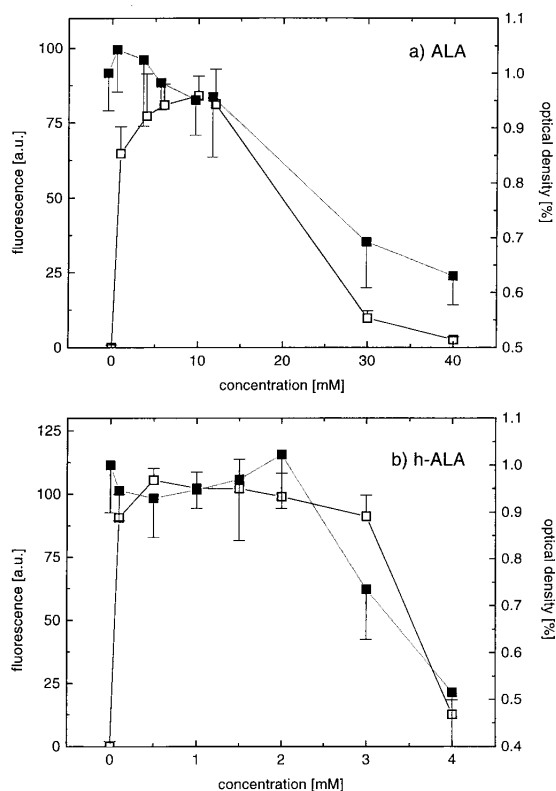


Figure 6: Correlation of PpIX fluorescence intensity ($-p-$) and mitochondrial activity test by means of an MTT test ($-n-$) in A549 cell for a) ALA and b) h-ALA (Description see materials and methods).

pH Dependence of the PpIX formation

It has been found that tumor tissues are generally more acidic than surrounding normal tissues. This is probably due to an overproduction of lactic acid and hydrolysis of adenosine triphosphate (ATP). Since this microenvironmental factor may influence PpIX generation, we incubated three cell lines with ALA, ch-ALA, and h-ALA solutions initially adjusted to pH values in the range between 5.5 and 8.5. In order to prevent saturation or cytotoxic effects provoked by the drug itself, concentrations inferior to c_{opt} ($c_{opt}/2$) were chosen. The values plotted in figure 7 indicate that optimal PpIX formation happens at physiological pH values of around 7.5 ± 0.5 . The total PpIX production approximately tripled at pH 7.4 compared to production induced at pH 5.5. Due to proton release to the non-buffered medium, the initial pH values decreased during incubation. While under alkaline this effect was more marked ($\Delta pH \sim 0.3$ / h at 8.5), the pH values under acidic conditions remained

nearly unchanged ($\Delta pH \sim 0.01$ / h at pH 6.5).

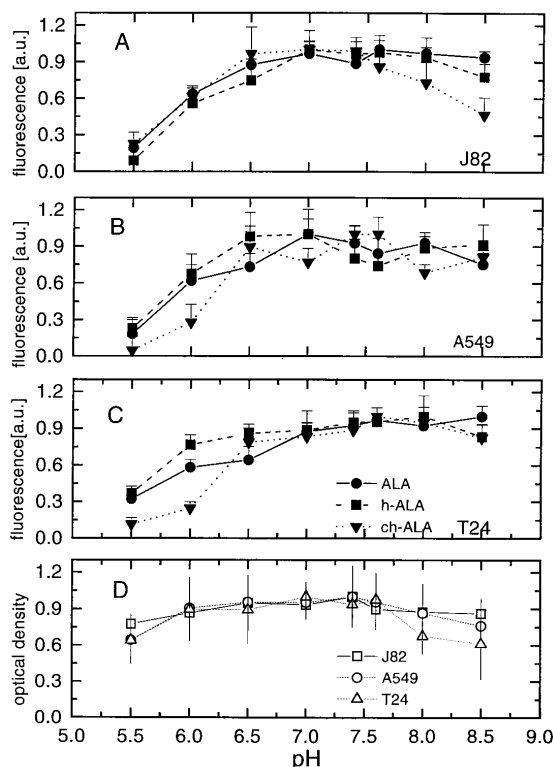


Figure 7: PpIX formation as a function of initial pH values in A) J82, B) A549 and C) T24 cell lines after 120 min of incubation with 0.1 mM h-ALA ($-n-$), 3.2 mM ch-ALA ($-t-$), and 5 mM ALA ($-l-$) solutions (Fluorescence values are normalized to the maximum of fluorescence).

Generally, PpIX production was more drastically reduced under acidic than under alkaline conditions, extending previously published results using ALA as a PpIX precursor [27, 35-36]. While the decrease of PpIX formation at higher pH values can be attributed to a reduction of cell viability, the decrease under acidic conditions can be attributed to either a pH-dependent drug uptake or a reduced enzymatic activity in the biosynthesis of heme. As has been shown, ALA uptake is regulated by a pH-dependent ion pump that is more active at pH 5.0 [37]. Hence, PpIX production would be expected to increase under acidic conditions. However, it is known that intracellular pH is also downregulated when extracellular pH falls below 6.5 [38]. This might inhibit the activity of enzymes involved in the biosynthetic pathway of heme, which have optimal activity between pH 7 and pH 7.5

[36]. A further indication for this pH-dependent intracellular process is given by the use of ALA esters since a major part of these amphiphilic compounds will not be taken up actively, as demonstrated by inhibitory tests [39].

From these experiments, it can be concluded that, for diagnostic as well as for therapeutic reasons, ALA formulations adjusted to physiological pH values should be applied. However, the instability of ALA implies the administration of ALA solution adjusted to lower pH values for the photodetection of early human bladder cancer in urology [6-9, 24]. Since these are physiological pH values for urothelial cells, the uptake of ALA may not be affected by solutions buffered to a pH of 5. In contrast, the production of PpIX under these conditions may be strongly dependent on this parameter. Novo and colleagues [24] have attributed the chemical instability of ALA to an irreversible dimerization of two parent molecules followed by an oxidation of the resulting dihydropyrazine derivative. Generally, the velocity of such bimolecular reactions is proportional to the product of the concentrations of the two involved reactants. Hence, under this assumption the drastic reduction of the concentration by a factor of about 20 [22] that is used with ALA esters enhances the stability of the corresponding solution by a factor of 400. This increase of stability opens the possibility for a further increase of PpIX formation after topical application of ALA derivatives by a simple adjustment of the pharmaceutical formulation to physiological pH values.

CONCLUSIONS

In summary, this study shows that using esters of ALA instead of ALA indicates a promising route to improve many clinical applications of PpIX-mediated PDT and fluorescence photodetection. The faster intracellular build-up of PpIX and the drastically reduced concentration relative to ALA enables treatments with significantly lower doses and shorter application times. Therefore, a significant decrease in costs should be associated with the use of such esters. Faster production of PpIX and hence shorter instillation times may play an important role for commercialization of this technique. Moreover, the enhancement of lipophilicity, which has been achieved by esterification, will result in deeper penetration of the drug into targeted lesions

after topical application and possibly also in a more homogenous distribution of the resulting photosensitizer. Therefore, more efficient PDT mediated by such prodrugs will be possible. No direct relationship between lipophilicity and total PpIX build-up has been found, indicating that two different processes, up-take and ester cleavage, are necessary for efficient PpIX formation. Moreover, long-chained esters should always be applied with lower doses compared to ALA. In most cell lines h-ALA has shown the most efficient PpIX formation.

A further enhancement of PpIX formation can be obtained by an adjustment of applied ALA and ALA prodrug formulations to physiological pH values.

ACKNOWLEDGMENTS

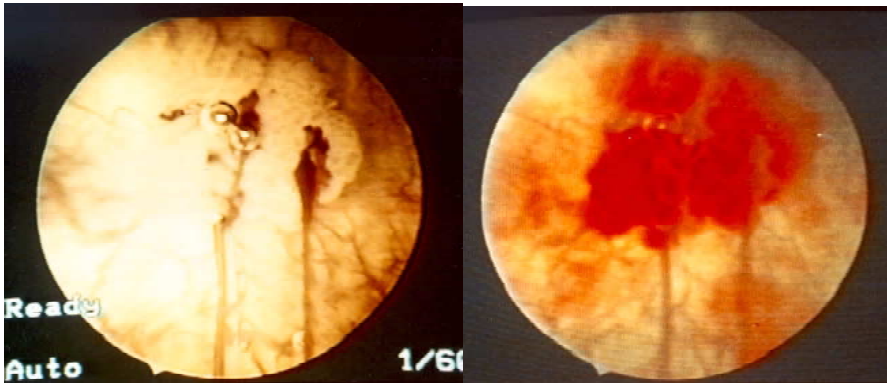
The authors would like to thank John-David Aubert (Department of Pulmonology, CHUV Hospital) for providing the BEAS-2B cell line and Pierrette Dessous l'église Mange (Department of Neuropathology, CHUV Hospital) for her assistance in maintaining the different cell lines. We gratefully thank Yann Berger and Reinhardt Neier (Institute of Chemistry, University of Neuchâtel) for the synthesis of ALA cyclohexyl ester. This work was supported in part of by the Swiss 'Fonds National' (Grant 20-50691), the Swiss National Priority Program in Optics, the Swiss Cancer Foundation, the Swiss Society for Multiple Sclerosis and the 'Fonds Vaud-Geneva' for their financial support. Norbert Lange would like to thank the Schering Research Foundation for providing his grant.

REFERENCES

- [1] Q. Peng, K. Berg, J. Moan, M. Kongshaug, J. M. Nesland, 5-Aminolevulinic acid-based photodynamic therapy: principles and experimental research, *Photochem. Photobiol.*, **65**, (1997), 235-251.
- [2] M. Kondo, N. Hirota, T. Takaoka, and M. Kajiwara, Heme-biosynthesis enzyme activities and porphyrin accumulation in normal and hepatoma cell lines of rats, *Cell Biol. Toxicol.*, **9**, (1993), 95-105.
- [3] P. Hinnen, F.W.M. De Rooij, M. L. F. van Velthuysen, A. Edixhoven, R. van Hillegersberg, H. W. Tilanus, J. H. P. Wilson, and P. D. Siersema, Biochemical basis of 5-aminolevulinic acid-induced

- protoporphyrin IX accumulation: a study in patients with (pre)malignant lesions of the esophagus, *Br. J. Cancer*, **78**, 679-682 (1998).
- [4] J. C. Kennedy and R. H. Pottier, Endogenous protoporphyrin IX, a clinically useful photosensitizer for photodynamic therapy., *J. Photochem. Photobiol., B: Biol.*, **14**, (1992), 275-292.
- [5] R. Baumgartner, R. M. Huber, H.-J. Schulz, H. Stepp, K. Rick, F. Gamarra, A. Leberig, and C. Roth, Inhalation of 5-aminolevulinic acid: a new technique for fluorescence detection of early stage lung cancer, *J. Photochem. Photobiol. B: Biology*, **36**, (1996), 167-174.
- [6] P. Jichlinski, M. Forrer, J. Mizeret, T. Glanzmann, D. Braichotte, G. Wagnières, G. Zimmer, L. Guillou, F. M. Schmidlin, P. Graber, H. van den Bergh, H.-J. Leisinger, Clinical evaluation of a method for detecting superficial transitional cell carcinoma of the bladder by light-induced fluorescence of protoporphyrin IX following topical application of 5-Aminolevulinic acid: Preliminary results, *Lasers Surg. Med.*, **20**, (1997), 402-408.
- [7] A. Kriegmair, R. Baumgartner, R. Knuechel, P. Steinbach, A. Ehsan, W. Lumper, Hostädter, F., Hofstetter, A. Fluorescence photodetection of neoplastic urothelial lesions following intravesical instillation of 5-aminolevulinic acid, *Urology*, **44**, (1994), 836-841.
- [8] M. Kriegmair, Baumgartner, R., Lumper, W., Waidelich, R., Hofstetter, A., Early clinical experience with 5-aminolevulinic acid for the photodynamic therapy of superficial bladder cancer, *British J. Urol.*, **77**, (1996), 667-671.
- [9] M. Kriegmair, Baumgartner, R., Knuechel, R., Stepp, H., Steinbach, P., Hofstaedter, F., Hofstetter, A., Detection of early bladder cancer by 5-aminolevulinic acid induced porphyrin fluorescence, *J. Urol.*, **155**, (1996), 105-110.
- [10] L. Gossner, M. Stolte, R. Sroka, K. Rick, A. May, E. G. Hahn, and C. Ell, Photodynamic ablation of high-grade dysplasia and early cancer in Barrett's esophagus by means of 5-aminolevulinic acid, *Gastroenterology*, **114**, (1998), 448-455.
- [11] K. F. M. Fan, C. Hopper, P. M. Speight, G. Buonaccorsi, A. J. MacRobert, and S. G. Bown, Photodynamic Therapy Using 5-Aminolevulinic Acid for Premalignant and Malignant Lesions of the Oral Cavity, *CANCER*, **78**, (1996), 1374-1383.
- [12] P. Wyss, M. Fehr, H. van den Bergh, U. Haller, Feasibility of photodynamic endometrial ablation without anesthesia, *Int. J. Gynec. Obstr.*, **60**, (1998), 287-288.
- [13] W. Stummer, S. Stocker, S. Wagner, H. Stepp, C. Fritsch, C. Goetz, A. E. Goetz, R. Kiefmann, and H. J. Reulen, Intraoperative detection of malignant glioma by 5-ALA-induced porphyrin fluorescence, *Neurosurgery*, **42**, 518-525 (1998).
- [14] G. Wagnières, C. Hadjur, P. Grosjean, D. Braichotte, J.-F. Savary, P. Monnier, and H. v. d. Bergh, Clinical evaluation of the cutaneous phototoxicity of a second generation photosensitizer for PDT: mTHPC, *Photochemistry and Photobiology*, **68**, (1998) 382-387
- [15] S. Grönlund-Pakkanen, Mäkinen, K., Talja, M., Kuusisto, A., Alhava, E., The importance of fluorescence distribution and kinetics of ALA-induced PpIX in the bladder in photodynamic therapy, *J. Photochem. Photobiol. B: Biol.*, **38**, (1997), 269-273.
- [16] A. Martin, W. D. Tope, J. M. Grevelink, J. C. Starr, J. L. Fewkes, T. J. Flotte, T. F. Deutsch, and R. R. Anderson, Lack of Selectivity of Protoporphyrin-IX Fluorescence for Basal-Cell Carcinoma After Topical Application of 5-Aminolevulinic Acid - Implications for Photodynamic Treatment, *ARCHIVES OF DERMATOLOGICAL RESEARCH*, **287**, (1995), 665-674.
- [17] J. Webber, D. Kessel, and D. Fromm, Side-Effects and Photosensitization of Human Tissues After Aminolevulinic Acid, *JOURNAL OF SURGICAL RESEARCH*, **68**, (1997), 31-37.
- [18] D. M. Fiedler, P. M. Eckl, and B. Krammer, Does Delta-Aminolevulinic-Acid Induce Genotoxic Effects, *JOURNAL OF PHOTOCHEMISTRY AND PHOTOBIOLOGY B-BIOLOGY*, **33**, (1996), 39-44.
- [19] A. Marti, N. Lange, H. van den Bergh, D. Sedmera, and P. Kucera, Optimisation of the formation and distribution of Protoporphyrin IX in the urothelium: an in vitro approach, *J. Urology*, (1999).
- [20] Kloek, J., Beijersbergen van Henegouwen, G. M. J., Prodrugs of 5-Aminolevulinic acid for photodynamic therapy, *Photochem. Photobiol.*, **64**, (1996), 994-1000.
- [21] J. Kloek, W. Akkermans, and G. M. J. Beijersbergen van Henegouwen, Derivatives of 5-aminolevulinic acid for photodynamic therapy: Enzymatic conversion into protoporphyrin, *Photochem. Photobiol.*, **67**, (1998), 150-154.
- [22] J.-M. Gaullier, Berg, K., Peng, Q., Anholt, H., Selbo, P. K., Ma, L.-W., Moan, J., Use of 5-aminolevulinic acid esters to improve photodynamic therapy on cells in culture, *Cancer Research*, **57**, (1997), 1481-1486.

- [23] N. Lange, P. Jichlinski, M. Zellweger, M. Forrer, A. Marti, L. Guillou, P. Kucera, G. Wagnières, and H. van den Bergh, Photodetection of early human bladder cancer based on the fluorescence of 5-aminolevulinic acid hexylester-induced protoporphyrin IX: a pilot study, *Br. J. Cancer*, (1999) 80(1/2), 185-193.
- [24] M. Novo, Hüttmann, G., Diddens, H., Chemical instability of 5-aminolevulinic acid used in the fluorescence diagnosis of bladder tumours, *J. Photochem. Photobiol B: Biology*, 34, (1996), 143-148.
- [25] J. W. Bridges, Sargent, N. S. E., Upshall, D. G., Rapid absorption from the urinary bladder of a series of n-alkyl carbamate: a route for the recirculation of drug, *British J. Pharmacol.*, 66, (1979), 283-.
- [26] S. Iinuma, S. S. Farshi, B. Ortel, and T. Hasan, A mechanistic study of cellular photodestruction with 5-aminolevulinic acid-induced porphyrin, *Br. J. Cancer*, 70, 21-28 (1994).
- [27] B. Krammer, K. Ueberriegler, In vitro investigation of ALA-induced protoporphyrin IX, *J. Photochem. Photobiol. B: Biology*, 36, (1996), 121-126.
- [28] J. Moan, G. Streckyte, S. Bagdonas, O. Bech, and K. Berg, Photobleaching of protoporphyrin IX in cells incubated with 5-aminolevulinic acid, *Int. J. Cancer*, 70, (1997), 90-97.
- [29] F. M. Rossi, Campbell, D. L., Pottier, R. H., Kennedy, J. C., Gudgin Dickson, E. F., In vitro study on the potential use of 5-aminolevulinic acid mediated photodynamic therapy for gynaecological tumours, *Br. J. Cancer*, 74, (1996), 881-887.
- [30] D. He, S. Behar, N. Nomura, S. Sassa, and L. H. W., The effect of ALA and Radiation on porphyrin/heme biosynthesis in endothelial cells, *Photochem. Photobiol.*, 61, (1995), 656-661.
- [31] S. L. Gibson, Haves, J. J., Foster, T. H., Hilf, R., Time-dependent intracellular accumulation of 5-aminolevulinic acid, induction of porphyrin synthesis and subsequent phototoxicity, *Photochem. Photobiol.*, 65, (1997), 416-421.
- [32] FRAGA CG, ONUKI J, LUCESOLI F, BECHARA EJ, DI MASCIIO P (1994). 5-Aminolevulinic acid mediates the in vivo and in vitro formation of 8-hydroxy-2'-deoxyguanosine in DNA. *Carcinogenesis* 15, 2241-2244
- [33] M. Hermes-Lima, How do Ca²⁺ and 5-aminolevulinic acid-derived oxyradicals promote injury to isolated mitochondria?, *Free Radical Bio. Med.*, 19, (1995), 381-390.
- [34] BERG K, ANHOLT H, BECH O, MOAN J (1996). The influence of iron chelators on the accumulation of protoporphyrin IX in 5-aminolevulinic acid-treated cells!. *Br. J. Cancer*, 74, 688-697.
- [35] C. Fuchs, Riesenber, R., Siebert, J., Baumgartner, R., pH-Dependent formation of 5-aminolevulinic acid-induced protoporphyrin IX in fibrosarcoma cells, *J. Photochem. Photobiol. B: Biology*, 40, (1997), 49-54.
- [36] L. Wyld, M. W. R. Reed, and N. J. Brown, The influence of hypoxia and pH on aminolevulinic acid-induced photodynamic therapy in bladder cancer cells in vitro, *Br. J. Cancer*, 77, (1998), 1621-1627.
- [37] M. Bermutz Moretti, C. G. S., C. Stella, E. Ramos, and A. d. C. Battle, Delta-aminolevulinic acid transport in *Saccharomyces cerevisiae*, *Int. J. Biochem.*, 25, (1993), 1917-1924.
- [38] E. Musgrove, M. Seaman, and D. Hedley, Relationship between cytoplasmic pH and proliferation during exponential growth and cellular quiescence, *Exp. Cell Res.*, 172, (1987), 65-75.
- [39] E. Rud, G. Gederaas, S. B. Brown, J. A. Holroyd, D. Vernon, A. Hogset, J. Moan, and K. Berg, Cellular uptake mechanisms for 5-aminolevulinic acid and 5-aminolevulinic methyl ester, 8th Congress of the European Society of Photobiology, Granada (Spain), Book of abstracts, S136, 85 (1999).



White-light and violet-light view of a carcinoma of the bladder following the instillation of an ALA hexylester solution.

Chapter 7

PPIX in the clinical context

7.1 Protoporphyrin IX in the clinical context

When in contact with ALA, the cells in vivo produce PPIX in the same way as cells in culture. Cancerous cells and, more generally, cells with a higher cellular turnover than normal cells, tend to synthesize more of it, thus leading to the build-up of a fluorescence emission contrast. This has been taken advantage of for the detection of lesions in several organs. Maybe the widest use of this technique in clinics has been reported for skin and urinary bladder affections. Indeed, the administration of an exogenous drug is easy in both organs and the delivery of the light is relatively straightforward.

In dermatology, ALA has been used topically to treat basal cell carcinomas (BCC) and squamous cell carcinomas (SCC) [1]. For the treatment of BCCs, ALA-PDTs give good results for superficial lesions [2,3], following the topical application of ALA in a cream formulation and the irradiation of the site, usually with light of 600+ nm wavelength. The results are reportedly good, ranging from 88% to 100% complete response [4-6] and similarly good for superficial SCCs [1].

However, this method of treatment is reported to be less efficient for nodular BCCs or SCCs [7-9]. The reasons for this limited clinical effectiveness are not fully understood but it is pointed out that the low depth of penetration of ALA into the lesions may well be at least one of the causes, as might be the heterogeneity of the lesions. One possibility to overcome this difficulty is to apply the ALA systemically. Peng et al [10] report that the systemic application (i.v., 25 mg/kg) of ALA for noduloulcerative BCCs can produce complete responses as well as a selectivity of the detected PPIX (tumor:normal ratio of 2 to 5) and point out the fact that the systemic application of ALA could be an optimal treatment since it is also well-tolerated. The oral ingestion of ALA reportedly seems to sometimes induce side-effects [11]. Indeed, these authors show that 40 mg/kg of ALA can induce mild (nausea, vomiting, neurological symptoms) or severe (vasodilatation and hypotension) side-effects, an observation that is confirmed by other authors [12], along with the confirmation that 40 mg/kg ALA p.o. is a way to induce full thickness PPIX fluorescence in all types of BCCs studied (including nodular lesions) and the observation that the build-up of PPIX fluorescence is faster in BCCs vs normal adjacent skin. These results seem to indicate that the PDT of non-melanoma skin tumors with systemic application of ALA could be more reliable than those with topical application of ALA.

The treatment of intraepidermal SCCs (Bowen's disease, squamous cell carcinoma in situ) by ALA PDT seems to be successful [5,6] as well as that of actinic keratosis [1]. It has also been successfully applied to the treatment of non-cancerous diseases of the skin such as psoriasis, among others.

Upon instillation of a solution of ALA in the urinary bladder, the urothelial cells produce PPIX. As stated above, the cancer cells tend to produce more PPIX than the normal cells thus making them easy to spot. This method allows the physician to localize and clearly delineate pre-/early cancerous lesions in the urinary bladder and to treat them. It is especially important as precancerous areas are thought to be responsible for the high rate of recurrence (50-75%) of superficial bladder cancer after endoscopic resection [2]. In a clinical study by Kriegmair et al [13], 68 patients with bladder cancer were investigated. The procedure used by these authors was to instill 50 ml of 3% aqueous solution of ALA into the bladder of the patients for at least 3 hours before the cystoscopy under violet light. The authors report that the demarcation of the tumors is clear-cut thanks to the intense red fluorescence of the PPIX in the lesions. They also present a sensitivity of 100% and a specificity of 68.5%, as well as no false negative results and no problematic side effect due to the ALA instillation. It should be noted, though, that these impressive figures are not achieved by random biopsy-taking but rather through a guided biopsy procedure. The good clinical results of the ALA instillation are confirmed in a subsequent study by Kriegmair et al [14]. Similar results are also reported by Jichlinski et al [15] in a study about 34 patients. As in the two preceding papers, the authors instill 50 ml of 3% aqueous ALA in the bladder of the patients during up to 4 hours and 45 minutes. They report that the fluorescence cystoscopy is twice as sensitive as white-light cystoscopy for the detection of invisible foci of carcinoma. In another paper, Jichlinski et al [16] take random biopsies and report a sensitivity of 82.9% and a specificity of 81.3% for superficial bladder cancer.

The ALA has been used in other organs for various cancerous and non-cancerous conditions, albeit with less width. We should mention the treatment of tumors of the aerodigestive tract [17, 18], the detection [19] and treatment [20] of endometriosis and the detection of early cancers in the lungs [21,22] and the detection of cancerous foci in patients suffering from Barrett's esophagus [23,24].

The good results that have been published should not offset the significant limitations of the method [25]. Indeed, for the urological application, the concentrations of the solutions of ALA (3% = 180 mM) are high and the instillation times are in the range of several hours. This means that further improvements of this method are essential. Several possibilities can be devised as ways to achieve this goal, namely to change the drug formulation (for example by using liposomes or an additional molecule to ease the transport through the membranes like DMSO), to use iron chelators to decrease the quantity of PPIX that is turned into heme or to use more lipophilic molecules that will penetrate the cellular membranes easier than the free acid [25].

Following the good results of both the study on cells in culture (Chapter 6) and the ex vivo tissue study [26], we decided to investigate the performance of the ALA-hexylester (h-ALA) in the urinary bladder in vivo. This clinical study is given in Section 7.3 and has been published as:

Norbert Lange, Patrice Jichlinski, Matthieu Zellweger, Martin Forrer, Alexandre Marti, Louis Guillou, Pavel Kucera, Georges Wagnières, and Hubert van den Bergh: 'Photodetection of Early Human Bladder Cancer Based on the Fluorescence of 5-Aminolevulinic Acid Hexylester-Induced Protoporphyrin IX: A Pilot Study', British Journal of Cancer, 1999, 80(1/2), 185-193.

This work took place in close collaboration between the urological endoscopy department of the CHUV hospital and the laboratory of Prof. Dr. Hubert van den Bergh under the supervision of Dr. Norbert Lange and Dr. Patrice Jichlinski. It includes preliminary work by Dr. Norbert Lange (synthesis of ALA ester derivatives, design of the study) and measurements in the clinics by Dr. Norbert Lange (documentation and supervision), Dr. Patrice Jichlinski and Dr. Alexandre Marti (endoscopical procedure, follow-up) and Matthieu Zellweger (fluorescence spectroscopy measurements and data processing).

7.2 Fluorescence spectroscopy of the PPIX in the bladder

In the course of the study presented in section 7.3, we measured the fluorescence spectra of several locations in the bladder of 25 patients with our optical fiber-based spectrofluorometer. The procedure is described in section 7.3, Materials and Methods. After the insertion of the optical fiber through the working channel of the rigid cystoscope, the light was switched off and the spectra were recorded. Typical spectra are presented in Fig. 7.1. We then assigned a spectrum to each location and correlated it to the histopathological status given by the biopsy. An example of the actual correlation of the spectroscopic data and the location is given in Fig. 7.2.

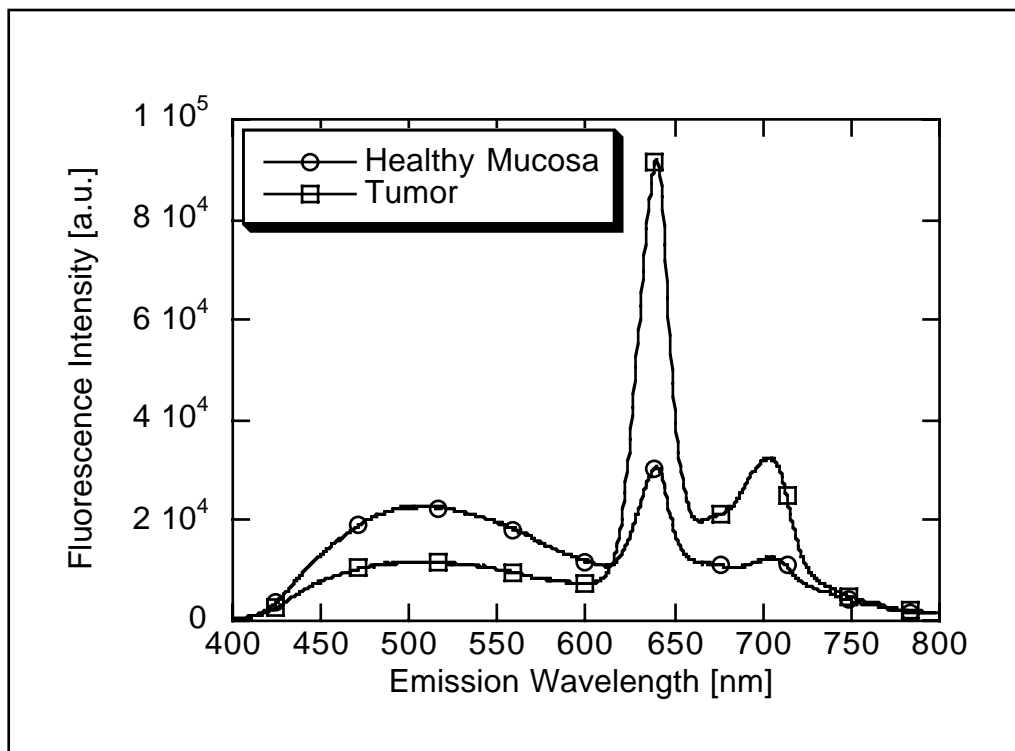


Figure 7.1: Fluorescence spectra recorded on healthy mucosa and on a tumor in the bladder of one patient after the instillation of ALA hexylester. The excitation wavelength is 405 nm.

In Fig. 7.1, the emission peaks of the PPIX are clearly visible in both spectra. However, the neoplastic tissue demonstrates a much more intense fluorescence of PPIX than the normal tissue. It is interesting to note that the autofluorescence contribution is smaller on the spectrum of the tumor than on the spectrum of normal tissue. Such decreases in autofluorescence intensity on neoplastic tissues in the bladder are reported [27,28]. Although we did not investigate this issue systematically, it is possible that it contributes to the modifications of our spectra. One point should be considered, though. Most of the autofluorescence that we observe in our spectra is due to the inherent fluorescence of the fiber. This is to be linked to the design of our measurement setup and its single fiber. Indeed, the autofluorescence generated within the fiber by the excitation light can easily be collected by the fiber on the way back to the detector. This is the reason why we did not study the autofluorescence in the bladder and why we could not do so. Another reason for the decrease observed in these spectra is the fiber tip. When the fiber is inserted into the working channel of the cystoscope, it is easily damaged. This can account for decreases in the signal due to the decreased collection efficiency of the fiber tip. All in all, our measurements are not able to produce reliable information about the modifications of the autofluorescence on neoplastic lesions in the bladder. This is not a tremendous loss, though, as ALA and its ester derivatives can induce a usable contrast in a reproducible manner.

Most of the results acquired by the author of this report during this study are presented in a condensed manner in section 7.3. Since his contribution mainly included the acquisition of spectroscopic data and the subsequent processing of these spectra, it seemed necessary to explicitly present some of this material. This has been done on p. 101 through a correlation of the pictures that were published in the article and the spectra that were measured by the author at these very locations. Three spectra are therefore presented. Each of them is correlated to one location and it can be seen that the amplitude of the PPIX peaks at 635 and at 690 nm is correlated to the fluorescence of the location. The whole study comprises 25 patients and, altogether, around 600 similar spectra.

This closes the part of our work dealing with ALA, its derivatives and PPIX. Recently, the interesting properties of ALA have been used more and more to mark selectively early neoplastic cells in many organs. The field of selective ALA marking of non-neoplastic lesions of different types is also developing fast. This should produce very interesting results and stimulate further improvements in this method of detection.

References

1. Peng, Q., T. Warloe, K. Berg, J. Moan, M. Kongshaug, K.-E. Giercksky, J. Nesland, '5-Aminolevulinic acid-based photodynamic therapy', *Cancer*, 79, 2282-2308, 1997.
2. Kennedy, J., S. Marcus, R. Pottier, 'Photodynamic therapy (PDT) and photodiagnosis (PD) using endogenous photosensitization induced by 5-aminolevulinic acid (ALA): mechanisms and clinical results', *Journal of Clinical Laser Medicine and Surgery*, 14(5), 289-304, 1996.
3. Fink-Puches, R., P. Wolf, H. Kerl, 'Photodynamic therapy of superficial basal cell carcinoma by instillation of aminolevulinic acid and irradiation with visible light', *Archives of Dermatology*, 133, 1494-1495, 1997.
4. Kennedy, J., R. Pottier, 'Endogenous protoporphyrin IX, a clinically useful photosensitizer for photodynamic therapy', *Journal of Photochemistry and Photobiology, B: Biology*, 6, 275-292, 1992.
5. Cairnduff, F., M. Stringer, E. Hudson, D. Ash, S. Brown, 'Superficial photodynamic therapy with topical 5-aminolevulinic acid for superficial primary and secondary skin cancer', *British Journal of Cancer*, 69, 605-608, 1994.
6. Svanberg, K., T. Andersson, D. Killander, I. Wang, U. Stenram, S. Andersson-Engels, R. Berg, J. Johansson, S. Svanberg, 'Photodynamic therapy of non-melanoma malignant tumours of the skin using topical d-amino levulinic acid sensitization and laser irradiation', *British Journal of Dermatology*, 130, 743-751, 1994.

7. Martin, A., W. Tope, J. Grevelink, J. Starr, J. Fewkes, Th. Flotte, Th. Deutsch, R. Anderson, 'Lack of selectivity of protoporphyrin IX fluorescence for basal cell carcinoma after topical application of 5-aminolevulinic acid: implications for photodynamic treatment', *Archives of Dermatological Research*, 287, 665-674, 1995.
8. Szeimies, R.-M., T. Sassy, M. Landthaler, 'Penetration potency of topical applied d-aminolevulinic acid for photodynamic therapy of basal cell carcinoma', *Photochemistry and Photobiology*, 59(1), 73-76, 1994.
9. Orenstein, A., G. Kostenich, Z. Malik, 'The kinetics of protoporphyrin fluorescence during ALA-PDT in human malignant skin tumors', *Cancer Letters*, 120, 229-234, 1997.
10. Peng, Q., T. Warloe, J. Moan, H. Heyerdahl, H. Steen, J. Nesland, K.-E. Giercksky, 'Distribution of 5-aminolevulinic acid-induced porphyrins in noduloulcerative basal cell carcinoma', *Photochemistry and Photobiology*, 62(5), 906-913, 1995.
11. Rick, K., R. Sroka, H. Stepp, M. Kriegmair, R.M. Huber, K. Jacob, R. Baumgartner, 'Pharmacokinetics of 5-aminolevulinic acid-induced protoporphyrin IX in skin and blood', *Journal of Photochemistry and Photobiology, B: Biology*, 40, 313-319, 1997.
12. Tope, W., V. Ross, N. Kollias, A. Martin, R. Gillies, R. Anderson, 'Protoporphyrin IX fluorescence induced in basal cell carcinoma by oral d-aminolevulinic acid', *Photochemistry and Photobiology*, 67(2), 249-255, 1998.
13. Kriegmair, A., R. Baumgartner, R. Knuechel, P. Steinbach, A. Ehsan, W. Lumper, F. Hofstädter, A. Hofstetter, 'Fluorescence photodetection of neoplastic urothelial lesions following intravesical instillation of 5-aminolevulinic acid', *Urology*, 44, 836-841, 1994.
14. Kriegmair, M., R. Baumgartner, R. Knuchel, H. Stepp, F. Hofstädter, A. Hofstetter, 'Detection of early bladder cancer by 5-aminolevulinic acid induced porphyrin fluorescence', *Journal of Urology*, 165, 105-110, 1996.
15. Jichlinski, P., M. Forrer, J. Mizeret, Th. Glanzmann, D. Braichotte, G. Wagnières, G. Zimmer, L. Guillou, F. Schmidlin, P. Graber, H. van den Bergh, H.-J. Leisinger, 'Clinical evaluation of a method for detecting superficial transitional cell carcinoma of the bladder by light-induced fluorescence of protoporphyrin IX following topical application of 5-aminolevulinic acid: preliminary results', *Lasers in Surgery and Medicine*, 20, 402-408, 1997.
16. Jichlinski, P., G. Wagnières, M. Forrer, J. Mizeret, L. Guillou, M. Oswald, F. Schmidlin, P. Graber, H. van den Bergh, H.-J. Leisinger, 'Clinical assessment of fluorescence cystoscopy during transurethral bladder resection in superficial bladder cancer', *Urological Research*, 25 [Supplement 1], S3-S6, 1997.
17. Gossner, L., M. Stolte, R. Sroka, K. Rick, A. May, E. Hahn, C. Ell, 'Photodynamic ablation of high-grade dysplasia and early cancer in Barrett's esophagus by means of 5-aminolevulinic acid', *Gastroenterology*, 114, 448-455, 1998.
18. Messmann, H., R. Knüchel, W. Bäuml, A. Holstege, J. Schölmerich, 'Endoscopic fluorescence detection of dysplasia in patients with Barrett's esophagus, ulcerative colitis, or adenomatous polyps after 5-aminolevulinic acid-induced protoporphyrin IX sensitization', *Gastrointestinal Endoscopy*, 49(1), 97-101, 1999.
19. Malik, E., A. Meyhöfer-Malik, D. Trutenau, H. Diddens, W. Küpker, K. Diedrich, 'Pilotstudie zur photodynamischen Diagnostik der Endometriose mittels 5-Aminolävulinsäure', *Geburtsh. u. Frauenheilk.*, 58, 420-425, 1998.
20. Wyss, P., M. Fehr, H. van den Bergh, U. Haller, 'Feasibility of photodynamic endometrial ablation without anesthesia', *International Journal of Gynecology and Obstetrics*, 60, 287-288, 1998.
21. Baumgartner, R., R. Huber, H. Schulz, H. Stepp, K. Rick, F. Gamarra, A. Leberig, C. Roth, 'Inhalation of 5-aminolevulinic acid: a new technique for fluorescence detection of early stage lung cancer', *Journal of Photochemistry and Photobiology, B: Biology*, 36, 169-174, 1996.
22. Huber, R., F. Gamarra, H. Hautmann, K. Häussinger, S. Wagner, M. Castro, R. Baumgartner, '5-aminolevulinic acid (ALA) for the fluorescence detection of bronchial tumors', *Diagnostic and Therapeutic Endoscopy*, 5, 113-118, 1999.

23. Messmann, H., R. Knuechel, E. Endlicher, T. Hauser, R.M. Seimies, F. Kullmann, W. Baeumler, J. Schoelmerich, 'Photodynamische Diagnostik gastrointestinaler Praekanzerosen nach Sensibilisierung mit 5-Aminolaevulinsaeure. Eine Pilotstudie', *Deutsche Medizinische Wochenschrift*, 123, 17, 515-521, April 1998.
24. Stepp, H., R. Sroka, R. Baumgartner, 'Fluorescence endoscopy of gastrointestinal diseases: basic principles, techniques, and clinical experience', *Endoscopy*, 30, 4, 379-386, May 1998.
25. van den Bergh, H., N. Lange, P. Jichlinski, 'ALA hexyl ester: a second-generation precursor for protoporphyrin IX in photodynamic therapy and photodetection of early bladder cancer', *Photodynamics News*, 2(1), 4-8, 1999.
26. Marti, A., N. Lange, H. van den Bergh, D. Sedmera, P. Jichlinski, P. Kucera, 'Optimalisation of the formation and distribution of protoporphyrin IX in the urothelium: An in vitro approach', *Journal of Urology*, 162, 546-552, 1999.
27. Anidjar, M., D. Etti, O. Cussenot, P. Meria, F. Desgrandchamps, A. Cortesse, P. Teillac, A. Le Duc, S. Avrillier, 'Laser induced autofluorescence diagnosis of bladder tumors: dependence on the excitation wavelength', *The Journal of Urology*, 156, 1590-1596, 1996.
28. Koenig, F., F. McGovern, H. Enquist, R. Larne, Th. Deutsch, K. Schomacker, 'Autofluorescence guided biopsy for the early diagnosis of bladder carcinoma', *The Journal of Urology*, 159, 1871-1875, 1998.

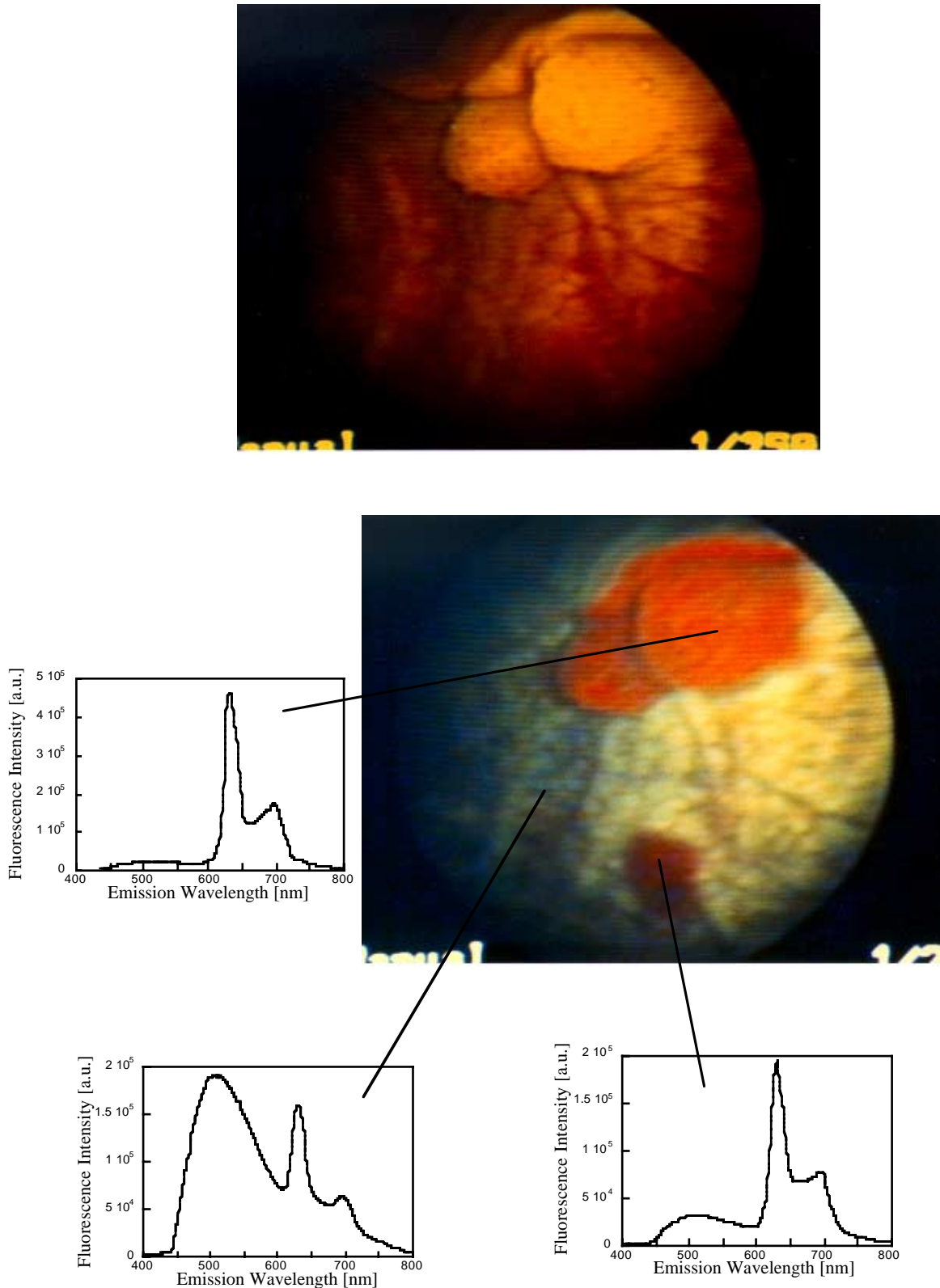


Figure 7.2: Endoscopic view under white light and under violet light of one site in the bladder of one patient. The fluorescence spectrum associated with each measurement zone is given. The respective scales of the spectra are comparable. These spectra are typical examples of the measurements acquired by the author of this report during the course of the clinical study presented in Section 7.3.

7.3

Photodetection of early human bladder cancer based on the fluorescence of 5-aminolevulinic acid hexylester-induced protoporphyrin IX: A pilot study.

Norbert Lange¹, Patrice Jichlinski², Matthieu Zellweger¹, Martin Forrer¹, Alexandre Marti², Louis Guillou⁴, Pavel Kucera³, Georges Wagnières¹, and Hubert van den Bergh¹

¹Institute of Environmental Engineering, Swiss Federal Institute of Technology (EPFL), CH-1015 Lausanne, ²Department of Urology, CHUV Hospital, CH-1011 Lausanne, ³Institute of Physiology, University of Lausanne, CH-1005 Lausanne, ⁴Department of Pathology, CHUV Hospital, CH-1011 Lausanne, Switzerland

Keywords: 5-aminolevulinic acid, 5-aminolevulinic acid hexyl ester, photodynamic therapy, fluorescence, protoporphyrin IX, human bladder cancer

ABSTRACT

Exogenous administration of 5-aminolevulinic acid (ALA) is becoming widely used to enhance the endogenous synthesis of protoporphyrin IX (PpIX) in photodynamic therapy (PDT) and fluorescence photodetection (PD). Recently, results have shown that the chemical modification of ALA into its more lipophilic esters circumvents limitations of ALA-induced PpIX like shallow penetration depth into deep tissue layers and inhomogeneous biodistribution and enhances the total PpIX formation. The present clinical pilot study assesses the feasibility and the advantages of a topical ALA ester-based fluorescence photodetection in the human bladder. In this preliminary study 5-aminolevulinic acid hexylester (h-ALA) solutions, containing concentrations ranging from 4-16 mM, were applied intravesically to 25 patients. Effects of time and drug dose on the resulting PpIX fluorescence level were determined *in vivo* with an optical fiber-based spectrofluorometer. Neither local nor systemic side-effects were observed for the applied conditions. All conditions used yielded a preferential PpIX accumulation in the neoplastic tissue. Our clinical investigations indicate that with h-ALA a twofold increase of PpIX fluorescence intensity may be observed using 20-fold lower concentrations as compared to ALA.

British Journal of Cancer, 1999, **80**(1/2), 185-193

INTRODUCTION

Fluorescence Photodetection (PD) and Photodynamic Therapy (PDT) are techniques currently under clinical assessment for both visualization and local destruction of malignant tumors and premalignant lesions. One drawback of these methods found with some photosensitizers is a more or less long-term cutaneous photosensitivity (Wagnières et al. (1998), Dougherty et al (1990)). A more recent strategy for administering photosensitizers involves 5-aminolevulinic acid (ALA) in order to stimulate the formation of protoporphyrin IX (PpIX) in situ. The exogenous (ALA) bypasses the negative feedback control from heme to ALA synthase that catalyzes the condensation of glycine and succinyl-CoA. Given in excess, exogenous ALA thus can result in a temporary accumulation of PpIX, in particular in cells with higher metabolic turnover. Since PpIX has fairly good photosensitizing properties (Cox et al. (1982)), Kennedy et al. (1990) proposed ALA as a possible photodynamic agent. Following this pioneering work, this treatment modality has been widely studied for various cancers (Kennedy et al. (1990); Peng et al. (1992); Svanberg et al. (1994)).

As well as for the PDT of malignant or premalignant lesions, ALA-induced PpIX is now being used for the detection of such lesions. This technique has been shown to work, among other applications, in urology, where easy instillation in the bladder, combined with the fact that this organ is readily accessible endoscopically, makes it an ideal object. Alongside classical techniques such as cytology or white-light examination, fluorescence photodetection by ALA-induced PpIX provides some advantages (Leveckis et al. (1994); Kriegmair et al. (1996); Jichlinski et al. (1997)). This inspection modality allows an exact mapping which pinpoints, with a high level of sensitivity and specificity, the locations of carcinoma in situ (CIS) as well as early stages of cancer-like dysplasias, which are normally difficult to recognize under white-light examination.

However, when using topically instilled ALA for the PDT of CIS and precancerous lesions, this modality appears to be limited by the amount of ALA that can enter the target cells or by the tissue penetration and the distribution of the resulting PpIX in the

targeted tissue. Almost all of these possible disadvantages accompanying the use of ALA can be ascribed to the physical-chemical properties of the molecule itself. Applied under physiological conditions, ALA is a zwitterion (Novo et al. (1994)). Because the lipid bilayer of biological membranes is relatively impermeable to charged molecules, the cellular uptake of ALA is shallow. Consequently, in order to increase the transport across cellular membranes, fairly high drug doses and increased administration times have to be used. This deficiency results in a low penetration depth (Loh et al. (1993); Warloe et al. (1992); Peng et al. (1995)) and an ALA-induced PpIX distribution which is not optimized for the PDT of the deep layers of nodular lesions in the urothelium (Iinuma et al. (1995); Chang et al. (1996)) after topical ALA application.

Systematic studies have shown that the modification of a drug to an ester, an amide or a urethane by the addition of a long-chained hydrocarbon improves penetration through biological barriers (Bridges et al. (1979); Jain (1987 a); Jain (1987 b)). After penetration into the cell, the ester derivative can then, for example, be hydrolyzed back to the free ALA by non-specific esterases. Recently, promising results were obtained with different alkylesters of ALA in vivo and in vitro (Peng et al. (1996); Kloek et al. (1996); Gaullier et al. (1997), Marti et al. (1998)). These groups demonstrated that the application of esterified ALA derivatives results in an up to 25-fold increase in PpIX fluorescence levels as compared to ALA.

This report covers initial clinical investigations with 5-Aminolevulinic acid hexylester hydrochloride (h-ALA)-induced fluorescence photodetection in the human bladder. Following our preclinical studies (Marti et al. 1998), we selected h-ALA from the multitude of possible ALA-alkylesters because it represents a good compromise between water/urine solubility and sufficient PpIX formation capacity at low doses. Furthermore, h-ALA has been shown to lead to a homogenous distribution of PpIX-related fluorescence over the entire urothelium in our pig bladder model (Marti et al. (1998)). In addition, it can be synthesized simply from ALA and hexanol (Kloek et al. (1997)). The goal of this clinical pilot study was to test h-ALA as a potential candidate for improving both the PD and PDT in the

urinary bladder. Therefore, topical application of h-ALA should result in higher PpIX formation than is the case with the same amount of ALA. It should enable shorter times between instillation and examination and lower drug concentrations while retaining the outstanding selectivity. This work presents a preliminary optimization of h-ALA-induced PpIX in respect to the resulting fluorescence intensities. Both the influence of the concentration and instillation time of h-ALA solutions on the total amount of PpIX were determined in vivo by the use of an optical fiber-based spectrofluorometer.

MATERIALS AND METHODS

1. Patients

25 patients (7 women and 18 men, 4 cases of ordinary ALA and 21 cases of h-ALA) have been involved in this first study conducted since August 1997. The mean age was 70 years, covering an age range of between 44 and 85. Local ethical committee approval was granted for this study, and written consent was obtained in each case.

2. Preparation and Administration of 5-Aminolevulinic Acid (ALA) 5-Aminolevulinichexylester Hydrochloride (h-ALA)

ALA (99%) was purchased from Merck

Patient no.	Concentration [mM]	Instillation time [h]	Resting time [h]	Fluorescence signal [r. u.]
1	4	2	-	16.2
2	4	2	-	11.2
3	4	4	-	34.5
4	4	4	-	20.5
5 ^{b)}	8	2	-	22.1
				38.4
6	8	2	-	36.2
7	8	2	-	46.7
8	8	2	-	-
9 ^{b)}	8	2	2	151.1
				102.0
10	8	2	2	115.8
11	8	2	2	147.5
12	8	4	-	66.4
13	8	4	-	72.6
14	8	4	-	63.4
15	8	4	-	73.8
16	8	4	-	94.4
17	8	4	-	77.1
18	8	4	2	102.7
19	8	4	2	95.0
20	16	2	-	15.8
21	16	2	-	16.7
22	180 ^{a)}	4	2	54.0
23	180 ^{a)}	4	2	43.6
24	180 ^{a)}	4	2	46.2
25	180 ^{a)}	4	2	45.3

Table 1: Experimental instillation conditions used in the first clinical trials with h-ALA and normalized fluorescence levels on papillary tumors (pTa G2) obtained by normalization to reference cuvette. ^{a)} Instillation of the 180 mM solution of ALA. ^{b)} Patient with two papillary tumors.

(Darmstadt, Germany). Other chemicals (thionyl chloride (99%) and 1-hexanol 99.9%) used for the synthesis of h-ALA were ordered from Fluka Chemie AG (Buchs, Switzerland) and were used without further purification.

The synthesis described here is a slight modification of the methods reported recently (Takeya (1992) and Kloek et al. (1996)). In brief, 3.5 ml of thionyl chloride were added drop by drop under stirring to an excess (~10 ml) of 1-hexanol cooled on ice in an argon atmosphere. The solution was stirred for a further 30 minutes to bring the reaction to completion; after warming up to room temperature, 2.5g of ALA ($M_r = 167.6$ g/mol) were added to the solution. The suspension was then stirred overnight at room temperature under argon. The final phase of the reaction was controlled on-line by thin layer chromatography (TLC) (TLC foils, Schleicher & Schuell, Merck, Darmstadt, Germany) in $\text{CH}_2\text{Cl}_2/\text{MeOH}$ (9:1) stained by KMnO_4 ($R_f = 0.6$). Once the reaction was complete, the solvent and hexylchloride were removed under reduced pressure (~ 0.5 torr). The viscous residue was dissolved in warm methanol. Then a small amount of methanol was evaporated until the first crystals of the reaction product appeared. A small quantity of diethylether was added and h-ALA was allowed to crystallize on ice. This dissolving and recrystallizing procedure was then subsequently repeated until only one spot was recognized on the TLC, yielding 80-90% of h-ALA ($M_r = 251.8$ g/mol) as a white powder. The product was characterized by proton nuclear magnetic resonance ($^1\text{H-NMR}$) with a 400 MHz (Bruker, Germany) spectrometer and identified as 5-aminolevulinic acid hexylester hydrochloride. The purity (> 95%) was further verified by high performance liquid chromatography (HPLC) with UV/VIS detection at 270 and 350 nm respectively (data not shown). No other products were observed.

The ALA solutions were administered in accordance with standard protocol used in Lausanne's CHUV Hospital (Jichlinski et al. (1997)). In brief, 1500 mg of ALA were dissolved in 38 ml of sterile water. Five ml of phosphate-buffered saline (PBS) were added and the pH was adjusted with a further 7 ml of aqueous sodium hydroxide

(1N) to a value of 5.3. This solution with a concentration of 180 mM of ALA was sterilized by filtration through a Millipore filter (Millipore, Millex GS 0.22 μm) and stored at -18°C one day before measurements were conducted. The solution was instilled into patients' bladders using a 16 French Foley catheter six hours prior to photodetection. Patients were asked to retain the solution for four hours. Their bladders were evacuated two hours prior to treatment.

Depending on the prodrug concentration to be applied, 50-200 mg (i.e. 4-16 mM) of crystalline h-ALA were dissolved in 35 ml of water. Then 13 ml of PBS were added to the aqueous solution and adjusted with 0.1 N HCl to give the same pH value of 5.3. The solutions were instilled as described above. Table 1 summarizes the different conditions under which ALA and h-ALA were applied. All patients treated with ALA (4 cases) and some instilled with h-ALA (5 cases) had a supplementary resting time of two hours after being exposed to the drug solution.

3. Procedure

3.1. Bladder inspection under white-light illumination

Prior to further treatment or measurement, the actual status of the bladder was documented under white-light illumination. The frame accumulation color CCD camera (Storz, Tuttlingen, Germany), connected to a video recorder (JVC, Japan) and an RGB Monitor (Sony, Japan) was plugged directly into the ocular of a 23.5 French cystoscope (Storz PDD, Tuttlingen, Germany) to record the standard endoscopic color image.

3.2. Fluorescence Spectroscopy

Fluorescence emission spectra were recorded with an optical fiber-based spectrofluorometer based on a Peltier cooled CCD coupled to a spectrograph (Cromex 250, SI Instruments, Germany). The experimental setup is shown in Figure 1. Arranged on a trolley, the whole setup can be easily transported. Excitation light ($\lambda_{\text{ex}} = 405$ nm) from a 75W high-pressure Xenon-lamp (UXL-75 XE, Ushio Inc., Japan) was spectrally resolved by a quarter meter monochromator (Chromex 250, SI Instruments, Germany) with a bandwidth of 5nm and an excitation filter, SCHOTT BG3 (Schott AG, Mainz, Germany), mounted on a filter wheel. A stepper motor (SMC 100, Princeton Instruments Inc., USA) controlled

this excitation filter wheel, which was equipped with different low-pass filters installed to purify the excitation light.

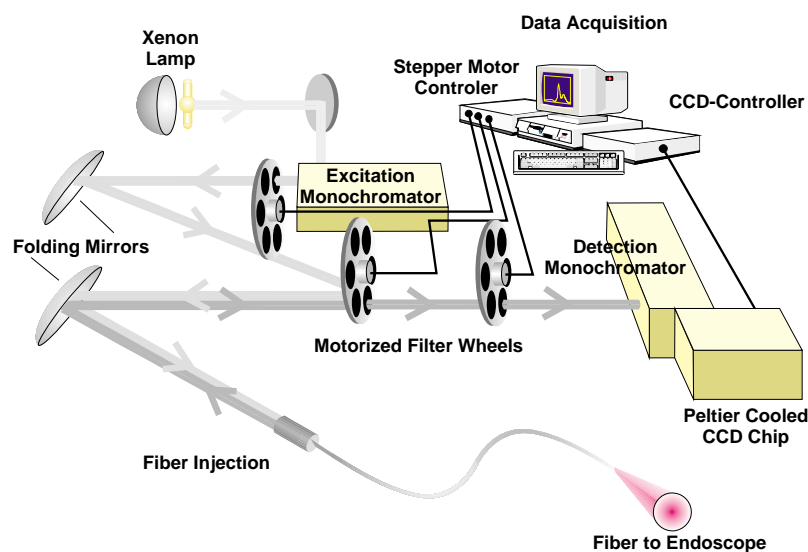


Figure 1: Schematic view of the optical fiber-based spectrofluorometer.

Fully reflective mirrors and a dichroic mirror (Reynard DC 450 (Reynard, USA)), mounted on a second filter wheel, were used to feed the light into a 600 μm core silicone-clad silica fiber with perpendicular polished end-faces. Excitation energy measured at the distal end of the fiber tip was determined with a calibrated power-meter (Optical Power Meter 840, Newport, USA). Fluorescence emitted by any sample was collected with the same fiber and separated from the excitation light by the dichroic optics described above. A long-pass filter (Reynard FG 455) mounted on a third filter wheel made further spectral separation, virtually eliminating all reflected excitation light prior to acquisition. This filter setup allows the acquisition of fluorescence emission spectra between 455-900nm. Detection based on this combination enables fast data acquisition combined with a low level of noise. The whole setup and data acquisition was controlled by a 486 personal computer using CSMA software (SI Instruments GmbH, Germany).

An aqueous solution of Rhodamine B ($c = 1 \cdot 10^{-6}$ mol/l) in a 10 mm quartz cuvette was used as a reference. Emission spectra of the reference were recorded before and after each measurement. All measurements were normalized to the peak value of the reference

to give comparable results corrected for day-to-day fluctuations of the excitation light energy or detection pathway alignment.

After inspection of the bladder under white light, the distal end of the fiber was introduced via the biopsy channel of the cystoscope. A background measurement was performed in the center of the bladder to allow the correction of the spectra for parasitic light and fluorescence generated by the fiber itself. Then the physician brought the distal end of the fiber directly into contact with the bladder wall.

3. 3. Bladder inspection under violet-light illumination

After measurement of the fluorescence spectra (see below) of healthy, cancerous and suspicious areas in the bladder, the camera was equipped with a long-pass filter ($\lambda > 520$ nm, Wratten filter No. 12, Kodak, Rochester, USA), positioned between the ocular of the cystoscope and the CCD-Chip. A footswitch allows the physician to place a bandpass filter (380-450 nm) in front of the 300 W Xenon-arc lamp (Storz, Tuttlingen, Germany) to give about 150 mW of violet light at the end of the cystoscope. Excitation with violet light generated a visible pale-green autofluorescence of the healthy mucosa. As a result of the absorption of autofluorescence, the blood vessels of the lamina propria appear somewhat darker. Filtration of the light below 520 nm allows these sites to be distinguishable from zones containing high PpIX concentrations, appearing in a clear, bright, fluorescing red. To improve the fluorescence images, the camera was switched into frame accumulation mode for enhanced sensitivity. The integration times ranged from one-eighth to one-half of a second, depending on observation distance.

3. 4. Biopsy sampling and pathology

Prior to transurethral resection of the bladder wall (TURB), a total number of 109 biopsies from fluorescent and non-fluorescent areas (average 5.2/patient; guided by light-induced fluorescence after excitation at 405 nm) were taken from the patients treated with h-ALA

solutions. Macroscopic fluorescence findings and locations were documented for each biopsy. All samples were sent for histopathological examination. The urothelial carcinomas were graded and staged according to the World Health Organization (W.H.O.) 1973 classification (Mostofi et al. (1973)) and the UICC/AJC 1992 system (UICC-TNM (1992)) respectively. Flat intraepithelial neoplastic lesions were graded according to the criteria of Nagy et al. (1982) and classified as grade 1 (mild dysplasia), grade 2 (moderate dysplasia), grade 3 (marked dysplasia) and carcinoma in situ.

RESULTS

Macroscopic Findings

All aqueous solutions of h-ALA stayed clear and colorless until use. Neither systemic nor local reactions following the examination with both h-ALA and ALA were observed under the conditions used in this study. Even the highest drug dose administered (16 mM) of h-ALA was well tolerated. h-ALA-induced synthesis of PpIX was observed in each patient. All papillary and planar tumors, also visible under white-light cystoscopy, showed bright red fluorescence. This red fluorescence was found to demarcate the outline the urothelial lesions with high precision. Using the violet light of the filtered Xenon arc lamp, it was possible to perform both fluorescence-guided biopsies as well as accurate resections of targeted tissues. Qualitatively, all conditions tested resulted in a clearly visible contrast between healthy and diseased sites of the bladder

wall.

Figure 2 demonstrates the advantageous use of h-ALA-induced PpIX for the fluorescence diagnosis of human bladder cancer. The two pictures show a sequence of a white-light (Fig. 2a) and a violet-light (Fig. 2b) examination after instillation of 8 mM of h-ALA over a period of two hours (Patient No. 10). White-light illumination shows two papillary tumors (pTa G2) situated below the air bubble of the bladder under investigation. Fluorescence photodetection of the same area (Figure 2b) indicates a further lesion (flat papillary tumor (pTa G2)) which is barely detectable under white light.

Fluorescence Findings and Histopathological Diagnosis

A total of 109 biopsies were taken under light-induced fluorescence from patients after instillation with h-ALA solutions. The correlation between the fluorescence findings and the histopathological analysis is summarized in Table 2. Thirty-two tissue samples were excised from healthy areas of the bladders investigated, containing eight samples, which were considered to be fluorescent. Histopathological diagnosis of the latter samples indicates the reasons for these 'false positive' responses. All these specimens showed tissular structures known for a higher cellular turnover, e.g. metaplasias, hyperplasias, chronic inflammation, or scar formation. In total, only six of the 77 biopsies, taken from malignant and premalignant sites, were not

Histopathological findings	Total number of biopsies	Fluorescence positive	Fluorescence negative
healthy mucosa	28	5	23
Metaplasia	1	1	-
Hyperplasia	3	3	-
Dysplasia G1	12	10	2
Dysplasia G2	5	3	2
Dysplasia G3	2	2	-
CIS	11	9	2
pTa G1	8	8	-
pTa G2	14	14	-
pTa G3	19	19	-
pT1 G2-G3	4	4	-
pT2a	2	2	-
Total	109	80	29

Table 2: Correlation between histopathological finding and fluorescence diagnosis following h-ALA instillation.

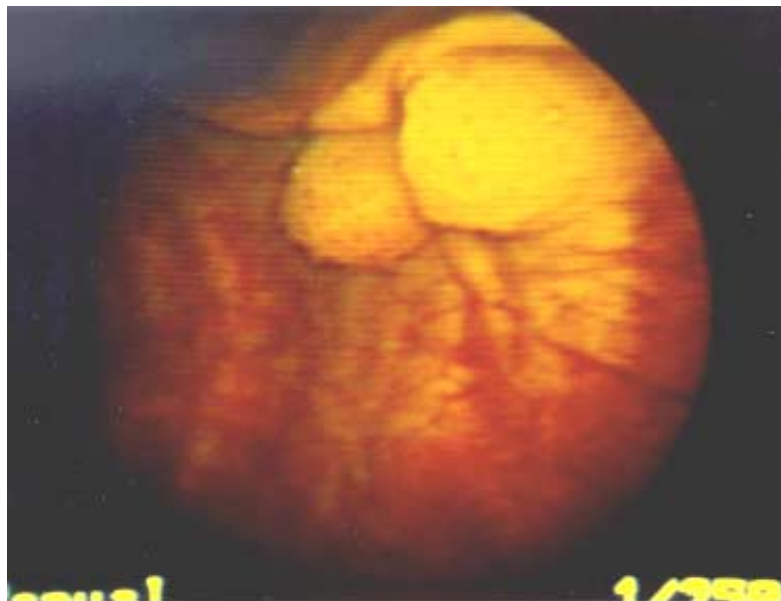
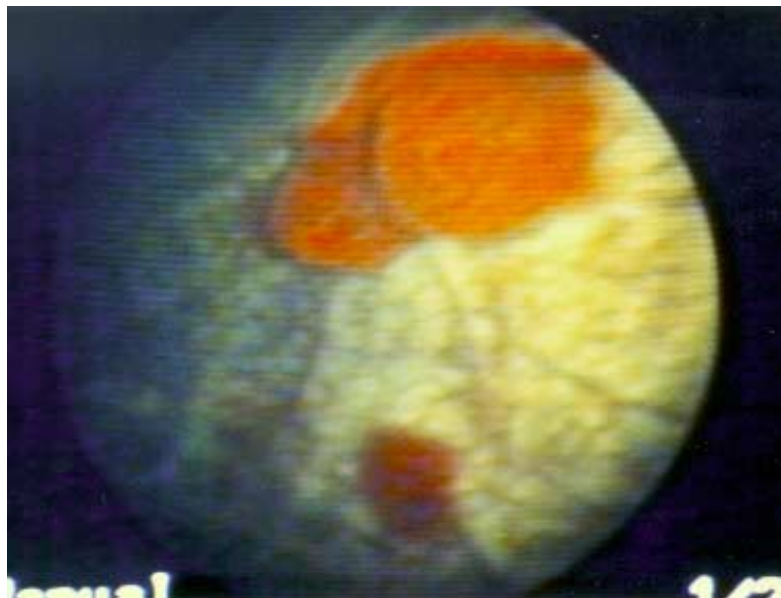
A**B**

Figure 2: Endoscopic view of a flat papillary tumor (pTa G2) after 2 hours of h-ALA exposure (description see text) under: 2a) white-light; 2b) violet-light examination.

fluorescing.

Three of these 'false negative' responses can be explained by non-optimized conditions with regard to the concentrations of h-ALA applied (two moderate dysplasias; Patient No. 4) as well as non-optimal incubation times (CIS; Patient No. 1). A further CIS was missed (Patient No. 13) probably due to an unusually long period of white-light illumination preceding photodetection, resulting in the photobleaching of PpIX. Without exception, histopathologically-

staged pTa G1 or higher samples were found by fluorescence photodetection.

Fluorescence Spectroscopy

Fluorescence emission spectra were measured on a total number of 24 patients (20 h-ALA, 4 ALA) (Table 1). ALA and h-ALA-induced porphyrins were excited at 405 nm on both healthy and malignant areas in the human bladder. The emission from the urothelial surface was spectrally resolved between 450 and 800 nm. A comparison of the emission spectra after ALA and h-ALA exposure is plotted in Figure 3. The total fluorescence intensity is normalized to the reference. As shown in this figure, the characteristic emission bands of PpIX at $\lambda = 635$ nm and $\lambda = 708$ nm after excitation in the Soret Band are clearly visible. According to the spectral shape, the fluorescence is attributed to PpIX. In none of the spectra recorded in vivo, an indication of porphyrins other than PpIX could be found. Depending on the duration of white and violet-light examinations before fluorescence measurements, a peak, attributed to a PpIX photobleaching product, of around 665-675 nm appeared (Fig. 3a, dotted line). The appearance of this supplementary fluorescence peak results in a line broadening because of overlapping fluorescence emission peaks and may suggest some degree of

heterogeneity. In addition to the fluorescence emission spectra recorded on a papillary tumor pTa G2 after four hours of h-ALA exposure, the corresponding spectra obtained on a healthy area were plotted (Fig. 3a, dashed line). From these spectra, it can be seen that the healthy mucosa's autofluorescence of around 513 nm exceeds the two typical fluorescence peaks of PpIX at 636 nm and 708 nm. All samples taken from sites with these fluorescence characteristics were confirmed as healthy after histopathological examination.

Evaluation of all fluorescence data available reveals that papillary tumor had the highest emission intensities. Premalignant lesions such as dysplasias and carcinoma in situ generally showed lower PpIX fluorescence intensities compared to malignant lesions. However, no direct relationship has been discovered between histopathological grading and relative fluorescence values.

Effect of exposure time and concentration

Three different solutions containing 50mg (4mM, 4 patients), 100mg (8mM, 15 patients) and 200mg of h-ALA (16mM, 2 patients) in 50ml of the solvent were instilled in human bladders between two and six hours prior to the fluorescence measurements (Table 1). Increased red fluorescence due to enhanced PpIX formation in premalignant and malignant lesions compared to the surrounding healthy sites was observed at all applied conditions. In order to quantify the resulting PpIX fluorescence, emission spectra were collected from different sites of the treated bladders. The fluorescence intensities of papillary tumors pTa graded G2 or G3 at 636nm were chosen as standard in order to determine the influence of the different treatment conditions applied. The selection is based on the presence of this type of lesion in each bladder examined. Table 1 summarizes the influence of the different conditions on the relative fluorescence intensities of the PpIX emission band at 636 nm.

Analysis of the data available from patients exposed for two hours (patient nos. 1, 2, 5, 6, 7, 20, and 21) to different h-ALA concentrations indicates a strong concentration dependent on the PpIX fluorescence. It appears that, within two hours, a solution of 8 mM h-ALA generates the highest fluorescence levels as compared to 4 mM and 16 mM of h-ALA. In Figure 4,

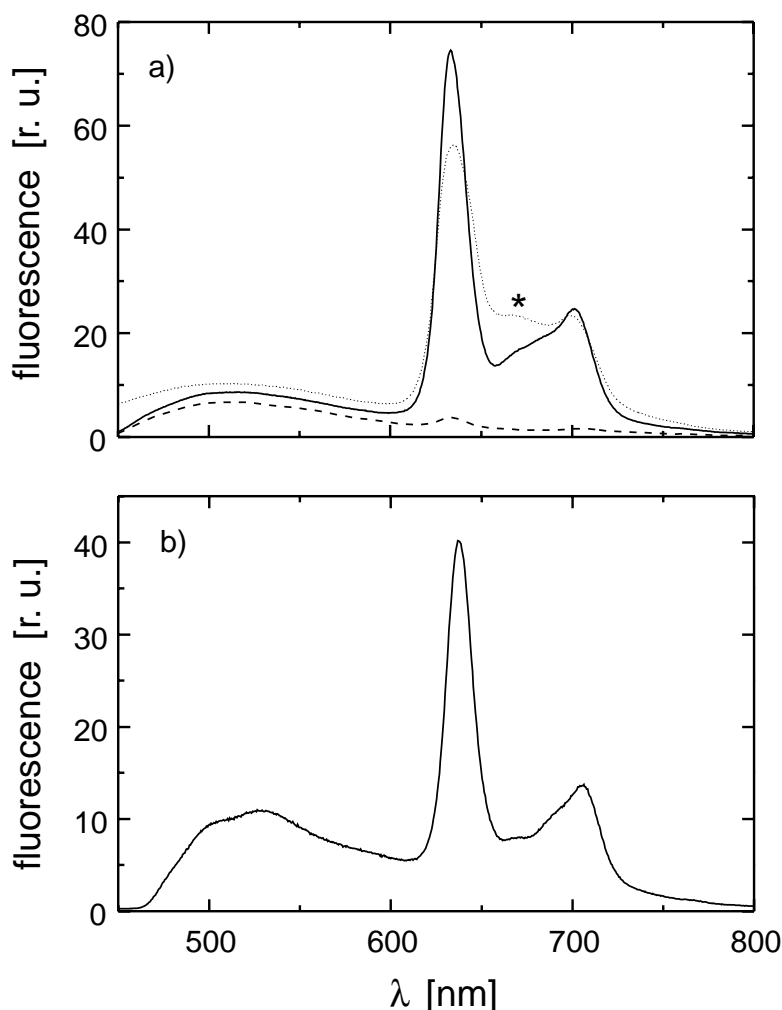


Figure 3: a) Fluorescence spectra of h-ALA-induced PpIX ($\lambda_{ex} = 405 \text{ nm}$) in normal mucosa (dashed line) and a papillary tumor (pTa G2, solid line) after 4 hours of instillation with 8mM h-ALA, dotted line: a fluorescence peak (*) at 670 nm becomes visible due to photobleaching of PpIX; b) Fluorescence spectra of ALA-induced PpIX ($\lambda_{ex} = 405 \text{ nm}$) in a papillary tumor (pTa G2, solid line) after 6 hours of installation with 180 mM ALA.

the time course of the relative fluorescence intensity is plotted for h-ALA concentrations of 4 mM and 8 mM. An increase of fluorescence intensity with instillation time was observed the two solutions. In addition, Figure 4 shows that, taking both the total fluorescence and the slope of the graphs into consideration, an instillation of 8 mM h-ALA solution is more efficient than that of a 4 mM solution.

In the course of our preliminary clinical study, a total of four patients (nos. 8-11) were instilled under slightly different conditions. The patients' bladders were exposed to the solutions for two hours.

Following this exposure time, the bladders were emptied and the patients were allowed a supplementary resting time of two hours. From Figure 4, it is clear that following this '(2+2)-concept' significantly enhanced fluorescence levels can be obtained compared to permanent exposure to the drug for four hours.

The comparison of the relative fluorescence intensities of an 8 mM h-ALA solution and a 180 mM solution of ALA under similar conditions (four hours of instillation, two hours of supplementary resting time) clearly demonstrates the advantage of using h-ALA. A treatment under these conditions with a topical 8 mM h-ALA solution resulted in a 2-fold increase of the fluorescence signal as compared to topical 180 mM ALA. After only four hours of h-ALA exposure (8 mM), the relative fluorescence intensity already exceeded that induced by ALA (180 mM) six hours after instillation.

DISCUSSION

Bladder cancer is a fairly common disease, appearing between the ages of 50 and 70 (Richie et al. (1989), Levi (1993)). This cancer, characterized by a high incidence (Levi (1993)), can appear in many distinct morphological forms, single or multiple, visible such as papillary or invisible such as 'flat' atypical lesions, mainly represented by low or high-grade dysplasia or CIS. Bladder tumor multiplicity and the presence of these different forms of atypia are indicators of poor disease prognosis. Recognition of all visible or invisible lesions is therefore a prerequisite for any kind of treatment, with the aim of reducing the risk of progression or the rate of recurrence.

Although topical application of ALA has proved to be a helpful and reliable tool in fluorescence photodetection of invisible lesions in human bladder disease (Kriegmair et al. (1994); Jichlinski et al. (1996)), some problems remain due to ALA's poor

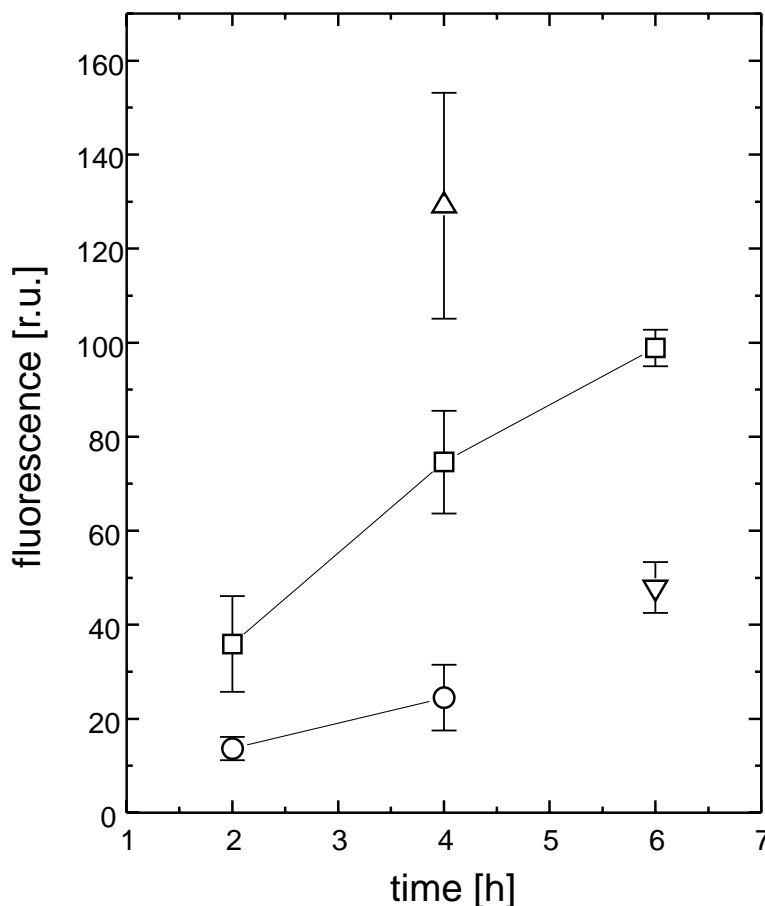


Figure 4: Effect of instillation time on the relative PpIX fluorescence intensity at 636nm in papillary tumors (pTa G2) (squares: 8mM h-ALA; circles: 4mM h-ALA; up-triangle: 8mM h-ALA (2 hours of instillation / 2 hours of resting time); down-triangle: 180mM ALA).

bioavailability. A small hydrophilic amino acid like ALA does not penetrate into all tissue compartments with great ease. Hence its concentration in tissue may remain relatively low and its distribution somewhat heterogeneous. Consequently, high drug doses over long instillation periods have to be used.

Three different concepts have been proposed to enhance the ALA-induced PpIX formation in deeper layers of the target tissue. Two of them are based on the use of chemicals, given along with ALA, in order to enhance both its penetration into deeper tissue layers and/or the total PpIX accumulation. This transepithelial penetration enhancement can be achieved either by prior DMSO exposure of the targeted area (Peng et al. (1995)) or by encapsulation of ALA into liposomes (Fukuda et al. (1992)). The second approach uses agents interfering directly with the biosynthetic pathway of heme. Tetrapyrrol modulators, such as 1,10-Phenanthroline

(Rebeiz et al. (1996)) and allyl-isopropyl-acetamide (AIA) (Schoenfeld et al. (1994)) stimulating the enzymatic activity associated with PpIX formation. Iron chelators (e.g. ethylenediaminetetraacetic acid (EDTA)) (Hanania et al. (1992); Orenstein et al. (1995), Warloe et al. (1995)), desferrioxamine (DFO) (Ortel et al. (1993)) and CP94 (Chang et al. (1997)) have been shown to increase PpIX concentration by preventing the ferrochelatase-mediated insertion of iron into the tetrapyrrole ring. This study followed a third approach, based on the thesis that the transformation of the hydrophilic ALA into more lipophilic prodrugs will enhance drug uptake.

In view of the results obtained using esters of ALA *in vitro* (Kloek et al. (1996), Gaullier et al. (1997), Marti et al. (1998)) and *in vivo* (Peng et al. (1996), Kloek et al. (1996)), it appeared reasonable to envisage developing such a substance for clinical tests in which superficial bladder carcinoma is detected by fluorescence and possibly even treated by PDT. From the variety of derivatives recently tested in our laboratory (Marti et al. (1998)), we selected h-ALA as it represents a good compromise between water/urine solubility and lipophilicity. It also gave an excellent *in vitro* dose drug response compared to ALA solutions. Furthermore, it can be synthesized with a fairly high yield and low cost. The goal of this first clinical study with h-ALA in urology was to evaluate the feasibility of fluorescence photodetection with this new agent and the advantages achieved by instillation of h-ALA as compared to ALA for use in the human bladder.

One criterion for the use of h-ALA as a potential candidate in replacing ALA, is the preservation of the outstanding selectivity of ALA-induced PpIX for malignant and premalignant tissues. Confirmed by histopathological examination, we have demonstrated that the fluorescence of PpIX in the urothelium induced by intravesically administered h-ALA correlated significantly with neoplastic lesions and was suitable for the detection of papillary tumors as well as for dysplasia and carcinoma *in situ*. The rate of false negative responses of 7% found in the present study is comparable to the value given by Jichlinski et al. in 1997 and slightly higher than that presented by the Munich group (Kriegmair et al. (1996)). A total

number of 28 biopsies were taken from areas proven to be benign. Only five of these samples revealed an enhanced red fluorescence under violet-light irradiation, yielding a rate of falsely positive fluorescence findings of 17%. This result seems to be quite small compared to both the results of Kriegmair et al. (1996) and Jichlinski et al. (1997). But it may be explained by the small number of biopsies taken or the fact that the fluorescence induced by the long-chained esters was found to be limited to the site of application (Peng et al. (1996)), hence no supplementary PpIX build-up from systemic ALA uptake is observed.

Clinical fluorescence spectroscopy has been used for measuring the PpIX accumulation kinetics, indicating an increase of h-ALA-induced PpIX with time in the human bladder within six hours. A quantitative comparison of the fluorescence intensities at 636 nm following similar instillation conditions with solutions of 180 mM of ALA or 8 mM of h-ALA respectively, clearly shows the advantages of h-ALA-induced PpIX. The more than twofold increase of the fluorescence signal due to the use of h-ALA is in good agreement with the *in vivo* results of Kloek et al. (1996).

The time course of the PpIX fluorescence intensity in neoplastic tissues shows that, following 8 mM h-ALA exposure for two or four hours, synthesis of PpIX continues within almost two hours after termination of the instillation. In this time range, the fluorescence intensity increases 400% (2 h of exposure, 2 h of resting time) and 25% (4 h of exposure, 2 h of resting time) respectively.

The significant increase of the fluorescence signal using the '(2+2)-concept' as compared to a permanent exposure to drug for four hours as well as the strong dependence on the instilled h-ALA concentration can be explained by an interference of high ALA concentrations with the biosynthetic pathway of heme. This observation was confirmed by *in vitro* experiments made by Gaullier et al. (1997) and Marti et al. (1998) with several ALA esters including h-ALA. Whereas the transport of ALA across the lipid bilayer of cell membranes probably represents a bottleneck in the PpIX formation, the

enhanced uptake of lipophilic h-ALA may saturate the intracellular PpIX biosynthesis. This saturation might cause a negative feedback to enzymatic activity. Furthermore, high intracellular ALA concentrations have been shown to be cytotoxic. A high cellular ALA content may induce the release of Ca^{2+} from mitochondria, mitochondria swelling and uncouple respiration (Hermes-Lima (1995)). It can also cause ferritin iron release (Berg et al. (1996)) or mediate the formation of 8-hydroxy-2'-deoxyguanosine in DNA (Fraga et al. (1994)).

The results presented in this study have shown that a two-hour instillation of h-ALA (8 mM) provides sufficient PpIX fluorescence for reliable photodetection of malignant and premalignant lesions. This reduction in instillation time to only two hours increases the patient's comfort. Moreover, this makes outpatient treatment feasible and helps to cut costs in view of the excessively increasing cost of hospitalization. Finally, the reduction of the drug dose will decrease drug cost and the potential risk of mild complications provoked by ALA, recently reported by Rick et al. (1997).

While for reliable fluorescence photodetection a two-hour instillation of 8 mM h-ALA has been shown to give satisfactory results, other conditions must be fulfilled with respect to an efficient bladder cancer therapy by PDT. Among other factors, the two key parameters high concentration of the photosensitizer and its homogeneous distribution in the target tissue play a major role for the effectiveness of PDT.

Fluorescence microscopic studies showed that, after topical application of ALA, the PpIX was restricted to the superficial layers of the bladder tumors (Steinbach et al. (1994)). On the contrary, preliminary fluorescence microscopic studies on some biopsies, taken in this study (data not shown), as well as the *in vitro* studies of Marti et al. (1998) demonstrated homogeneously distributed PpIX fluorescence over the entire urothelium after topical application of h-ALA solutions.

Considering the photobleaching of porphyrins during irradiation (Rotomski et al. (1996), Bezdetnaya et al. (1996), Moan

et al. (1997)), a threshold concentration of PpIX necessary for tissue destruction, and the high selectivity of h-ALA-induced PpIX, a small PpIX amount in healthy areas of the bladder, observed in this study will probably not induce any damage in these regions. However, the twofold increase of PpIX fluorescence after 6 hours in neoplastic tissues by using h-ALA may further enhance the PDT effect as compared to the use of ALA. The latter appeared insufficient as observed in recent studies (Kriegmair et al. (1996)).

It can be concluded that the use of h-ALA is a promising way to improve the photodetection of neoplastic and pre-neoplastic lesions as compared to ALA. In future, h-ALA may replace the use of ALA for clinical intravesical instillation because it is easy to use, real time observation without major auxiliary devices is possible and it is relatively cheap. Finally it looks more promising as a PDT agent than ALA itself.

ACKNOWLEDGEMENTS

The authors are grateful to the Swiss 'Fonds National', the Common Research Program in biomedical technology between Lausanne Hospital (CHUV), the Swiss Federal Institute of Technology (EPFL), Lausanne University (UNIL), the Swiss National Priority Program in Optics, and the 'Fonds Vaud-Geneva' for their financial support. Norbert Lange thanks Patrick Gerber (ICO, University of Lausanne) for many fruitful discussions. The Deutsche Forschungsgemeinschaft (DFG), Bonn, Germany, provided the grant for Dr. N. Lange.

REFERENCES

- BERG K, ANHOLT H, BECH O, MOAN J (1996). The influence of iron chelators on the accumulation of protoporphyrin IX in 5-aminolevulinic acid-treated cells!. *Br. J. Cancer*, **74**, 688-697
- BEZDETNAYA L, ZEGHARI N, BELITCHENKO I, BERBERI-HEYOB M, MERLIN JL, POTAPENKO A, GUILLEMIN F (1996) Spectroscopic and biological testing of photobleaching of porphyrins in solutions. *Photochem. Photobiol*, **64**, 382-386
- BRIDGES JW, SARGENT NSE, UPSHALL DG (1979). Rapid absorption from the urinary bladder of a series of n-alkyl carbamate: a route for the recirculation of drug. *British J. Pharmacol.*, **66**, 283-289

- CHANG SG, MACROBERT AJ, BOWN SG (1996). Biodistribution of protoporphyrin IX in rat urinary bladder after intravesical instillation of 5-aminolevulinic acid, *J. Urol.*, **155**, 3, 1744-1748
- CHANG SG, MACROBERT AJ, PORTER JB, BOWN SG (1997). The efficacy of an iron chelator (CP94) in increasing cellular protoporphyrin IX following 5-aminolevulinic acid administration: an in vivo study, *J. Photochem. Photobiol. B: Biol.*, **38**, 114-122
- DOUGHERTY TJ, COOPER MT, MANG TS (1990). Cutaneous phototoxic occurrences in patients receiving Photofrin. *Lasers Surg. Med.*, **10**, 485-488
- FRAGA CG, ONUKI J, LUCESOLI F, BECHARA EJ, DI MASCIO P (1994). 5-Aminolevulinic acid mediates the in vivo and in vitro formation of 8-hydroxy-2'-deoxyguanosine in DNA. *Carcinogenesis* **15**, 2241-2244
- FUKUDA H, PAREDES S, DEL BATTLE AM (1992). Tumor localizing properties of porphyrins in vivo studies using free and liposome encapsulated aminolevulinic acid. *Comp. Biochem. Physiol.*, **102b**, 433-436
- GAULLIER JM, BERG K, PENG Q, ANHOLT H, SELBO PK, MA LW, MOAN J (1997). Use of 5-aminolevulinic acid esters to improve photodynamic therapy on cells in culture. *Cancer Research*, **57**, 1481-1486
- GIBSON SL, HAVES JJ, FOSTER TH, HILF R (1997). Time-dependent intracellular accumulation of d-aminolevulinic acid, induction of porphyrin synthesis and subsequent phototoxicity. *Photochem. Photobiol.*, **65**, 416-421
- HANANIA J, MALIK Z (1992). The effect of EDTA and serum on endogenous porphyrin accumulation and photodynamic sensitization of human leukemic cells, *Cancer Lett.*, **65**, 127-131
- HERMES-LIMA M (1995). How do Ca^{2+} and 5-aminolevulinic acid-derived oxyradicals promote injury to isolated mitochondria?, *Free Radical Biol. Med.*, **19**, 381-390
- IINUMA S, BACHOR R, FLOTTE T, HASAN T (1995). Biodistribution and phototoxicity of 5-aminolevulinic acid-induced PpIX in an orthotopic rat bladder tumor model, *J. Urol.*, **153**, 802-806
- JAIN R (1987 a). Transport of molecules in the tumor interstitium: a review. *Cancer Res.*, **47**, 3039-3305
- JAIN RK (1987 b). Transport of molecules across tumor vasculature. *Cancer Metast. Rev.*, **6**, 559-593
- JICHLINSKI P, FORRER M, MIZERET J, GLANZMANN T, BRAICHOTTE D, WAGNIÈRES G, ZIMMER G, GUILLOU L, SCHMIDLIN FM, GRABER P, VAN DEN BERGH H, LEISINGER HJ (1997). Clinical evaluation of a method for detecting superficial transitional cell carcinoma of the bladder by light-induced fluorescence of protoporphyrin IX following topical application of 5-Aminolevulinic acid: Preliminary results. *Lasers Surg. Med.*, **20**, 402-408
- KENNEDY JC, POTTIER RH, PROSS DC (1990). Photodynamic therapy with endogenous protoporphyrin IX: Basic principles and present clinical experience. *J. Photochem. Photobiol. B: Biol.*, **6**, 143-148
- KENNEDY JC, POTTIER RH (1992). Endogeneous protoporphyrin IX a clinically useful photosensitizer for photodynamic therapy. *J. Photochem. Photobiol. B: Biol.*, **14**, 275-292
- KLOEK J, BEIJERSBERGEN VAN HENEGOUWEN GMJ (1996). Prodrugs of 5-aminolevulinic acid for photodynamic therapy. *Photochem. Photobiol.*, **64**, 994-1000
- KRIEGMAIR M, BAUMGARTNER R, LUMPER W, WAIDELICH R, HOFSTETTER A (1996). Early clinical experience with 5-aminolevulinic acid for the photodynamic therapy of superficial cancer, *Br. J. Urol.*, **77**, 667-671
- KRIEGMAIR A, BAUMGARTNER R, KNUECHEL R, STEINBACH P, EHSAN A, LUMPER W, et al. (1994). Fluorescence photodetection of neoplastic urothelial lesions following intravesical instillation of 5-aminolevulinic acid. *Urology*, **44**, 836-841
- LEVECKIS J, BURN JL, BROWN NJ, REED MWR (1994). Kinetics of endogeneous protoporphyrin IX induction by aminolevulinic acid: preliminary studies in the bladder. *J. Urol.*, **152**, 550-553
- LEVI F (1993). Incidence of infiltrating cancer following superficial bladder carcinoma. *Int. J. Cancer*, **55**, 419-421
- MALIK Z, KOSTENICH G, ROITMAN L, EHRENBERG B, ORENSTEIN A (1995). Topical application of 5-aminolevulinic acid, DMSO and EDTA: protoporphyrin IX accumulation in skin and tumors of mice. *J. Photochem. Photobiol. B.*, **28**, 213-218
- MARTI A, LANGE N, VAN DEN BERGH H, SEDMERA D, JICHLINSKI P, KUCHERA P (1998). Optimalisation of the formation and distribution of protoporphyrin IX in the urothelium: An invitro approach, *J. Urol.* (in press)

- MOSTOFIO FK, SOBIN LH, TORLONI, H (1973). Histological typing of urinary bladder tumors. In: World Health Organization. Ed. 'International Histological Classification of tumors.' Geneva 1973
- NAGY GK, FRABLE WJ, MURPHY WM (1982). Classification of premalignant urothelial abnormalities: A Delphi study of the National Bladder Cancer Collaborative Group A. In: Sommers SC, Rosen PP, eds. Norwalk, CT: Appleton, pp. 219-233
- NOVO M, HUETTMANN G, DIDDENS H (1996). Chemical instability of 5-aminolevulinic acid used in the fluorescence diagnosis of bladder tumours, *J. Photochem. Photobiol. B: Biology*, **34**, 143-148
- ORENSTEIN A, KOSTENICH G, TSUR H, ROITMAN L, EHRENBERG B, MALIK Z (1995). Photodynamic therapy of human skin tumors using topical application of 5-aminolevulinic acid, DMSO and EDTA. Proc. SPIE, **2325**, 100-105
- ORTEL B, TANEW A, HONIGSMANN H (1993). Lethal photosensitization by endogenous porphyrins of PAM cell-modification by desferrioxamine, *J. Photochem. Photobiol. B: Biol.*, **17**, 273-278
- PENG Q, MOAN J, WARLOW T, NESLAND JM, RIMINGTON C (1992). Distribution and photosensitizing efficiency of porphyrins induced by application of endogenous 5-aminolevulinic acid in mice bearing mammary carcinoma. *Int. J. Cancer*, **52**, 433-443
- PENG Q, WARLOE T, MOAN J, HEYERDAHL H, STEEN HB, NESLAND JM, GIERCKSKY KE (1995). Distribution of 5-aminolevulinic acid-induced porphyrins in noduloulcerative basal cell carcinoma, *Photochem. Photobiol.*, **62**, 906-913
- PENG Q, MOAN J, WARLOE T, IRANI V, STEEN HB, BJORSETH A, NESLAND JM (1996). Build-up of esterified aminolevulinic-acid-derivative-induced porphyrin fluorescence in normal mouse skin. *J. Photochem. Photobiol. B: Biology*, **34**, 96-96
- POTTIER WR, MANG S, DOUGERTHY TJ (1987). The theory of photodynamic therapy dosimetry: Consequences of photodestruction of sensitizer. *Photochem. Photobiol.*, **46**, 97-101
- REBEIZ N, ARKINS S, REBEIZ CA, SIMON J, ZACHARY JF, KELLY KW (1996). Induction of tumor necrosis by d-Aminolevulinic acid and 1,10-Phenanthroline photodynamic therapy, *Cancer Res.*, **56**, 339-344
- RICHE, JP, SHIPLEY WU, YAGODA A (1989). Cancer of the bladder. In: DE VITA VT, HELLMANN S, ROSENBERG SA (eds.) Cancer principles and practice of oncology. JB Lippincott, Philadelphia, 1008-1020
- RICK K, SROKA R, STEPP H, KRIEGMAIR M, HUBER RM, BAUMGARTNER R (1997). Pharmacokinetics of 5-aminolevulinic acid-induced protoporphyrin IX in skin and blood, *J. Photochem. Photobiol. B: Biol.*, **40**, 319-313
- ROTOMSKI R, BAGDONAS S, STRECKYTE G (1996) Spectroscopic studies of photobleaching and photoproduct formation of porphyrins used in tumour therapy, *J. Photochem. Photobiol. B: Biol.*, **33**, 61-67
- SCHOENFELD N, MAMET R, NORENBERG Y, SHAFRAN M, BABUSKIN T, MALIK Z (1994). Protoporphyrin biosynthesis in melanoma B 16 cells stimulated by 5-aminolevulinic acid and chemical inducers: characterization of photodynamic inactivation, *Int. J. Cancer*, **56**, 106-112
- STEINBACH P, KRIEGMAIR M, BAUMGARTNER R, HOFSTADTER F, KNUECHEL R (1994). Intravesical instillation of 5-aminolevulinic acid: the fluorescent metabolite is limited to urothelial cells. *Urology*, **44**, 676-681
- SVANBERG K, ANDERSSON T, KILLANDER D, WANG I, STENRAM U, ANDERSSON-ENGELS S, BERG R, JOHANSSON J, SVANBERG S (1994). Photodynamic therapy of non-melanoma malignant tumors of the skin using topical d-aminolevulinic acid sensitization and laser irradiation. *Br. J. Dermatol.*, **130**, 743-751
- TAKEYA H (1992). Preparation of 5-aminolevulinic acid alkyl esters as herbicides. *Chem. Abstr.* **116**, P189633
- 'UIC-TNM Classification of Malignant Tumors'. (1992) 4th ed. Berlin: Springer Verlag
- WARLOE T, PENG Q, HEYERDAHL H, MOAN J, STEEN HB, GIERCKSKY KE (1995). Photodynamic therapy with 5-aminolevulinic acid induced porphyrins and DMSO/EDTA for basal cell carcinoma. In CORTESE, DA, Proc. SPIE, **2371**, 226-235
- WARLOE T, PENG Q, STEEN HB, GIERCHSKY KE (1992). Localization of porphyrins in human basal cell carcinoma and normal tissue induced by topical application of 5-aminolevulinic acid. In: SPINELLI P, DAL FANTE M, MARCHESINI R (eds.), Photodynamic therapy and biomedical lasers, pp. 454-458. Amsterdam: Elsevier Science Publishers B. V.

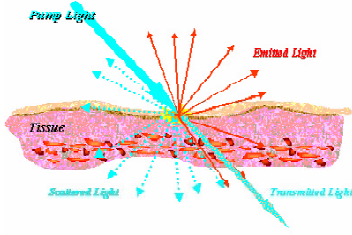
Part III

***ENDOGENOUS
FLUOROPHORES***

The third and last part of this thesis deals with the uses of fluorescence spectroscopy to investigate endogenous fluorophores (for a definition of exogenously-induced fluorophores, see p. 14). Because, in this case, the biological tissues emit fluorescence without the adjunction of any additional fluorophores, this native fluorescence is sometimes called autofluorescence.

We have separated this third part in two chapters. The first of these two chapters deals with a spectroscopic study of the autofluorescence of the bronchial tissue. We carried out a study about this phenomenon and tried to link the shape and intensity of the autofluorescence spectra to the histopathological status of the tissue. This chapter has resulted in two publications that have been submitted to peer-reviewed journals.

The main goal of the spectroscopic study that is presented in chapter 8 was to optimize a cancer photodetection system based on the autofluorescence on the bronchial tissue. This work is presented in chapter 9. Based on the spectroscopic study we present in chapter 8, we developed a new photodetection system, in close collaboration with the company *Richard Wolf Endoskope GmbH* (Germany). This device is presented in detail together with some clinical results.



Light-tissue interactions

Chapter 8

Autofluorescence of the human bronchial tissue

The autofluorescence of the biological tissues is a well-known phenomenon [1]. It is due to the natural presence of fluorophores within the tissue. In section 8.1, we briefly survey the molecules that are responsible for the autofluorescence, their structure and their functions. Section 8.2 focuses on the autofluorescence of healthy and non-healthy tissues with the main interest on bronchial tissue. The abovementioned spectroscopic study is presented in section 8.3 (additional work that has been carried out in Lausanne about the autofluorescence of the bronchi is given in the Appendix A3). The following section (8.4) presents another part of our study about the autofluorescence of bronchial tissue. Indeed, we calculated the absolute intensity of the emitted autofluorescence for a given fluorescence excitation power expressed in physical units. This work has also been submitted to a peer-reviewed journal, 'Applied Optics'.

8.1 The endogenous fluorophores

All biological tissues emit fluorescence when excited by UV or visible light. This fluorescence is emitted by naturally-occurring fluorophores (FPs) and is therefore often called autofluorescence.

It has already been reported that early cancerous tissues have a different autofluorescence emission spectrum than healthy tissues. This is not new work [2-5]. Although the origin of the autofluorescence itself is usually related to the structure of tissues or metabolic processes [1,6], the reasons behind the modifications of the autofluorescence spectra in early tumors remain controversial. Nevertheless, the ensuing contrast has been taken advantage of for cancer detection purposes, eventually leading to the commercialization of several systems.

Biological tissues are made up of a very complex mixture of molecules. Several of these molecules are fluorescence emitters, when excited with an appropriate wavelength. The mixture of all these emission spectra as well as the diffusion and scattering properties of the biological tissues make the overall autofluorescence spectrum broad and quite featureless (Fig. 8.1).

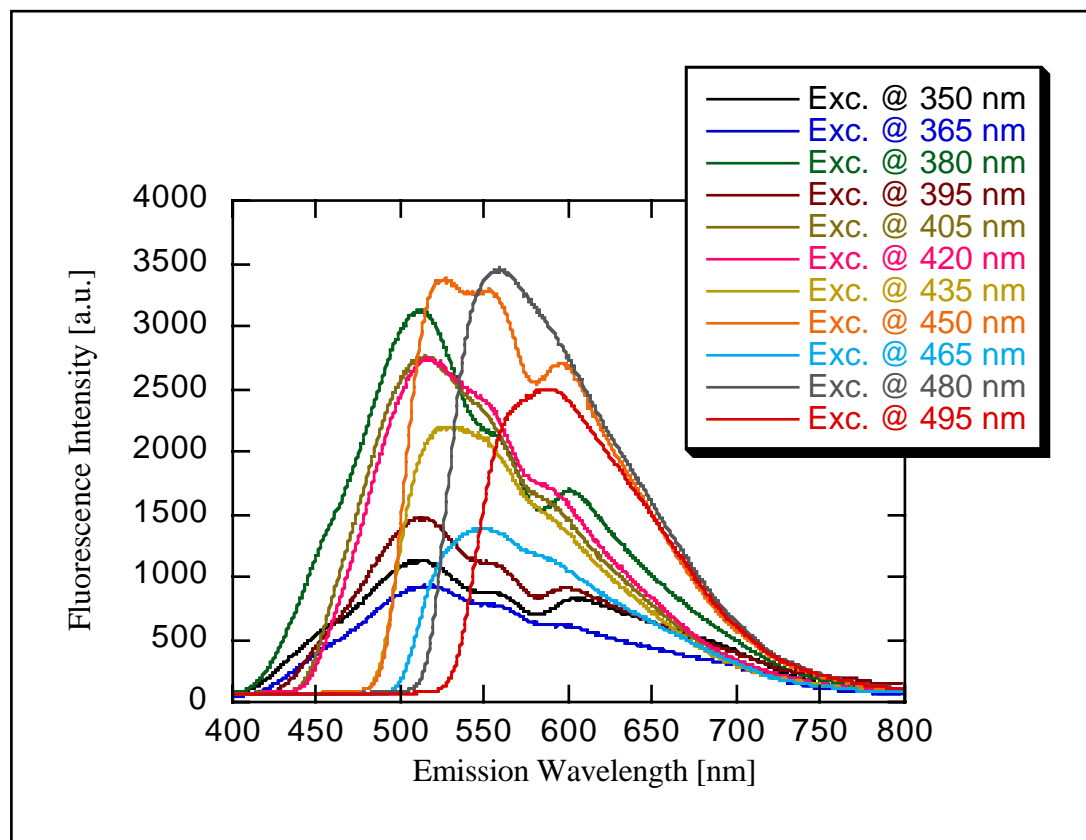


Figure 8.1: Emission spectra of normal bronchial tissue in vivo for several excitation wavelengths (for details about these measurements, see Section 8.3, Materials and Methods).

Figure 8.1 shows the autofluorescence spectrum emitted by normal bronchial tissue in vivo following an excitation at different wavelengths. The longpass filters are not necessarily the same for each excitation wavelength. This explains why the spectra at longer wavelengths seem to be shifted. For details about the experimental setup, see Section 8.3, Table 1 and Materials and Methods section.

The molecules responsible for the autofluorescence of tissues have recently been reviewed by Richards-Kortum and Sevick-Muraca [1] and the corresponding excitation and emission spectra have been published by Wagnières et al. [6]. They are presented in Fig. 8.2a (absorption spectra) and 8.2b (emission spectra).

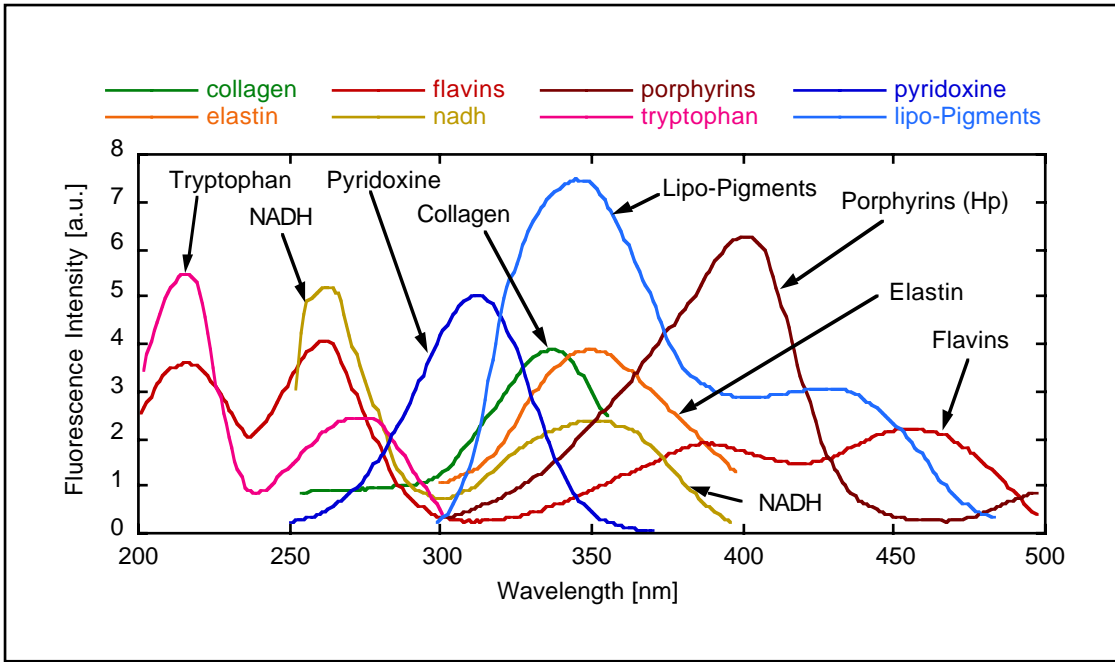


Figure 8.2a: Absorption spectra of biomolecules in the biological tissue [6].

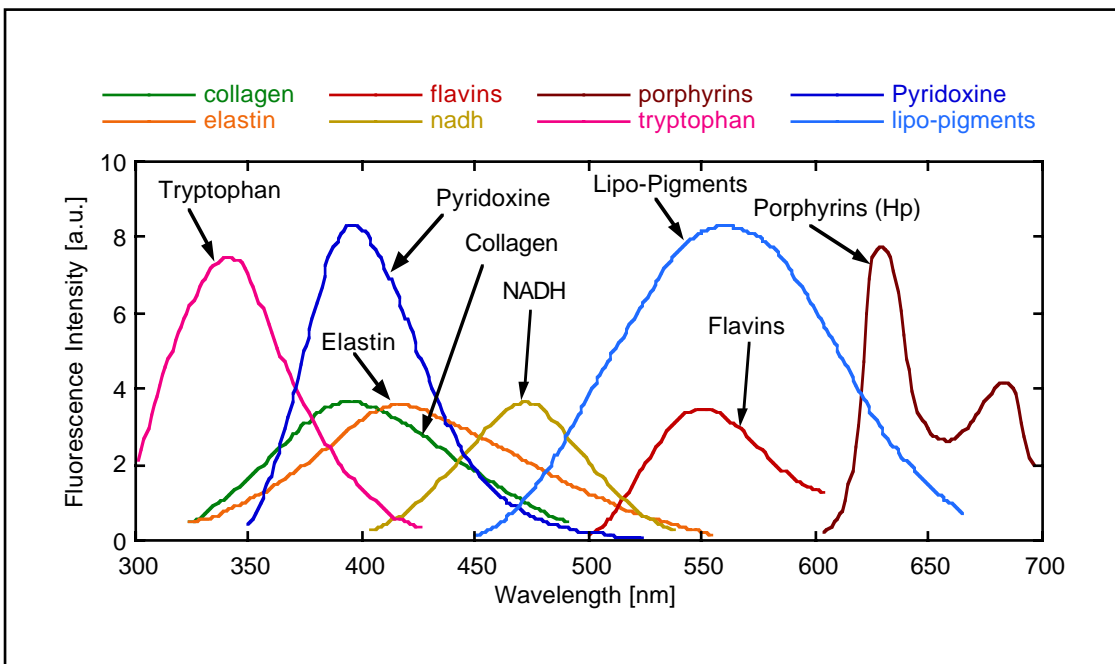


Figure 8.2b: Emission spectra of biomolecules in the biological tissue [6].

The endogenous fluorophores can be classified in four groups, the porphyrins, the amino-acids and the proteins, the flavins and the pyridine nucleotides (NADH, NADPH) [7].

The porphyrins are synthesized in mammals from 5-aminolaevulinic acid (see Part II). They are typically made of a substituted tetrapyrrole ring with an 18-electron conjugated system. The main molecule of this family is heme (although heme is not itself fluorescent, many other endogenous porphyrins are). The structure of the tetrapyrrole ring is given in Fig. 8.3 and more detailed porphyrin structures for the particular case of the biosynthesis of heme are given in Chapter 6. This tetrapyrrole ring is called porphine. It does not occur in nature [8].

The porphyrins emit red fluorescence when excited, and their emission spectrum bears the typical two peaks around 635 and 690 nm. They have a maximum of excitation around 400 nm (the so-called Soret band). In their functional structure, the porphyrins are often associated with a metal

ion (Fe in hemoglobin, myoglobin or cytochromes, Mg in chlorophyll¹). The porphyrins function as electron donors or acceptors and, in the case of chlorophylls, light absorbers [9]. Their fluorescence intensities are dependent on the pH value of their environment. High concentrations of halogenides can cause porphyrin fluorescence quenching [8]. The hydrogenation of the pyrrole ring (from porphyrins to chlorins and further from chlorins to bacteriochlorins) shifts the fluorescence maxima to longer wavelengths.

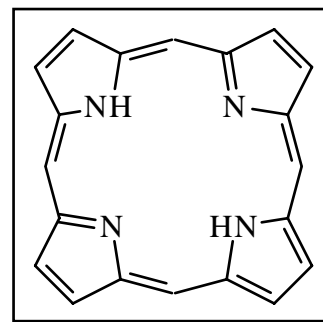


Figure 8.3: The tetrapyrrole ring (common moiety of the porphyrins).

The only proteins exhibiting native fluorescence are those which possess phenylalanine (Phe), tyrosine (Tyr) or tryptophane (Trp) or combinations thereof [8]. Their fluorescence (essentially collagen and elastin [1,6]) stems in fact from cross-links between the amino-acids that compose them [1]. The cross-links are of two types, both involving a pyridine moiety [1]. Collagen is a rigid protein found in the skin, the bones, the teeth, and so on. It absorbs around 340 nm and emits around 380 nm [9]. Richards-Kortum and Sevick-Muraca report excitation and emission maxima for collagen of 280 and 310 nm, 265 and 385 nm, 330 and 390 nm, 450 and 530 nm respectively in their review [1, adapted from previous work in their group]. Elastin is a flexible protein whose absorption maximum lies around 350 nm and emission around 410 nm [9].

The fluorescent amino-acids are the aromatic ones, namely phenylalanine, tyrosine and tryptophane, whose structure is given in Fig. 8.4.

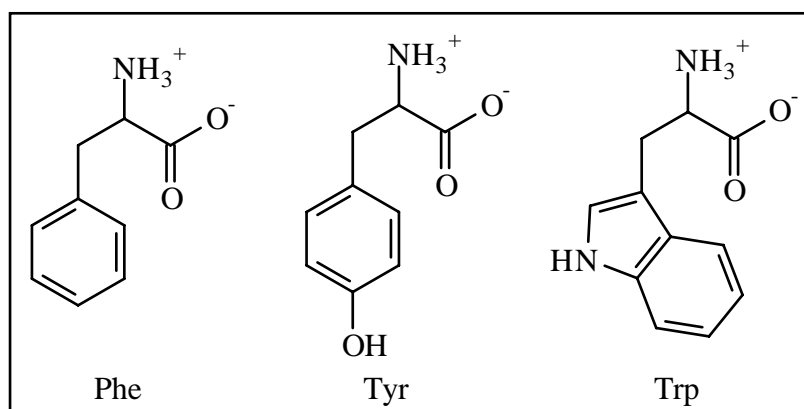


Figure 8.4: Structure of the fluorescent amino-acids phenylalanine (Phe), tyrosine (Tyr) and tryptophane (Trp).

Their photophysical data are summarized in Table 8.1 (compiled from [8]). Phenylalanine has a weaker fluorescence than tyrosine or tryptophane because its quantum yield and its molar extinction are lower, with values of 0.025 and $200 \text{ cm}^{-1}\text{M}^{-1}$ respectively in water [8]. It is reported that the fluorescence of Phe decreases by around 30% at pH below 2.3 [8].

The emission spectrum of Tyr is strongly pH-dependent and is also influenced by factors such as temperature, ionic strength of the medium or presence of energy acceptors (Trp, peptide bonds). Free Tyr possesses the highest fluorescence quantum yield of the three aminoacids. Its value is 0.2 in water but decreases by 40-90% when bound into a protein. Its molar extinction is $1500 \text{ cm}^{-1}\text{M}^{-1}$ at its excitation maximum.

¹Although, strictly speaking, chlorophyll is made up of a chlorin ring and not of a porphyrin ring, it can be considered a member of the same family of molecules (along with bacteriochlorins).

Tryptophane fluorescence is very useful as an intrinsic probe for the investigation of the structure of proteins and enzymes [8] because it is quenched by several ions (bromide, iodide, nitrate), molecules (oxygen, hydrogen peroxide, acrylamide, NADH, NADPH, glucose, histidine) or groups (SH, S-S bonds). Its quantum yield is 0.14 in water and its molar extinction amounts to $6000 \text{ cm}^{-1}\text{M}^{-1}$ at its excitation maximum.

Name	Excitation Wavelength [nm]	Emission Wavelength [nm]	Molar extinction ($\text{cm}^{-1}\text{M}^{-1}$) at maximum	Fluorescence quantum yield
Phenylalanine	260	282	200	0.024
Tyrosine	275	303	1500	0.2
Tryptophane	287	348	6000	0.14

Table 8.1: Photophysical data of the fluorescent amino-acids in water at $\text{pH} = 7.0$.

In aerobic organisms, the oxygen molecule is the final electron acceptor in the process of oxidation of fuel molecules. The flavins and the pyridine nucleotides are electron carriers dedicated to these reactions. The major flavin-related electron carrier is Flavin Adenine Dinucleotide (FAD) whose oxidized form (FAD) is fluorescent, while its reduced form (FADH₂) is not [1,9]. The other important naturally-occurring flavin derivatives include Flavin Mononucleotide (FMN) and riboflavin (Vitamin B₂). The structure of the reactive site of FAD is shown in the Fig. 8.5.

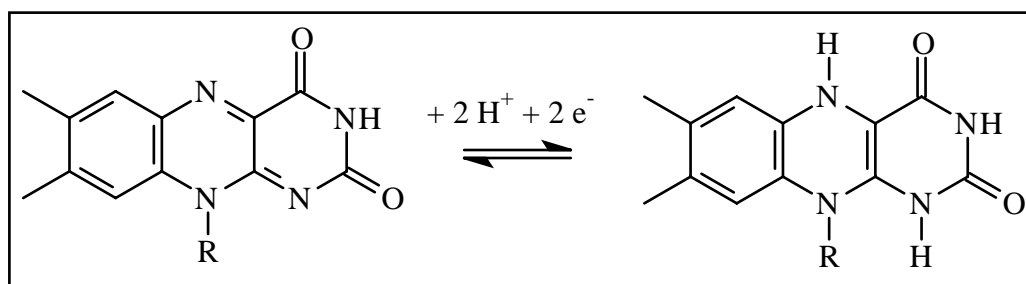


Figure 8.5: The structure of the reactive part of FAD (left) and FADH₂ (right) and the reaction of electron acceptance.

The molecule of FAD has an absorption maximum around 450 nm and an emission maximum around 515 nm [1,9]. As a family, the flavins are involved in near-UV and blue light reception (300 - 500 nm). This part of the spectrum is known to induce and regulate important events in almost all organisms [8,10]. For instance, in plants and fungi, the blue light can induce a response from the β -carotene synthesis mechanisms or, in insects, it influences the development of eggs and their hatching [10]. All the emission spectra of the flavins are broad and structureless [8]. The flavins are quenched as a result of their interaction with iodide, bromide, tryptophan, cysteine or upon binding to proteins. Interestingly, Wolfbeis [8] reports that concentration changes of flavins in intact organs may be followed directly by measuring their fluorescence. The concentrations of flavins in biological tissues have been reported in several studies [11,12]. There seems to be an agreement that a relevant concentration in tissue is around $10 \mu\text{M}$. The photophysical data of the flavin derivatives are summarized in Table 8.2 (compiled from [8]).

The other main metabolic molecules involved in tissue autofluorescence are Nicotinamide Adenine Dinucleotide (NAD⁺, reduced into NADH) and Nicotinamide Adenine Dinucleotide Phosphate (NADP⁺, reduced into NADPH). Although these molecules are used for different biochemical pathways, they carry electrons in much the same way [9]. The structure of their reactive moiety (the pyridine nucleotide) is given in Fig. 8.6.

Name	Excitation Wavelength [nm]	Emission Wavelength [nm]	Fluorescence quantum yield
Riboflavin	370	520	0.25
FMN	450	530	0.25
FAD	450	530	0.025

Table 8.2: Photophysical data of the flavin derivatives in water at pH = 7.0.

the adenine part of the molecule does not absorb [8]. The fluorescence of these species can be used to follow the kinetics of some dehydrogenases or to assay substrates or metal ions [8]. When NADH or NADPH are bound to proteins, their fluorescence excitation and emission maxima may drastically change and their fluorescence quantum yield is increased by approximately a factor of four [1]. Maximal values of 325/440 to 365/478 nm (excitation/emission maxima) have been reported [8 and references therein]. This form of NADH or NADPH is present mainly in mitochondria and is thought to account for 80% of tissue fluorescence [13]. The photophysical data of the nicotinamide derivatives are summarized in Table 8.3 (compiled from [8]).

More molecules are thought to be involved in the autofluorescence of the living tissues. We should mention Pyridoxine (Vitamin B₆, a pyridine-like molecule) and its metabolites, Retinol (Vitamin A), lipopigments (products of lipid oxidation whose chemical structure is not well-known [1]) and eosinophils (a type of white blood cell). It should also be mentioned that all purine and pyrimidine bases, as well as DNA and RNA are fluorescent. Their intensity is, however, very low [8], and especially so in neutral aqueous solutions at room temperature.

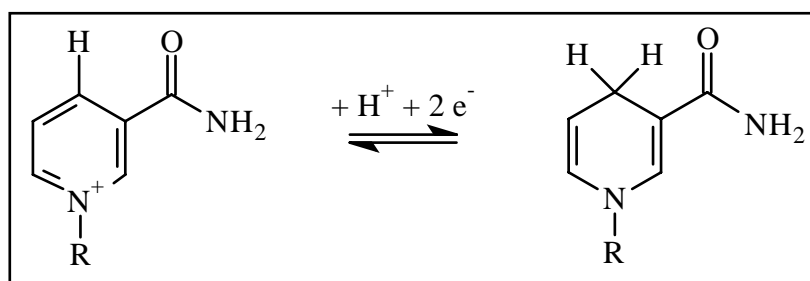


Figure 8.6: The structure of the reactive part of NAD⁺ (left) and NADH (right) and the reaction of electron acceptance.

Name	Excitation Wavelength [nm]	Emission Wavelength [nm]	Fluorescence quantum yield
NADH	340	435	0.019
NADPH	340	460	0.019

Table 8.3: Photophysical data of the nicotinamide derivatives in water at pH = 7.0.

8.2 The autofluorescence of healthy tissues and of early cancerous lesions

The modifications in the autofluorescence characteristics of the tissue during the process of cancerization have been widely studied. The reasons behind these contrasts seem less clear but can be sorted into two broad categories: biochemical effects and architectural effects. It should also be kept in mind that the non-fluorescing heme also influences the spectral shape of tissue autofluorescence. Its negative imprint due to the absorption of the fluorescence photons by hemoglobin, can be found in most of them as two dips at 540 and 580 nm.

Published work

Early reports of autofluorescence as a way of diagnosing early cancers include the work of Yang et al [3] on ex vivo tissue samples. They noticed characteristic peaks appearing in the red region

Only the reduced form of these molecules is fluorescent. They have an absorption maximum at around 340 nm and emit fluorescence around 450 nm. Wolfbeis reports that the emission of NADH or NADPH comes from the nicotinamide moiety whereas

(630-690 nm) on cancer specimens when excited by a lamp at 365 nm. They found good agreement between the autofluorescence modifications and the results of the biopsies. Moreover, they reported very similar spectroscopic features for cancers of various organs and the similarity of the peaks in the red region with the peaks of HpD. They concluded therefore that the new peaks might be due to additional porphyrin compounds in cancers.

Harris et al [4] also reported bright autofluorescence of human buccal tissues but found little reproducibility and hence little relevance in its observation. They attributed it however to bacteria-produced porphyrins.

In a work about human breast and lung tissues *ex vivo* (tumor and normal), Alfano et al [14] excited the autofluorescence with laser light at 488 and 457 nm. They observed a loss of structure in the spectral shape of the breast tumor tissues and suggested it might be due to a reduction in fluorophores like porphyrins. Moreover, they observed a blue shift of the main peak of the spectra and attributed this shift to physiological and biochemical transformations, namely the accumulation of positively-charged ions in the malignant cells' intracellular environment. However, the color shift was observed to be in the opposite direction for lung tumor tissues. The common features of the cancerous tissues are the loss of structure in the porphyrin region, which is attributed to a reduction in the density of the porphyrin molecules in the cancer cells [14].

Anthony et al [15] reported autofluorescence spectra of bronchial tissue *in vivo*. They showed that the tissue, when excited at 407, 413 and 415 nm, displays, after an emission peak around 500 nm, a monotonically decreasing spectrum along the wavelength range. Moreover, they reported that the spectra of the tumor and the healthy tissue were, after normalization, very well overlapped between 500 and 600 nm but then the spectrum from the tumor displayed an increase in the red region that could not be found in the spectrum of the healthy tissue. They also reported that the autofluorescence spectra measured at different sites of the healthy bronchi are remarkably constant in shape (within a few percent). It is interesting to note that our results (see Section 8.3) are in very good agreement with both these observations. Anthony et al do not however try to give an explanation about the differences in autofluorescence but rather dismiss this result for lack of enough diagnostic usefulness.

In another paper, Tang et al [16] reported about the autofluorescence of human lung and breast tissues *ex vivo*. They observe that, when excited at 457 nm, lung cancer tissues have less features than their normal counterparts, namely they lose two emission peaks at 555 and 600 nm. They relate these differences in spectral shape to the absorption of hemoglobin. Indeed, the absorption bands of hemoglobin are centered at 540 and 580 nm and they suggest the decrease in the lung cancer spectrum be due to a decrease of hemoglobin in these samples.

In a more recent paper by Hung et al [17] or Palcic et al [18], it is reported about the autofluorescence of bronchial tissue *in vivo*, excited at 405, 442 and 488 nm. The main observations of the authors are a sharp decrease (around a factor of 10) in the green autofluorescence of the tissue in the carcinoma *in situ* with respect to healthy mucosa. However, an amplification of the signal showed that the spectral shape was not changed. The observations were similar for the excitation wavelength of 442 nm and the only notable difference for the excitation wavelength of 488 nm was that the shape of the spectrum was not retained. These authors suggest that these differences in autofluorescence intensity and spectral shape might well be due to differences in the amount of oxidized and reduced forms of flavins in tumors and normal tissues. This would be in agreement with the idea that the metabolism of an early tumor cell is indeed different from that of a normal cell and agree with a study by Pollack et al [19]. However, neither Hung et al nor Palcic et al reported any observation of an increase in the red autofluorescence.

A relative increase in the red region (in this case proposed as porphyrin fluorescence) has been observed by Schomacker et al [20] in colonic adenomatous polyps *in vivo* when excited at 337 nm. These authors use LIF to distinguish normal colonic mucosa and hyperplastic polyps from adenomatous polyps and adenocarcinomas. They achieve a sensitivity of 70% and specificity of 91% with a Multivariate Linear Regression of four wavelengths. They seem to achieve a good

discrimination between the adenocarcinomas and the normal colonic mucosa but the size of the former (22.6 ± 10 mm) hints at relatively large lesions. The discrimination is less convincing in the case of adenomatous and hyperplastic polyps as they overlap substantially. It should also be noted that adenomatous polyps, although considered premalignant, are benign neoplasms.

In a study about bladder tissue autofluorescence following excitation at 308, 337 or 480 nm, Anidjar et al [21] reported a marked decrease in autofluorescence for carcinomas in situ with respect to normal bladder mucosa when excited at 480 or 337 nm. The spectral shape of the autofluorescence underwent no change, however. At 308 nm excitation wavelength, they observed not only a change in intensity but also a change in spectral shape between the normal bladder mucosa and the CIS. They related these changes to the emission of oxidized flavoproteins (480 nm), tryptophan (selectively excited by 308 nm) and NADH (337 nm). They report that these results make it possible to distinguish normal bladder mucosa from carcinomas in situ. This is in partial agreement with König et al [22], who also used 337 nm as an excitation wavelength but found a spectrum with a different shape. Indeed, these authors found not only a difference in fluorescence intensity but also a modification of the spectral shape between the healthy mucosa and the carcinoma in situ. The disagreements might be due to differences in data manipulation as Anidjar et al provided no explanation on how and whether their spectra were corrected for background fluorescence, the spectral response of their setup, or to differences in their acquisition system, as Anidjar et al used a long pass filter centered at 400 nm whereas König et al used a gated intensifier [22,23]. Moreover, the results of König et al rely on the largest series of random biopsies to date [22]. Their explanation about the autofluorescence changes is that the spectrum is influenced by the epithelial thickness.

The epithelial thickness is also the reason invoked by Leonhard [24] and Häussinger et al [25] for the modifications in the autofluorescence of bronchial tissues. Their idea is that the autofluorescence photons are reabsorbed on their way out by the thicker tissues. It should be added that their imaging system (Storz) uses a combination of autofluorescence and blue backscattered excitation light to enhance the contrast. This idea had been devised already by Hürzeler, although without the use of fluorescence [26].

More studies about the use of the autofluorescence contrast in vivo as a diagnostic tool have been published. We should mention the report of use of fluorescence and red reflectance light in the GI tract by Weiss et al [27]. The modifications of autofluorescence in the oral cavity have been reviewed by Gillenwater et al [7]. They conclude that a considerable amount of further research is necessary to actually link the altered fluorescence to a clearly architectural or biochemical cause. As for the increase in red fluorescence sometimes observed, these authors seem to favour its porphyrin origin. Dhingra et al also report a relative increase in the red region after an excitation at 410 or 370 nm [28]. These investigators related the modifications of the spectral shape and of the fluorescence intensity to both an architectural effect and an increased production of porphyrins due to a metabolic change. These results are in agreement with similar findings by Gillenwater et al [29], who analyzed the autofluorescence of lesions in the oral cavity after an excitation at 337, 365 and 410 nm. The increase in red fluorescence is also reported by Ingrams et al [30] in ex vivo samples of oral cavity tissue.

In a study about colon tissues ex vivo, Bottiroli et al [31] clearly observed a change in the fluorescence intensity and in the spectral shape between normal and tumor tissues. They linked the latter observation to modifications of the redox equilibrium and the former to the varying thickness of the tissue, hence combining architectural and biochemical effects. They also suggest that short UV excitation wavelengths (< 350 nm) favor the modifications of fluorescence intensity and longer wavelengths (> 350 nm) favor the modifications of spectral shape. In a study about breast tissues ex vivo, Gupta et al [32] found an increase in the fluorescence of the cancerous tissues with respect to normal tissues (they linked it to an enhanced concentration of fluorophores) but no change in the shape of the spectra. However, it should be noted that the results from an ex vivo study are by no means transposable to the in vivo case because the biochemical properties of tissues may significantly change within relatively short periods [20,33].

Phenomenology and optimization

As has been seen above, the controversy is going on. There is no agreement at all about the 'best' parameters (excitation wavelengths, detection windows), the findings of the autofluorescence analysis (loss of structure, loss of intensity, appearance of new peaks) or the reasons behind the modifications (thickening of the epithelium, increased production of porphyrins by bacteria, endogenous increase of the production of porphyrins, increased absorption by hemoglobin, modifications of the metabolism and of the related species). The only agreed-upon observation is that some modifications of the autofluorescence occur during the cancerization process and that, under certain circumstances, they may be useful as a diagnostic tool.

The parameters of autofluorescence have been studied in a very scattered way and, to our knowledge, there is still a lack of a very wide study about autofluorescence that would cover a large range of excitation wavelengths with a large number of patients. To a limited extent, this is what we propose for the bronchial tissues in Section 8.3. Many more similar studies are needed for the lungs and other organs before any agreement can be reached about the parameters of autofluorescence. However, upon reaching such an agreement, a noticeable improvement should be possible in the field of autofluorescence imaging and in the design of relevant devices.

The findings of the autofluorescence spectral analysis and the reasons behind these findings are closely related since the latter are the cause of the former. However, due to the great number of different tumors, the number of changes occurring in cells along the cancerization process, the various experimental designs and the inhomogeneity of a cancerous tissue, there is still much to be investigated until an unequivocal explanation can be found to these observations. Moreover, it is likely that, in most cases, the modifications of autofluorescence are due to a combination of both architectural effects and biochemical effects.

This could be true in the case of the autofluorescence of the bronchi. Indeed, if the modifications were due to architectural effects alone, it is likely that one would observe a continuous change of the autofluorescence spectrum from the healthy tissue's towards the carcinoma in situ's (namely a gradual spectroscopical change following the gradual thickness change from healthy to metaplasia to dysplasia and to CIS [34-36]). Consequently, in the light of our results, one would observe a continuous change in the intensity of the spectrum (actually observed) and a continuous change in the shape of the spectrum (not observed as the metaplastic tissues exhibit the same spectral shape as the healthy tissues). On the other hand, if the modifications were due to biochemical effects only, it is likely that one would observe no change of the autofluorescence spectrum, neither in its shape nor in its intensity, between the healthy tissue's and the metaplasia's, since both are considered normal and non-malignant. As a matter of fact, we do not observe a change in the spectral shape of the spectra but it is clear that the metaplastic tissues exhibit a little less fluorescence when excited in the violet-blue region. These elements seem to give us a hint that the modifications of the fluorescence are probably not due to one clear-cut reason only but rather to an ensemble of subtle changes. A modality of investigation that could produce more information about this issue lies in the fluorescence lifetime methods [13,37] because they could distinguish between a quenching (biochemical effect) and a shielding (architectural effect). As relevant technologies become available, new devices should enter the clinical world to push the limits of the knowledge in this area a bit further.

The successes and recent developments of detection methods are encouraging for the future. Still, much remains to be done and many more developments will be necessary until cancer can be dealt with easily and successfully on a routine basis. All these efforts will require a great deal of financing and, due to demographic patterns, it is likely that more and more financial efforts will incumb to fewer and fewer people as the population ages and the disease becomes more common. This fact, along with the exponential increase in the cost of public health raises at least one other crucial issue: next to being the most frequent cancer in the western world, lung cancer is also characterized by a more puzzling feature, namely it is the most *avoidable* of all cancers. The way to avoid it is just not to smoke. It is therefore legitimate to ask whether an efficient method of prevention would maybe be the best investment for all the efforts in the search of a solution to this disease. But this, in turn, could be the subject of another thesis...

References

1. Richards-Kortum, R., E. Sevick-Muraca, 'Quantitative optical spectroscopy for tissue diagnosis', Annual Review of Physical Chemistry, 47, 555-606, 1996.
2. Policard, A., 'Etudes sur les aspects offerts par les tumeurs expérimentales à la lumière de Wood', CR. Séances Soc. Biol. Fil., 91, 1423, 1924.
3. Yang, Y., Y. Ye, F. Li, Y. Li, P. Ma, 'Characteristic autofluorescence for cancer diagnosis and its origin', Lasers in Surgery and Medicine, 7, 528-532, 1987.
4. Harris, D. M., J. Werkhaven, 'Endogenous porphyrin fluorescence in tumors', Lasers in Surgery and Medicine, 7, 467-472, 1987.
5. Alfano, R., D. Tata, J. Cordero, P. Tomashefsky, F. Longo, M. Alfano, 'Laser Induced Fluorescence Spectroscopy from Native Cancerous and Normal Tissue', IEEE Journal of Quantum Electronics, Vol. QE-20, No.12, dec 1984.
6. Wagnières, G., W. Star, B. Wilson, 'In vivo fluorescence spectroscopy and imaging for oncological applications', Photochemistry and Photobiology, 68(5), 603-632, 1998.
7. Gillenwater, A., R. Jacob, R. Richards-Kortum, 'Fluorescence spectroscopy: a technique with potential to improve the early detection of aerodigestive tract neoplasia', Head & Neck, 556-562, 1998.
8. Wolfbeis, O., 'The fluorescence of organic natural products', in Molecular Luminescence Spectroscopy: Methods and Applications - Part I, Stephen G. Schulman Editor, John Wiley and Sons, 167-370, 1985.
9. 'Biochemistry', L. Stryer, Fourth Edition, W.H. Freeman and Company, New York, USA, 1995.
10. Galland, P., H. Senger, 'The role of flavins as photoreceptors', Journal of Photochemistry and Photobiology, B: Biology, 1, 277-294, 1988.
11. Benson, R., R. Meyer, M. Zaruba, G. McKhann, 'Cellular autofluorescence - is it due to flavins', Journal of Histochemistry and Cytochemistry, 27(1), 44-48, 1979.
12. Höhne, W., W. Schramm, M. Nittka, H.-D. Kronfeldt, 'Characterization of endogenous fluorophores by psec laser fluorescence spectroscopy', Proceedings of the Society for Photo-Optical Instrumentation Engineering, 2324, 300-306, 1995.
13. Jérôme Mizeret, 'Cancer detection by endoscopic frequency-domain fluorescence lifetime imaging', PhD thesis #1839, EPFL, 1998.
14. Alfano, R., G. Tang, A. Pradhan, W. Lam, D. Choy, E. Opher, 'Fluorescence Spectra from Cancerous and Normal Human Breast and Lung Tissues', IEEE Journal of Quantum Electronics, Vol. QE-23, No.10, Oct 1987.
15. Anthony, D., A. Profio, O. Balchum, 'Fluorescence spectra in lung with porphyrin injection', Photochemistry and Photobiology, 49, 583-586, 1989.
16. Tang, G., A. Pradhan, R. Alfano, 'Spectroscopic differences between human cancer and normal lung and breast tissues', Lasers in Surgery and Medicine, 9, 290-295, 1989.
17. Hung, J., S. Lam, J. C. LeRiche and B. Palcic, 'Autofluorescence of normal and malignant bronchial tissue', Lasers Surg. Med., 11 (1991) 99-105.
18. Palcic, B., S. Lam, J. Hung and C. Mac Aulay, 'Detection and localization of early lung cancer by imaging techniques', Chest, 99 (1991) 742-743.
19. Pollack, M., A. Taylor, J. Taylor, R. William, 'B vitamins in cancerous tissues. I. Riboflavin', Cancer Research, 2, 739-743, 1942.
20. Schomacker, K., J. Frisoli, C. Compton, Th. Flotte, J. Richter, N. Nishioka, Th. Deutsch, 'Ultraviolet laser-induced fluorescence of colonic tissue: basic biology and diagnostic potential', Lasers in Surgery and Medicine, 12, 63-78, 1992.

21. Anidjar, M., D. Etti, O. Cussenot, P. Meria, F. Desgrandchamps, A. Cortesse, P. Teillac, A. Le Duc, S. Avriillier, 'Laser induced autofluorescence diagnosis of bladder tumors: dependence on the excitation wavelength', *The Journal of Urology*, 156, 1590-1596, 1996.
22. Koenig, F., F. McGovern, H. Enquist, R. Larne, Th. Deutsch, K. Schomaker, 'Autofluorescence guided biopsy for the early diagnosis of bladder carcinoma', *The Journal of Urology*, Vol. 159, 1871-1875, 1998.
23. Koenig, F., F. McGovern, A. Althausen, Th. Deutsch, K. Schomaker, 'Laser induced autofluorescence diagnosis of bladder cancer', *The Journal of Urology*, Vol. 156, 1597-1601, 1996.
24. Leonhard, M., 'New incoherent autofluorescence/fluorescence system for early detection of lung cancer', *Diagnostic and therapeutic endoscopy*, 5, 71-75, 1999.
25. Häussinger, K., F. Stanzel, R. M. Huber, J. Pichler, H. Stepp, 'Autofluorescence detection of bronchial tumors with the D-Light/AF', *Diagnostic and therapeutic endoscopy*, 5, 105-112, 1999.
26. Hürzeler, D., 'Blue light endoscopy', *Laryngoscope*, 85(8), 1374-1378, 1975.
27. Weiss, A., H. Zeng, R. Kline, C. Macauley, N. Mackinnon, 'Use of Endoscopic Autofluorescence Imaging in Diagnosis of Disease of the Esophagus and Stomach', *Gastrointestinal Endoscopy*, 47(4), 70-70, 1998.
28. Dhingra, J., D. Perrault, K. McMillan, E. Rebeiz, S. Kabani, R. Manoharan, I. Itzkan, M. Feld, S. Shapshay, 'Early Diagnosis of Upper Aerodigestive Tract Cancer by Autofluorescence', *Arch Otolaryngol Head Neck Surg*, Vol 122, November 1996.
29. Gillenwater, A., R. Jacob, R. Ganeshappa, B. Kemp, A. El-Naggar, L. Palmer, G. Clayman, M. Mitchell, R. Richards-Kortum, 'Noninvasive diagnosis of oral neoplasia based on fluorescence spectroscopy and native tissue autofluorescence', *Arch Otolaryngol Head Neck Surg*, Vol. 124, 1251-1258, Nov 1998.
30. Ingrams, D., J. Dhingra, K. Roy, D. Perrault, I. Bottrill, S. Kabani, E. Rebeiz, M. Pankratov, S. Shapshay, R. Manoharan, I. Itzkan, M. Feld, 'Autofluorescence characteristics of oral mucosa', *Head & Neck*, 27-32, January 1997.
31. Bottioli, G., A. Croce, D. Locatelli, R. Marchesini, E. Pignoli, S. Tomatis, C. Cuzzoni, S. Di Palma, M. Dalfante, P. Spinelli, 'Natural Fluorescence of Normal and Neoplastic Human Colon: A Comprehensive "Ex Vivo" Study', *Lasers in Surgery and Medicine*, 16, 48-60, 1995.
32. Gupta, P., S. Majumder, A. Uppal, 'Breast cancer diagnosis using N₂ laser excited autofluorescence spectroscopy', *Lasers in Surgery and Medicine*, 21: 417-422, 1997.
33. Bigio, I., J. Mourant, 'Ultraviolet and visible spectroscopies for tissue diagnostics: fluorescence spectroscopy and elastic scattering spectroscopy', *Physics in Medicine and Biology*, 42, 803-814, 1997.
34. Qu, J., C. MacAulay, S. Lam and B. Palcic, 'Laser-induced Fluorescence Spectroscopy at Endoscopy: Tissue Optics, Monte-Carlo Modeling and in vivo Measurements', *Optical Engineering*, 34(11), 3334-3343, 1995.
35. Khanavkar, B., F. Gnudi, A. Muti, W. Marek, K.-M. Müller, Z. Atay, T. Topalidis, J. Nakhosteen, 'Grundlagen der LIFE[®]-Autofluoreszenzbronchoskopie', *Pneumologie*, 52, 71-76, 1998.
36. Häussinger, K., J. Pichler, F. Stanzel, A. Markus, H. Stepp, A. Morresi-Hauff, R. Baumgartner, 'Interventional bronchoscopy beyond the year 2000: autofluorescence', *Respiratory Bronchology*, in press, 1999.
37. Thomas Glanzmann, 'Steady-state and time-resolved fluorescence spectroscopy for photodynamic therapy and photodetection of cancer', PhD thesis #1920, EPFL, 1998.

8.3

In vivo autofluorescence spectroscopy of human bronchial tissue to optimize the detection and imaging of early cancers.

Matthieu Zellweger¹, Pierre Grosjean², Didier Goujon¹, Philippe Monnier², Hubert van den Bergh¹, and Georges Wagnières¹

¹DGR-LPAS, Institute of Environmental Engineering, Swiss Federal Institute of Technology (EPFL), CH-1015 Lausanne, ²ENT clinic, CHUV Hospital, CH-1011 Lausanne, Switzerland

Keywords: autofluorescence, lung cancer, early detection, imaging, spectroscopy.

ABSTRACT

We are developing an imaging system to detect pre-/early cancers in the tracheo-bronchial tree. Autofluorescence might be useful but many features remain sub-optimal. We have studied the autofluorescence of human healthy, metaplastic and dysplastic/CIS bronchial tissue, covering excitation wavelengths from 350 to 480 nm. These measurements are performed with a spectrofluorometer whose distal end is designed to simulate the spectroscopic response of an imaging system using routine bronchoscopes. Our data provides information about the excitation and emission spectral ranges to be used in a dual range detection imaging system to maximize the Tumor vs Healthy and the Tumor vs Inflammatory/Metaplastic contrast in detecting pre-/early malignant lesions. We find that the excitation wavelengths producing the highest contrasts are between 400 and 480 nm with a peak at 405 nm. We also find that the shape of the spectra of healthy tissue is similar to that of its inflammatory/metaplastic counterpart. Finally we find that, when the spectra are normalized, the region of divergence between the tumor and the non-tumor spectra is consistently between 600 and 800 nm and that the transition wavelength between the two spectral regions is around 590 nm for all the spectra regardless of the excitation wavelength, thus suggesting that there might be one absorber or one fluorophore. The use of backscattered red light enhances the autofluorescence contrast.

accepted for publication in the 'Journal of Biomedical Optics'

Introduction

Carcinoma of the bronchus is the commonest cancer in the western world. In determining the 5-year survival associated with the disease, tumor staging is a very important parameter [1, 2] as precancerous (dysplasia) and early cancerous lesions (carcinoma in situ and microinvasive carcinoma) are indeed much more successfully treated than invasive cancers [3]. The only method of localizing and delineating such lesions is bronchoscopy. However, the changes occurring during the first stages of the cancerization process make it difficult in most cases for the endoscopist to accurately localize the lesions under white-light illumination. Several examples of the use of Light-Induced Fluorescence (LIF) have been proposed for point fluorescence measurements and imaging applications with [4-8] and without [4, 9-15] the addition of an exogenous drug to enhance the contrast between the early cancerous lesion and the healthy surrounding area [16]. Because they rely upon the natural fluorescence of the tissues, the latter are termed 'autofluorescence' methods. Due to the geometry of the bronchi and the behavior of particles in the air flow, it is difficult to homogeneously distribute an inhaled exogenous drug to the bronchial epithelium and it is also difficult to perform point fluorescence measurements. Consequently, no exogenous fluorescent markers or exogenously induced drugs (PPIX) have shown convincing results up to now according to our knowledge. In this paper, we are thus reporting on a study about the autofluorescence of the bronchial tissue. Several experimental [8, 17, 18] and commercially available systems (Xillix [10, 11], Storz [19], SAFE-1000 (Pentax), [20]) use autofluorescence to create images of the bronchial tissue. The goal of these systems is to detect and distinguish the precancerous and early cancerous lesions from the healthy surrounding area. To do so, most of these systems excite the autofluorescence with blue and/or violet light and detect the autofluorescence in one [20], or several spectral regions [8, 10, 11, 19]. However, no systematic optimization work has been reported for the spectral design of these systems. Improvement might be possible by optimizing the domains of excitation and detection wavelengths. We propose here a study of the optimization of the excitation wavelength covering a range of excitation

wavelengths from 350 nm to 480 nm, and the detection spectral ranges to detect and characterize the precancerous and early cancerous lesions by autofluorescence in the tracheo-bronchial tree. Our choice of a dual range detection method is based on our aim of optimizing an imaging system. At least two spectral domains are necessary for efficient contrast enhancement. In fact, due to the tridimensional geometry of the bronchi, both a background and a contrast bearing foreground image are necessary. However, detection over many spectral regions is detrimental to the intensity of the fluorescence detected in each region and is consequently shot-noise limited.

Our measurements of the autofluorescence properties of the bronchial tissue in vivo are correlated to the histopathological status of the examined sites. Moreover, our measurements took place at a fixed distance between the tissue and the probe. This characteristic is also based on our goal of optimizing an imaging endoscopic system that probes the tissue from a certain distance.

Materials and Methods

Patients.

Forty-eight patients were involved in this study (see Table 1) from November 1996 to September 1999. The patients were scheduled for rigid bronchoscopy for screening purposes (positive cytology or primary cancerous lesion in the upper aerodigestive tract). Biopsies were taken in the case of a suspicion of an early cancerous lesion. The LIF measurements were executed during the general anesthesia required by rigid bronchoscopy. For safety reasons, not all patients were measured at all wavelengths.

Fluorescence Spectroscopy

Our optical fiber-based spectrofluorometer has been described elsewhere [21] and has only been slightly modified (Fig. 1) for this study. In brief, it consists of an excitation source (UXL-75 XE, 75W high pressure Xenon lamp, Ushio Inc., Japan) whose light is passed through a spectrograph (Chromex 250, Chromex, Albuquerque NM 87107, USA), filtered (filter #1, see Table 2) and injected into a quartz optical fiber hexagonal bundle (7 fibers, HPSUV300A, Oxford Electronics Ltd, Four Marks, Hants, UK; NA=0.22, 300 μ m core diameter).

This bundle is then connected to a similar bundle that has been adapted to fit the biopsy channel of a standard flexible bronchoscope (Olympus BF Type 20). Four of the seven fibers are used for the excitation light and the remaining three fibers collect the fluorescence light. The distance between the fiber bundle tip and the tissue to be investigated is kept constant (at 3.5 mm, [22]) by a spacer (Fig. 2a and 2b) in order to detect the same

spectroscopic response as an imaging system that does not come into actual contact with the tissue during routine inspection. The excitation wavelength is scanned between 350 nm (it is difficult to obtain enough excitation power below this wavelength with a clinically acceptable setup and shorter wavelengths are too far into the UV range to be compatible with this environment) and 480 nm (above this wavelength, the spectral domain of the 'green' image becomes too narrow to detect enough fluorescence power - see below for the definition of the 'green' image) (see Table 2) by steps of 10 or 15 nm.

The resolution of the excitation is ± 10 nm (FWHM) and the typical excitation power at the distal end of the setup is given in Table 2. The fluorescence is collected and separated from the backscattered excitation light by a dichroic mirror (filter #2, see Table 2). It is then filtered by a long pass filter (filter #3, see Table 2) and dispersed by a spectrograph (Chromex 250, Chromex,

Excitation Wavelength	Histopathological status	Number of patients	Number of spectra
350 nm	Healthy	9	59
	Inflammation/Metaplasia	3	60
	Dysplasia/CIS	2	21
365 nm	Healthy	15	182
	Inflammation/Metaplasia	3	60
	Dysplasia/CIS	2	20
380 nm	Healthy	8	80
	Inflammation/Metaplasia	3	66
	Dysplasia/CIS	2	18
395 nm	Healthy	8	75
	Inflammation/Metaplasia	3	66
	Dysplasia/CIS	2	15
405 nm	Healthy	34	435
	Inflammation/Metaplasia	14	295
	Dysplasia/CIS	5	61
420 nm	Healthy	23	193
	Inflammation/Metaplasia	13	167
	Dysplasia/CIS	4	33
435 nm	Healthy	21	185
	Inflammation/Metaplasia	13	150
	Dysplasia/CIS	5	41
450 nm	Healthy	26	344
	Inflammation/Metaplasia	13	162
	Dysplasia/CIS	5	67
465 nm	Healthy	14	121
	Inflammation/Metaplasia	12	149
	Dysplasia/CIS	3	24
480 nm	Healthy	13	132
	Inflammation/Metaplasia	8	90
	Dysplasia/CIS	3	27

Table 1: Number of patients and of spectra for each excitation wavelength and each pathological status.

Albuquerque NM 87107, USA) to be detected by a Peltier cooled CCD (TE/CCD-256, UV coated, Spectroscopy Instruments GmbH, D-82205 Gilching, Germany). LIF is observed in the range between 425 nm and 800 nm (depending on the excitation wavelength) with a resolution of 11 nm (FWHM). The whole setup is controlled by a 486 PC (Fast 486/50, Spectroscopy Instruments GmbH, D-82205

Gilching, Germany) with CSMA software (Spectroscopy Instruments GmbH, D-82205 Gilching, Germany) and mounted on a trolley for transport to the medical facility. The acquisition time of one spectrum is 2 seconds.

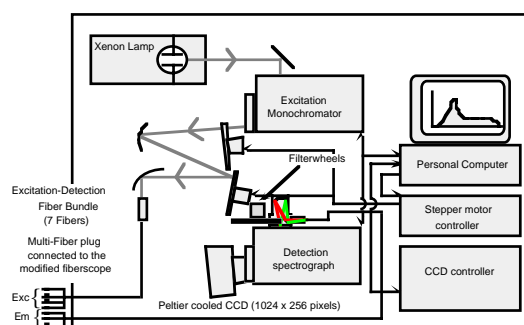


Figure 1: Apparatus for fluorescence measurements.

Before each clinical autofluorescence measurement session, the fluorescence spectrum of an aqueous solution of Rhodamine B ($c = 1 \cdot 10^{-6}$ M) in a 10 mm quartz cuvette is measured. The magnitude of the peak at 575 nm allows for a certain

degree of lamp output fluctuations to be taken into account and corrected for. Fluorescence excitation of the Rhodamine takes place at each of the excitation wavelengths and detection is between 450 and 800 nm (depending on the excitation wavelength). The fluorescence excitation light power is measured by placing the distal end of the modified bronchoscope into the detector of an optical power meter (Newport Instruments, 840-C). The spectrum of a non-fluorescent tissue-like phantom [23] is also measured. This spectrum is a background spectrum and allows for the subtraction of the fluorescence generated within the optical system (fiber bundle, filters, etc).

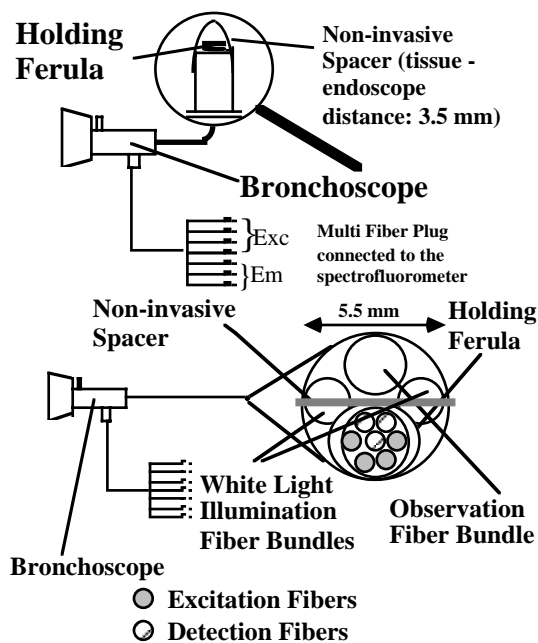


Figure 2: Probe for calibrated fluorescence spectroscopy (above: side view; below: front view).

Correction of the raw spectra

The raw spectra are corrected for the spectral response of the detector. This procedure has been described in detail elsewhere [22]. In brief, the spectrum of a calibrated lamp (the spectral emission of which is close to the emission of a perfect blackbody) was acquired with our setup. The resulting curve combined with the measurement of the fluorescence excitation power is used to divide the raw spectra, thus producing corrected spectra expressed in pW of fluorescence collected by the spectrofluorometer per nm and per μW of excitation power ([pW/(μW * nm)]). In our study, this correction produces spectra whose shape is correct, and whose

magnitude is correct down to a certain multiplicative factor that in turn depends on the instrumentation that was used. Nevertheless, the spectra throughout this study can be compared between themselves and are therefore expressed in 'relative units' (r.u.).

Procedure.

After the routine endoscopic observation of the tracheobronchial tree, the modified fiberoscope was passed through the rigid sheath. It was then placed onto the site to be measured. The spacer ensured a gentle contact with the tissue at a fixed distance (3.5 mm) between the fibers and the tissue. This distance was chosen as the best trade-off between the geometrical distortion of the spectra requiring as long a distance as possible and the SNR decrease requiring as close a distance as possible to minimize the integration time [22]. The endoscopic standard white-light illumination was switched off. Ten spectra were recorded on the same location for each excitation wavelength. The endoscopic light was then switched on again. The site was checked for the absence of blood prior to proceeding to further measurements and its macroscopical aspect was recorded. At the end of the measurement session, a biopsy was taken at the site of the measurements to check the histopathology of the site.

Histological examination

The biopsies were processed and analyzed in a routine fashion in the Institute of Pathology at the CHUV Hospital. The pathologists reported the results of microscopy and they were assigned to three different groups for the treatment of our spectral data: normal mucosae without any trace of inflammation or metaplasia were grouped under the label 'Healthy'. Inflammatory or metaplastic mucosae without malignant changes were grouped under the label 'Inflammation/Metaplasia'. The mucosae bearing pre-/early malignant features (mild, moderate and severe dysplasia as well as carcinoma in situ) were grouped under 'Dysplasia/CIS'. This grouping makes sense as it separates the healthy from the non-healthy but non-cancerous (inflammatory or metaplastic) tissues and from the early cancerous tissues.

Excitation Wavelength (FWHM: 20 nm)	Excitation Filter (#1) (0°)	Dichroic Filter (#2) (45°)	Emission Filter (#3) (0°)	Typical power at the distal tip of the probe (\pm SD)
350 nm (\pm 10 nm)	Bandpass UV, UG5*	Dichroic 425 nm, DC425**	Longpass 425 nm, FG425**	9.2 μ W (\pm 2.9 μ W)
365 nm (\pm 10 nm)	Bandpass UV, UG5*	Dichroic 425 nm, DC425**	Longpass 425 nm, FG425**	14.9 μ W (\pm 4.4 μ W)
380 nm (\pm 10 nm)	Bandpass UV, UG5*	Dichroic 425 nm, DC425**	Longpass 425 nm, FG425**	13.8 μ W (\pm 4.0 μ W)
395 nm (\pm 10 nm)	Bandpass Blue, BG3*	Dichroic 425 nm, DC425**	Longpass 435 nm, FG435**	14.2 μ W (\pm 4.0 μ W)
405 nm (\pm 10 nm)	Bandpass Blue, BG3*	Dichroic 450 nm, DC450**	Longpass 450 nm, FG450**	17.7 μ W (\pm 4.8 μ W)
420 nm (\pm 10 nm)	Bandpass Blue, BG3*	Dichroic 450 nm, DC450**	Longpass 450 nm, FG450**	16.4 μ W (\pm 5.3 μ W)
435 nm (\pm 10 nm)	Dichroic 450 nm, DC450**	Dichroic 450 nm, DC450**	Longpass 495 nm, FG495**	13.7 μ W (\pm 4.6 μ W)
450 nm (\pm 10 nm)	Dichroic 450 nm, DC450**	Dichroic 475 nm, DC475**	Longpass 495 nm, FG495**	15.6 μ W (\pm 6.4 μ W)
465 nm (\pm 10 nm)	Dichroic 550 nm, DC550**	Dichroic 475 nm, DC475**	Longpass 515 nm, FG515**	11.5 μ W (\pm 3.8 μ W)
480 nm (\pm 10 nm)	Dichroic 550 nm, DC550**	Dichroic 550 nm, DC550**	Longpass 530 nm, FG530**	24.4 μ W (\pm 4.4 μ W)

Table 2: characteristics of the filters used for the fluorescence spectroscopy (* filters by Schott Glaswerke, D-55116 Mainz, Germany, ** filters by Reynard, San Clemente CA 92673-6227, USA).

Analysis of results.

Mean and typical autofluorescence spectra

The background spectrum of the phantom was subtracted from each measurement. For each set of 10 raw spectra at a given site, a mean spectrum was calculated. This mean spectrum was corrected by the Rhodamine reference value to correct for some instabilities of our setup. All the mean spectra of a given excitation wavelength were then grouped according to the histopathological status (see above for the classifications) of their corresponding biopsy, normalized and averaged. This produced three (see Table 1) spectra (thereafter called 'typical' spectra) for each excitation wavelength (see an example in Fig. 3 for 405 nm as the excitation wavelength). These typical spectra are given for a histopathological status and a standard deviation of the mean was computed (also in Fig. 3). They were corrected for the spectral sensitivity of the optical setup and detector (see above or [22] for the procedure).

Cut-on wavelength

The first parameter to determine for the spectral optimization of a dual range detection imaging device is the cut-on wavelength which separates the spectral domains corresponding to the foreground

and background images. For this purpose, the typical non-healthy spectra and the typical healthy spectrum were superimposed (see an example in Fig. 4 for 405 nm as the excitation wavelength). The difference between the 'Dysplasia/CIS' and the 'Healthy' typical spectra, or the difference between the 'Dysplasia/CIS' and the

'Inflammation/Metaplasia' typical spectra was calculated (see an example for the difference between the 'Dysplasia/CIS' and the 'Healthy' in Fig. 4 for 405 nm as the excitation wavelength). The shortest wavelength corresponding to the half-maximum value produced the 'cut-on' wavelength (600 nm in the Fig. 4). This wavelength is used below for the optimization of the sensitivity ('Dysplasia/CIS' vs 'Healthy') and the optimization of the specificity ('Dysplasia/CIS' vs 'Inflammation/Metaplasia'). This separation of the autofluorescence spectra into two regions, namely a short-wavelength region (thereafter 'green' region) and a long-wavelength region (thereafter 'red' region) is justified because it has been reported in several papers that the decrease of autofluorescence on pre-/early cancerous lesions is larger in the 'green' part than in the 'red' part of the spectrum.

Sensitivity and specificity

To optimize the sensitivity and the specificity of our method, we need to compare the typical 'Dysplasia/CIS' spectrum with either the typical 'Healthy' spectrum (sensitivity) or with the typical 'Inflammation/Metaplasia' spectrum (specificity). We named the

fluorescence relative power of the green and the red regions of the 'Dysplasia/CIS' spectrum 'A' and 'B' respectively, the fluorescence relative power of the green and the red regions of the 'Healthy' spectrum 'C' and 'D' respectively, and the fluorescence relative power of the green and the red regions of the 'Inflammation/Metaplasia' spectrum 'E' and 'F' respectively (see an example in Fig. 3 for 405 nm as the excitation wavelength). A, B, C, D, E and F were calculated for each measurement whenever the spectra were available. The corresponding R, R' and R'' ratios (see below) were then calculated for each measurement, as well as a subsequent mean R, R' or R'' for the relevant patient. The general mean of these mean ratios is plotted in Fig. 6a, 6b and 6c as a function of the excitation wavelength.

As stated above, we defined three ratios to quantify the modifications of the spectra associated with different histopathological statuses in order to optimize both the sensitivity (Tumor vs Healthy modifications) and the specificity (Tumor vs Inflammation/Metaplasia modifications), namely R, R' and R'' as:

$$R_{\text{Sens.}} = \frac{C}{A} \div \frac{D}{B} = \frac{B \times C}{A \times D} \text{ and}$$

$$R_{\text{Spec.}} = \frac{E}{A} \div \frac{F}{B} = \frac{B \times E}{A \times F}$$

$$R'_{\text{Sens.}} = \frac{C}{A} \text{ and } R'_{\text{Spec.}} = \frac{E}{A}$$

$$R''_{\text{Sens.}} = \frac{D}{B} \text{ and } R''_{\text{Spec.}} = \frac{F}{B}$$

These ratios express the ratio of the modifications in the green over the modifications in the red ($R_{\text{Sens.}}$ for the Tumor vs Healthy modifications and $R_{\text{Spec.}}$ for the Tumor vs Inflammation/Metaplasia modifications), the modifications in the green ($R'_{\text{Sens.}}$ for the Tumor vs Healthy modifications and $R'_{\text{Spec.}}$ for the Tumor vs Inflammation/Metaplasia modifications) and the modifications in the red ($R''_{\text{Sens.}}$ for the Tumor vs Healthy modifications and $R''_{\text{Spec.}}$ for the Tumor vs Inflammation/Metaplasia modifications). It should be noted that these ratios are monotonic functions of the Tumor vs

Healthy and Tumor vs Inflammation/Metaplasia contrasts and that R is a monotonic function of the chromatic contrast. It should also be taken into account that R is independent of the tissue-probe distance whereas this is not the case for R' and R''. To optimize the autofluorescence detection method, we need to find the excitation wavelength maximizing one or several of these ratios, depending on the approach that has been chosen.

Results

Typical autofluorescence spectra

The typical autofluorescence spectra of the healthy tissue, inflammatory/metaplastic tissue and dysplasia/CIS excited at 405 nm are presented in Fig. 3. The typical spectrum of the healthy tissue is the average of 435 measurements, the typical spectrum of the inflammatory/metaplastic tissue is the average of 295 measurements and the typical spectrum of the dysplasia/CIS is the average of 61 measurements. The three typical spectra are plotted on the same scale to reflect their relative intensity. The Dys/CIS vs Healthy cut-on wavelength (600 nm) is plotted just for the sake of clarifying the concept, along with the 6 regions of interest (A, B, C, D, E and F). The regions at shorter (longer) wavelengths than the cut-on wavelength are named 'green' ('red') regions respectively. The units are relative units as a multiplicative factor, which depends on the geometry of the optical coupling of the fluorescence light into the detection fiber at the distal end of our device, would intervene to actually have units independent of our spectrofluorometer. The error bars in Fig. 3 express the 67% confidence interval.

It should be noted that such typical spectra were measured and computed (see Table 1) for the other excitation wavelengths (350 nm, 365 nm, 380 nm, 395 nm, 420 nm, 435 nm, 450 nm, 465 nm and 480 nm) but are not displayed for the sake of readability.

It is interesting to note that the 'Healthy' and the 'Inflammation/Metaplasia' typical spectra are very reproducible from one patient to another, hence the small error bars (this was observed at all excitation wavelengths). Moreover, it should be noted that, when superimposed, the Inflammation/Metaplasia typical spectra and the 'Healthy' typical

spectra are quite close in shape (data not shown).

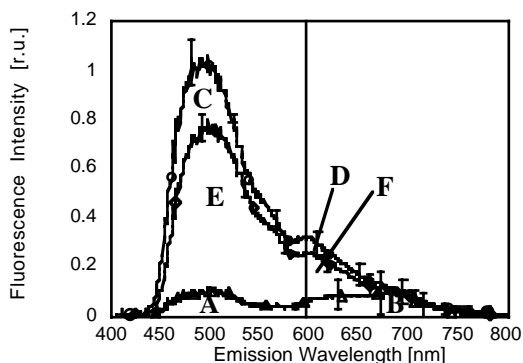


Figure 3: Typical autofluorescence spectrum of healthy (circles), inflammatory/metaplastic (diamonds) and pre-/early cancerous (triangles) lung tissue excited at 405 nm in vivo. The error bars represent the 67% confidence interval and the vertical line is drawn for the separation of the short-wavelength (green) and long-wavelength (red) regions of the spectra. The green region of the healthy spectrum is termed C, of the inflammatory/metaplastic, E and of the pre-/early cancerous, A. Similarly, the red regions are termed D, F and B.

This feature is especially striking for the excitation wavelength 405 nm: both typical spectra ('Healthy' and 'Metaplasia') are overlapped and nearly indistinguishable. This seems to indicate that there is little, if any, difference in the spectral shape of the healthy and the inflammatory/metaplastic lung tissue whereas the intensity of the latter is significantly smaller than that of the former. Moreover, the small error bars observed on the 'Inflammatory/Metaplasia' typical spectra tend to indicate that this measurement is also highly reproducible. These features are observable for each excitation wavelength (data not shown) and are in agreement with previously reported results [24].

The error bars of the 'Dysplasia/CIS' typical spectrum are also plotted in Fig. 3. They appear to be larger than on the 'Healthy' typical spectrum. This might partly be due to the much smaller statistics (the product of the error bar and the square root of the number of measurements is not constant) and partly to an inherent inhomogeneity of the early cancerous lesions.

Figure 4 shows the superimposed typical spectra for the healthy tissues and the early

cancerous tissues excited at 405 nm. The difference of the two typical spectra is also plotted along with the cut-on wavelength (half-maximum).

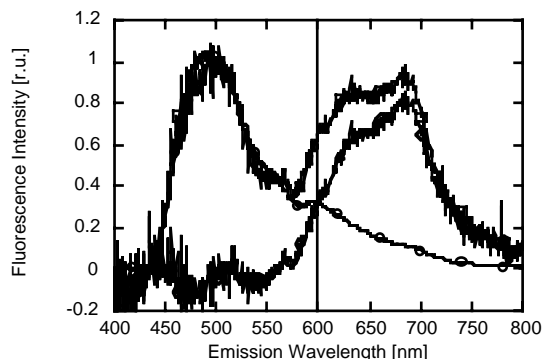


Figure 4: Superimposed normalized typical autofluorescence spectra of healthy (circles) and pre-/early cancerous (squares) lung tissue excited at 405 nm in vivo and difference (diamonds) between the pre-/early cancerous and the healthy spectra. The half-maximum of the difference defines the cut-on wavelength and is displayed as a vertical line.

This calculation was carried out for each excitation wavelength and the results are given in Figure 5 as the cut-on wavelength for the optimization of the sensitivity ('Dysplasia/CIS' vs 'Healthy') and the optimization of the specificity ('Dysplasia/CIS' vs 'Inflammation/Metaplasia') together with the average cut-on wavelength for both cases.

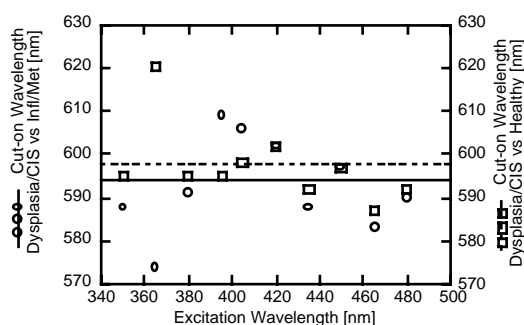


Figure 5: Cut-on wavelength as a function of the excitation wavelength. The mean cut-on wavelength for the Dysplasia/CIS vs healthy tissues (squares and broken line) and Dysplasia/CIS vs Inflammatory/Metaplastic tissues (circles and plain line) is displayed.

It is interesting to note that the cut-on wavelengths for sensitivity and specificity are very close to each other within an excitation wavelength (with one exception, 365 nm) and also very close to each other

from one wavelength to another (again, with the exception of 365 nm) at around 600 nm. It is likely that this reflects a general property of the biological tissue.

The ratios R and R' and R'' are plotted for the optimization of both sensitivity and specificity as a function of the excitation wavelength in Fig. 6a (R), 6b (R') and 6c (R''). Such a graph is intended to provide an answer to the issue of the best excitation wavelength for maximum sensitivity and maximum specificity. The nominal values of R' are larger than those of R because the decrease in the autofluorescence in the green is offset by a smaller decrease of the autofluorescence in the red. The UV excitation wavelengths (350-395 nm) seem to be less efficient in generating a contrast than the blue-violet excitation wavelengths (400-465 nm) and excitation around 405 nm seems to produce the highest contrast. It is also interesting to note that this excitation region seems to hint at the same fluorescence excitation wavelengths for both the optimization of sensitivity and the optimization of specificity. The fact that the 'pure' decrease in the green (as given by R') is more important than the R ratio is in agreement with the previously stated observation that the autofluorescence decrease is larger in the green than in the red. This is further demonstrated by the fact that R' is almost systematically larger than R . Consequently, the use of backscattered red light would allow the clinician to take advantage of the whole decrease in the green region (because it would correspond in our case to $R'' = 1$ or $R = R'$) without the offset of the modifications of the red autofluorescence.

Discussion

Since the first 'blue light endoscopies' by Hürzeler [25], much has been learnt about the fluorescence techniques applied to detect early cancerous lesions of the bronchi. Several commercial systems have been built and tested throughout the world. However, no optimization study preceded these developments [26-29]. Such a study could lead to significant improvements in future photodetection systems. A possible way to contribute to this improvement is to optimize the spectral designs of the systems. To do so, a study of the excitation wavelengths and the detection windows was necessary over a

large range of excitation wavelengths. This was the main goal of our work.

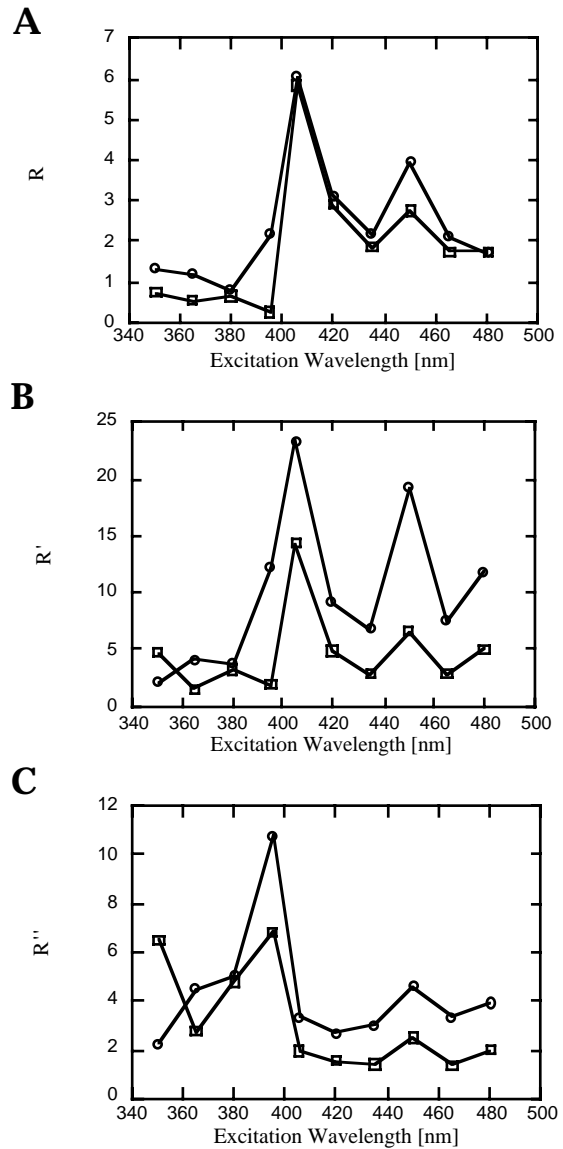


Figure 6: Ratios $R_{Sens.}$ ($(B * C) / (A * D)$, Dysplasia/CIS vs Healthy, circles) and $R_{Spec.}$ ($(B * E) / (A * F)$, Dysplasia/CIS vs Inflammatory/Metaplastic, squares) as a function of the excitation wavelength (a). Ratios $R'_{Sens.}$ (C/A , Dysplasia/CIS vs Healthy, circles) and $R'_{Spec.}$ (E/A , Dysplasia/CIS vs Inflammatory/Metaplastic, squares) as a function of the excitation wavelength (b). Ratios $R''_{Sens.}$ (D/B , Dysplasia/CIS vs Healthy, circles) and $R''_{Spec.}$ (F/B , Dysplasia/CIS vs Inflammatory/Metaplastic, squares) as a function of the excitation wavelength (c).

Bearing this goal in mind, we decided to consider a dual range detection method. It is possible to imagine detection algorithms with many channels as has been done for the detection of early lesions in the cervix [30] but this method works fine for point

spectroscopic measurements only. For real-time imaging purposes in the tracheo-bronchial tree, the intensity of the fluorescence signal in each detection region also has to be considered. Increasing the number of detection regions will decrease the number of photons in each region. This will eventually be detrimental to the quality of the images that are to be detected.

Several papers report a sharp autofluorescence decrease on early cancerous lesions around 500 nm and/or a relatively less important decrease after 600 nm when excited between 400 and 450 nm [7, 9, 31]. This is the fundamental base behind all the autofluorescence imaging systems. The Pentax system works with a single range detection principle [20] whereas a multiple range approach has been preferred for the Xillix and the Storz systems [19, 31] and some laboratory systems [8, 17, 18]. It is interesting to note that our results are in good agreement with these previous results. Indeed, we also found that the autofluorescence of the early cancerous lesions sharply decreases when excited in the blue-violet range and decreases less significantly in the red region. The comparison of the typical spectra takes place through their superimposition, a method that has been used by other groups [7, 24].

The first computation that was performed with the typical spectra was the determination of the cut-on wavelength. From its definition, this is the wavelength that delineates the green and the red regions. In the perspective of a dual range detection system, this would correspond to the transition wavelength of a dichroic mirror. This cut-on wavelength was found to be around 595-600 nm with no measurable dependence on the excitation wavelength. Moreover, the cut-on wavelength for the optimization of sensitivity and for the optimization of specificity were found to be similar. This result seems to indicate that the choice of an excitation wavelength should have little, if any, impact on the spectral specifications of a dichroic mirror. This observation is fortunate for possible future developments of novel photodetection devices. Indeed, it means that the spectral transition producing the highest sensitivity is the same as the one producing the highest specificity. The design of such a system could therefore avoid a trade-off between

those two concepts. Moreover, this observation seems to hint at the fact that only one class of fluorophores or only one class of absorbers are involved in the modifications of the shape of the autofluorescence spectra.

The previously mentioned observation that the overall autofluorescence decreases between a healthy bronchial tissue and an early cancerous lesion dictated our approach for the treatment of the data. Having defined the green and the red regions of both the healthy and the early cancerous typical spectra, we compared their surfaces. The R ratio takes into account the modifications of the green autofluorescence and the modifications of the red autofluorescence. Since these modifications seem to be different for both regions (hence the relative 'increase' in the red region when the typical spectra are superimposed), this is used to generate a color contrast in a dual range detection method. However, the use of the modifications in the red region partly offsets the decrease in the green region (as can be seen with the R' ratio that is larger than the R ratio). This decrease can then be used at its maximum with a single range detection method, but it then loses the advantage of the endoscope-tissue distance independence and is subject to artefacts since it does not rely on two images anymore. This is the trade-off that faces future developers of autofluorescence imaging systems. Another method to avoid this problem is to be found in the use of reflectance light (which, in our case, corresponds to $D = B$ for red reflected light, in which case $R = R'$). Assuming the level of backscattered light does not depend on the tissue-probe distance, it is possible to use the whole range of the decrease in the green region of the spectra. This has been implemented in at least one commercial system with blue backscattered light [19] and has been reported with red backscattered light in the GI tract by Weiss et al [32].

The superimposition of the typical spectra produces interesting information about the modification of the spectral shape along the cancerization process. The ultimate goal of photodetection is to unequivocally separate the precancerous and early cancerous lesions from the healthy and metaplastic/inflammatory mucosae. Since we chose a dual range detection mode, this means that the shape of the spectra should be

such that the modifications in one window are different from the modifications in the other window in a Dysplasia/CIS only and not on metaplastic/inflammatory tissue. It also means that the shape of the spectra for the healthy mucosae and the inflammatory/metaplastic mucosae should be similar enough to be assigned to the same sub-group of non-cancerous spots. According to this study, it is very striking that the spectra for the inflammatory/metaplastic tissue often overlap the spectra for the healthy tissue to a large extent. Moreover, the error bars are small on these spectra ($\pm 8.5\%$ on average between 500 and 700 nm for the typical spectrum of healthy tissue excited at 405 nm), thus indicating not only a striking similarity between the spectra of the inflammatory/metaplastic and healthy tissue but also a stable similarity, hence a very high degree of interpatient reproducibility of our measurements. This is in good agreement with results reported by others about the similarity of the spectra acquired on healthy and on inflammatory bronchial tissue [24]. These features tend to indicate that the implementation of this method into an optimized imaging system could produce few false-positive results as the inflammatory or metaplastic areas would be consistently similar to the healthy ones.

A more sensitive issue is the stability of the spectral shape of the precancerous/early cancerous areas. Because they are frequently invisible to the naked eye, these lesions are hard to find and hence the possible measurement sites are few. Some excitation wavelengths produce a more important contrast between these lesions and healthy tissue than others, as can be seen in the Fig. 6a. The contrast seems to be building up at 395 nm, stays high for blue excitation wavelengths (405 to 450 nm) and goes down again after 450 nm. This clearly speaks for blue-violet excitation wavelengths instead of UV or longer wavelength light. This observation seems to be consistent whatever the ratioing method (see Fig. 6a, 6b and 6c). A non-negligible problem is the large error bars on the 'Dysplasia/CIS' typical spectra (a fact that is observed at each excitation wavelength). Part of the reason behind this fact is the smaller number of measurements on such locations. Nevertheless, most of it might also be due to a naturally higher inhomogeneity of the pre-

/early cancerous lesions. Still, at least one other reason should be considered, namely the sampling error, either the fluorescence measurements or the biopsy taking. If a measurement and a biopsy are from different sites, a suspicious-shaped spectrum could be included in the healthy group of spectra or, vice-versa, a possibility that would be more detrimental to our study because of the very much smaller number of proven suspicious areas. Although very difficult to prove, such an error could obviously bear heavily on the error bars if found to be true. It is likely, though, that this could easily happen. Indeed, the pre-/early cancerous lesions that we measured were very small patches of diseased cells surrounded by mainly healthy mucosa. In such a situation, one could easily imagine that the shifting of the biopsy forceps by say 1 mm could lead to the sampling of a normal tissue area whereas the measured spectrum indicated the opposite. As a matter of fact, the smaller statistics of the Dysplasia/CIS group of spectra is not a sufficient reason to explain the larger noise on these measurements (the product of the error bar and the square root of the number of measurements is not constant). This observation clearly speaks in favor of a non-negligible sampling error.

A major drawback of our method would be the instability of the autofluorescence measurements. It is obvious that not only two normal mucosae in two different patients should produce a similar autofluorescence spectrum (interpatient variations of the spectra), but also that several normal sites in the bronchi of the same patient should produce a similar spectrum (inpatient variations of the spectra). Moreover, if the autofluorescence method were to be used in a routine fashion to detect early cancerous lesions, it should also be able to discriminate between malignant lesions and bruised or irritated mucosae. To study this issue, we therefore measured six autofluorescence spectra on 3 healthy sites in the bronchi of five patients. We included in these measurements such areas that were normal but macroscopically different (such as erythroplastic/bruised (4), leucoplasic (2), thickened (1) areas). The typical spectra are very similar from one patient to another (interpatient similarity) and very similar to each other (inpatient similarity) as can be seen from the small error bars on the Fig. 7 (data for one patient, data from the other

patients not shown for the sake of readability). An example of these results is given in Fig. 7. The areas measured for Fig. 7 are both healthy but differ in their macroscopic aspect. The second spot is reddish (bruised).

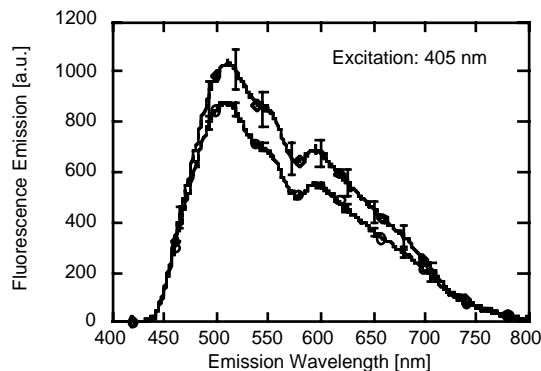


Figure 7: Measured mean spectra (six measurements each) of the autofluorescence of two spots (both normal: one with a normal appearance (circles) and one bruised (diamonds)) in the bronchi of the same patient. Excitation wavelength: 405 nm.

It is interesting to note that this result tends to demonstrate that the macroscopic aspect of a normal area in the bronchi is of little influence on the shape of the autofluorescence spectra. This is reassuring as the opposite would mean that the method is close to useless to the clinician. This also demonstrates that the autofluorescence measurements have a good inpatient stability in addition to a good interpatient stability. This is in agreement with previously published data [7]. This is reassuring as to the possibility of optimizing an imaging photodetection apparatus as it means that these benign lesions would not be positive on the autofluorescence images and would also be stable against inpatient variability.

Such a study over hundreds of spectra can provide knowledge not only about the spectroscopy of early lesions but also about non-malignant tissues. Clearly, a detection method that produced a positive result for metaplasias would prove quite useless to the clinician. It is therefore of crucial importance to find a way to assign both the healthy tissues and the non-healthy but benign (namely the inflammatory and metaplastic tissues) to the same group unequivocally. This means that the spectra should be as

stable as possible. Our results tend to show that this is the case.

The use of autofluorescence as a detection method for pre-/early cancerous lesions has been reported in several organs. In the lungs, the most often described system is the LIFE system. This system relies on a dual range detection method [10]. It is recognized as a valuable complement to the standard white-light bronchoscopy [11, 12, 33, 34]. The results behind the development of this system by Hung et al [9] and Palcic et al [31] are confirmed by our findings that the fluorescence of the pre-/early cancerous lesions are reduced by around one order of magnitude in the green region with respect to healthy tissue whereas the decrease is less marked in the red region. As for the modifications of the spectral shape, the authors did not observe any of them for excitation wavelengths of 405 or 442 nm [9]. Still, the decrease in the region around 500 nm is in agreement with their results. In a study about the autofluorescence of bronchial tissue, Qu et al [24] also report a decrease in autofluorescence intensity between healthy and inflamed tissue as well as between healthy and CIS tissue. They also report that the shape of the spectra of inflamed tissue is similar to that of the spectra of healthy tissue, a result that is confirmed by our findings. However, these authors do not report any modification of the spectral shape of the CIS with respect to the healthy tissue. On the contrary, they show that when their intensity is adjusted accordingly, the spectra of both the healthy tissue and the CIS overlap. Our results are in disagreement with this finding and it is probably a sign that the controversy is still going on as to the exact reasons behind the modifications of the autofluorescence spectra. It should be noted, though, that these authors performed their measurements with a probe in contact with the tissue. It is a critical point as such a measuring procedure only allows a very small volume of tissue to be probed. A possible element of explanation might be that the modifications to the intensity of the autofluorescence spectra might be due to some modifications to the contents in biomolecules (flavins) in the tissue, a feature that is observed by both Qu et al [24] and ourselves. On the other hand, the modifications in the shape of the autofluorescence spectra might be linked to a deeper lying effect (such as maybe an

increase of the relative vascular volume, hence an increase in the relative hemoglobin contents) which would be probed only when observing the tissue from a certain distance. This might be an element of explanation for the discrepancy between the work of these authors and ours. Indeed, the large peak on Fig. 6a could be reminiscent of a similar peak on the absorption spectrum of hemoglobin.

As an extension of the studies on the Xillix system, Takehana et al [35] found that it could be useful in the GI tract and report autofluorescence spectra similar to ours in normal and precancerous tissues in the esophagus. Again, the behavior of the autofluorescence is a decrease on moderate dysplasia and a modification of the spectral shape, in this work a relative increase of the red (580+ nm) contribution. Although this is reported for a different organ, it is interesting to note the striking similarity to our results. Another interesting extension of the Xillix system is reported by Weiss et al [32] for the esophagus and stomach. In this work, the authors used a fluorescence/reflectance mode by means of red backscattered light. They report an improved contrast with the latter with respect to the former. This corresponds to our R' ratio (because in this case $B = D$ which is the desired effect when adding red reflectance light) and our results are also in agreement with these findings (Fig. 6a). The reflectance mode has also been used in the Storz system but this time blue instead of red light is detected [19]. The Storz system was used in a clinical context by Häussinger et al [14], who report a similar decrease in the autofluorescence on severe dysplasia with respect to normal epithelium when excited in the 380-460 nm range. The spectral shape of their measurements is not investigated in great detail but their assumption that the color of pre-/early cancerous lesions will be different is a hint that the spectral shape could change. It is indeed the case in the spectra they report although only one spectrum for each pathological status is given. The blue backscattered light is intended to produce a constant distance-independent background image for dual range detection. Nevertheless, the strong absorption of the blood in this part of the spectrum could cause benign small bruised areas to appear red and thus generate a false positive site.

Another commercially available system that relies on autofluorescence to detect pre-/early cancerous lesions is the SAFE-1000 system. This system uses a single range detection method in the green region of the autofluorescence spectrum. It corresponds to our R' ratio. In such a system, the positive-looking sites appear darker than the surrounding mucosa rather than having a different color [20]. Kakihana et al report of a clinical study with this system [13] and report a similar decrease in the autofluorescence of an invasive squamous cell carcinoma (excitation at 440 nm) with a relative increase in the fluorescence emission above 540 nm. However, these authors also report that the thickening of the epithelium because of chronic inflammation induces false negative results. Moreover, such a single range system is subject to difficulties due to the fact that the tridimensional geometry of the bronchi induces darker areas that are not lesions but rather areas at a greater distance from the source. The inhomogeneity of the illumination could possibly induce false positive results in a single range system.

There is a recurrent controversy about the reasons of the decrease of the autofluorescence in the green region of the spectrum. A possible explanation is that the fluorescence is reabsorbed by the thickened epithelium (architectural effect). This is a partial explanation proposed by Qu et al [24] who report interesting changes in intensity of the autofluorescence spectra and parallel changes in the mean thickness of the bronchial epithelium from $46 \pm 3 \mu\text{m}$ in normal epithelium, to $70 \pm 7 \mu\text{m}$ in dysplasia to $116 \pm 16 \mu\text{m}$ for CIS. However, they do not provide any thickness measurement for the inflammatory tissues, shown in their work to undergo a similar intensity decrease. The epithelial thickening is also invoked by other authors [14] to explain the changes in the autofluorescence emission from pre-/early cancerous tissues. Another possible explanation is a change in the microenvironment (pH, cell metabolism, redox state of the flavins or the nicotinamides), namely a biochemical effect. Several authors invoke this possibility [9, 36, 37], but the clear-cut unequivocal reason behind the changes in autofluorescence emission remains unclear.

In the light of our results, it seems that an architectural effect alone is unlikely. If this were the case, we would observe a continuous change of the autofluorescence spectrum from that of the healthy tissue towards that of the carcinoma in situ (namely a gradual spectroscopic change following the gradual thickness change from healthy to metaplasia to dysplasia to CIS). Consequently, we would observe a continuous change in the intensity of the spectrum (actually observed) and a continuous change in the shape of the spectrum (not observed as the inflammatory/metaplastic tissues exhibit the same spectral shape as the healthy tissues). It might well be that the thickening of the epithelium along the process of cancerization is not the only reason that accounts for the modifications to the spectroscopy of the biological tissues during cancerization.

On the other hand, if the modifications were due to biochemical effects only, it is likely that one would observe no change in the autofluorescence spectrum, neither in its shape nor in its intensity, between those of the healthy tissue and the metaplasia, since both are considered normal and non-malignant. As a matter of fact, we do not observe a change in the spectral shape of the spectra but it is clear that the metaplastic tissues exhibit less fluorescence when excited in the violet-blue region. These elements seem to give us a hint that the modifications in fluorescence are probably not due to one clear-cut reason alone but rather to a group of changes.

The sampling error proved to be a possible problem. When probing a tissue, it might be difficult to take a biopsy at the exact place where the measurements took place. Although this might lead to a spectrum being assigned to the wrong group, it is a negligible problem regarding the typical spectra of healthy tissue. As a matter of fact, the number of stable reproducible spectra that we measured on healthy or metaplastic tissue is such that it allows a small number of possibly wrong measurements to be disregarded. However, such an argument is invalid for the early lesions group of spectra. Due to the relatively small number of lesions, one wrongly assigned spectrum can bear quite heavily on the statistics. Moreover, due to the difficulty of actually seeing these lesions, it is likely that the

possible error in the biopsy taking (as well as in the histopathological analysis) could be higher for pre-/early cancerous lesions than for the normal mucosa. Unfortunately, it is hard to imagine any way to overcome such a possible error, especially since small early lesions are surrounded by much larger areas of healthy mucosa.

One goal of the clinician is to clearly separate the tissues that present some malignant change from the tissues that do not (specificity). In this sense, they require some methodology that would assign healthy, inflammatory and metaplastic tissues to the same group and light and moderate and severe dysplasias as well as carcinoma in situ to another group. Our results seem to show that this is the case for spectroscopic measurements. Obviously, there is much more variability from one spectrum to another in the 'Dysplasia/CIS' group than in the 'Healthy' and 'Metaplasia' groups. This is probably due to a much wider range of possible alterations of the tissue. A further similar study could benefit greatly from the investigation of light or moderate or severe dysplasias only. Classifying the spectra of these lesions in three subgroups instead of grouping them into only one category would produce the spectra of all the tissue stages along the cancerization process. However, due to the aforementioned difficulties, great care will have to be exercised when collecting the data.

Our study also produces very interesting results about healthy tissues. They clearly show that there might be something like a 'typical' spectrum for both absolutely healthy bronchial tissue in vivo and metaplastic or inflammatory tissue. Moreover, it seems that the spectral shape of these two typical spectra are similar and that they are reproducible. The interpatient and inpatient fluctuations seem negligible, as can be seen on the error bars of the typical spectra. Such an observation is of great importance not only for developers of future autofluorescence imaging systems but also for clinicians that will eventually use them as it suggests a low level of false positive results.

Acknowledgements

We gratefully acknowledge support from the Swiss National Fund for Scientific Research, Grants #20-50691 and #21-

43507.95, the Swiss Priority Program in Optics (PPO II), the 'CHUV-EPFL-UNIL' Fund for collaboration in the area of biomedical technology, the 'Fonds de Service' and 'Fonds de Perfectionnement' of the ENT, Head and Neck Surgery Department at the CHUV Hospital.

References

- [1] R. Souhami and J. Tobias, *Cancer and its Management*, Blackwell Science, Oxford, 1995.
- [2] S. Lam and H. Becker, "Future diagnostic procedures", *Thoracic endoscopy*, **6**(2) 363-380, (1996).
- [3] P. Norwell, "Mechanisms of tumor progression", *Cancer Research*, **46**, 2203-2207, (1986).
- [4] S. Lam, J. Hung and B. Palcic, "Detection of lung cancer by ratio fluorimetry with and without Photofrin II", *Proceedings SPIE*, **1201**, 561-568, (1990).
- [5] R. Baumgartner, R. M. Hubber, H. Schultz, H. Stepp, K. Rick, F. Gamarra, A. Leberig and C. Roth, "Inhalation of 5-aminolevulinic acid: a new technique for fluorescence detection of early stage lung cancer", *J. Photochem. Photobiol. B: Biol.*, **36**, 169-174, (1996).
- [6] Y. Hayata, H. Kato, J. Ono, "Fluorescence fiberoptic bronchoscopy in the diagnosis of early stage lung cancer", in: *Recent results in cancer research*, pp. 121-130, Springer Verlag, Berlin-Heidelberg, 1982.
- [7] D. J. Anthony, A. E. Profio and O. J. Balchum, "Fluorescence spectra in lung with porphyrin injection", *Photochem. Photobiol.*, **49**, 583-586, (1989).
- [8] G. Wagnières, A. Studzinski, D. Braichotte, P. Monnier, C. Depeursinge, A. Châtelain and H. van den Bergh, "Clinical imaging fluorescence apparatus for the endoscopic photodetection of early cancers by use of Photofrin II", *Applied Optics*, **36**(22), 5608-5620, (1997).
- [9] J. Hung, S. Lam, J. C. LeRiche and B. Palcic, "Autofluorescence of normal and malignant bronchial tissue", *Lasers Surg. Med.*, **11**, 99-105, (1991).
- [10] S. Lam, C. MacAulay, J. Hung, J. LeRiche, A. E. Profio and B. Palcic, "Detection of dysplasia and carcinoma in situ with a lung imaging fluorescence endoscope device", *J. Thorac. Cardiovasc. Surg.*, **105**, 1035-1040, (1993).
- [11] S. Lam, T. Kennedy, M. Unger, Y. E. Miller, D. Gelmont, V. Rusch, B. Gipe, D. Howard, J. C. Leriche, A. Coldman and A. F. Gazdar, "Localization of bronchial intraepithelial neoplastic lesions by fluorescence bronchoscopy", *Chest*, **113**(3), 696-702, (1998).
- [12] N. Ikeda, H. Honda, T. Katsumi, T. Okunaka, K. Furukawa, T. Tsuchida, K. Tanaka, T. Onoda, T. Hirano, M. Saito, N. Kawate, C. Konaka, H. Kato and Y. Ebihara, "Early detection of bronchial lesions using lung imaging fluorescence endoscope", *Diagnostic and therapeutic endoscopy*, **5**, 85-90, (1999).
- [13] M. Kakihana, K. K. II, T. Okunaka, K. Furukawa, T. Hirano, C. Konaka, H. Kato and T. Ebihara, "Early detection of bronchial lesions using system of autofluorescence endoscopy (SAFE) 1000", *Diagnostic and therapeutic endoscopy*, **5**, 99-104, (1999).
- [14] K. Häussinger, F. Stanzel, R. M. Huber, J. Pichler and H. Stepp, "Autofluorescence detection of bronchial tumors with the D-Light/AF", *Diagnostic and therapeutic endoscopy*, **5**, 105-112, (1999).
- [15] S. Lam, C. MacAuley and B. Palcic, "Detection and localization of early lung cancer by imaging techniques", *Chest*, **103**, 12S-14S, (1993).
- [16] G. Wagnières, W. Star and B. Wilson, "In vivo fluorescence spectroscopy and imaging for oncological applications", *Photochem. Photobiol.*, **68**(5), 603-632, (1998).
- [17] D. R. Doiron, A. E. Profio, R. G. Vincent and T. J. Dougherty, "Fluorescence bronchoscopy for detection of lung cancer", *Chest*, **76**, 27-32 (1979).
- [18] A. E. Profio and D. R. Doiron, "A feasibility study of the use of fluorescence bronchoscopy for localization of small lung tumors", *Phys. Med. Biol.*, **22**, 949-957 (1977).
- [19] M. Leonhard, "New incoherent autofluorescence/fluorescence system for early detection of lung cancer", *Diagnostic and therapeutic endoscopy*, **5**, 71-75 (1999).
- [20] R. Adachi, T. Utsui and K. Furusawa, "Development of the autofluorescence endoscope imaging system", *Diagnostic and therapeutic endoscopy*, **5**, 65-70 (1999).
- [21] M. Zellweger, P. Grosjean, G. Wagnières, P. Monnier and H. van den Bergh, "Stability of the fluorescence measurement of Foscan® in the normal human oral cavity as an indicator of its content in early cancers of the esophagus and bronchi", *Photochem. Photobiol.*, **69**(5), 605-610 (1998).
- [22] M. Zellweger, D. Goujon, M. Forrer, H. van den Bergh and G. Wagnières, "Absolute

autofluorescence spectra of healthy bronchial tissue in vivo", submitted to 'Applied Optics'.

[23] G. Wagnières, S. G. Cheng, M. Zellweger, N. Utke, D. Braichotte, J.-P. Ballini and H. E. van den Bergh, "An Optical Phantom with Tissue-Like Properties in the Visible for Use in PDT and Fluorescence Spectroscopy", *Phys. Med. Biol.*, **42**(7), 1415-1426, (1997).

[24] J. Qu, C. MacAulay, S. Lam and B. Palcic, "Laser-induced Fluorescence Spectroscopy at Endoscopy: Tissue Optics, Monte-Carlo Modeling and in vivo Measurements", *Optical Engineering*, **34**(11), 3334-3343, (1995).

[25] D. Hürzeler, "Blue light endoscopy", *Laryngoscope*, **85**(8), 1374-1378 (1975).

[26] J. M. Kurie, J. S. Lee, R. C. Morice, G. L. Walsh, F. R. Khuri, A. Broxson, J. Y. Ro, W. A. Franklin, R. Yu and W. K. Hong, "Autofluorescence Bronchoscopy in the Detection of Squamous Metaplasia and Dysplasia in Current and Former Smokers", *Journal of the National Cancer Institute*, **90**(13), 991-995, (1998).

[27] P. J. M. George, "Fluorescence Bronchoscopy for the Early Detection of Lung-Cancer", *Thorax*, **54**(2), 180-183, (1999).

[28] M. Zargi, L. Smid, I. Fajdiga, B. Bubnic, J. Lenarcic and P. Oblak, "Laser-induced fluorescence in diagnostics of laryngeal cancer", *Acta Otolaryngol*, **S527**, 125-127, (1997).

[29] M. Dal Fante, "Diagnostica endoscopica in fluorescenza della displasia e del CIS bronchiale", <http://www.villaggiodelsalute.com/&Na/sem-2/dalfante.htm>, (1999).

[30] N. Ramanujam, M. F. Mitchell, A. Mahadevan, S. Thomsen, A. Malpica, Th. Wright, N. Atkinson, R. Richards-Kortum, "Development of a multivariate statistical algorithm to analyse human cervical tissue fluorescence spectra acquired in vivo", *Lasers in Surgery and Medicine*, **19**(1), 46-62, (1996).

[31] B. Palcic, S. Lam, J. Hung and C. Mac Aulay, "Detection and localization of early lung cancer by imaging techniques", *Chest*, **99**, 742-743, (1991).

[32] A. A. Weiss, H. Zeng, R. W. Kline, C. Macauley and N. Mackinnon, "Use of Endoscopic Autofluorescence Imaging in Diagnosis of Disease of the Esophagus and Stomach", *Gastrointestinal Endoscopy*, **47**(4), 70-70, (1998).

[33] B. Kulapaditharom and V. Boonkitticharoen, "Laser-Induced Fluorescence Imaging in Localization of Head and Neck Cancers", *Annals of Otolaryngology and Laryngology*, **107**(3), 241-246, (1998).

[34] B. Venmans, T. van Boxem, E. Smit, P. Postmus and T. Sutedja, "Results of two years experience with fluorescence bronchoscopy in detection of preinvasive bronchial neoplasia", *Diagnostic and Therapeutic Endoscopy*, **5**, 77-84, (1999).

[35] S. Takehana, M. Kaneko and H. Mizuno, "Endoscopic diagnostic system using autofluorescence", *Diagnostic and therapeutic endoscopy*, **5**, 59-63, (1999).

[36] Y. Yang, Y. Ye, F. Li, Y. Li and P. Ma, "Characteristic autofluorescence for cancer diagnosis and its origin", *Lasers in Surg. Med.*, **7**, 528-532, (1987).

[37] D. M. Harris and J. Werkhaven, "Endogenous porphyrin fluorescence in tumors", *Lasers Surg. Med.*, **7**, 467-472, (1987).

8.4

Absolute autofluorescence spectra of human healthy, metaplastic and early cancerous bronchial tissue in vivo.

Matthieu Zellweger, Didier Goujon, Ramiro Conde, Martin Forrer, Hubert van den Bergh and
Georges Wagnières

DGR-LPAS, Institute of Environmental Engineering, Swiss Federal Institute of Technology
(EPFL), CH-1015 Lausanne, Switzerland

Keywords: autofluorescence, lung cancer, early detection, imaging.

Abbreviations: Charge-Coupled Device, CCD; Light-Induced Fluorescence, LIF; Signal to Noise Ratio, SNR.

ABSTRACT

Autofluorescence emerges as a useful tool for the detection of early cancers in the bronchi. It has already produced interesting results, which have been implemented in commercial imaging devices. Their design relies on the spectroscopy of the tissues of interest. However, a large majority of these autofluorescence spectroscopy studies have been presented in arbitrary units. This is a drawback for, in particular, the designing of imaging devices based on autofluorescence.

Using correction factors and a spectral sensitivity correction curve, we determined the absolute spectral distribution of the tissue autofluorescence in vivo. These measurements have been performed on healthy, metaplastic and dysplastic bronchial tissues at several excitation wavelengths ranging from 350 nm to 495 nm. Moreover, we did so at a fixed distance between the tissue and the probe to avoid geometric distortions of the spectra due to the optical characteristics of tissue. We found that the order of magnitude of the autofluorescence brightness was stable as the excitation wavelengths varied (in the order of $5 \text{ pW}/\mu\text{W} \times \text{nm}$ at the maximum of the fluorescence emission spectra).

submitted to 'Applied Optics'

INTRODUCTION

The autofluorescence of biological tissues for the detection of early cancers has been under investigation for many years (1). The method is promising as it seems to produce useful information about the histopathological status of the tissue in the lungs (2-6), breast (7-10), oral cavity and upper aero-digestive tract (11-16), colon (17, 18), cervix (19-21), bladder (22, 23), esophagus (24), skin (25) and brain (26). Providing the excitation wavelength and detection ranges are chosen in a sensible way, much can be learnt from the spectra. This has been implemented in commercial autofluorescence cancer detection devices (27-30).

A major difficulty when dealing with autofluorescence is its dependence upon tissue optics and instrumental parameters. Both can induce a distortion of the autofluorescence spectra, because of the wavelength dependence of, in the former, the diffusion and absorption processes and in the latter, of most optical components (CCDs, optical fibers, monochromator). Consequently, it might be difficult to compare the results from one study or one setup to the results from another one. Moreover, the actual design of an apparatus based on the autofluorescence of biological tissues is crucially dependent upon the absolute fluorescence intensity detected at each wavelength.

For these reasons, we propose here an extension of a previous study by our group (31) on the autofluorescence of healthy bronchial tissue. We corrected the spectra collected by our setup for the instrumental parameters and kept the distance between the tissue and the probe fixed. Thus, we found absolute autofluorescence spectra expressed in physical units which are independent of our instrumentation.

MATERIALS AND METHODS

Fluorescence Spectroscopy

Our optical fiber-based spectrofluorometer has been described elsewhere and has not undergone any modification with respect to a previous study (31). Very briefly, it consists of an excitation source (UXL-75 XE, 75W high pressure Xenon lamp, Ushio Inc., Japan) whose light is passed through a spectrograph (Chromex 250, Chromex,

Albuquerque NM 87107, USA), filtered by a short-pass filter and injected into a quartz optical fiber hexagonal bundle (7 fibers, HPSUV300A, Oxford Electronics Ltd, Four Marks, Hants, UK; NA=0.22, 300 μm core diameter). This bundle is then connected to a similar bundle that has been adapted to fit the biopsy channel of a standard flexible bronchoscope (Olympus BF Type 20). Four of the seven fibers are used for the excitation light and the remaining three fibers collect the fluorescence light. The excitation wavelength is scanned between 350 nm (it is difficult to obtain enough excitation power below this wavelength with a clinically acceptable setup and shorter wavelengths are too far into the UV range to be compatible with this environment) and 495 nm (above this wavelength, the spectral domain of the 'green' image becomes too narrow to detect enough fluorescence power) by steps of 10 or 15 nm. The typical total power at the distal end of the fibers is 15 μW and the Full Width at Half Maximum of the excitation is 15 nm. The fluorescence is collected and separated from the backscattered excitation light by a dichroic mirror. It is then filtered by a long-pass filter and dispersed by a spectrograph (Chromex 250, Chromex, Albuquerque NM 87107, USA) to be detected by a Peltier cooled CCD (TE/CCD-256, UV coated, Spectroscopy Instruments GmbH, D-82205 Gilching, Germany). The whole setup is controlled by a 486 PC (Fast 486/50, Spectroscopy Instruments GmbH, D-82205 Gilching, Germany) with CSMA software (Spectroscopy Instruments GmbH, D-82205 Gilching, Germany) and mounted on a trolley for transport to the medical facility. Before each clinical autofluorescence measurement session, the fluorescence spectrum of an aqueous solution of Rhodamine B ($c = 1 \cdot 10^{-6}$ M) in a 10 mm quartz cuvette is measured. The magnitude of the peak at 575 nm allows for a certain degree of lamp output fluctuations to be taken into account and corrected for. Fluorescence excitation of the Rhodamine takes place at each of the excitation wavelengths and detection is between 450 and 800 nm (depending on the excitation wavelength). The fluorescence excitation light power is measured by placing the distal end of the modified bronchoscope into the detector of an optical power meter (Newport Instruments, 840-C).

Determination of the optimal distance between the tissue and the probe to measure the spectroscopy of the autofluorescence detected by an endoscopic imaging device.

The first part of this study involved the determination of the optimal distance between the tissue to be investigated and the fiber's distal tip to avoid spectral distortions of the detected signal. As will be seen below, short distances induce underestimation of the red autofluorescence, thus distorting the spectroscopy of what would be seen by an imaging device. On the other hand, long distances are detrimental to the SNR. To determine the optimal tissue-probe distance, spectra of the authors' buccal mucosa were recorded with the excitation wavelengths 360 nm and 415 nm. Using a hand piece, the distance between the fiber tip and the sample was varied from 0 mm (actual contact) to 10 mm. A relevant background spectrum (acquired on a non-fluorescent phantom (32)) was then subtracted to produce a pure autofluorescence spectrum of the sample. This allowed us to calculate color ratios within the spectra and to find out which was the optimal tissue-probe distance for the subsequent part of the study, on patients.

Patients.

Forty-eight patients were involved in this study. The patients were scheduled for rigid bronchoscopy for screening purposes (positive cytology or primary cancerous lesion in the upper aerodigestive tract). Biopsies were taken in the case of a suspicion of an early cancerous lesion. The LIF measurements were executed during the general anesthesia required by rigid bronchoscopy. Not all patients have been measured at all excitation wavelengths. This is due to safety reasons as the anesthesia cannot be extended indefinitely. A typical patient has therefore been measured at 4 excitation wavelengths. Altogether, over 1900 autofluorescence spectra have been measured. Details can be found in another paper (31).

Procedure of endoscopic measurements.

After the routine endoscopic observation of the tracheobronchial tree, the modified fiberscope (31) was passed through the sheath of the rigid bronchoscope. It was then placed onto the site to be measured. The spacer ensured a gentle contact with the tissue at a fixed distance (3.5 mm) between

the fibers and the tissue. The endoscopic standard white-light illumination was switched off. Ten spectra on average were recorded on the same location for each excitation wavelength. The endoscopic light was then switched on again. The site was checked for the absence of blood prior to proceeding to further measurements. At the end of the measurement session, a biopsy was taken at the site of the measurements to check the histopathology of the site.

Histological examination

The biopsies were processed in a routine fashion. The pathologists reported the results of microscopy. Normal mucosae without any trace of inflammation or metaplasia were grouped under the label 'Healthy'. Inflammatory or metaplastic mucosae without malignant changes were grouped under 'Inflammation/Metaplasia'. Mucosae bearing pre-/early malignant features (mild, moderate and severe dysplasia as well as carcinoma in situ) were grouped under 'Dysplasia/CIS' and under 'Invasive' in case of more advanced changes.

Analysis of results.

Principle

For this study, the emission spectrum of a calibrated lamp (EH-100, 1000 W tungsten halogen, Eppley Laboratory Inc, Newport, RI02840, USA) was used. Its emission spectrum is, down to fit parameters that are specific to the lamp, close to that of a blackbody, at a specific temperature (3055 °K). By comparing the theoretical emission spectrum $theor(\lambda)$ and the emission spectrum measured with our experimental setup $meas(\lambda)$, it is possible to compute the global efficiency of the setup as a function of the wavelength. This produces a correction spectrum $corr(\lambda)$. This correction spectrum can then be used to correct any measured spectrum, thus avoiding the distortions due to the instrumental setup. These correction spectra have been determined for all spectral configurations of the optical fiber-based spectrofluorometer.

Correction spectrum

The measurement of the lamp's spectrum, $meas(\lambda)$, is made by directing the fibers of our setup (31) towards the lamp, at a distance of 3 m. As the units of our raw spectrum are given in counts per pixel (of the

CCD detector), we have to correct by a factor (thereafter F) that gives the number of nanometers covered by one pixel of the detector. The measured spectrum of the lamp $meas(\lambda)$ also has to be divided by the integration time t [s]. Finally, as stated above, it has to be divided by $theor(\lambda)$ to generate $corr(\lambda)$:

$$corr(\lambda) = \frac{meas(\lambda)}{theor(\lambda) \times \frac{\pi}{4} d^2 \times F \times t}$$

with

d: diameter of the entrance fibers [m]

F: 0.53 nm/pix

t: integration time, $t = 1$ s

$meas(\lambda)$: [cts/pix]

$theor(\lambda)$: [W/m^3]

The units of $corr(\lambda)$ are therefore [cts/($W_m \cdot s$)], with W_m the emitted power [W].

Tissue spectra

The background spectrum of the non-fluorescent phantom was subtracted from each tissue spectrum. Ten spectra were measured at each site and averaged because they were fairly stable. This average spectrum was then divided by the excitation power and the integration time, thus producing a raw spectrum $spectr(\lambda)$ whose units are:

$$\left[\frac{cts}{W_x \times s \times pix} \right]$$

with

cts: counts

W_x : excitation power [W]

s: seconds [s]

pix: number of pixels

Our goal is to represent tissue spectra in terms of fluorescence power per unit of excitation power per nm (hence [$W_m/(W_x \cdot nm)$], with W_m the collected power and W_x the excitation power). It is possible to do so by dividing $spectr(\lambda)$ by the correction curve $corr(\lambda)$ to obtain a corrected spectrum $cs(\lambda)$:

$$cs(\lambda) = spectr(\lambda)/corr(\lambda)$$

whose units are:

$$\left[\frac{cts}{W_x \times s \times pix} \right] \div \left[\frac{cts}{W_m \times s} \right] = \left[\frac{W_m}{W_x \times pix} \right]$$

and, after division by the conversion factor (F) defined above:

$$\left[\frac{W_m}{W_x \times nm} \right]$$

which is the expression of the autofluorescence spectra in absolute physical units.

Distal end of the probe

The distal end of our setup has been described in detail previously (31). It keeps a fixed distance (3.5 mm) between the probe and the tissue sample. This implies that it only detects a fraction of the photons that are emitted by the tissue. This fraction has experimentally been measured by placing the distal end of the probe at 3.5 mm of a surface which diffusely reflects more than 99% of the incident light in the visible (white reflectance coating, Eastman Kodak Company, Rochester, NY, USA). The incident power and the power of the reflected light were measured. After correcting for attenuation of the fibers and connectors, it was found to be 1/545. To express the absolute fluorescence intensity that is actually emitted by the tissues, the autofluorescence spectra have therefore to be multiplied by 545. This enables to calculate the absolute intensity of emitted fluorescence in pW for every μW of excitation power for every nm of spectral width.

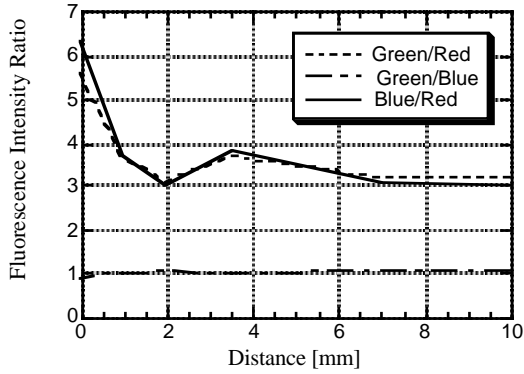
RESULTS

Tissue-probe distance

The fluorescence spectra depend on distance for two reasons. Firstly, the closer the probe to the tissue, the higher the fluorescence signal. That means that the probe has to be as close as possible to the tissue. Secondly, tissue optics effects, associated with the geometry of the measurement, distort the spectra. Red fluorescence photons, because they are less absorbed by the tissue than blue or green photons, propagate further away within the tissue than them. If the probe is too close to the tissue, some red fluorescence photons can possibly propagate further than the area covered by the probe. The red

contribution is therefore too small. This effect is very important when the probe is in contact with the tissue. Past a certain probe-tissue distance, it becomes negligible.

A



B

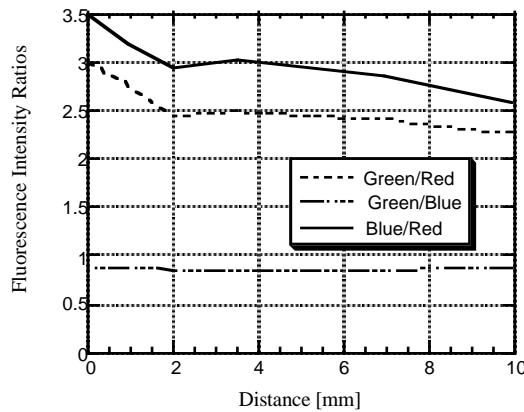


Figure 1: Ratio of the autofluorescence in the 'blue' (480-510 nm), the 'green' (510-560 nm) and the 'red' (600-650 nm) windows as a function of the probe-sample distance. These results have been acquired on the authors' buccal mucosa with an excitation wavelength of 360 nm (a) and 415 nm (b).

The modifications of the red part of the spectrum were then calculated by calculating the 'blue', 'green' and 'red' values of the spectra, (namely the values of the fluorescence in the 'blue' (480-510 nm), the 'green' (510-560 nm) and the 'red' (600-650 nm) windows) and ratioing them. A plot of these ratios as a function of the sample-probe distance is given above (Fig. 1a and 1b, spectra acquired on the authors' buccal mucosa with excitation wavelengths of 360 nm on Figure 1a and 415 nm on Figure 1b).

From these figures, it can be seen that the Green/Blue ratios are fairly constant over the

whole range of distances. This is hardly surprising as the diameter of the fiber bundle (1.9 mm) is larger than the propagation distance of the blue photons. The ratios involving the red photons undergo more drastic variations as the distance increases. At short distances (0 to 2 mm), the red photons diffuse further away than the diameter of the fiber and hence are not detected. As the fiber is pulled further from the sample, the relative number of red photons increase and hence the Green/Red and Blue/Red ratios decrease. Up to a certain distance (around 2 mm), this effect is important. For longer distances, it becomes less crucial. According to these results, it was decided to use a distance of 3.5 mm between the sample and the probe to minimize the geometrical distortion of the spectra when measuring the autofluorescence in vivo. This also implied acceptable loss of autofluorescence signal, as illustrated below. This is why a non-invasive spacer has been designed to ensure a gentle contact while maintaining a constant distance between the probe and the tissue.

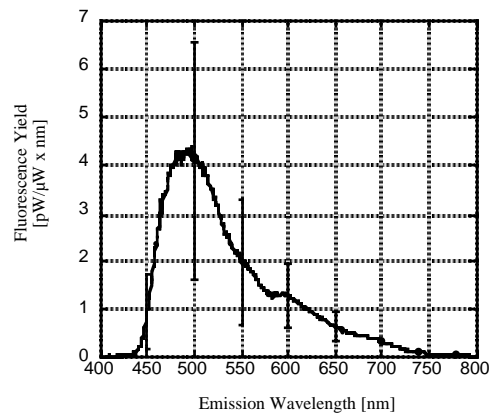


Figure 2: Absolute autofluorescence emission spectra of healthy bronchial tissue in pW per μW of excitation power per nm of spectral width as a function of the emission wavelength. The excitation wavelength is 405 nm. The curve represents the average autofluorescence spectra observed at this excitation wavelength and the bars delimit the corresponding 67% confidence interval.

Absolute fluorescence emission of healthy tissue

As example, the average absolute autofluorescence spectra of the healthy tissue

Excitation Wavelength [nm]	Maximal Emission Wavelength [nm]	Fluorescence Yield at the Emission Maximum [pW/ μ W x nm]	Standard Deviation at the Emission Maximum [pW/ μ W x nm]
350	460	7.9	5.5
365	460	6.9	3.2
380	475	4.7	2.8
395	480	4.5	2.3
405	490	4.2	2.5
420	500	4.5	3.5
435	515	4.0	3.3
450	520	3.5	2.7
465	530	3.1	2.4
480	550	3.5	3.3
495	575	2.3	2.1

Table 1: Emission wavelength of the maximum [nm], average fluorescence yield at the autofluorescence maximum of normal bronchial tissue in vivo for different excitation wavelengths.

is presented in Fig. 2 with an excitation wavelength of 405 nm.

It is interesting to note that, the autofluorescence variations from one patient to another (interpatient autofluorescence variations, given by the 67% confidence interval) are significant. It should also be noted that the integrated fluorescence yield between 600 and 800 nm is around one order of magnitude smaller than the integrated fluorescence yield between 450 and 600 nm. This observation has to be taken into account for the designing of imaging devices relying on these two spectral windows (31).

Table 1 summarizes the emission maximum's wavelength and the fluorescence yield at that point. It can be seen that the maximum is shifted. This is due to the use of a different long-pass filter for each excitation wavelength (details are provided in another paper (31)). The fluorescence yield decreases monotonically as the excitation wavelengths increase. It is likely to be due to the combination of the previous observation about the long-pass filters and to the fact that

the autofluorescence spectra are those of a mixture of fluorophores. The intensity of these spectra decreases as the emission wavelengths increase.

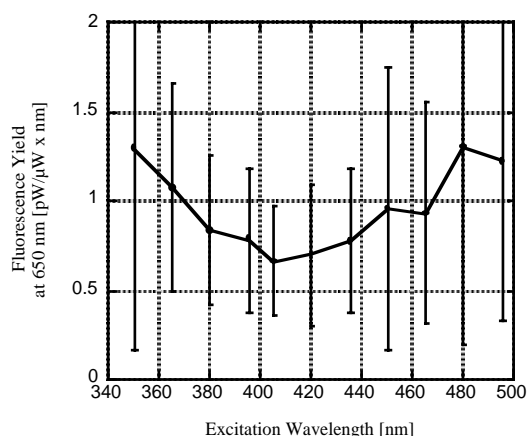


Figure 3: Absolute autofluorescence yield at 650 nm as a function of the excitation wavelength.

To determine the excitation spectra of the bronchi autofluorescence yield, the absolute intensity of the spectra has been recorded at

650 nm. This emission wavelength is present in all autofluorescence spectra regardless of the experimental conditions (long-pass filter used). Figure 3 summarizes the intensities that were measured at an emission wavelength of 650 nm as a function of the excitation wavelength.

The structure of the curve of Figure 3 is likely to be due to the following factors. As the excitation wavelength changes towards longer wavelengths, deeper layers of tissue are probed. This effect, combined with the reduced wavelength difference between the excitation and the detection, is probably responsible for the large fluorescence yield observed between 460 and 495 nm. Finally, the dip around 400 nm could be a hint that hemoglobin is involved in the process. This observation seems compatible with observations reported elsewhere (1) that a non-negligible part of the tissue's autofluorescence might be due to its flavin components.

DISCUSSION

The autofluorescence of biological tissues can bring crucial information about their pathological or metabolic status. Many groups have taken advantage of these properties to detect and characterize early cancerous lesions as well as non-cancerous ones (1). The measurement of the autofluorescence itself suffers from a major limitation: its setup dependence. For instance, the results of several investigators have been acquired in vivo with an actual contact between the probe and the sample (13, 14, 23). Such measurement geometry induces some spectral distortion and virtually no information is provided regarding the absolute intensity of the autofluorescence.

The setup dependence stems from the tissue optics involved in the measurement and the geometry of the measurement. The propagation of photons within the biological tissue is a function of their wavelength, with the longer wavelength photons propagating further away from their emission spot than the shorter wavelength ones. Consequently, past a certain distance between the fiber and the tissue, the photons 'missed' by the probe become so small a proportion that the spectrum is no longer noticeably distorted. As one increases the probe-tissue distance, one decreases the signal to noise ratio (SNR) and the only possibility to measure with a

given SNR is then to increase the integration time. However, especially for in vivo applications, the integration time should be kept at a minimum.

Hence, when dealing with these issues, it is necessary to balance two antagonist effects, namely, an increase in the probe-sample distance to minimize the geometrical distortion of the spectra and a decrease in this distance to maximize the SNR.

Our results show that, in our conditions, the actual contact between the sample and the probe leads to significant distortions in the red part of the spectrum. They can be avoided in shifting the probe back from the tissue and, we found on a distance of 2 mm. Past this distance, the geometrical distortions become less crucial. The lack of precise control of this distance is at the origin of our choice of 3.5 mm, which corresponds to a trade-off between a minimal spectral distortion and a reasonable SNR. Due to the natural elasticity of the biological tissues, some deformation of the organ was expected on the spot where the spacer was to rest. This inevitably brings the tissue closer to the probe than the actual length of the spacer. We designed the spacer accordingly, thus avoiding unwanted contact between the fibers and the tissue.

The modifications we sometimes observed within one measurement session between the spectra of one patient (namely the intrapatient fluctuations of the autofluorescence spectra) involved the intensity of the spectra and not the spectral shape as would have been the case if the spectroscopy was to be distorted by too close a distance. It should be noted that, in the context of our measurements, the intra-patient fluctuations are significantly smaller than the interpatient fluctuations (data not shown). It is reported (33) that some of the fluorophores contributing to the natural fluorescence of the biological tissues are metabolic products. Since metabolism should vary from one patient to another, it was expected that the autofluorescence would also undergo some variations. This is reflected in the standard deviations attached to our results. Interestingly, the fluctuations seem to be consistent from one excitation wavelength to another. This suggests that these variations are not due to changes in the tissue optical properties. Comparable fluctuations have been found in previous

studies of metabolic processes (involved, for example, in the metabolism of the photosensitizers used in photodynamic therapy) (34-36) and of autofluorescence of the tongue as reported by Gillenwater et al (13) or autofluorescence in the oral cavity of healthy individuals reported by Dhingra et al (14) and Gillenwater et al (37) (although not totally quantified in the latter).

The absolute spectra and data we present here have been corrected for all the instrumental biases. Consequently, spectra acquired with another setup could be similar if corrected for the instrumental factors. It is interesting to note, however, that most of the analyses presented in the literature (2, 20, 21, 23, 33), rely on the use of qualitative methods to treat the data in arbitrary units rather than on true quantitative data. This also makes sense as the true quantitative information is frequently of little diagnostic use. The most useful information, however, is that contained in the spectra's shape. It could therefore be imagined that a semi-quantitative correction could be applied to spectra measured with different setups. This correction would produce spectra whose shape is correct, but whose intensity is only relative. This would mean that these spectra could be given as true spectra, down to an uncomputed multiplicative factor. This treatment has been used for the spectra presented in our previous study (31).

It is interesting to note that metaplastic and inflammatory tissues also display an autofluorescence decrease. We reported in a previous study that their shape remains essentially constant, however (31). This decrease is then more marked on dysplastic tissues and on carcinoma in situ. It seems that this trend can also be observed on more invasive lesions, but it is beyond the scope of this study and the previous one (31) that deliberately focused on healthy tissues and on early lesions respectively. This observation is in agreement with the observations of other authors about the autofluorescence decrease but the reasons behind it remain unclear (2, 38, 39).

It should be noted that this decrease has to be taken into account while calculating the SNR of autofluorescence images obtained on dysplasia and early carcinoma. Typical examples are presented in Fig. 4 for an excitation wavelength of 405 nm. As can be

seen, the SNR of curve 1 is larger than that of curve 3. It should be remembered, however, that curve 1 is a mean over more spectra than curve 3 (435 vs 61). The same measurements were performed at the other wavelengths (data not shown).

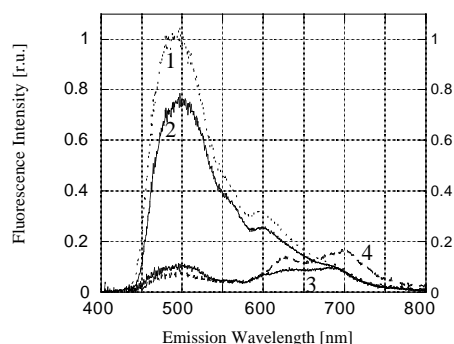


Figure 4: Relative modifications of the average autofluorescence spectra as the healthy tissue (curve 1) turns metaplastic or inflammatory (curve 2), dysplastic or CIS (curve 3) and to carcinoma in situ (curve 4). The spectra are expressed relatively to the healthy spectrum that has been normalized (excitation wavelength: 405 nm).

The autofluorescence decrease at the emission maximum is expressed in relation to the 'healthy' normalized spectrum. These decreases are summarized in Fig. 5.

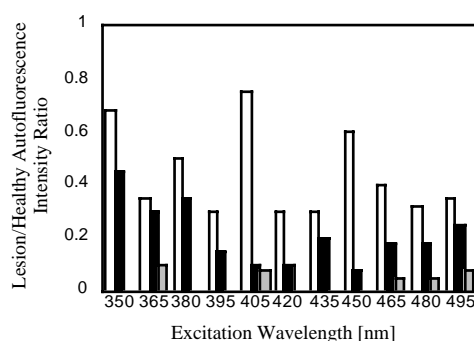


Figure 5: Lesion/healthy autofluorescence intensity ratio at the emission maximum as a function of the tissue histopathological status and the excitation wavelength, metaplastic or inflammatory (white), dysplastic or CIS (black) and invasive lesions (gray, whenever available).

It can be seen in Fig. 5 that the sharp decrease of autofluorescence on cancerous lesions is present for all the excitation wavelengths. Nevertheless, this decrease seems to be more marked for violet than for UV excitation wavelengths, and the violet-blue excitation wavelengths (400-450 nm) seem to be the most promising ones in terms of generating a contrast between healthy and early cancerous bronchial tissue (31). There is a smaller decrease on metaplastic and inflammatory tissues and a more marked decrease on dysplasias or CIS. Whenever available, the corresponding values for more invasive lesions are also given.

In conclusion, our results give useful information about the absolute autofluorescence of tissues and will provide information to the designers of future autofluorescence imaging photodetection systems in terms of photon budget, components to be chosen and autofluorescence modifications to be expected.

ACKNOWLEDGMENTS

We gratefully acknowledge support from the Swiss National Fund for Scientific Research, Grants #20-50691 and #21-43507.95, and the Swiss Priority Program in Optics.

REFERENCES

1. G. Wagnières, W. Star and B. Wilson, "In vivo fluorescence spectroscopy and imaging for oncological applications", *Photochem. Photobiol.*, 68(5), 603-632, (1998).
2. Hung, J., S. Lam, J. C. LeRiche, and B. Palcic (1991) Autofluorescence of normal and malignant bronchial tissue. *Lasers Surg. Med.* 11, 99-105.
3. Häussinger, K., F. Stanzel, R. M. Huber, J. Pichler, and H. Stepp (1999) Autofluorescence detection of bronchial tumors with the D-Light/AF. *Diagnostic and therapeutic endoscopy.* 5, 105-112.
4. Horvath, T., M. Horvathova, F. Salajka, B. Habanec, L. Foretova, J. Kana, H. Koukalova, P. Pafko, F. Wurst, E. Novotna, J. Pecina, V. Vagunda, R. Vrbacky, R. Talac, H. Coupkova, and Z. Pacovsky (1999) Detection of bronchial neoplasia in uranium miners by autofluorescence endoscopy (SAFE-1000). *Diagnostic and therapeutic endoscopy.* 5, 91-98.
5. Kurie, J. M., J. S. Lee, R. C. Morice, G. L. Walsh, F. R. Khuri, A. Broxson, J. Y. Ro, W. A.

Franklin, R. Yu, and W. K. Hong (1998) Autofluorescence Bronchoscopy in the Detection of Squamous Metaplasia and Dysplasia in Current and Former Smokers. *JOURNAL OF THE NATIONAL CANCER INSTITUTE.* 90, 991-995.

6. George, P. J. M. (1999) Fluorescence Bronchoscopy for the Early Detection of Lung-Cancer. *THORAX.* 54, 180-183.

7. Gupta, P. K., S. K. Majumder, and A. Uppal (1997) Breast-cancer diagnosis using N-2 laser-excited autofluorescence spectroscopy. *Lasers in Surgery and Medicine.* 21, 417-422.

8. Alfano, R. R., G. C. Tang, A. Pradhan, W. Lam, D. S. J. Choy, and E. Opher (1987) Fluorescence spectra from cancerous and normal breast and lung tissue. *IEEE J. Quant: Elect.* QE23, 1806-1811.

9. Tang, G. C., A. Pradhan, and R. R. Alfano (1989) Spectroscopic differences between human cancer and normal lung and breast tissues. *Lasers in Surgery and Medicine.* 9, 290-295.

10. Pradhan, A., B. B. Das, K. M. Yoo, J. Cleary, R. Prudente, E. Celmer, and R. R. Alfano (1992) Time-resolved UV photoexcited fluorescence kinetics from malignant and non-malignant human breast tissues. *Lasers in the Life Science.* 4, 225-234.

11. Ingrams, D. R., J. K. Dhingra, K. Roy, D. F. Perrault, I. D. Bottrill, S. Kabani, E. E. Rebeiz, M. M. Pankratov, S. M. Shapshay, R. Manoharan, I. Itzkan, and M. S. Feld (1997) Autofluorescence Characteristics of Oral-Mucosa. *Head and Neck Journal for the Sciences and Specialities of the Head and Neck.* 19, 27-32.

12. Fryen, A., H. Glanz, W. Lohmann, T. Dreyer, and R. M. Bohle (1997) Significance of autofluorescence for the optical demarcation of field cancerisation in the upper aerodigestive tract. *Acta Oto-Laryngol.* 117, 316-319.

13. Gillenwater, A., R. Jacob, and R. Richards-Kortum (1998) Fluorescence spectroscopy: a technique with potential to improve the early detection of aerodigestive tract neoplasia. *Head & Neck* 556-562.

14. Dhingra, J. K., D. F. Perrault, K. Mcmillan, E. E. Rebeiz, S. Kabani, R. Manoharan, I. Itzkan, M. S. Feld, and S. M. Shapshay (1996) Early diagnosis of upper Aerodigestive tract cancer by autofluorescence. *Arch. Otolaryngol Head Neck Surg.* 122, 1181-1186.

15. Onizawa, K., H. Saginoya, Y. Furuya, and H. Yoshida (1996) Fluorescence Photography as a Diagnostic Method for Oral-Cancer. *Cancer Letters.* 108, 61-66.

16. Zargi, M., L. Smid, I. Fajdiga, B. Bubnic, J. Lenarcic, and P. Oblak (1997) Laser-induced fluorescence in diagnostics of laryngeal cancer. *Acta Otolaryngol* 125-127.
17. Schomacker, K. T., J. K. Frisoli, C. C. Compton, T. J. Flotte, J. M. Richter, N. S. Nishioka, and T. F. Deutsch (1992) Ultraviolet laser-induced fluorescence of colonic tissue: basic biology and diagnostic potential. *Lasers in Surgery and Medicine*. 12, 63-78.
18. Bottiroli, G., A. C. Croce, D. Locatelli, R. Marchesini, E. Pignoli, S. Tomatis, C. Cuzzoni, S. Dipalma, M. Dalfante, and P. Spinelli (1995) Natural fluorescence of normal and neoplastic human colon - a comprehensive 'ex-vivo' study. *Lasers in Surgery and Medicine*. 16, 48-60.
19. Ramanujam, N., M. F. Mitchell, A. Mahadevan, S. Thomsen, A. Malpica, T. Wright, N. Atkinson, and R. Richards-Kortum (1996) Spectroscopic diagnosis of cervical intraepithelial neoplasia (CIN) in vivo using laser-induced fluorescence spectra at multiple excitation wavelengths. *Lasers Surg. Med.* 19, 63-74.
20. Ramanujam, N., M. F. Mitchell, A. Mahadevan-Jansen, S. L. Thomsen, G. Staerckel, A. Malpica, T. Wright, N. Atkinson, and R. Richards-kortum (1996) Cervical precancer detection using a multivariate statistical algorithm based on laser-induced fluorescence spectra at multiple excitation wavelengths. *Photochemistry and Photobiology*. 64, 720-735.
21. Ramanujam, N., M. F. Mitchell, A. Mahadevan, S. Thomsen, and e. al. (1996) Development of a multivariate statistical algorithm to analyse human cervical tissue fluorescence spectra acquired in vivo. *Lasers in Surgery and Medicine*. 19, 46-62.
22. Koenig, F., F. J. McGovern, H. Enquist, R. Larne, T. F. Deutsch, and K. T. Schomacker (1998) Autofluorescence guided Biopsy for the Early Diagnosis of Bladder-Carcinoma. *J. Urology*. 159, 1871-1875.
23. Anidjar, M., D. Etori, O. Cussenot, P. Meria, F. Desgrandchamps, A. Cortesse, P. Teillac, A. Leduc, and S. Avrillier (1996) Laser-Induced Autofluorescence Diagnosis of Bladder-Tumors - Dependence on the Excitation Wavelength. *J. of Urology*. 156, 1590-1596.
24. Weiss, A. A., H. Zeng, R. W. Kline, C. Macauley, and N. Mackinnon (1998) Use of Endoscopic Autofluorescence Imaging in Diagnosis of Disease of the Esophagus and Stomach. *Gastrointestinal Endoscopy*. 47, 70-70.
25. Colasanti, Colasanti, Fabbrocini, Liuzzi, Quarto, Riccio, Roberti, and Villani (1995) Non-invasive spectroscopic analysis of dermatological lesions excited with N2 laser. *SPIE*. 2627, 77-89.
26. Bottiroli, G., A. Croce, D. Locatelli, R. Nano, K. Lanza, E. Giombelli, F. Tancioni, and E. Benericetti (1999) Brain tissue autofluorescence properties: application to glioma resection margin delineation during surgical operation. *Photochemistry and Photobiology*. 69, Special Issue, 38S, MPM-E11.
27. Kakihana, M., K. K. II, T. Okunaka, K. Furukawa, T. Hirano, C. Konaka, H. Kato, and T. Ebihara (1999) Early detection of bronchial lesions using system of autofluorescence endoscopy (SAFE) 1000. *Diagnostic and therapeutic endoscopy*. 5, 99-104.
28. Leonhard, M. (1999) New incoherent autofluorescence/fluorescence system for early detection of lung cancer. *Diagnostic and therapeutic endoscopy*. 5, 71-75.
29. Takehana, S., M. Kaneko, and H. Mizuno (1999) Endoscopic diagnostic system using autofluorescence. *Diagnostic and therapeutic endoscopy*. 5, 59-63.
30. Adachi, R., T. Utsui, and K. Furusawa (1999) Development of the autofluorescence endoscope imaging system. *Diagnostic and therapeutic endoscopy*. 5, 65-70.
31. Zellweger, M., P. Grosjean, D. Goujon, P. Monnier, H. van den Bergh, and G. Wagnières, In vivo autofluorescence spectroscopy of human bronchial tissue to optimize the detection and imaging of early cancers. accepted for publication in 'The Journal of Biomedical Optics'.
32. Wagnières, G., S. G. Cheng, M. Zellweger, N. Utke, D. Braichotte, J.-P. Ballini, and H. E. van den Bergh (1997) An Optical Phantom with Tissue-Like Properties in the Visible for Use in Pdt and Fluorescence Spectroscopy. *Phys. Med. Biol.* 42, 1415-1426.
33. Richards-Kortum, R. and E. Sevick-Muraca (1996) Quantitative optical spectroscopy for tissue diagnosis. *Annu. Rev. Phys. Chem.* 47, 555-606.
34. Braichotte, D. R., J.-F. Savary, P. Monnier, and H. E. van den Bergh (1996) Optimizing light dosimetry in photodynamic therapy of early-stage carcinomas of the esophagus using fluorescence spectroscopy. *Lasers in Surgery and Medicine*. 19, 340-346.
35. Braichotte, D., J.-F. Savary, T. Glanzmann, P. Monnier, G. Wagnières, and H. E. van den Bergh (1996) Optimizing Light Dosimetry in Photodynamic Therapy of the Bronchi by

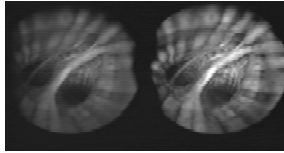
Fluorescence Spectroscopy. *Lasers in Med. Sci.* 11, 247-254.

36. Glanzmann, T., C. Hadjur, M. Zellweger, P. Grosjean, M. Forrer, J. P. Ballini, P. Monnier, H. van den Bergh, C. K. Lim, and G. Wagnieres (1998) Pharmacokinetics of tetra(m-hydroxyphenyl)chlorin in human plasma and individualized light dosimetry in photodynamic therapy. *Photochemistry and Photobiology.* 67, 596-602.

37. Gillenwater, A., R. Jacob, R. Ganeshappa, B. Kemp, A. K. Elnaggar, J. L. Palmer, G. Clayman, M. F. Mitchell, and R. Richardskortum (1998) Noninvasive Diagnosis of Oral Neoplasia Based on Fluorescence Spectroscopy and Native Tissue Autofluorescence. *Archives of Otolaryngology-Head & Neck Surgery.* 124, 1251-1258.

38. Palcic, B., S. Lam, J. Hung, and C. Mac Aulay (1991) Detection and localization of early lung cancer by imaging techniques. *Chest.* 99, 742-743.

39. Anthony, D. J., A. E. Profio, and O. J. Balchum (1989) Fluorescence spectra in lung with porphyrin injection. *Photochem. Photobiol.* 49, 583-586.



Two images on one CCD.

Chapter 9

Cancer photodetection in the tracheo-bronchial tree by autofluorescence imaging

In this final chapter, we present the industrial prototype that has been designed based on the spectroscopic studies described previously. Chapter 8 dealt with the autofluorescence spectroscopy of the tracheo-bronchial tree and its modifications according to the histopathological status of the site. In the course of this work, we showed that there are consistent differences of autofluorescence between the healthy and the non-healthy tissues if the excitation wavelength and the autofluorescence detection domains are carefully chosen. This can be seen as a kind of optimization study for the development of a future photodetection system that would be based on the autofluorescence properties of the bronchial tissue to image large portions of tissue. This is one of the ultimate uses of the spectroscopic contrasts between normal and early cancerous tissues. As a matter of fact, a complete system based on our autofluorescence measurements was developed first in our laboratory and then refined in the Knittlingen factory of the firm *Richard Wolf Endoskope GmbH* (Germany).

Although some commercial devices do exist for this purpose (Xillix, Pentax, Storz), they mostly lack the optimization that our study yielded. The fundamental studies upon which they are based have been presented in Chapter 8.

9.1 Commercial systems

Of all the commercial systems, the Xillix (LIFE) is the oldest. Its first version used a He-Cd laser (442 nm) to excite the autofluorescence of the bronchial tissue. It now relies on a filtered Xe lamp (blue light excitation) [1]. The fluorescence is then separated in two spectrally different components, each of them being then passed through an image intensifier and imaged on a CCD. Not much is publicly known about the spectral characteristics of these two components but Lam et al [2] report that one is in the green region (480-520 nm) and the other in the red region (630+ nm) of the spectrum in an early version (1993) of the system. In today's commercial system, the lesions appear reddish-brown [3] against a greenish background. The Xillix system is credited with successes in many papers [2,4-8] with a sensitivity of 72.5% in detecting moderate to severe dysplasia and carcinoma in situ (white-light bronchoscopy: 48.4%) and a specificity of 94% (white-light bronchoscopy: 94%, same specificity) [4]. A controversy about the performance of the system is still going on, as some authors [9,10] cannot reproduce these seemingly impressive results. Nevertheless, if a controversy exists, this means that some successes must have helped in detecting early lesions and, in fact, the conclusion of most studies is that autofluorescence bronchoscopy must be considered a complement of rather than a substitute for the conventional white-light bronchoscopy. Most authors agree that the use of this system requires some training, and, from a purely practical point of view, it is often stated that the device is quite cumbersome. It should not be forgotten that the use of image intensifiers is detrimental to the resolution of the images and that these devices are expensive and consumable. An imaging system with no such devices would certainly gain in image quality and in weight. Other known drawbacks of the Xillix system are its inability to rapidly switch from its white-light mode into its autofluorescence mode and its price.

The Pentax system (SAFE-1000) is more recent. In this device, autofluorescence is excited by a filtered Xe lamp in the 420-480 nm region [11]. It is externally similar to the Xillix system with an articulated arm and a large main unit behind the clinician. However, the Pentax system only detects the autofluorescence in one spectral domain, namely the green region of the spectrum (490-590 nm) [12] and images it on an intensified CCD. This gives a simpler device and certainly fewer problems of alignment, synchronization and tuning but this also neglects the difficulties linked to the distribution of the photons in a 3-dimensional environment. Using this system, the lesions appear darker green against a lighter green background. Not much has been published about this system so far [11-14 (this last study has been carried out with a prototype of the SAFE-1000 system)] but successes [13,14] are reported (sensitivity of the autofluorescence technique in detecting bronchial (pre-) neoplasia: 78.95% vs. 21.05% for white-light illumination [11,13]). Due to its principle, it is likely that this system generates a non-negligible number of false positive results. This is actually reported by Horvath et al [13] for reasons such as anatomically related shadows, adherent mucus (in agreement with Kakihana et al [14] for bronchitis patients), biopsy accuracy and cicatricial formation among others). Moreover, although it is true that it takes advantage of the full decrease in the autofluorescence of bronchial tissue in the green region, some doubt reasonably remains as to the real efficiency of such a single range imaging system (see below).

In the light of our results, it seems that neither of these systems can take full advantage of the modifications of the autofluorescence when the normal tissue turns dysplastic and to carcinoma in situ. The Xillix system is likely to detect such lesions but it probably loses intensity in the detection path because of the limited width of the spectral windows. This loss is possibly a drawback for the color contrast that should be generated. It is however certainly a drawback for the intensity of the detected image, a crucial point when it regards a system that uses image intensifiers. A better spectral optimization of this system could maybe lead to some simplifications in its design or some improvements in the images' quality. On the other hand, the Pentax system takes full advantage of the decrease in the green region. Our results tend to show that the modified but non-neoplastic tissues like inflammatory or metaplastic tissues emit less fluorescence than healthy ones. Hence, such a system as the Pentax probably generates false-positive results not only due to geometrical effects (see previous paragraph), but also because areas of metaplastic or inflammatory tissues also appear darker with this imaging system, thus making it a priori

impossible to distinguish metaplasias or inflammations from early cancers. This might be overcome by using two detection ranges instead of one.

The Storz system is also very recent. It has several advantages over the two previously described systems. First, its size should be mentioned as it is just of the same size as a standard one-CCD mosaic chip color endoscopic camera (it actually is a standard color endoscopic camera). This camera is clipped at the proximal tip of the bronchoscope and linked to a standard-sized driver and a television screen. The illumination comes from a filtered Xe lamp (380-460 nm). At this stage, it should be mentioned that this system can be used in two different modes, namely the AF mode for the autofluorescence and the ALA mode, which is more specifically aimed at the PPIX detection. The particularity of this system in the AF mode is the use of backscattered light on top of the autofluorescence. Indeed, the detection long-pass filters let through around 1% of the backscattered excitation light, thus achieving the goal of imaging the changing autofluorescence against a 'constant' background image [15]. The lesions should therefore appear reddish against a bluish background. It is neither known which are the spectral domains that have been chosen for the foreground images nor which electronic treatment (if any) is applied to the different signals before the imaging. Despite its relative novelty, the Storz system is already reported to have had a number of successes [16] with few false positive findings and an impressive gain in sensitivity from 33% to 83% in detecting the dysplasias or the CIS [16,17]. It should be noted, though, that the use of backscattered violet-blue excitation light has at least one disadvantage: the blood cannot be discriminated from the lesions because it absorbs the excitation light that should be backscattered. There is consequently no difference on the screen between the excitation light absorbed by the blood and the smaller autofluorescence emitted by the lesions. This potentially generates false-positive results. Another drawback of this system is the possible spectral crosstalk of the color filters of the camera. As they have probably not benefited from an optimization study in the same manner as our system has, it is possible that the filters are chosen in such a way that their transmission ranges overlap or that the natural fluorophores emit in two of their spectral ranges. This would be detrimental to the contrast between the early lesions and the healthy tissue. It should also be mentioned that the images given by this system are of limited quality because the integration time usually needs to be set on 2 to 4 frames. Next to these disadvantages, this system is a real improvement over the previously commercialized systems as it images the autofluorescence of the bronchial tissue at a fraction of their size.

Table 9.1 summarizes the main spectroscopic features of these different systems as well as their mode of action.

Name	Excitation region	Detection range(s)	Mode
Xillix	blue light	green: 480-520 nm red: 630+ nm	Dual range
Pentax	420-480 nm	green: 490-590 nm	Single range
Storz	380-460 nm	N/A	Dual range + Retrodiffusion

Table 9.1: Commercially available photodetection imaging systems and their spectral characteristics.

The last system is the Wolf-EPFL system. It has not yet been commercialized but it is now in the first set of clinical tests in the ENT clinic of the CHUV Hospital in Lausanne. We describe it in more detail in the next section.

9.2 The Wolf-EPFL System

Introduction

The aim of this part of our work was to develop a photodetection imaging system for the early lesions in the bronchi based on our autofluorescence measurements. Such a system should be seen as an improvement and a simplification of a previous system developed in Lausanne and described by Wagnières et al [18].

The specifications of the system read as follows: it should

- allow for a rapid switch between the white-light and the autofluorescence modes,
- avoid the use of an image-intensifier,
- be adjustable to flexible and rigid Wolf bronchoscopes,
- rely on a Xenon-lamp and not a laser,
- rely on standard commercial components (monitor, VCRs),
- rely on a sensitive B/W microhead CCD camera,
- image both color components on one CCD chip,
- superimpose both color components,
- avoid the use of a computer,
- be as compact as possible.

These specifications aimed at providing some advantages for this system with respect to the previously developed as well as the early commercial systems. These advantages should make this system less cumbersome (use of a lamp instead of a laser), more flexible (availability, at the switch of a button, of both the autofluorescence and white-light observation) than other systems. It should also be less delicate, less expensive and consumable (no use of image intensifiers), simpler and more reliable (no use of a computer) and optimized (autofluorescence *in vivo* measurements). Finally, all these specifications should make the final system, when marketed, less expensive than similar earlier systems.

Materials and Methods

Principle

The principle of the system is given in Fig. 9.1.

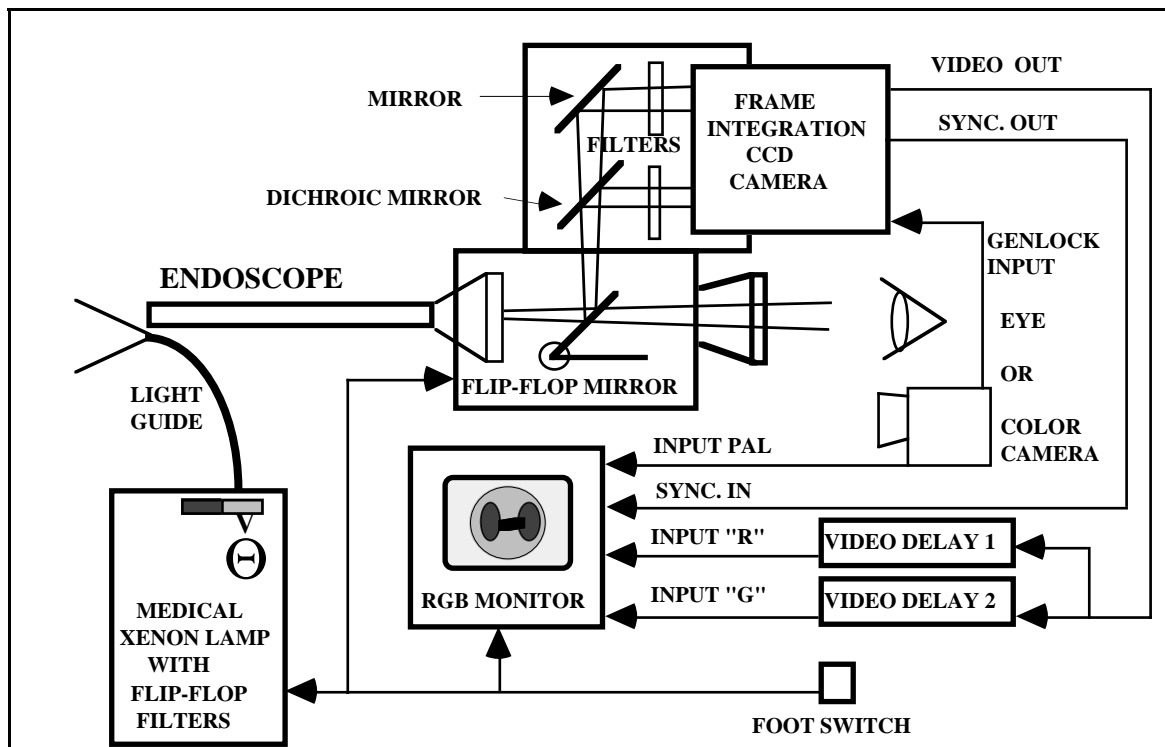


Figure 9.1: Principle diagram of the Wolf/EPFL autofluorescence photodetection system.

This system relies on one B/W CCD camera only. Two images are formed on the chip, one for each spectral region (color components: one 'green' region and one 'red' region as described in Chapter 8). A video processor then delays these two images. The delay is different for the green and for the red component, thus allowing their superimposition on the screen. A switchable mirror also permits observation of the endoscopic site under white-light illumination.

Detection

The detection of the autofluorescence takes place in a device that is clipped at the eyepiece of a standard bronchoscope. It is composed of three stages. The first stage includes the switchable mirror and the eyepiece. The second stage contains the focusing optics and the third stage frames the optical elements to separate the color components (dichroic mirror), to filter the unwanted light (long pass filter, color filters) and to image the resulting light streams (micro-head B/W CCD camera). A general view of this device can be found in Fig. 9.2.

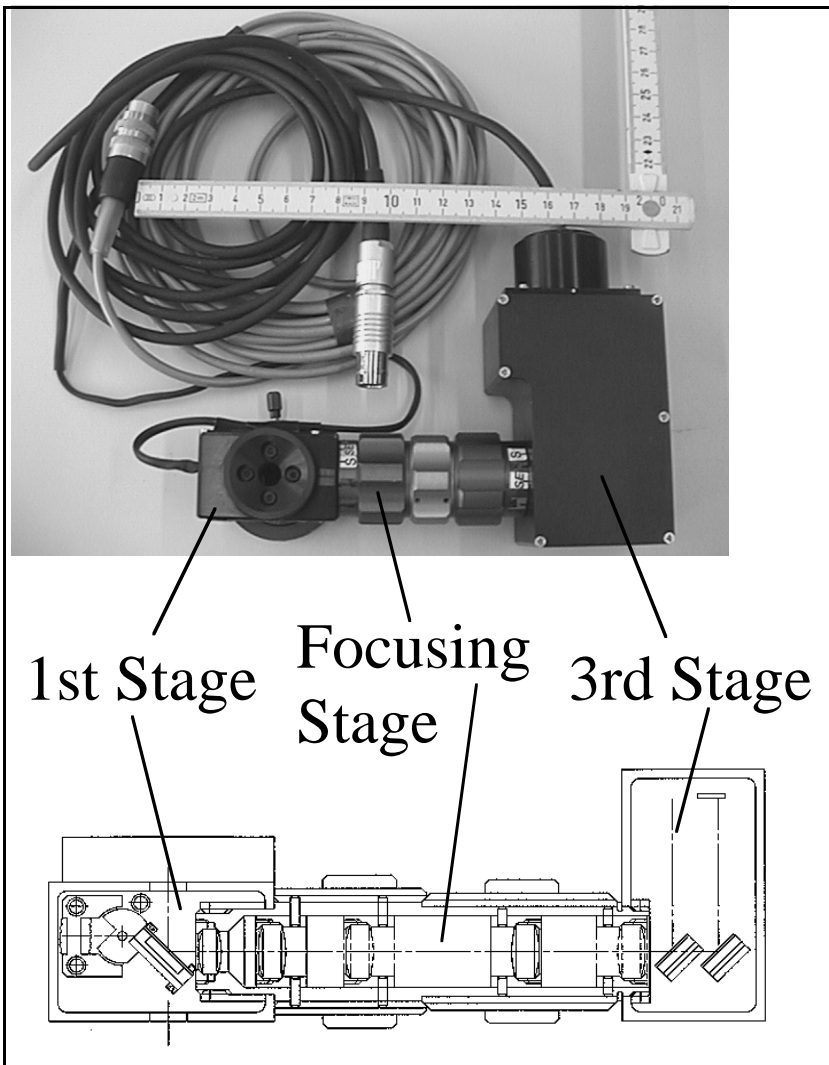


Figure 9.2: General view and drawing of the detection device developed at the EPFL. The drawing does not take into account the 90° rotation of the third stage with respect to the first stage that is shown on the photograph of the actual prototype (drawing by Nicolas Chauvin). For this reason, the drawing presents a side view of the first stage and the photograph a back view. The photograph of the side view of the first stage can be found in Fig. 9.3.

The first stage of the device that was developed at the EPFL was designed to divert the light stream into the focusing optics when in autofluorescence mode (design by Nicolas Chauvin). In white-light mode, it should only let the light through. This goal has been achieved with a switchable mirror. It is powered by an electromagnet. Figure 9.3 gives a close-up view of the first stage in both the open and the closed configuration.

The second stage, the focusing stage, consists of three lenses. The first lens is fixed and is inserted in the first stage. Its mount stops the motion of the switchable mirror. The second and third lenses can be shifted by rotation of the outer rings (blue rings) of this part of the device. All three lenses are supplied by Spindler & Hoyer GmbH (37081 Göttingen, Germany). Their characteristics are given in Table 9.2 below. The third stage of this device aims at separating the green and the red color components from the backscattered excitation light first and then from each other. To do so, this stage includes a long pass filter, a dichroic filter and color filters if necessary. The

characteristics of these filters are given in Table 9.2. Figure 9.4 gives a close-up view of the third stage. The prism in the third stage aims at correcting the optical path of the channel that has been

transmitted by the dichroic mirror. In fact, by shifting back the focus point of the green channel, it allows for the two color components to be imaged at the same point although the optical path of the red component is shorter than that of the green component.

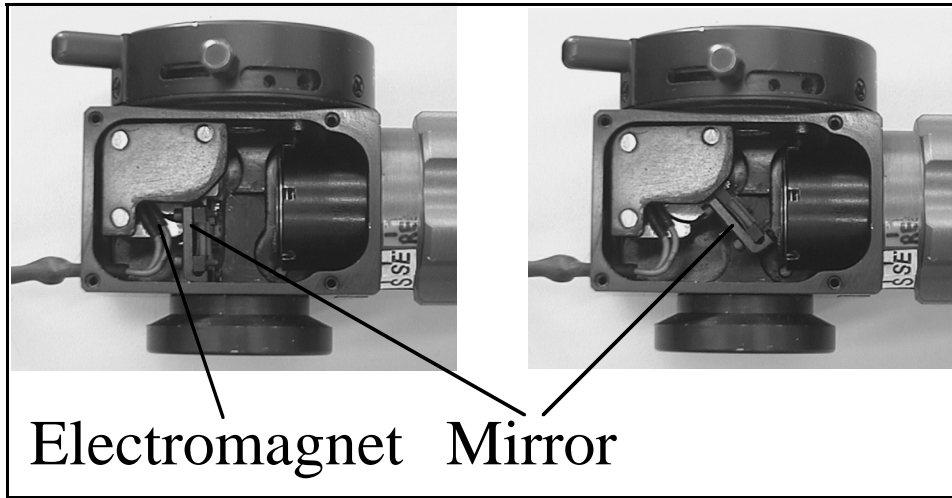


Figure 9.3: Close-up view of the first stage of the prototype developed at the EPFL in the open (white-light, left) and the closed (autofluorescence, right) configurations (design by Nicolas Chauvin).

The Mark II Wolf system has been developed as an improvement of the device developed at the EPFL. It is based on the same principle (imaging of two color components next to each other on the same CCD chip). It also contains a switchable optical element and is also clipped to the eyepiece of a standard bronchoscope. Not much is known about the exact elements that compose it, however, for proprietary reasons. Figure 9.5 gives an external view of this device and Table 9.2 summarizes the details of the system developed at the EPFL.

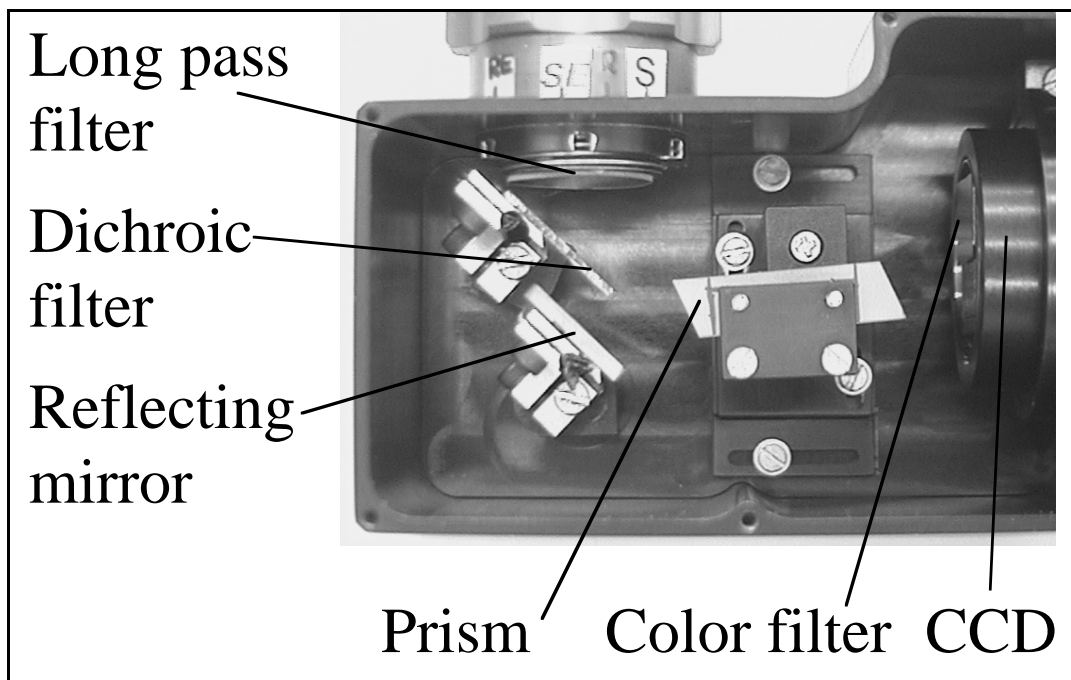


Figure 9.4: Close-up view of the third stage of the prototype developed at the EPFL.

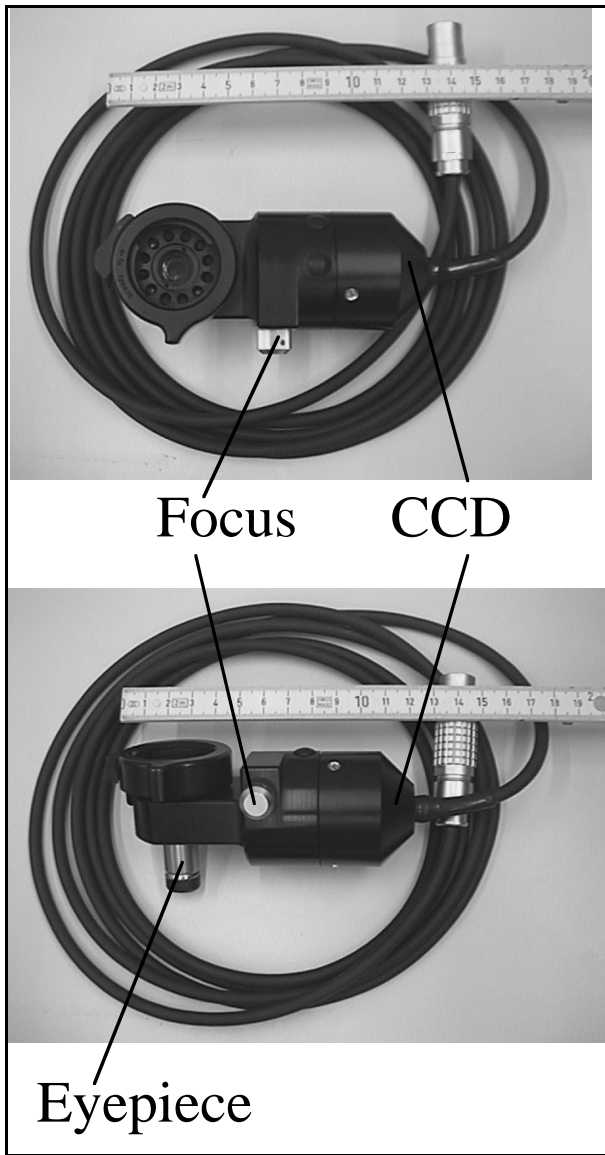


Figure 9.5: Close-up view of the prototype developed at Knittlingen.

Delay line

The B/W CCD camera detects two images next to each other, one for the green channel and one for the red channel. This signal is taped for documentation purposes with a standard VCR. An example of the raw signal as it can be measured at the output of the camera driver is given in Fig. 9.6.

Element	Prototype developed at the EPFL
Long-pass filter	Schott, Germany, custom-made long pass, 50% trans. at 520 nm
Focusing optics	3 lenses (1 fixed, 2 movable, all from Spindler & Hoyer): 1. f = 16 mm, d = 8 mm 2. f = 25 mm, d = 12.5 mm 3. f = 30 mm, d = 12.5 mm
Dichroic mirror	Andover Corporation, Salem, NH, USA Red reflective, 45°, 50% trans. at 580 nm, 0% trans. at 600 nm
Color filter (green)	None
Color filter (red)	Schott, Germany, custom-made long pass, 50% trans. at 600 nm
Prism	Gueissaz Präzisionsoptik, 8706 Meilen, Switzerland, rhombic prism, SF5 optical glass, n = 1.67270, $\alpha = 70^\circ$, l = 23.2 mm
Size (L x W x D)	164 mm x 115 mm x 53 mm
Weight	500 g (770 g incl. wiring)
CCD camera	Kappa Messtechnik GmbH, CF 8/1 FMC
Pixel number	752 (H) x 582 (V)
Active area	6.4 mm (H) x 4.8 mm (V)
Line number	752
Sensitivity	0.12 lx, at video frequency
Quantization	8 bits
S/N	> 50 dB (> 16.7:1)
Shutter maximal speed	1/10'000 s
Shutter minimal speed	10 s

Table 9.2: Description of the optical components of the EPFL prototype.

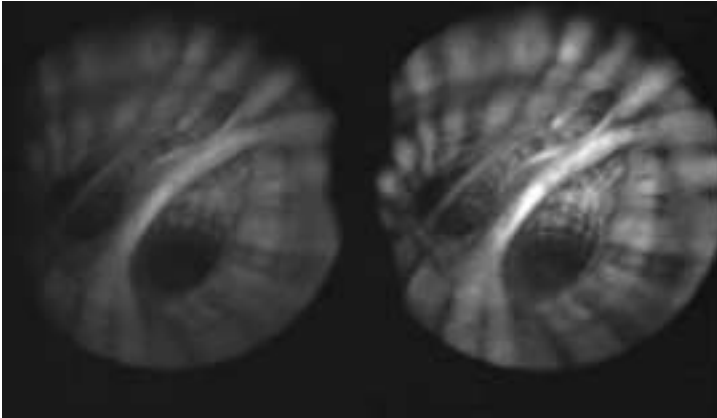


Figure 9.6: Screen result of the raw video signal at the output of the camera driver. It can be observed that the two images are next to each other.

The signal is then processed by a delay line that has been developed by Studzinski Ltd, La Tour de Peilz, Switzerland. In this device, the signal is first duplicated and each of the signals is delayed from a given amount of time, thus allowing the superimposition of the two components in false colors on a television screen by displaying the green component on the 'G' channel and the red component on the 'R' channel of an RGB screen. For the screen, a black band is added on each side to hide the remaining half-circular signal. The block diagram of the delay line is given in Fig. 9.7.

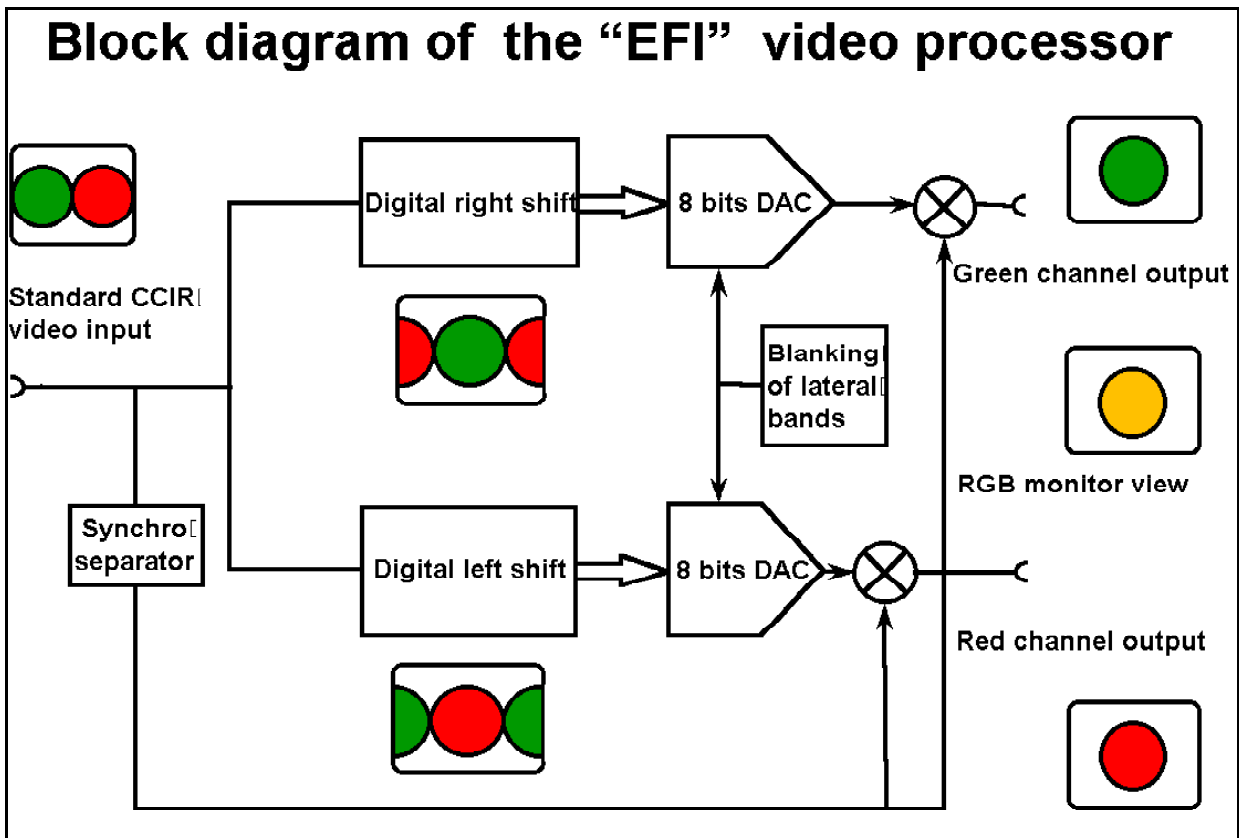


Figure 9.7: Block diagram of the video delay line.

This special feature of this system has been included in a patent filed by Wolf Endoskope GmbH: German Patent Application DE 198 00 312 A1 'Diagnosegerät zur bildgebenden Aufnahme fluoreszierender biologischer Gewebereiche', filed on January 7th 1998, by G. Wagnières, M. Zellweger, N. Lange, N. Chauvin, U Zanger, A. Studzinski, H. van den Bergh (status pending); European Patent Application EP 0 928 597 A2, filed on March 18th 1998 (status pending); United States Patent Application US 09/098 286 (status pending).

On the screen, the healthy tissue appears greenish-yellowish and the lesions appear brownish-red. On the other hand, blood appears bright red and can be discriminated from the lesions.

Fluorescence excitation

The excitation of the autofluorescence is achieved by means of a filtered 300W Xe lamp (Wolf Endoskope, Knittlingen, Germany) in the violet-blue range (380-460 nm, custom made filters). A major problem when dealing with the autofluorescence of the bronchial tissue is the faintness of the detected signals. In imaging applications, this becomes a crucial issue for the choice of the lamp. It should emit as much excitation light as possible in the chosen region. It should not emit IR or unwanted visible light as it could pass through the long pass filter, be reflected on (transmitted through) the dichroic mirror and be mistakenly detected by the CCD as red (green) light. The light guide (which transmits light from the lamp to the endoscope) should transmit as much as possible of the excitation light while blocking IR and should also be non-fluorescent. The same remark applies to the endoscopes. Finally, the filters in the detection head should be non-fluorescent, they should block as much of the unwanted light and transmit as much of the desired light as possible. In the case of the Wolf system, the spectral characteristics of the filters are proprietary information. The light power at the distal end of different light guides or bronchoscopes with the Wolf 300 W standard Xenon lamp has been measured and is given in Table 9.3. This measurement was performed by placing the tip of the endoscope or of the light guide within the detection head of a surface absorbing calorimeter (Sciencetech, Boulder CO, USA).

Functional system

The actual Wolf/EPFL system has been completed with standard VCRs and a standard monitor. The recorded raw signal (two B/W images next to each other) can be reprocessed if necessary by feeding it into a delay line. It is also helpful, when judging the suspiciousness of a lesion, to watch the B/W images as one should clearly see a sharp

decrease in autofluorescence on the green channel and a smaller decrease in the red channel, as shown by the spectroscopy. The autofluorescence result image and the corresponding white-light image are taped for documentation purposes. The Wolf system has been wired on a trolley to allow its transportation to the medical facility. The wiring diagram is given in Fig. 9.8 and the general view of the Wolf system is presented in Fig. 9.9.

An interesting feature of this system is its ability to rapidly switch from the white-light mode to the autofluorescence mode. This is steered by the autofluorescence detection stage, with a manual switch. Upon pressing of this button, the light source switches from white to violet light by placing a filter in the light beam. This also switches the observation channel of the monitor from PAL to RGB, thus displaying the autofluorescence image instead of the white-light image. This is done through the video switch (see Fig. 9.8). This device receives two standard PAL video signals, one from the color camera and one from the RGB-PAL encoder that has been fed with the raw RGB B/W signals, and delivers either of them to the VCR and the monitor. The gamma value of the B/W CCD camera is set to 0.45.

This completes our description of the Wolf system prototype. As stated before, it is still a prototype and can be improved further. On a purely practical point of view, some clinicians complain of its weight as it adds a non-negligible contribution to the proximal tip of the endoscope, thus modifying the usual weight and balance of the ensemble. Some of them also notice that the switching between the standard white-light and blue-light autofluorescence excitation mode can be activated unwillingly due to the positioning of the switch (just above the back of the clinician's hand depending on where they hold the ensemble). These small drawbacks will be easily corrected. As for the principle of the autofluorescence photodetection with this system, our results seem to show that the detection of early lesions is possible (see following

	Wolf Light Guide
Rigid 0° Wolf bronchoscope	Violet: 260 mW White: 530 mW
Flexible Wolf bronchoscope	Violet: 65 mW White: 160 mW
No bronchoscope (light guide only)	Violet: 565 mW White: 1100 mW

Table 9.3: Light power at the distal end of the Wolf bronchoscopes and/or light guide with the Wolf lamp.

section). As with any imaging method, care must be taken when interpreting the results and some experience must be gained to take full advantage of the information yielded by the method. This learning curve seems to be relatively short however and this system could therefore reach wide acceptance in the clinical settings. This is especially true since its use is easy (very little tuning) and it is functional within minutes from being plugged in.

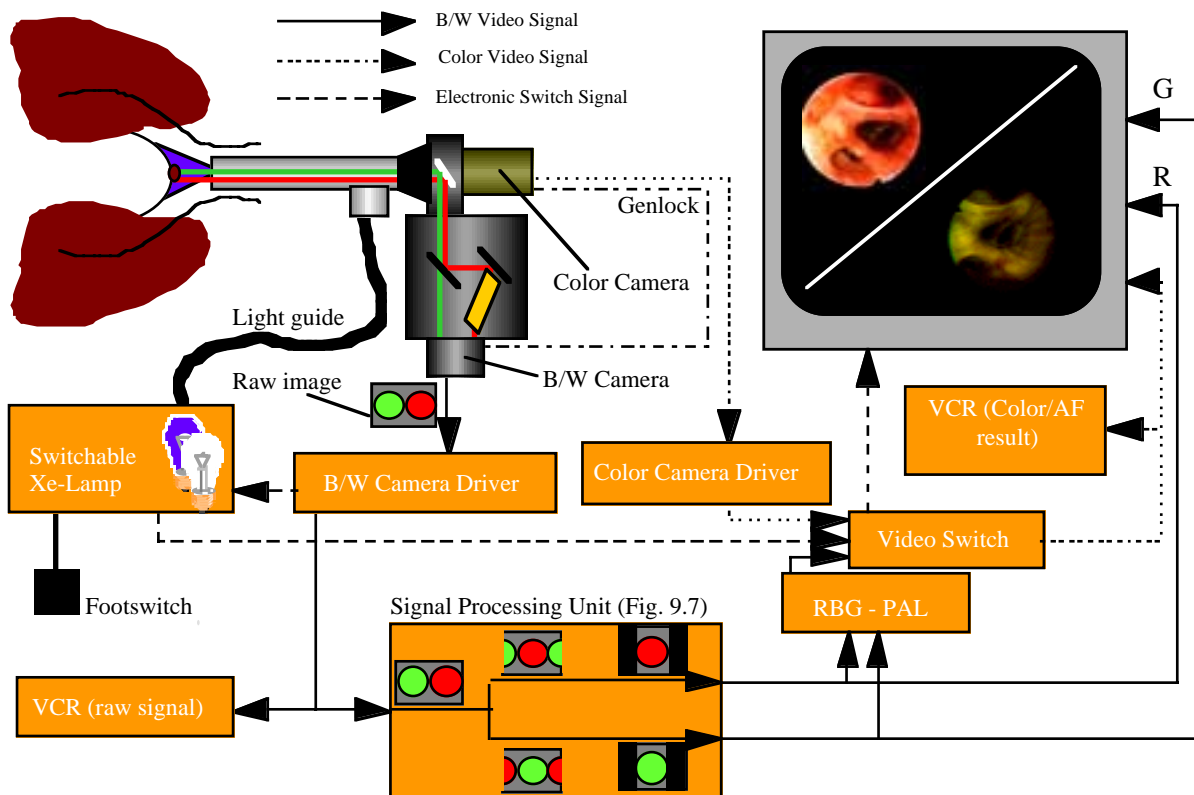


Figure 9.8: Diagram of the Wolf/EPFL system.

Another main advantage of this system over previous ones is its ability to work at video frequency, thus making it possible to perform a complete bronchial examination under fluorescence excitation light if necessary. This means that, although we did the opposite for scientific and learning purposes, it is imaginable to perform one survey of the bronchi with this device only. The autofluorescence images are bright enough to allow the clinician to navigate in the tracheo-bronchial tree and the ability to rapidly switch to white light ensures that a suspicious site can be observed in a conventional way at the press of a button. Finally, when marketed, this system could be more reliable (no computer) and less expensive than its competitors as it avoids the use of costly devices (image intensifiers) and of non-standard components.

The main point of such a prototype is to assess its clinical relevance. To do so, we performed 15 endoscopies with this device in the CHUV between July and November 1999. We used the system on relevant high risk patients (positive sputum cytology, positive resection margin following lobectomy, patients within the regular follow-up of lung cancers) and gathered images and biopsies of the sites appearing positive and negative.

Protocol of the photodetections

The photodetections took place in the following manner: a brief survey of the bronchi was undertaken by the endoscopist under standard white light. This was intended to assess the state of the mucosa and the presence or absence of notable lesions under white light. The bronchi were then examined one more time under violet-blue autofluorescence excitation light. Care was taken not to damage the mucosa during these examinations as blood can absorb the excitation light. It can then cover the mucosa as a thick layer of dark fluid, thus generating difficulties in assigning the true color of the mucosa.

A biopsy was taken on each suspicious white-light or autofluorescence site and the results were compared. Reddish brown sites under the violet-blue light were considered positive and greenish sites negative. Some examples of the resulting images are given in the following section and the complete summary of the biopsies that have been taken during these examinations is given in Table 9.4.



Figure 9.9: General view of the functional system.

The Wolf Xe source was used to excite the autofluorescence through the illumination channel of the fiberscope. The fluorescence was then collected by the detection fibers of the modified fiberscope (described in Section 8.3, Materials and Methods), filtered and dispersed on the CCD of our optical fiber-based spectrofluorometer. Since the excitation power at the distal end could vary, only normalized spectra are given and the comparison of the shapes of the spectra is the only relevant information that can be gathered from this data.

9.3 Clinical results: examples

This section aims to provide an answer to the question of the clinical relevance and usefulness of the Wolf-EPFL autofluorescence imaging system to detect early cancerous lesions in the bronchi. For each patient, the following data is given:

- The age and the sex of the patient.
- The reason why they have been investigated in the endoscopy center in the first place as well as the reason why they seemed to be relevant photodetection candidates.
- The fluorescence image of the relevant site(s) that has/have been found.
- The corresponding white-light image of the same site.
- The corresponding histopathological result of the biopsy(ies).
- The B/W image of the same site.
- Any further information that seemed relevant.
- A 'simulated' normalized autofluorescence spectrum obtained with our spectrofluorometer on the lesion and on healthy tissue (whenever available).

Patient #1: 71-year-old male

This patient underwent a control endoscopy at 2 years after an epidermoid carcinoma of the pharynx (treated by radiotherapy) as part of the regular follow-up for cancer patients. No actual sign of relapse had been recorded.

These images have been included as an example of images taken of healthy tissue. No fluorescence positive site have been found during this endoscopy and, consequently, no biopsies were taken.



Figure 9.10: White-light image of healthy bronchial tissue.

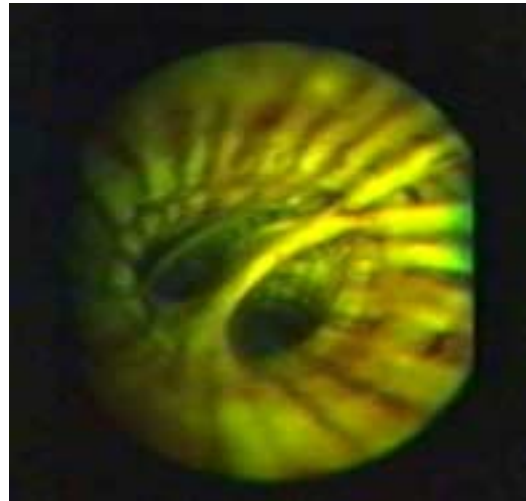


Figure 9.11: Autofluorescence image of healthy bronchial tissue.

The Fig. 9.10-9.12 only are intended to provide examples of autofluorescence images. No suspicious site has been found in the bronchi of this patient.

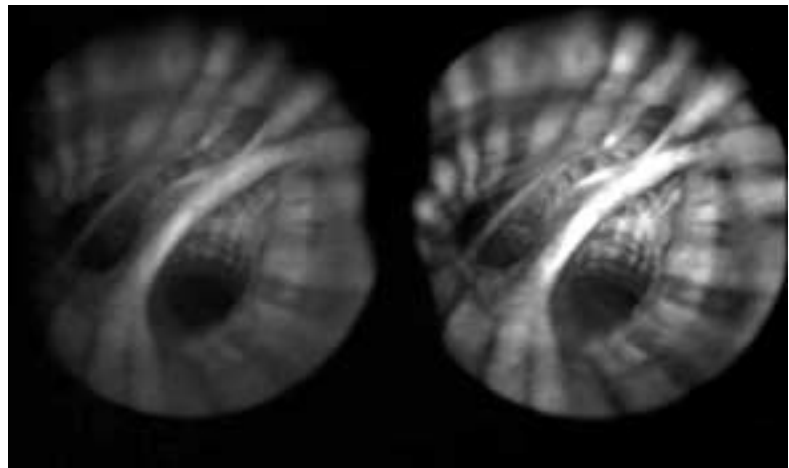


Figure 9.12: Raw video signal of the two color components of the autofluorescence image of healthy bronchial tissue. The red component is on the left and the green component is on the right.

Patient #2: 62-year-old male

This patient underwent a bronchoscopy following a positive esophageal cytology (high grade dysplasia).

Three suspicious sites were found in the bronchi of this patient, two under white light and one under autofluorescence excitation light. Three biopsies were taken. Two biopsies were taken on the white-light positive-appearing sites. These sites were negative under autofluorescence excitation light. The last biopsy was taken on the only autofluorescence-positive site. It had been missed under white-light examination. The images of this site are given in Fig. 9.13-9.15. During the first white-light examination of the bronchi, this site had not been noticed as suspicious. The histopathological analysis confirmed the presence of low grade epithelial dysplasia.

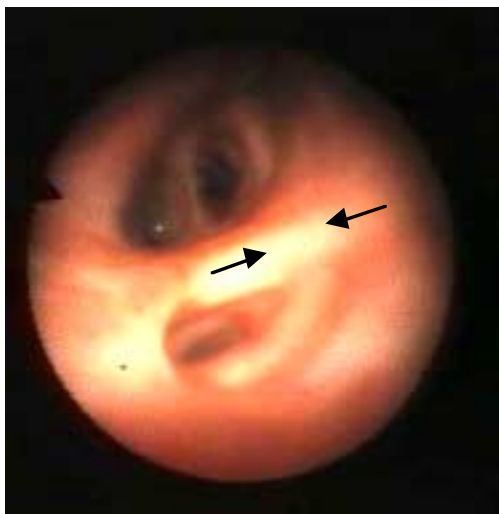


Figure 9.13: White-light image of a site bearing a low grade dysplasia in the bronchi (missed during WLB).

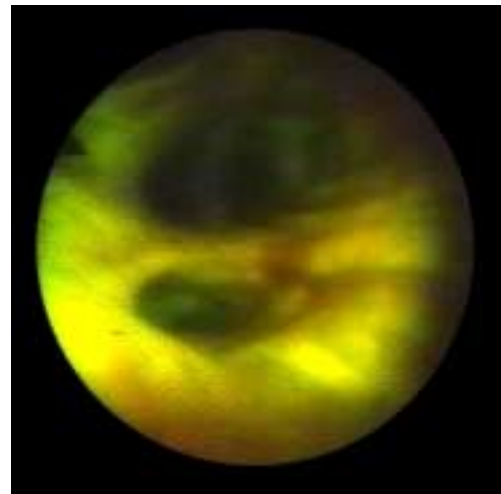


Figure 9.14: Autofluorescence image of a site bearing a low grade dysplasia in the bronchi.

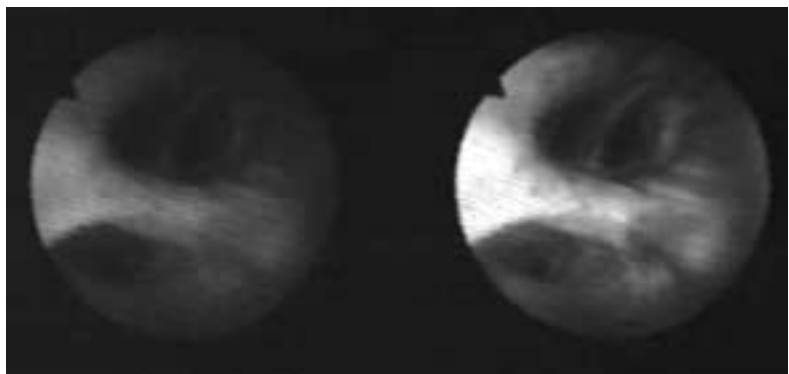


Figure 9.15: Raw video signal of the two color components of the autofluorescence image of bronchial tissue bearing a low grade dysplasia. The red component is on the left and the green component is on the right.

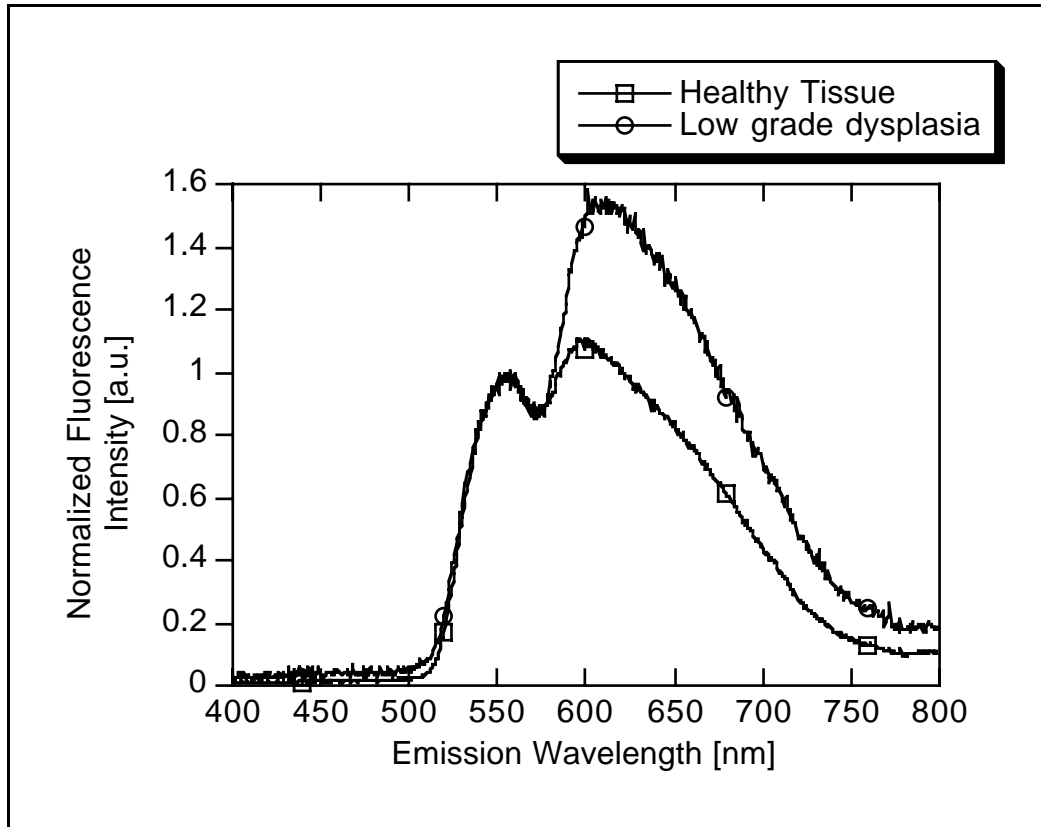


Figure 9.16: Normalized autofluorescence spectra of the healthy bronchial tissue and of the site bearing low grade dysplasia. The spectra are normalized at 550 nm (local maximum in the 'green' region) as the excitation power may have varied due to the experimental setup. They can therefore only be compared in terms of spectral shape.

It can be seen from Fig. 9.13-9.15 that the low-grade dysplasia appears as a reddish spot against a greenish background whereas the same spot is barely visible under white-light illumination. Considering our autofluorescence spectroscopic measurements, this finding is in agreement with what could be expected on images of the autofluorescence of bronchial tissue. It can also be observed that the B/W image of this site (Fig. 9.15) displays a major autofluorescence decrease in the green channel (right image), whereas this decrease is less marked in the red channel (left image). This is also in full agreement with our spectroscopic observation that the intensity of the autofluorescence sharply decreases in the green region of the spectrum and decreases to a lesser extent in the red region. A further agreement is found in the 'simulated' spectra given in Fig. 9.16. These spectra are the ones observed by our imaging system under excitation by the filtered Xe lamp. It can be seen that the spectrum of the lesion has a relatively larger 'red' contribution than the spectrum of the healthy tissue. These spectra have been obtained by sampling an area of bronchial tissue of roughly 3 mm in diameter with a modified bronchofiberscope (described in Section 8.3 Materials and Methods).

Patient #3: 71-year-old male

This patient underwent a control bronchoscopy 4 months after a lobectomy (right upper lobe). He also had undergone a PDT in the left upper lobe 3 months earlier.

Two suspicious sites were found in the bronchi of this patient, one on the lobectomy scar and the second on the site of the previous PDT. Both were found under autofluorescence excitation light, although it should be mentioned that the first site appeared erythroplastic under white-light illumination. Two biopsies were taken, one on each site. The histopathological analysis of the first biopsy (lobectomy scar) confirmed the presence of an infiltrating little-differentiated epidermoid carcinoma. The second biopsy (taken on the division carina on the site of the PDT) was analyzed as moderate dysplasia. The images of this second site are given in Fig. 9.17-9.19.



Figure 9.17: White-light image of a site bearing a moderate dysplasia in the bronchi (this site appeared negative during WLB).

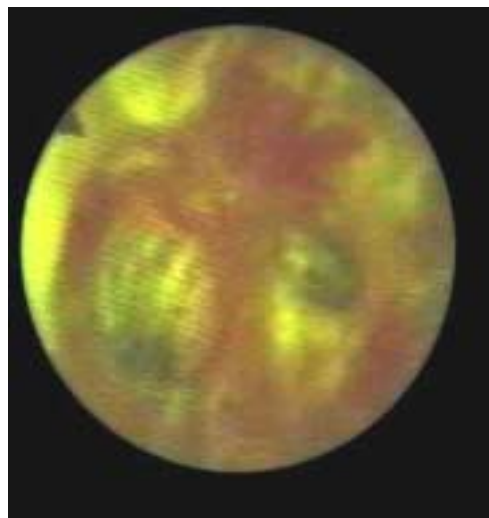


Figure 9.18: Autofluorescence image of a site bearing a moderate dysplasia in the bronchi.

It can be seen from Fig. 9.17-9.19 that the moderate dysplasia appears as a reddish spot against a greenish background whereas the same spot is barely suspicious under white-light illumination. The autofluorescence image also clearly shows the delineation of the lesion. Again, it can also be observed that the B/W image of this site (Fig 9.19) displays a major autofluorescence decrease in the green channel (right image), whereas this decrease is less marked in the red channel (left image).

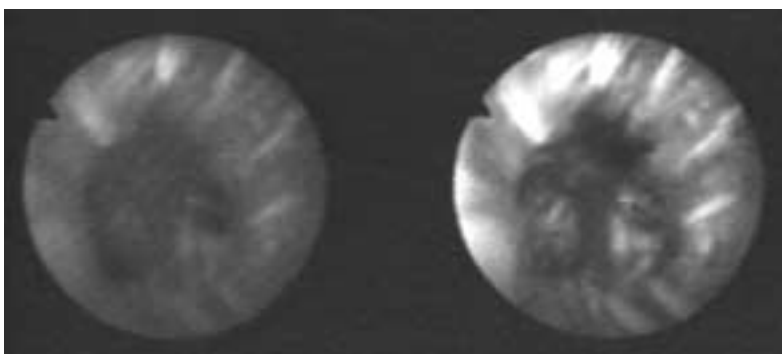


Figure 9.19: Raw video signal of the two color components of the autofluorescence image of bronchial tissue bearing a moderate dysplasia. The red component is on the left and the green component is on the right.

Patient #4: 60-year-old female

This patient underwent a bronchoscopy for suspicion of a tumor on the vocal cords.

No suspicious site has been found in the bronchi of this patient, neither during WLB nor under autofluorescence excitation light. The observation of the vocal cords however produced highly suspicious images on the right vocal cord. The left vocal cord appeared swollen under white-light illumination and negative under autofluorescence excitation light. Two biopsies were taken, one on each vocal cord. The histopathological analysis of the first biopsy (left vocal cord) confirmed the absence of malignant tissue. The second biopsy (right vocal cord) was analyzed as a little-differentiated epidermoid carcinoma. The images of the vocal cords are given in Fig. 9.20-9.22.



Figure 9.20: White-light image of the vocal cords. The right vocal cord bears a little differentiated epidermoid carcinoma and the left vocal cord, though swollen, bears no sign of malignant change.



Figure 9.21: Autofluorescence image of the vocal cords. The right vocal cord bears a little-differentiated epidermoid carcinoma and the left vocal cord bears no sign of malignant change.

It can be seen from Fig. 9.20-9.22 that the little-differentiated epidermoid carcinoma appears as a reddish spot on the right vocal cord whereas the contralateral vocal cord, bearing no malignant change, appears green. Again, it can also be observed that the B/W image of this site (Fig. 9.22) displays a major autofluorescence decrease in the green channel (right image), whereas this decrease is less marked in the red channel (left image).

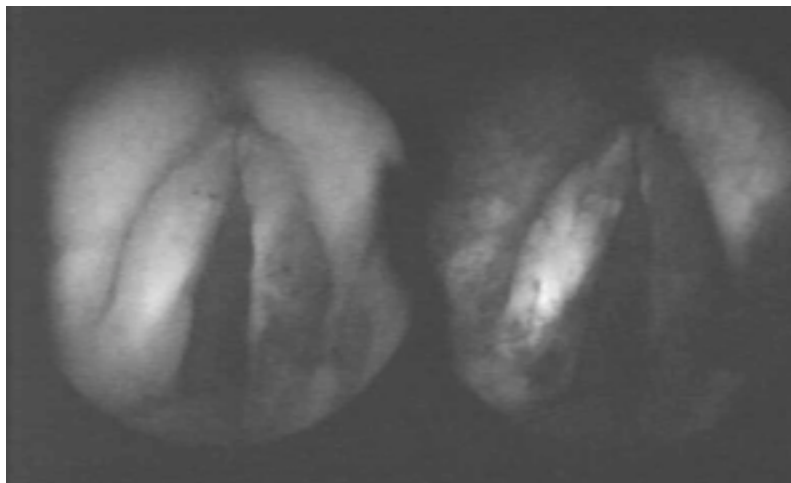


Figure 9.22: Raw video signal of the two color components of the autofluorescence image of the vocal cords. The right vocal cord bears a little-differentiated epidermoid carcinoma and the left vocal cord bears no sign of malignant change.

Patient #5: 70-year-old male

This patient underwent a bronchoscopy as part of the follow-up after a lobectomy (right upper lobe, 6 months beforehand).

Three highly suspicious areas were found in the left main bronchus both under white light and violet light. These sites appeared as small whitish spots slightly protruding into the left main bronchus (Fig. 9.23). Under autofluorescence excitation light, these sites appeared dark red (Fig. 9.24). One biopsy was taken. The histopathological analysis of this biopsy confirmed the presence of a little-differentiated epidermoid carcinoma.

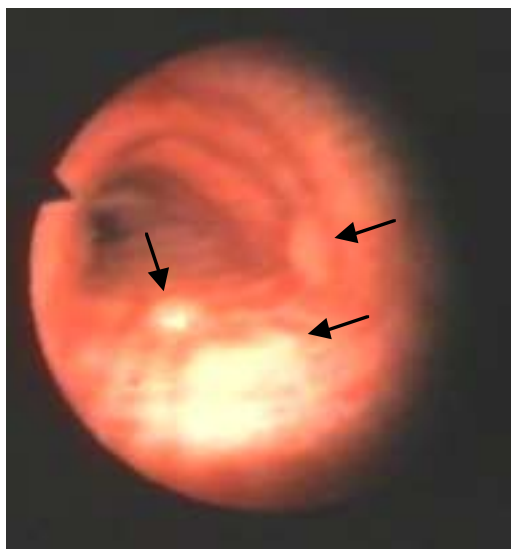


Figure 9.23: White-light image of a site bearing a little-differentiated epidermoid carcinoma in the bronchi.

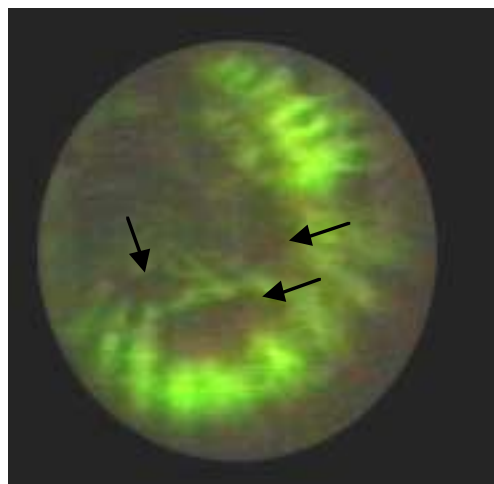


Figure 9.24: Autofluorescence image of a site bearing a little-differentiated epidermoid carcinoma in the bronchi.

It can be seen from Fig. 9.23-9.25 that the little-differentiated epidermoid carcinoma appears as a dark red spot against a greenish background. Again, it can also be observed that the B/W image of this site (Fig. 9.25) displays a major autofluorescence decrease in the green channel (right image), whereas this decrease is less marked in the red channel (left image). In this case, the autofluorescence image is of help to clearly assess the delineation of the lesion. Figure 9.26 is a close-up view of one such lesion bearing a little blood. The white-light image leaves no doubt as to the extension of the blood on the lesion.

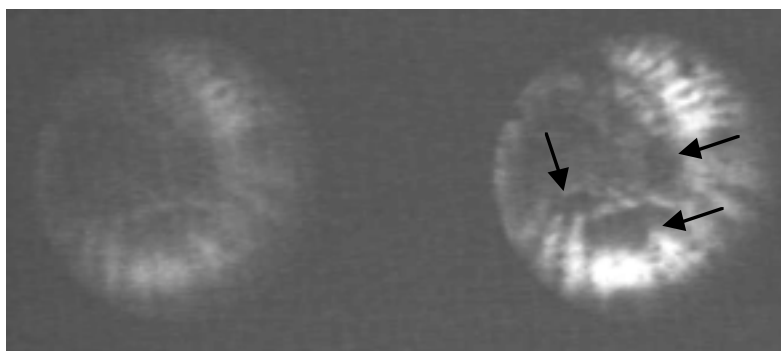


Figure 9.25: Raw video signal of the two color components of the autofluorescence image of bronchial tissue bearing a little-differentiated epidermoid carcinoma. The red component is on the left and the green component is on the right.

Figure 9.26 is a close-up view of one such lesion bearing a little blood. The white-light image leaves no doubt as to the extension of the blood on the lesion.

A major difficulty when using violet light to excite the autofluorescence of tissue is the possible interference of blood as it strongly absorbs light around 410 nm. It might therefore appear very dark, a potentially confusing property as the diseased tissue should also appear darker than the healthy tissue. The autofluorescence image of the site displayed in Fig. 9.26 is given in Fig. 9.27 and the corresponding raw B/W image is given in Fig. 9.28.



Figure 9.26: White-light image of a site bearing blood on a little-differentiated epidermoid carcinoma in the bronchi

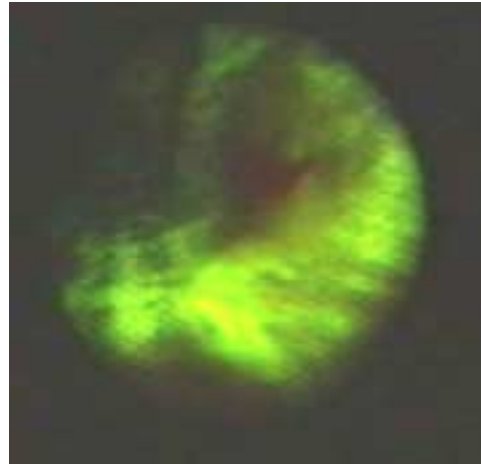


Figure 9.27 Autofluorescence image of a site bearing blood on a little-differentiated epidermoid carcinoma in the bronchi.

It can be seen in Fig. 9.27 that the blood and the lesion do not have the same color under autofluorescence excitation light. The blood appears bright red whereas the lesion looks rather dull and brownish. This is further demonstrated in Fig. 9.28 as the green color component (right image) shows the blood as very dark against a less dark lesion. Although this could be confusing under some circumstances, it is reassuring to see that our system seems to provide some discrimination between the blood and the lesions. Moreover, since it allows the operator to rapidly switch from autofluorescence excitation to white-light illumination, it is unlikely that blood could dramatically impair the detection of such lesions.

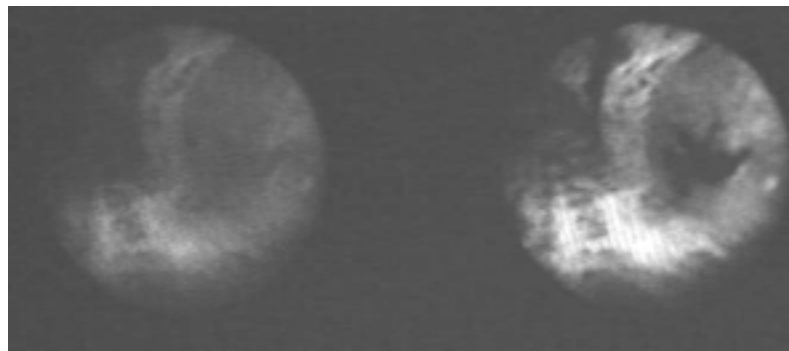


Figure 9.28: Raw video signal of the two color components of the autofluorescence image of bronchial tissue bearing blood on a little-differentiated epidermoid carcinoma in the bronchi. The red component is on the left and the green component is on the right.

Patient #6: 52-year-old male

This patient underwent a bronchoscopy as part of the follow-up after a lobectomy (left upper lobe, 6 weeks beforehand). The section of the lobectomy showed areas bearing malignant cells.

One highly suspicious area was found on the lobectomy scar. This site appeared as an erythroplastic area under white-light illumination (Fig. 9.29). Under autofluorescence excitation light, it appeared dark red (Fig. 9.30). The area was brushed twice. The cytopathological analysis of these brushings confirmed the presence of atypical cells with abnormally large nuclei. There are therefore suspicions that this area bears a carcinoma.

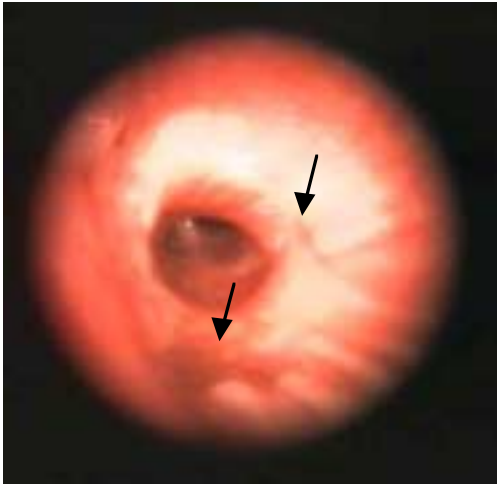


Figure 9.29: White-light image of a site whose cells are suspected of carcinoma (foreground) in the bronchi. The lobectomy scar is visible in the background.

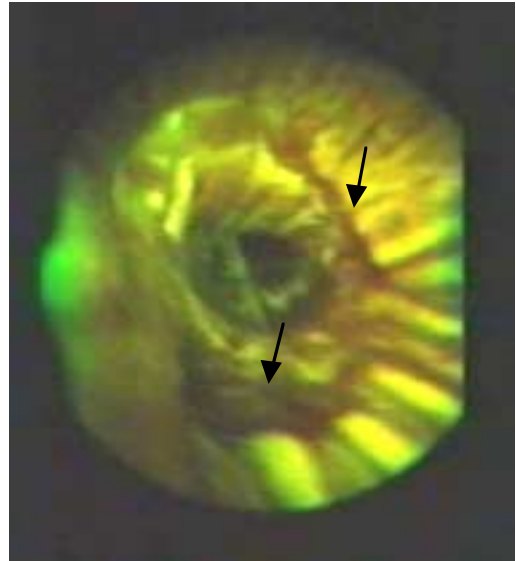


Figure 9.30: Autofluorescence image of a site whose cells are suspected of carcinoma (foreground) in the bronchi. The lobectomy scar is visible in the background.

It can be seen in Fig. 9.30 that the scar is clearly visible under autofluorescence excitation light. In the case of this patient, it could be mistaken as a false-positive result as it seems to have the same appearance and color as the truly suspicious area. This could be due to the fact that this scar was very recent (6 weeks) and still in within the scarring process. Further studies of such areas will be necessary to properly assess the contribution of the scars to the false-positive results.

As described in Chapter 8, it is possible to enhance the contrast by taking advantage of the full decrease of the green

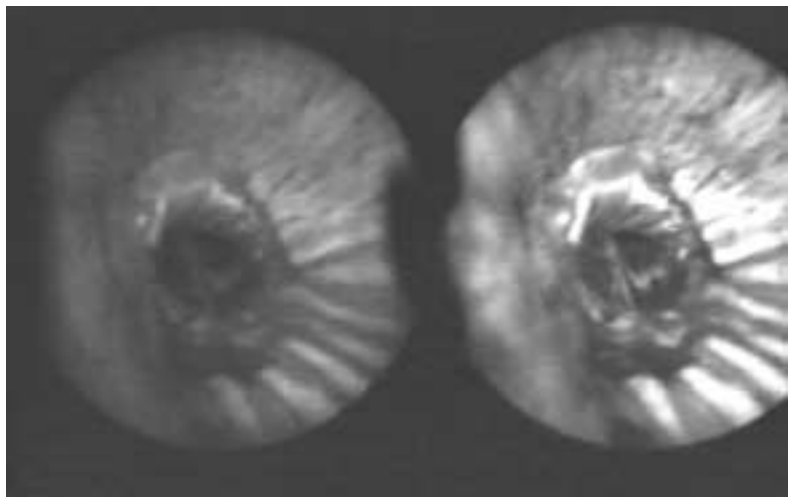


Figure 9.31: Raw video signal of the two color components of the autofluorescence image of a site whose cells are suspected of carcinoma (foreground) in the bronchi. The lobectomy scar is visible in the background. The red component is on the left and the green component is on the right.

autofluorescence. To do so, we need a 'constant' background image. This can be done by adding a red contribution to the violet-blue excitation light of around 0.1%. The red image will become 'constant'. By doing so, it is possible to fully take advantage of the decrease in green autofluorescence. This approach should improve the SNR of the resulting images while also increasing the contrast. This experiment has been carried out on the same patient, on the same spot and the results are given in Fig. 9.32-9.33.

It can be seen in Fig. 9.32 that the contrast of the autofluorescence and backscattered red light image of this site is enhanced as compared to the autofluorescence-only image of the same site (Fig. 9.30). It should be noted, however, that more locations appear red in this image and it is not known whether this could be detrimental to the overall usefulness of the autofluorescence imaging. The experiments that have been carried out with this method so far tend to show that the backscattering method induces more locations to appear red and eventually hinders discrimination between unsuspecting and suspicious areas. For instance, the blood appears bright red under such an illumination method and so do the lesions and the scarring tissue (Fig. 9.32). The pure autofluorescence excitation allows for a discrimination of the blood and the lesions (Fig. 9.27). It can be seen in Fig. 9.33 that the red channel (left image) is indeed very homogeneously illuminated, thus offsetting the decrease in the red autofluorescence. The green image has not changed.

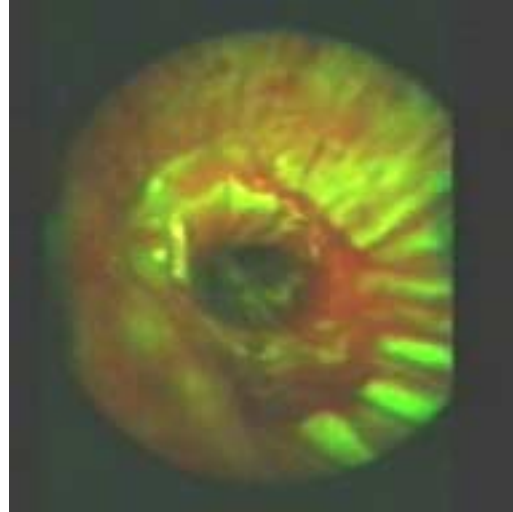


Figure 9.32: Autofluorescence and red backscattered image of a site whose cells are suspected of carcinoma (foreground) in the bronchi. The lobectomy scar is visible in the background.

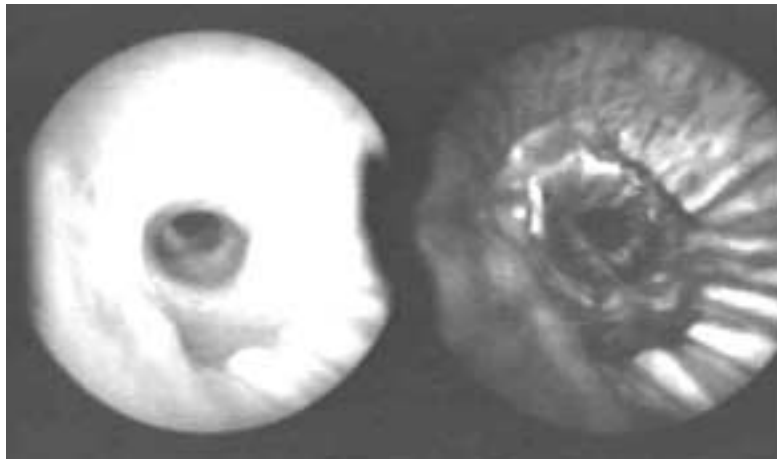


Figure 9.33: Raw video signal of the two color components of the autofluorescence and the red backscattered image of a site whose cells are suspected of carcinoma (foreground) in the bronchi. The lobectomy scar is visible in the background. The red component is on the left and the green component is on the right.

Patient #7: 66-year-old male

This patient underwent a bronchoscopy as part of the follow-up after a lobectomy (left upper lobe, 2 months beforehand). The section of the lobectomy showed areas bearing malignant cells during histopathological analysis.

One suspicious area was found on the lobectomy scar. This site appeared as an erythroplastic area under white-light illumination (Fig. 9.34). Under autofluorescence excitation light, it appeared dark red (Fig. 9.35). One biopsy was taken. The histopathological analysis of the biopsy was negative. It showed no malignant cells.



Figure 9.34: White-light image of a lobectomy scar. The lobectomy section bore malignant cells.

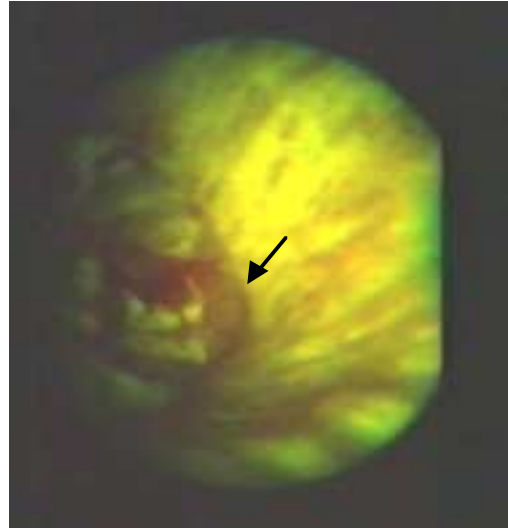


Figure 9.35 Autofluorescence image of a lobectomy scar. The lobectomy section bore malignant cells.

Figure 9.35 clearly shows an area that appears positive on the scar. This area is also visible on the white-light image of the site (Fig. 9.34). The raw B/W image confirms that the area should be considered suspicious (Fig. 9.36). Considering the presence of malignant cells on the lobectomy section, this appears at first as a highly suspicious area. The biopsy was negative, however. Several reasons may account for this fact. As seen in Patient #6, recent scars may appear positive. This might be due to cell multiplication characteristics of the scarring tissue that make it resemble the proliferative tissue of tumors. It might be that the scarring tissue requires a higher blood supply than the surrounding non-scarring locations. It cannot be excluded either that a slight displacement of the biopsy forceps in this difficult area might have taken a sample of healthy tissue rather than of a malignant area. Maybe other unexplained reasons account for this false-positive result.

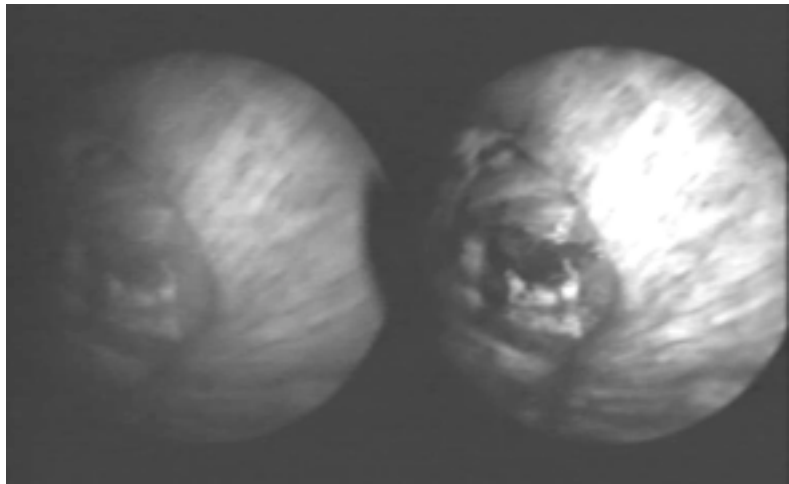


Figure 9.36: Raw video signal of the two color components of the autofluorescence image of a lobectomy scar. The lobectomy section bore malignant cells. The red component is on the left and the green component is on the right.

Summary of the patients and of the corresponding results

Pat	Site	White Light	Fluorescence	Histopathology	TP (F)	FP (F)	TP (W)	FP (W)	AF	WL
A	None	Negative	Negative	None						
B	Carina	Thickened	± Positive	CI/HYP		1		1		
C (#4)	Left vocal cord	Thickened	Negative	HK				1		
	Right vocal cord	Thickened	Positive	EpCarc	1		1			
D	Trachea	Dip	Negative*	Negative				1		
	Trachea	Negative	Negative	Negative						
E	None	Negative	Negative	None						
F (#1)	None	Negative	Negative	None						
G (#2)	Right lower lobe	Negative	Positive	LDys	1				1	
	Left stem bronchus	Positive	Negative	LI				1		
	Left stem bronchus	Positive	Negative	LI				1		
H	Left vocal cord	Leucoplasia	Negative	LI				1		
	Right vocal cord	Leucoplasia	± Positive	LI		1		1		
	False vocal cord (R)	Leucoplasia	Positive	CIS	1		1			
	Right arytenoid	LE	Positive	EpCarc	1		1			
I	LB/AB carina	Negative	Positive	HYP		1				
	LB/AB carina	Positive	Positive	WS						
J (#7)	Intermediary Trunk	Negative	Positive	CI		1				
	Lobectomy scar	E	Positive	CI/Scar		1		1		
K (#6)	Lobectomy scar	E	Positive	AtCells	1		1			
	Lobectomy scar	E	Positive	± CIS	1		1			
L (#3)	Lobectomy scar	E	Positive	EpCarc	1		1			
	Apico-dorsal trunk	Negative	Positive	Mdys	1				1	
M	Trachea	Negative	± Positive	Mmet		1				
	Nelson/B carina, L	Negative	Positive	Mmet		1				
	Left Nelson	E	Positive	Mmet		1		1		
	Nelson/B carina, R	Negative	Positive	Mmet		1				
N (#5)	Trachea	Positive	Positive	EpCarc	1		1			
O	Stem/Upper carina, L	Negative	Negative	Negative						
P	Paracardiac carina	Negative	Positive	CIS	1				1	
	Paracardiac carina	Negative	Positive	Sdys/CIS	1				1	
Tot 16	31**				11	9	7	9	4	0

Table 9.4: Summary of the results obtained with the autofluorescence photodetection system. The abbreviations are as follows (sorted by column): Patient: the number links to the cases in previous pages. Site: LB: left basal; AB: anterior basal; B: basal; ** one biopsy has not been included because it might have been taken on the wrong site. White light: negative: unsuspecting or missed under white light; positive: suspicious under white light; LE: leuco-erythroplasia; E: erythroplasia. Fluorescence: positive: reddish area; negative: greenish area; *: intense green autofluorescence. Histopathological result: CI: chronic inflammation; HYP: hyperplasia; HK: hyperkeratosis; EpCarc: epidermoid carcinoma; Ldys: light dysplasia; LI: light inflammation; CIS: carcinoma in situ; WS: biopsy on the wrong site likely; AtCells: atypical cells; Mdys: moderate dysplasia; Mmet: mature metaplasia; Sdys: severe dysplasia; TP (F): true positive in autofluorescence; FP (F): false positive in autofluorescence; TP (W): true positive in white light; FP (W): false positive in white light; AF: true positive in autofluorescence and negative under white light (equivalent to the false-negative results in white-light illumination); WL: true positive under white light and negative in autofluorescence (equivalent to the false-negative results in autofluorescence).

Two approaches have been used in the course of this work to assess the positivity of a site and the subsequent calculations. One of them is the learning curve approach and it is described first. The second approach relies upon the quantification of the color modifications and is described second. It is called the threshold approach. All the patients that are reported in Table 9.4 are patients that were scheduled for a bronchoscopy because of their risk factor. Some of them, however, did not bear any suspicious spot. They have been included in Table 9.4 anyway and make up for the patients with negative white-light bronchoscopy, negative autofluorescence bronchoscopy and negative histopathological result.

Learning curve approach

Under this approach, the sites labeled 'fluorescence positive' in Table 9.4 were the sites that appeared as red spots during bronchoscopy. This assignation does not stem from an objective criterion, as will be the case below. The data in Table 9.4 allows us to calculate the positive predictive value of the autofluorescence bronchoscopy, and of the white-light bronchoscopy. The negative predictive value cannot be calculated as the false negative rate is impossible to evaluate (although the lesions that have been detected by autofluorescence only make-up for some of the white-light false-negative results). The positive predictive value is given as the ratio of the true positive results (TP) on the overall positive results (true and false positive (FP)). For the sake of this calculation, the white-light results have been considered positive when the observation of the physician was such that they would have taken a biopsy after the white-light bronchoscopy. In our data, it means in the cases where the macroscopic description was 'thickened', 'dip', 'leucoplasia', 'erythroplasia' or 'leucoerythroplasia' [19]. This yields the following values of PPVs:

$$\text{Positive Predictive Value: PPV} = \frac{\text{TP}}{\text{TP} + \text{FP}}$$

$$\text{White-light bronchoscopy: } \frac{7}{7 + 9} = 44\%$$

$$\text{Autofluorescence: } \frac{11}{11 + 9} = 55\%$$

$$\text{Autofluorescence + white light: } \frac{7}{7 + 4} = 64\%$$

The PPV gives the probability that a lesion is actually a lesion if it is visible with a given method (as opposed to the sensitivity, which gives the capability of a method to find a lesion if there actually is a lesion). One can compare these positive predictive values, although they only apply to our small number of patients. It is clear from this data that the autofluorescence is helpful. The PPV goes from 44% for white-light bronchoscopy alone to 55% for the autofluorescence alone and up to 64% for both methods together. This shows that both methods are good complements as their concomitant use produces a better outcome than either of them alone. Moreover, it should

be noted that some lesions have been detected by autofluorescence only (see Table 9.4), namely two early cancerous lesions (light dysplasia and moderate dysplasia) and two CIS/severe dysplasias, whereas none have been detected under white-light illumination only. Although it is impossible at this stage to calculate values for the sensitivity or the specificity of the method, this means that the sensitivity of the autofluorescence bronchoscopy must be higher than the sensitivity of the white-light bronchoscopy. This, again, is a significant contribution of the autofluorescence detection. A difficult encountered with this data is the issue of the objective criterion for a site's positivity. Indeed, there are many false positive sites in the figures above. This was the reason of our trying to calculate these values with better parameters – objective criteria for the positivity of a site. This has been achieved with the threshold approach (see below).

It is interesting to address the issue of the agreement of the spectroscopy with the imaging. Some spectra are given for one patient (Fig. 9.16), and similar measurements were performed in other patients, but we decided not to explicitly show this data for all the measurements. These results are summarized in Table 9.5. The sites are the same as in Table 9.4. The spectra are by placing the light guide in front of the illumination bundle of the modified fiberscope (see Section 8.3). The detection takes place through the optical fibers that have been fitted into the biopsy channel.

Patient	Site	White Light	Fluorescence	Spectroscopy	Histopathology
G	Right lower lobe	Negative	Positive	Positive (Fig. 9.16)	Light dysplasia
I	Lower basal-anterior basal carina	Negative	Positive	Positive*	Hyperplasia
J	Lobectomy scar	Positive (E)	Positive	± Positive**	Chronical inflammation, scar
K	Lobectomy scar	Positive (E)	Positive	Positive**	Atypical cells

Table 9.5: Correlation of the white-light result, autofluorescence result, spectroscopic result and histopathological result of the relevant biopsies (whenever applicable); *: possible wrong biopsy site; **: possible wrong measurement site.

For every patient, autofluorescence spectra have been measured on the suspicious area and on a control healthy site. The spectra acquired on the suspicious area were considered positive whenever, after normalization at 550 nm, their red part was not within the standard deviation of the average normalized spectra of the healthy tissue. For these patients, the spectroscopy is in agreement with the autofluorescence imaging results. However, these results show that the spectroscopic measurement with our modified fiberscope is tricky. In the case of patient J, the positive-appearing site on the images was in a difficult localization next to a scar. In the case of patient K, the measurement sites were very tangential in the bronchial lumen and, consequently, it was very difficult to accurately hold the fiberscope in a given position. Only patient G could be measured in the best conditions, as the suspicious area was on a carina. It is therefore difficult to draw a conclusion with this data.

Under white-light illumination, the trained endoscopist relies on a wide expertise in observing the tissue and its modifications. Years of practice leave little doubt in their opinion as to where biopsies should be taken. It is not so clear-cut with autofluorescence detection. This method of detection, like other methods, has a learning curve. As we stand now at the beginning of the clinical tests of this system, it should be expected that the criteria of positivity could change if they are subjective and thus operator-dependent. Two options are therefore available for the design of large-scale clinical studies. Firstly, the operators of such studies should gain some experience with this system and receive some kind of training. This will be best achieved with

Histopathological status	Code
Blood	0
Healthy	1
Chronic inflammation	2
Mature metaplasia	3
Light dysplasia	4
Moderate dysplasia	5
Severe dysplasia/CIS	6
Epidermoid carcinoma	7

Table 9.6: Histopathological codes of the tissue sites that have been observed with our autofluorescence imaging system.

excitation. The green and red resulting images were digitized using 8-bit quantization. The average intensity (and the corresponding standard deviation) of the green and red pixels was computed on the site of the biopsy and next to it on presumably healthy tissue. The green intensities were then normalized by the total green, and the red intensities by the total red intensity of the image, because the green gain and the red gain are set independently for each patient. The ratio (green/red) of these normalized green and normalized red contribution was computed, together with its standard deviation and plotted vs. the histopathological status of the site as given by the histopathologist. For the sake of the readability of Fig. 9.37, the histopathological status has been coded with a number. These numbers are given in Table 9.6.

The histopathological status codes have been separated in three arbitrary groups. Blood and healthy tissue are assigned green color in Table 9.6 and Fig. 9.37 because they represent non-malignant sites. Although we observed blood in several spots, it has only been included here as an example (it can usually be distinguished from suspicious spots under white-light illumination). Chronic inflammation and metaplasias have been assigned blue color. This intends to group together the tissue changes that are not malignant. The red color has been attributed to the dysplasias and cancers. This grouping could be justified in a system of optical biopsy. It will probably be difficult to design a system that can distinguish a moderate dysplasia from a severe dysplasia. It is imaginable, however, to distinguish the lesions in broader categories.

Figure 9.37 summarizes the quantification of the autofluorescence changes observed during our preliminary study. Each point is given with its standard deviation. This is due to the fact that the color contribution of the green and red components are not fully homogenous. They are fairly stable, however, as can be seen in the small error bars. Assuming that these points represent a normal distribution, a curve can be drawn to express it. This has been done and is represented in Fig. 9.37 as three projected color curves on the right side of the graph. For the sake of clarity, the mean values of the three point groups are given with the 67% confidence interval. It can be seen that the three points are actually separated. This should not be interpreted as if this separation were unequivocal and final. As can be seen on the curves, the overlap of the healthy group (green curve) and the metaplastic group (blue curve) is non-negligible and so is also the overlap of the metaplastic group (blue curve) and the cancer group (red curve). This is the reason why some sites appear as false-positive results in Table 9.4 and on the screen during the investigations. The aim of such a quantification, however, is to fix a threshold at an objective value to distinguish early cancers from non-malignant changes. As the curves overlap, it is likely that there will always be some wrong results. This threshold can, in the light of our results, be estimated. It should lie within the gap between the two horizontal plain lines (at y-axis value of 0.82 and 0.71, respectively). This gap is indeed delimited by the maximal extent of the 95% confidence interval of the healthy and the malignant tissue's green/red ratio. As expected, the distribution curves of the healthy and of the malignant tissues overlap in this gap, at y-axis value

one single operator conducting the whole study since their criteria will be refined as they gain experience with the system. Another option would be to find a way to quantify the positivity of the autofluorescence sites and to define a threshold of positivity. Indeed, some sites appear reddish and some other sites appear more orange-looking and this might be correlated to the actual status of the tissue.

Threshold approach

We quantified the green and the red contribution in the images taken with our system and thus generated a graph correlating the histopathological status of the tissue with the green/red ratio of the lesions and healthy tissue for the small number of patients that we investigated. The result is given in Fig. 9.37. The points have been calculated in the following way: for each biopsy taken, an autofluorescence image was recorded with our system under broad band violet-light

of 0.75. At this point, the probability that a tissue with a ratio above 0.75 is healthy is 98.89% and the probability that a tissue with a ratio below 0.75 is malignant is 99.22%. Although this calculation has been done on a small number of patients, it is still a promising result as this ratio could be computed automatically by a simple software. Thus, after the setting of a threshold to a given value, it could be imaginable that an 'optical biopsy' producing three-way results such as 'nothing to worry about', 'suspicious' and 'highly suspicious' could be done.

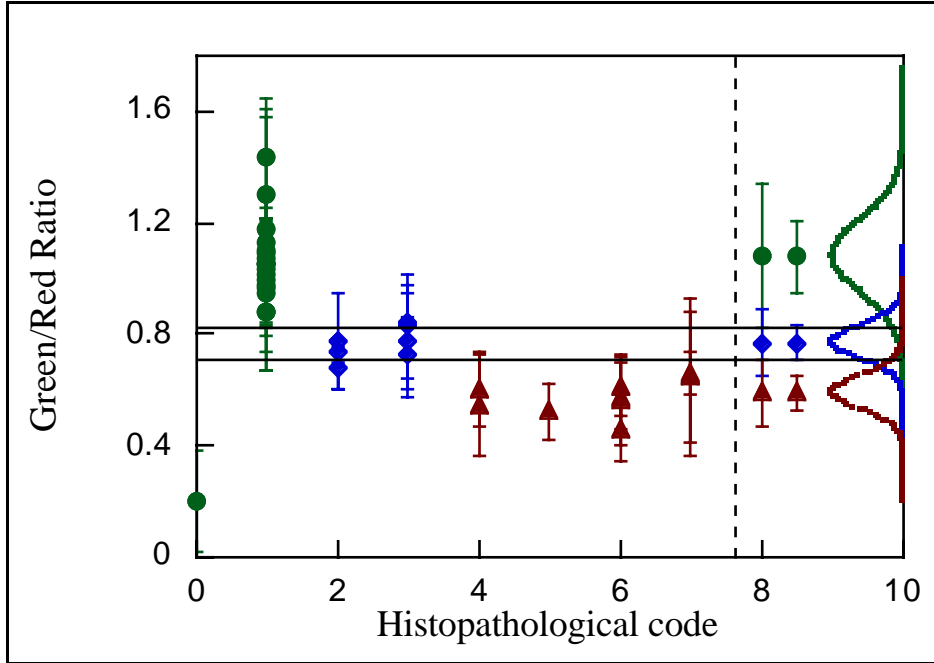


Figure 9.37: Green to Red ratio of healthy (green circles), of metaplastic/inflammatory (blue diamonds) and of malignant (red triangles) tissues as a function of the histopathological status (left of the vertical dotted line). The bars represent the 67% confidence interval. The points at the right of the vertical dotted line represent the mean values and the 95% (at x-axis value of 8) or the 67% (at x-axis value of 8.5) confidence interval. The curves at the right of the vertical dotted line (x-axis values between 9 and 10) are the projected normal distribution curves corresponding to the green/red ratios. The horizontal plain lines represent the maximal extent of the 95% confidence intervals of the healthy and the malignant ratios.

At their intersection, the healthy and metaplastic curves represent 89.3% and 90.5% of the points respectively and, similarly, the metaplastic and cancerous curves represent 86.6% and 86.6% of the points respectively.

It is also interesting to note that the quantification of the green/red ratio leads to a better discrimination of the results as the positivity criterion is now objective. In the case of our results, a threshold set below 0.8 would lead to hardly any false-positive result on healthy tissue and below 0.72, it would lead to hardly any false-positive result at all. It should be reminded, however, that the lowering of the threshold (better specificity) is detrimental to the sensitivity and vice-versa. The above-mentioned positive predictive value of the autofluorescence detection can be recalculated for this set of patients with a threshold set at 0.72 (positive results have a Green/Red ratio < 0.72):

$$\text{Positive Predictive Value: PPV} = \frac{\text{TP}}{\text{TP} + \text{FP}}$$

True positive results: 10

False positive results: 1

Positive predictive value (for autofluorescence): 91%

These PPVs are better than the similar values computed with the subjective criteria (learning curve approach, see above). This means that the setting up of an objective threshold is necessary to take full advantage of the method. Given that the treatment applied to the images is simple and quick, it would only require a frame-grabbing unit and a standard imaging software. Then, it would be possible to compute the green/red ratio of any site in the bronchi and to assign it to a group with a given probability. The setting up of the actual threshold should be done on a greater number of patients, however, as these results are only valid on the small number of sites that have been investigated between September and December 1999.

The green/red ratios that have been computed in Fig. 9.37 can be used to calculate the contrast between the early lesions and the healthy tissues in much the same way as the R ratio that had been calculated in Chapter 8 (Section 8.3). To do so, we divided the individual green/red values for healthy tissues by the corresponding green/red values for cancerous lesions. This is equivalent to the R ratio that had been defined as the ratio of the decrease in green autofluorescence by the decrease in red autofluorescence:

$$\frac{\left(\frac{\text{Green}_{\text{Healthy}}}{\text{Red}_{\text{Healthy}}}\right)}{\left(\frac{\text{Green}_{\text{Tumor}}}{\text{Red}_{\text{Tumor}}}\right)} = \frac{\left(\frac{\text{Green}_{\text{Healthy}}}{\text{Green}_{\text{Tumor}}}\right)}{\left(\frac{\text{Red}_{\text{Healthy}}}{\text{Red}_{\text{Tumor}}}\right)} = R$$

By calculating this ratio for every patient from Fig. 9.37 and taking an average value, it is found that it equals

$$R = 1.78 \pm 1.03$$

This value is of the same order of magnitude as the one calculated from the data given in Section 8.3 ($R = 2.91 \pm 1.69$). This shows that the contrast calculated on spectra in Section 8.3 can actually be transposed to images that have been gathered under similar spectral conditions. A narrowing of the excitation window (thus approaching what is described in Chapter 8), could mean an increased R for the images, but the price for it would also be a decreased power of excitation light. It is not certain that such a trade-off would eventually be a gain for the images.

Discussion

The spectroscopic study that we conducted as a preliminary study provided interesting results (Chapter 8). It demonstrated that autofluorescence could be helpful to characterize and detect early cancerous lesions in the bronchi. However, this study also demonstrated that the variability of lesions' autofluorescence is greater than that of healthy tissue. It also demonstrated that some non-malignant tissues might have a smaller autofluorescence than healthy tissue while retaining the same spectral shape. These reasons are also applicable to imaging systems. Moreover, whereas autofluorescence is intense enough to be recorded with a good SNR for point measurement applications, its faintness might be such that imaging applications become very difficult. In fact, as far as images' quality goes, the major drawback of the Xillix, the Pentax or the Storz systems are their use of image intensifiers (Xillix, Pentax) or of integration times longer than one frame (Storz). These two reasons are closely related to the faintness of autofluorescence signals. The criticism also applies to our system, although to a more limited extent, maybe because we rely on a very sensitive B/W CCD camera and not on a color camera. The images delivered by rigid bronchoscopes are bright enough to be used by the clinician to navigate in the bronchi. Most of the time, it is also the case with flexible bronchoscopes. Some patients, however, have a less intense autofluorescence than other ones. This reflects an observation that we already reported during the spectroscopic study – that the autofluorescence level can vary

from up to one order of magnitude between patients. As expected, this is also observed in imaging applications.

An interesting result of the spectroscopic study was that the spectral shape of the healthy spectra was very reproducible from one patient to another. For our imaging application, this means that the relative intensity of the green component and the red component of the autofluorescence images should vary little from one patient to another. In our system, the gain of the red channel and that of the green channel are separated, thus allowing their individual tuning. During this preliminary study, the color balance of the autofluorescence image has been checked on the carina of every patient and adjusted accordingly. As expected, the inter-patient adjustments of the red and green channel were small but not negligible ($\pm 10\%$). It is reasonable to assume that the autofluorescence of patients may change from one individual to another as it is likely that it reflects their metabolism. Different patients with different metabolism should therefore probably have different autofluorescence levels and slightly different spectral shapes. Our daily observations during endoscopies are in agreement with both statements.

Our results are encouraging as they show that the detection of early cancerous lesions in the bronchi by means of the autofluorescence is possible. Although our spectroscopic measurements (Chapter 8) showed that this might be the case, the implementation of an imaging system based on this preliminary study was by no means certain to produce good results as imaging applications suffer from drawbacks or edge-effects that are specific to them. Nevertheless, the Wolf-EPFL system is working and even seems to be compatible with a routine clinical use. This is central as it makes a large-scale clinical study with this system imaginable.

The goals that had been set for the design of this system have been reached. It is a non-intensified, mono-camera computerless system. The results presented in this chapter are the first preliminary clinical results with this new generation device. They confirm the findings of other system based on the same principles [2,3,18] but the hardware is simplified and its manipulation is user-friendlier. Its results appear promising but large-scale clinical studies are now necessary to assess its statistical value on a large number of patients.

The clinical experiments carried out showed that some situations may induce false positive results, as expected. Several reasons may account for this fact. First of all, our preliminary study includes the learning curve of the system. It is likely that some of the spots that were mistakenly assigned a positive autofluorescence result at the beginning of this study might be assigned a negative one by now. This is especially true since we lacked quantitative assignation criteria and hence sometimes the reddest spot in the bronchi was assigned a positive result, even though it might have not been considered positive in another patient. This demonstrates that a threshold is not only useful, it is necessary for maximal efficiency of the method.

It is very likely that some types of non-cancerous tissues will appear positive under the autofluorescence excitation light. This has been described by several authors working with commercial systems [13,14]. We found one false positive on a thick secretion very early in our tests. Distance effects are reported with a single-wavelength range detection system but are unlikely in a dual wavelength range system. Häussinger [16] et al report false positive results on scars with the Storz system. There seems to be a rather general agreement that scars can induce false positive autofluorescence results (also seen with our system). Although this issue is controversial, some authors report that, in some cases, even early tumors might grow by co-opting existing host vessels [20]. If found to be applicable to the tumors that we are investigating, this could mean that, in contrast with the prevailing view that most tumors begin as non-vascularized masses, the blood contents of such early tumors could be higher than that of the surrounding healthy tissue. This might also be the case in fresh scarring tissue, as it might be possible that, from the autofluorescence point of view, early tumors and fresh scars are both seen as proliferative tissues, no matter whether malignant or not.

The issue of false-positive sites (as seen above) is not specific to our system, however. For instance, Ikeda et al [21] report that false positive results have been observed on hyperplastic tissues using the Xillix system. False-positive results are a drawback for a new method. It is

clearly a major question to find out how to minimize or even avoid them. It is especially striking for the secretions. Most of the patients we investigated have very thick secretions due to their ailment and they can be detrimental to the quality of the images and measurements. Bearing that in mind, the operator will be very careful if the positive-appearing site is fuzzy and/or sensitive to the aspiration. Caution will be exercised when aspirating, however, as this might also damage an already fragile mucosa and induce some bruising which will eventually also be worsening the images' quality and the results' reliability. Again, a clear objective threshold to separate the true-positive results from the false-positive ones would be helpful as it would leave some of these artifacts on the side.

The bruising of the mucosa is another issue that can be crucial. As seen above, blood can cover the interesting sites and mask the mucosa. This is unwanted. A carefully designed large-scale clinical study would have to include two bronchoscopies. The first bronchoscopy, under white-light illumination, would assess the state of the mucosa in the bronchi and allow the clinician to decide which sites would be biopsied. The second bronchoscopy, in autofluorescence, would then let the clinician assess which sites were missed under white light and which additional sites should be biopsied. The mere fact that this method requires two bronchoscopies implies that the operator should be very careful not to bruise the mucosa during the first one as it will impair the second one. On the other hand, if the clinician decides to carry out the autofluorescence bronchoscopy first, they risk that they carry over sites that they would have missed otherwise into the second (white-light) bronchoscopy. Finally, no matter whether the first investigation is the white-light or the autofluorescence bronchoscopy, the fact that this would involve two full bronchoscopies in a row makes such a study time-consuming and not necessarily compatible with the priorities of the clinics.

The distance effects are unlikely with our dual wavelength range system. It should be considered, however, that dynamic viewing of the sites sometimes gives information as the far edges of the observation might suffer from slight differences in the size of the B/W images on the CCD for instance. This induces an imperfect overlap at the edges of the observation area and a consequent imbalance of the green and the red contribution to the resulting image. Moreover, it should be reminded that the autofluorescence bronchoscopy is a dynamic examination. If a site appears reddish on a static image (print out of the screen or digitized image taken from a video recording or static observation of a site in the bronchi), it should not be considered positive until one is certain that it remains reddish whenever the distal end of the bronchoscope is slightly shifted to observe the site. This observation also applies to the Storz system [16,17]. As for hyperplastic tissues, further studies are necessary to gain enough experience with the response of our system to them.

A further difficulty might be the taking of biopsies. This is no simple task. A slight displacement of the biopsy forceps with respect to the site that actually appeared positive in autofluorescence is very possible and may go unnoticed. It can have serious consequences on the result of such a preliminary clinical study however, as the early lesions that we are trying to detect are very limited in size. A possible way to overcome this difficulty would be to take the biopsies under violet-light illumination. This might also be difficult, however, as many biopsies have to be taken through a flexible bronchoscope, in sub-optimal illumination and brightness conditions. As for our preliminary study, we took images of the biopsy site after the biopsy to assess the exact location of the taking. In this case, a storing of the memorized early autofluorescence images for future reference could be of help (see Section 9.4)

There is a learning curve for the use of our system. This has been described for other systems (Xillix, Pentax) and is no surprise. Most if not all tumor detection methods have such a curve. This photodetection system is a complement to white-light bronchoscopy and should by no means replace it. The autofluorescence positive-appearing sites are hints to the operator attention should be directed more specifically to those sites and they should be biopsied as a priority. The ability to rapidly switch towards white light is then crucial for their final assessment of the tissue.

These first clinical results are encouraging but development of this system has not been concluded. In particular, the constructive criticism of the operators as well as the further testing of new methods is likely to bring them one more step forward.

One method that we also tested is the retrodiffusion method. Just as in the Storz system, we tried to take images with some part of the autofluorescence light mixed with backscattered light. In the Storz system, some of the blue excitation light is transmitted through the eyepiece's long-pass filter, whereas we tried to inject a very small fraction (0.1%) of additional red light in the violet excitation light. The reason behind our choice of the red part of the spectrum is that it should offset the decrease in red autofluorescence and that it should be minimally absorbed by tissue (unlike the violet light which is strongly absorbed by blood and might therefore prove disappointing). To carry out these tests, we used a y-shaped light-guide. One branch was connected to the standard light source and the other one to a similar light source fitted with red filters instead of a violet filter. The mixture was then normally fed into the bronchoscopes. Our findings have been disappointing. Although it seems that the contrast is actually enhanced by the addition of red light into the excitation light (the images look sharper), it also generates a large number of red patches on unsuspecting areas. The structure of the bronchi appears bright red and so do the scars or blood traces. Further studies will be necessary to determine the real contribution of additional red light to the detection of early lesions. The first part of such studies will have to involve some kind of tuning of the quantity of red light. One thing can be said at the present time, however. The additional red light so far did not bring any improvement in the detected images. It rather impaired the detection by making a lot of unsuspecting spots appear bright red, while spoiling some of the discrimination power between different shades of red.

It is fairly difficult to assess the number of false negative results of an autofluorescence photodetection method for bronchial carcinoma. To do so, one would have to take random biopsies in the whole tracheo-bronchial tree on negative appearing sites and, maybe, find a positive site. This would be difficult, time-consuming and not very efficient. On the other hand, it is possible to determine the number of false-positive of the conventional white-light bronchoscopy with respect to the autofluorescence photodetection method. This also gives the measure of the contribution of the autofluorescence method. In the case of our preliminary study, it is striking to see that four sites out of eleven (36%) have been seen by the autofluorescence method only. It is clear that this figure has to be considered with caution as the overall number of lesions is small. It shows however that the autofluorescence detection method can bring something to the clinician as it attracts their attention onto lesions that they might have overlooked otherwise. The interesting feature of the two spots that have been detected by the autofluorescence only is their histopathological status – both are dysplasias. It is a very promising observation as the whole spectroscopic study presented in Chapter 8 was designed to investigate the characteristics of such lesions. In this sense, it appears that the basic spectroscopy that has been carried out might have brought some significant improvement to the method.

Conclusion

These early clinical results are very encouraging and show good consistency with their spectroscopic counterparts. Despite its currently sub-optimal performances, it is clear that the autofluorescence detection contributes to the localization of early cancerous lesions that would otherwise be missed by the endoscopist, as can be seen in the increase in positive predictive value. In our short preliminary study, 4 lesions have been detected by autofluorescence only. This is a good sign as further improvements are possible on our system. These modifications should however be conducted with a concomitant large-scale clinical study to assess its real clinical contribution. The main improvement could be the implementation of a real-time quantification method of the green/red ratio. This is currently done afterwards using video recordings of the endoscopies. The improvement generated by this treatment method is impressive however (from 55% to 91% of positive predictive value).

These results also demonstrate that basic science can be of much help to improve applied systems. The optimization study presented in Chapter 8 and the subsequent clinical study show an interesting case of direct contribution of basic science to the clinical world. It is likely that

other sub-optimal systems aimed at a clinical use would greatly benefit from similar optimization studies.

9.4 Future prospects

The development of a functional commercial prototype for the autofluorescence photodetection of early cancers is an achievement in itself. Still, further improvements are necessary to make the detection of these lesions a better, less expensive and more widely accepted method. The paths to this goal are multiple.

Instrumental improvements include the user friendliness of the system. In this respect, our system brings the method further than the Xillix or the Pentax systems and it is second only to the Storz system. It is conceivable to make it lighter and a bit more ergonomic to facilitate its acceptance. These are details, however, because the principle that lies behind our results, namely the major changes in autofluorescence of the early cancerous tissues seems to be now agreed-upon.

The use of backscattered red light might be a good approach to enhance the already existing contrast but it needs to be refined and thoroughly studied before its use can bring more to the operator than autofluorescence alone. At the present time, it does not bring anything but this is not a final configuration. A possible improvement will be to use less red light than with the present system (0.1% of the violet). However, the choice of backscattered red light appears to be a sensible choice as it should not interfere with other mechanisms. In fact, the aim of the backscattered light is to generate a constant background image. It should therefore be created with a wavelength that will interact very little with the observed sites. In this respect, the choice by Storz to use backscattered blue light might prove a bit disappointing as blue light will be absorbed by the blood. It will consequently appear dark and possibly be confused with autofluorescence-positive lesions. More refinements may be devised, such as electronic treatment of the signal to enhance the contrast with or without use of threshold functions to trigger the treatment. This is, however, a subject for many more clinical tests.

Improvements in the method might be provided by a deeper understanding of the mechanisms underlying autofluorescence. We observed, for instance, that the fluorescence brightness could vary from one patient to another. As it is suspected that this property is linked to the metabolism of the patients, it cannot be excluded that the absorption of appropriate substances might enhance the already existing autofluorescence brightness. Whether it will also enhance the contrast, enhance both components or decrease the contrast is a matter of debate and the subject of further clinical tests, as well as the search for the appropriate substance.

A very promising way of detecting early cancers is to rely on the induction of protoporphyrin IX by ALA or a derivative. Although the few experiments to use this method in the bronchi have proven disappointing so far, the spectroscopy of PPIX makes it detectable by our system. It actually has been tested in the frame of the GI tract in Lausanne as a complement to white-light endoscopy to detect early malignancies of the esophagus in patients suffering from Barrett's esophagus. In such a case, it means that the main limit for the use of this method in the detection of early malignancies in the bronchi is the homogeneous topical application of ALA. Again, the exploration of this path might lead to further improvements in the detection of early cancers of the bronchi.

An interesting improvement would be achieved with the combination of both the autofluorescence spectroscopy and the autofluorescence imaging. It is possible to imagine investigating the tracheo-bronchial tree with an imaging system and to use a spectroscopic probe to measure the autofluorescence spectrum whenever a suspicious site is found. It would then combine both methods and probably, through a carefully chosen algorithm, allow the clinician to have a quantitative measurement of the suspiciousness of a site. Such a system could display the autofluorescence spectrum in real time and automatically compare it with previously recorded typical spectra. The deviation from the shape of the typical spectra could be quantified to express the caution to be applied to this site. This would come close to the 'optical biopsy' concept.

These possible improvements in our cancer detection system clearly show that our achievement of designing a functional device of autofluorescence imaging might well be a starting point rather than an achieved goal...

References

1. Wagnières, G., W. Star, B. Wilson, 'In vivo fluorescence spectroscopy and imaging for oncological applications', *Photochemistry and Photobiology*, 68(5), 603-632, 1998.
2. Lam, S., C. MacAulay, J. Hung, J. LeRiche, A. Profio, B. Palcic, 'Detection of dysplasia and carcinoma in situ with a lung imaging fluorescence endoscope device', *The Journal of Thoracic and Cardiovascular Surgery*, 105(6), 1035-1040, June 1993.
3. <http://www.xillix.com/life/lifelung.html>
4. Lam, S., C. MacAulay, B. Palcic, 'Detection and localization of early lung cancer by imaging techniques', *Chest*, 103, 12S-14S, 1993.
5. Lam, S., T. Kennedy, M. Unger, Y. Miller, D. Gelmont, V. Rusch, B. Gipe, D. Howard, J. LeRiche, A. Coldman, A. Gazdar, 'Localization of bronchial intraepithelial neoplastic lesions by fluorescence bronchoscopy', *Chest*, 113, 3, 696-702, March 1998.
6. Kulapaditharom, B., V. Boonkitticharoen, 'Laser-induced fluorescence imaging in localization of head and neck cancers', *Annals of Otolaryngology, Rhinology and Laryngology*, 107, 241-246, 1998.
7. Khanavkar, B., F. Gnudi, A. Muti, W. Marek, K.-M. Müller, Z. Atay, T. Topalidis, J. Nakhosteen, 'Grundlagen der LIFE[®]-Autofluoreszenzbronchoskopie', *Pneumologie*, 52, 71-76, 1998.
8. Takehana, S., M. Kaneko, H. Mizuno, 'Endoscopic diagnostic system using autofluorescence', *Diagnostic and Therapeutic Endoscopy*, 5, 59-63, 1999.
9. Kurie, J., J. Lee, R. Morice, G. Walsh, F. Khuri, A. Broxson, J. Ro, W. Franklin, R. Yu, W. Hong, 'Autofluorescence bronchoscopy in the detection of squamous metaplasia and dysplasia in current and former smokers', *Journal of the National Cancer Institute*, 90(13), July 1, 1998.
10. Venmans, B., T. van Boxem, E. Smit, P. Postmus, T. Sutedja, 'Results of two years experience with fluorescence bronchoscopy in detection of preinvasive bronchial neoplasia', *Diagnostic and Therapeutic Endoscopy*, 5, 77-84, 1999.
11. Pentax SAFE-1000, Technical Data, Description leaflet.
12. Adachi, R., T. Utsui, K. Furusawa, 'Development of the autofluorescence endoscope imaging system', *Diagnostic and Therapeutic Endoscopy*, 5, 65-70, 1999.
13. Horvath, T., M. Horvathova, F. Salajka, B. Habanec, L. Foretova, J. Kana, H. Koukalova, P. Pafko, F. Wurst, E. Novotna, J. Pecina, V. Vagunda, R. Vrbacky, R. Talac, H. Coupkova, Z. Pacovsky, 'Detection of bronchial neoplasia in uranium miners by autofluorescence endoscopy (SAFE-1000)', *Diagnostic and Therapeutic Endoscopy*, 5, 91-98, 1999.
14. Kakihana, M., K. K. II, T. Okunaka, K. Furukawa, T. Hirano, C. Konaka, H. Kato, Y. Ebihara, 'Early detection of bronchial lesions using system of autofluorescence endoscopy (SAFE) 1000', *Diagnostic and Therapeutic Endoscopy*, 5, 99-104, 1999.
15. Leonhard, M., 'New incoherent autofluorescence/fluorescence system for early detection of lung cancer', *Diagnostic and Therapeutic Endoscopy*, 5, 71-75, 1999.
16. Häussinger, K., F. Stanzel, R.M. Huber, J. Pichler, H. Stepp, 'Autofluorescence detection of bronchial tumors with the D-Light/AF', *Diagnostic and Therapeutic Endoscopy*, 5, 105-112, 1999.
17. Häussinger, K., J. Pichler, F. Stanzel, A. Markus, H. Stepp, A. Morresi-Hauff, R. Baumgartner, 'Interventional bronchoscopy beyond the year 2000: autofluorescence', *Respiratory Bronchology*, in press, 1999.

18. Wagnières, G., A. Studzinski, D. Braichotte, P. Monnier, C. Depeursinge, A. Châtelain and H. van den Bergh, 'Clinical imaging fluorescence apparatus for the endoscopic photodetection of early cancers by use of Photofrin II', *Applied Optics*, 36(22), 5608-5620, 1997.

19. Dr Pierre Grosjean, CHUV, personal communication

20. Holash, J., P. Maisonpierre, D. Compton, P. Boland, C. Alexander, D. Zagzag, G. Yancopoulos, S. Wiegand, 'Vessel cooption, regression and growth in tumors mediated by angiopoietins and VEGF', *Science*, 284, 1994-1998, June 18th 1999.

21. Ikeda, N., H. Honda, T. Katsumi, T. Okunaka, K. Furukawa, T. Tsuchida, K. Tanaka, T. Onoda, T. Hirano, M. Saito, N. Kawate, C. Konaka, H. Kato and Y. Ebihara, 'Early detection of bronchial lesions using lung imaging fluorescence endoscope', *Diagnostic and therapeutic endoscopy*, 5, 85-90, 1999.

希
望

Hope

Conclusion

The time has now come to draw a conclusion from this report. Although the readers will have done so for themselves, it is a useful exercise to put in words one's own feelings towards such a work.

The central theme of this work, cancer, is more than just another disease. It is associated with terrible stories of wasting and suffering for patients and their loved ones. It is not unusual that these sufferings are also due to the treatment of the disease. Moreover, the invasive nature of the disease probably makes it impossible for those who have suffered from a cancer once to ever be fully sure that it is indeed eradicated. This no doubt bears quite heavily on the mind of the patients. In this regard, any progress, no matter whether a small step or a giant leap, towards an improved detection or improved management of cancer is a success in itself. This surely makes a Ph.D. thesis in this field a very rewarding time.

As a scientific project, such a work is certainly a model of what science should become to evolve: multidisciplinary. Most neighboring fields are merging into new larger fields, most once clear-cut borders between specialties are becoming fuzzy and little defined. This is encouraging as it drives people from once-separated domains to close collaborations, certainly to everyone's benefit. The potential for learning new things in such an environment is huge, making again a Ph.D. thesis in this field a very rewarding time.

Unlike many other fields, the photodetection and the photodynamic therapy of early cancers are applied topics. Despite this fact, most of the research presented here is basic in its nature. Certainly, this is not basic science in the sense where theoretical particle physics is basic, but it is basic in its application of methods like fluorescence spectroscopy and the study of tissues down

to its properties as a mix of fluorophores. This shows that the improvement of applied science need some basic studies. This also shows how the addressing of basic questions can be implemented into 'real-world' answers.

Dealing with patients suffering from cancer, involvement in a clinical environment (whose priorities are very different from those of the research laboratories) and the interaction with other people to apply knowledge to the management of 'real world' problems were by no means the least interesting parts of the job. In this respect, the greatest satisfaction is clearly the successful eradication of a lesion which may mean extended survival or improved life quality for the patient. In this respect too, the successful identification of an early lesion is also highly significant as it means increased hope for the patient. This is invaluable. Hence, every effort should be made, both in terms of time and financing, for this increased hope or extended survival. Clearly, it is a public health priority and it clearly requires much patience and much financial effort from society.

In a period of economic crisis, in a period of increasing cost of public health and in a period of an ageing population, with an increasing number of patients for a decreasing number of active people, this issue raises at least two questions. Considering that many diseases, from cardiovascular diseases to many non-cancerous lung affections and, in our specific case, from lung cancers to bladder cancers (and certainly more) are linked to the consumption of tobacco products, the issue of screening has first to be raised.

One can divide the whole population into four risk groups for developing lung cancer: a very small percentage of people who already have an invasive lung lesion and are hence at very high risk (> 80 %) of developing a recurrence of the same cancer or another one. A larger percentage of people who have had a lung lesion that has been successfully managed in the past and who therefore have a moderate risk of developing a recurrence or another one (> 20 %). A very large percentage of the population who are heavy smokers or are exposed to some other known lung carcinogen who have a moderate risk of developing lung cancer (around 10 %). And the rest of the population who are a much larger group of people and have a very small probability of ever suffering from lung cancer (< 0.01 %). It is therefore questionable as a public health issue to invest much effort (both human and financial) into the detection of very early lesions in the lungs of a small number of people who are at high risk. Indeed, most studies tend to show that systematic screening techniques do not significantly improve cancer survival rates because relevant lesions are few and expensive to detect. Moreover, the gain in time with most current methods such as radiology or sputum cytology is not significant when one considers the natural history of the disease, thus making these detections 'a little less late' rather than 'early'. This is also true for the screening of moderate- to high-risk populations (i.e. smokers). In the light of these observations, it is meaningful to wonder whether such an effort could be put with more benefit to society in general into the development of detection or treatment methods for other diseases. This would also corroborate the view of that wise clinician who once stated that the best screening test for lung cancer is to ask the simple question "*Do you smoke?*".

Finally, considering also that the ailments that are linked to the consumption of tobacco products are therefore avoidable, would it not be fruitful to invest at least a fraction of these efforts into the prevention and the decrease of the smoking habit? This would be one way to fight some cancers much earlier as it would cut the cause and not treat the consequences. This would obviously require effective smoking cessation techniques (to be found) and huge educational efforts (whose efficiency remains to be proven). Nevertheless, as far as fighting lung or bladder cancer goes, such an achievement would probably be situated closer to a giant leap than to a small step. But this is a subject for some other Ph.D. theses.

Acknowledgments

Biomedical optics is a multidisciplinary domain. Many people have therefore contributed to this work, be it directly or indirectly. I would like to thank them all. I also would like to apologize to those whose name does not appear below, my memory is no longer what it used to be.

I am very grateful to Georges Wagnières and to Prof. Hubert van den Bergh for having accepted me as a Ph.D. student in their laboratory. I appreciated their interest for my work as well as their availability for constructive discussion. Their advice was always useful and sensible and I liked their sincere search for the best solution no matter what the problem was. After four years in their lab, however, I must admit that they maybe also are responsible for these memory problems I mentioned ;-).

The people I worked with in the LPAS have often been of invaluable help. I would like to extend special thanks to Martin Forrer who took care of me when I started and taught me the smallest details about the spectrofluorometer, to Norbert Lange who had an equally competent answer to every question from math to jazz, to Didier Goujon who never let go of a problem until he found a solution and to Jean-Pierre Ballini whose positive approach to science and to other people made it great to work with him. Christophe Hadjur, Ramiro Conde and Claude-André Porret also deserve my gratitude for the good atmosphere they contributed to perpetuate in the LPAS – it made working here a pleasant time.

My fellow Ph.D. students need my attention here. Thomas Glanzmann always answered my questions with patience, Nora Dögnitz, Thomas Stepinac and Vijay Sathya shared with me their culinary talents as well as quite a few drinks and ski days – thank you for these moments. I would also like to thank Jérôme Mizeret and Karim Mosbah for the good times we spent together. My diploma student, trainee and finally fellow Ph.D. student Pascal Uehlinger should be thanked here for the excellent work he did and for his everlasting good mood and positive motivation, even when underway for unpleasant activities. Tanja Gabrecht is an indefatigable writer and biscuit baker, she made the lab a friendlier place late at night and around the coffee machine. Véronique Bauler spills some smile onto the whole lab. May she be thanked for that. This whole work would not have been possible without the commitment of Flavio Comino, André Studzinski and Nicolas Chauvin.

Alain Woodtli deserves special thanks for his patience. His knowledge and kindness made it easier for me to slip back into the world of science when I started. I would also like to thank Roland Bays for his bottomless address book and for his sense of humor. Thank you also to Laurent Mosimann and Martin Brunner for the nice chats we shared.

The people at the CHUV have had much patience with our strange systems with sub-optimal performances. I would like to acknowledge here the competent and conscientious work of Pierre Grosjean, with whom I did most of the autofluorescence measurements. Many thanks also to Alexandre Radu, who displayed the same motivation for hamster studies, autofluorescence spectroscopy and autofluorescence imaging. My deepest gratitude goes to Prof. Philippe Monnier, head of the ENT clinics. The privileged access to the endoscopy rooms that he secured for us is certainly a major strength of this group. Thank you also to the ENT clinics resident physicians for always welcoming us.

The same gratitude applies to the people of the urology department, namely Alexandre Marti, Karim Kellou, Patrice Jichlinski and Prof. Hans-Jürg Leisinger. Thank you for the good work we did together. A special thanks to Karim and Alexandre for the moments we spent talking or snowboarding together.

Some people at the CHUV, who were not directly involved in the project, yet had their daily work disturbed by our experiments deserve special consideration. This is especially true because they never stopped smiling and being patient. Thank you Petra de Jonge, Philippe Garmond,

Sylvie Perret, Christine Dardel, Jorge Dias, Doriana Riva, Maïtena Ilharreguy, Madeleine Chollet, Domenico Panno, Jean-Marc Guglielmetti, Brigitte Théry, Eléonore Kischka, Marzia Gasser - I am sure I could extend the list with many more people.

The people working in the laboratory of Lucienne Juillerat should be thanked here for their significant contribution to the advances in my understanding of cell culture. I appreciated the patience of the people I met there and their friendly helpfulness. I also very much appreciated their flexibility, their positive attitude and their tolerance when it came to work together in a peaceful atmosphere. A special mention to Lucienne Juillerat for her genuine commitment to the advancement of the project, to Lucia Peduto for her sense of humor and dedicated work and to Judit Miklossy and Phillip Shaw for their kindness.

Although they did not contribute directly to this work, two of my teachers deserve my gratitude for what they taught me. Reinhard Neier and Max Jendly definitely contributed to the completion of my Ph.D. thesis.

I would like to thank my friends and family for their care and support. I would not have made it without you all. A special thought for Julia and Jade – may happiness and harmony enlighten both your lives.

Finally, I would like to thank Elena for having been my companion during these past four years.

APPENDIXES

A1.
***The optical fiber
based-spectrofluorometer***

During the course of a post-doctoral work in our laboratory, Dr. Martin Forrer built an optical fiber-based spectrofluorometer. This device has been the central tool for our work. Its main advantages are its sensitivity that allows us to detect very faint signals like the autofluorescence of biological tissues *in vivo* with a reasonable SNR, its versatility that is of utmost importance to measure signals at several excitation wavelengths within a short time frame and its 'home-made-ness' that lets us modify the setup for the conditions of each measurement. As the exact setup is described in each chapter, we propose here a general overview of this device only: the light is delivered by a high-pressure Xenon lamp and diverted into a spectrograph. This spectrograph is intended to allow the selection of the excitation wavelength. The light is then filtered and injected into an optical fiber. The filter is mounted on a wheel that holds 8 filters. This wheel is steered by a stepper motor and under the control of a computer. This setup allows the operator to change the excitation filter within seconds. The resolution of the excitation pathway is 20 nm (nominal excitation wavelength ± 10 nm, FWHM). The fluorescence light is then collected by the same fiber (or a separate fiber for the *in vivo* autofluorescence measurements, in which case it is directly injected into the detection spectrograph) and separated from the backscattered excitation light by a second filter (also held by a stepper motor-driven computer-controlled wheel). It is then filtered one more time and dispersed in a second spectrograph. Again, thanks to a similar wheel, the filter can be changed easily within seconds. A Peltier-cooled CCD finally detects the light. In our usual setup, the resolution of the detection is 15 nm but it can be taken down to below 2 nm. It has been measured that its sensitivity is around 1 pW per pixel at 500 nm for a SNR of 200. The whole setup is mounted on a trolley to allow its easy (it weighs around 200 kg) transportation wherever needed. The block diagram of our setup is presented in Fig. A1.1.

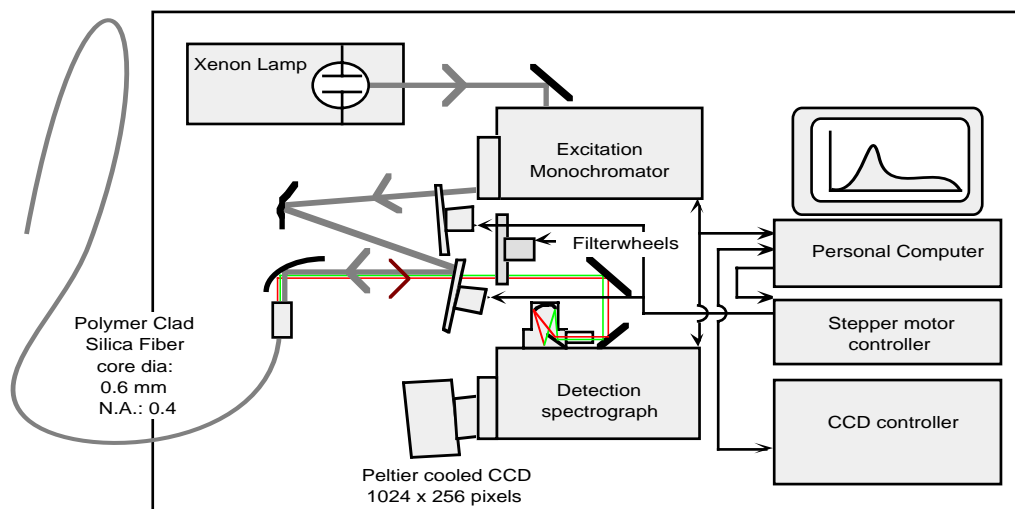


Figure A1.1: Block diagram of our optical fiber-based spectrofluorometer in its monofiber configuration.

A2.
***Some additional
exogenous fluorophores***

There are countless substances that are potential photodetection agents or PSs. In Chapter 5, we presented the Sytox[®] Green. Some work has been done with additional fluorophores and it is summarized here. All the molecules we tested are listed in Table A2.1. As will be seen, some of them are metachromatic (Sytox[®] Green, RuDPP, Di-4-ANEPPS, CFDA, Glycosylated Fluorescein) and some are not (EtNBS, 2I-EtNBS).

We took advantage of the availability of the hamster cheek pouch model to test some interesting potential photodetection substances. For the sake of brevity, we deliberately chose to focus here on two of them, EtNBS, 2I-EtNBS. The other substances proved disappointing during the preliminary tests. Consequently, no further tests were carried out. The administration of the substances (solvent, concentration) was adjusted in healthy untreated animals first. Then, a basic pharmacokinetics curve was measured on their cheek pouch by LIF. The same pharmacokinetics curve was measured on the cheek pouches of treated hamsters to determine the maximal intensity of fluorescence of both the healthy and the treated cheek pouch and hence the maximal contrast as a function of the elapsed time.

Name	Type	Exc. Max. [nm]	Em. Max. [nm]	Comments
EtNBS	tumor localizer [2]	600	700+	3 healthy hamsters, 2 x 2 mg/kg, 1 x 5 mg/kg, follow-up: 7 hours. Signal down to undetectable levels on the cheek pouch mucosa and on ventral skin 7 hours after the injection. 3 painted hamsters, 3 x 2.5 mg/kg, follow-up: 2 days. see details below - September 1998 4 painted hamsters, 2 x 0.5 mg/kg, 2 x 0.25 mg/kg, follow-up: 30 hours. no reproducible selectivity was found - February 1999
2I-EtNBS	tumor localizer [2]	600	700+	4 healthy hamsters, 2 x 2 mg/kg, 2 x 10 mg/kg, follow-up: 7 hours. Signal down to undetectable levels on the cheek pouch mucosa and on ventral skin 7 hours after the injection. 3 painted hamsters, 3 x 2.5 mg/kg, follow-up: 2 days. see details below - September 1998 9 painted hamsters, 9 x 2.5 mg/kg, follow-up: 24 hours. see details below - October 1998 4 painted hamsters, 2 x 1 mg/kg, 2 x 0.5 mg/kg, follow-up: 30 hours. no reproducible selectivity was found - February 1999

Sytox [®] Green	nucleic acid marker, Molecular Probes (MP), S-7020, [3]	470	525	2 painted hamsters, 2 x 0.3 mg/kg, follow-up: 3 hours. No pharmacokinetics could be measured. Point measurements were recorded. 7 painted hamsters, 7 x 0.3 mg/kg. Images were recorded. 1000-fold fluorescence enhancement upon nucleic acid binding.
Ruthenium-(4,7-diphenyl-1,10-phenanthroline), RuDPP	oxygen sensor (quenched by oxygen)	450	600+	4 painted hamsters, 4 x 1.5 mg/kg, follow-up: 11 days. No signal was detected following the injection. This lipophilic drug might have precipitated in the vascular system or might have been trapped in the liver or in some other organ.
sulfonated Ruthenium-(4,7-diphenyl-1,10-phenanthroline), RuDPP	oxygen sensor (quenched by oxygen) [4]	450	600+	3 painted hamsters, 3 x 6 mg/kg, follow-up: 7 days. 3 painted hamsters, 3 x 1.5 mg/kg, follow-up: 1 day. No useful contrast was found. Fluorescence lifetime measurements showed a shorter lifetime in invasive tumors than in healthy tissue [5,6].
Carboxy-fluorescein Diacetate, CFDA	pH marker MP, C-195 [3]	465	520	2 painted hamsters, 2 x 5 mg/kg, follow-up: 3 hours. No useful contrast was found. pH sensitive fluorescence intensity.
Glycosylated Fluorescein	Metabolism of the sugars Sigma, F-4396	495	520	5 painted hamsters, 3 x 1 mg/kg, 2 x 0.5 mg/kg, follow-up: 24 hours. No useful contrast was found.
Di-4-ANEPPS (ANEP: amino naphthylethenyl pyridinium)	membrane potential marker MP, D-1199, [3]	475	620	3 painted hamsters, 3 x 0.4 mg/kg. No pharmacokinetics could be measured. Point measurements and images were recorded. 10% change of fluorescence intensity per 100 mV change of membrane potential.

Table A2.1: List of the substances that were tested as possible novel metachromatic and non-metachromatic photodetection agents, along with their spectroscopic properties.

The protocol of regular painting of the hamster cheek pouch with a carcinogenic agent is described in section 4.3, Materials and Methods as well as in a paper by Andrejevic et al. [7]. The healthy untreated animals were kept following the same rules as the painted animals.

A2.1 EtNBS and 2I-EtNBS: the fluorophores

The PSs 5-ethylamino-9-diethylaminobenzo[a]phenothiazinium chloride (EtNBS) and 2-iodo-5-ethylamino-9-diethylaminobenzo[a]phenothiazinium chloride (2I-EtNBS) are members of the benzophenothiazine family [8], along with the Nile Blue dyes. Their structure is given in Fig. A2.1.

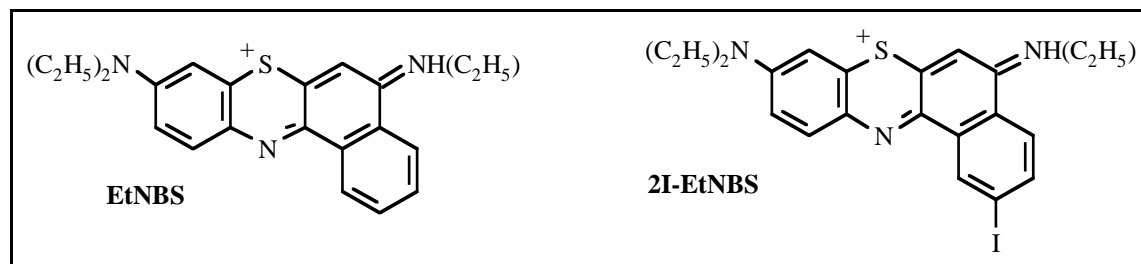


Figure A2.1: EtNBS and 2I-EtNBS (for simplicity, the chloride counter ion associated with each molecule is not shown).

In general, Nile Blue dyes are tumor-localizing but not photoactive molecules [8,9]. However, structural modifications (in this case, the alkylation of the amino-group in C-5 and the substitution of an oxygen by a sulfur atom in the benzophenoxazine's position 7) can increase their singlet oxygen yield [9]. Two such modified molecules are EtNBS and 2I-EtNBS (the iodine atom mainly prevents the formation of aggregates in solution [2]).

The EtNBS and 2I-EtNBS possess a delocalized positive charge, they absorb red light efficiently ($\epsilon = 68'600 @ 652 \text{ nm}$ [10], about 20 times more than Photofrin), are very lipophilic and, probably due to some steric hindrance that leads to a decreased tendency to form insoluble aggregates, are reasonably soluble in aqueous solutions [2,10]. They have a singlet oxygen generation quantum yield of about 2.5% (compared to 0.5% for EtNBA) and, in cell culture, EtNBS appears to be about 100 times more phototoxic than Photofrin [10-12]. Finally, they have a fluorescence quantum yield of 15% in methanol [2,11] and, when excited at appropriate wavelengths, emit fluorescence above 650 nm. Their excitation spectrum is given in Fig. A2.2a (detection wavelength: 700 nm) and emission spectrum in hamster tumor-bearing cheek pouch tissue is given in Fig. A2.2b (excitation wavelength: 600 nm).

The EtNBS is currently under preclinical investigations as tumor diagnostic and therapeutic agents in cell cultures [10,12,13] and, due to its properties as a tumor localizing molecule in vivo (up to 8:1 with respect to muscle), in subcutaneously implanted tumors in mice [12]. In this study, Cincotta et al report a pharmacokinetics curve in three types of tissue, in the skin of the mice, the muscle and the implanted tumor. The tumor vs muscle ratio of dye fluorescence is highest 3 hours after the s.c injection of the dye solution. Moreover, the authors perform PDTs by means of EtNBS sensitization with a good deal of selectivity for the tumor over the surrounding irradiated tissue. The authors also devise that a possible reason underlying this fact is the intracellular localization of the PS [12,14]. This could induce cellular damage to the tissue as opposed to a vascular effect observed with most other PSs, especially porphyrins [11,15]. This is also exemplified by the small fraction of the PS in the plasma of the animal [12] and the authors link this low level to the low levels of vascular damage to the tumor and the surrounding tissue. Twenty-four hours after the injection, no dye is detectable by LIF anymore, neither in the skin, nor in the muscle nor in neoplastic tissue.

In a subsequent study about the combined use of EtNBS with BPDMA [11], Cincotta et al investigate the synergistic effect of the PSs used together in an attempt to take advantage of the direct cellular effect of EtNBS and the mostly vascular effect of BPDMA and the ensuing hypoxia [16]. The authors succeed in eradicating large implanted tumors with PDT and devise a synergistic effect of the two PSs rather than an additive effect but feel that the actual mechanism leading to the destruction of these large tumors need further studies to become completely and clearly understood.

The EtNBS and 2I-EtNBS are therefore interesting molecules for further testing and we carried out some experiments with our hamster cheek pouch model.

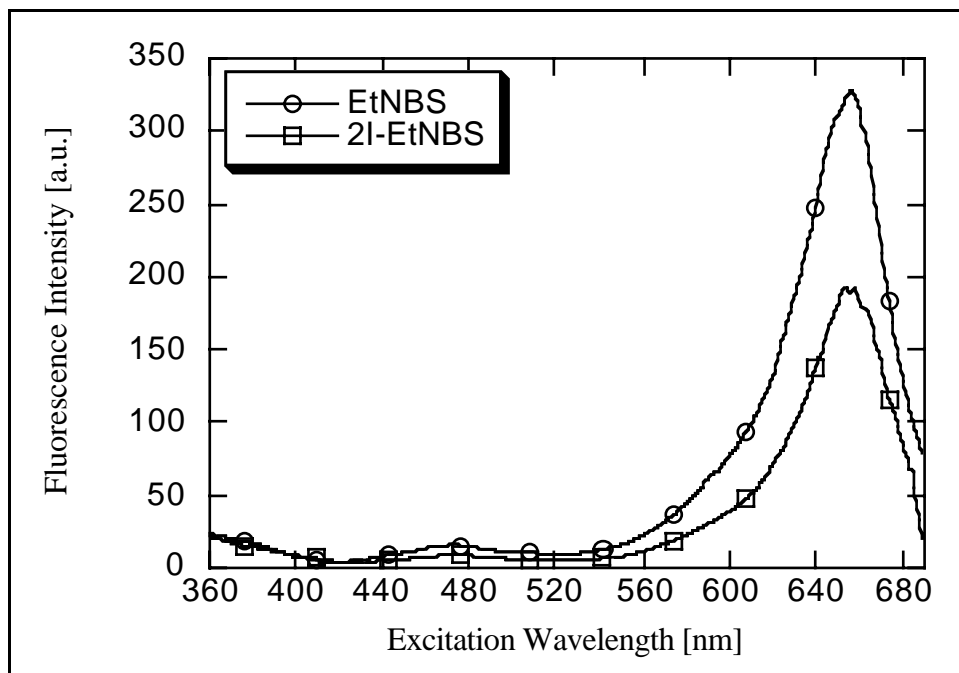


Figure A2.2a: Excitation spectrum of the EtNBS and 2I-EtNBS in the sucrose solution ($c = 2.8 \mu\text{M}$ and $c = 31.9 \mu\text{M}$ respectively), after the protocol described in section 'Preparation and administration'. The detection wavelength is 700 nm.

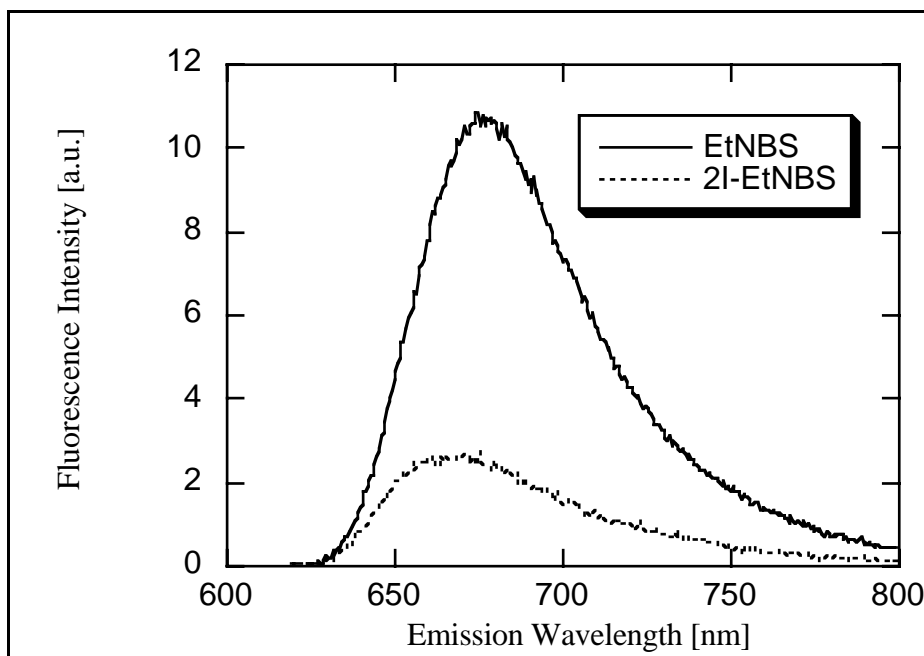


Figure A2.2b: Emission spectrum of the EtNBS and 2I-EtNBS in the hamster tumor-bearing cheek pouch tissue (measured *in vivo* after the protocol described in section 'Preparation and administration'). The excitation wavelength is 600 nm.

A2.2 EtNBS and 2I-EtNBS: the study

Preparation and administration

The dry, dark blue powder of EtNBS and 2I-EtNBS (generously provided by Dr Louis Cincotta, Ergoscience, Charlestown, MA, USA) was dissolved in an isotonic sucrose solution (9.25 % sucrose in sterile distilled water) at a concentration of 1.25 mg/ml. The solution was then filtered through an anti-bacterial filter to ensure its cleanliness.

Each hamster was first anaesthetized. A background spectrum was then measured on both cheek pouches before the injection, along with a reference spectrum acquired on a Nile Blue cuvette (this was intended to correct the actual value later measured on the peak of the dyes for the slight variations of excitation power delivered by the lamp). Then, the hamster received an intracardiac injection of 0.2 ml/100 g of this solution to achieve a dose of 2.5 mg/kg. Tests on healthy hamsters showed that doses above this value were toxic for the animal. Shortly after the injection, we started to measure the pharmacokinetics of the dye by Light-Induced Fluorescence (LIF) in both the untreated cheek pouch (thereafter labeled 'healthy') and the treated cheek pouch ('cancerous').

The measurements were done by spectrofluorometry, using our optical fiber-based spectrofluorometer described in Appendix A1. The excitation wavelength was 600 nm and detection took place above 645 nm (Filters: Short Pass 625 nm; Dichroic 625 nm; Long Pass 645 nm). The spectra were acquired at different time intervals after the injection (4 spectra for each point in time), thus allowing us to calculate a mean value and a standard deviation, both plotted on the graphs. The spectra were normalized before their evaluation by dividing them by a corresponding reference value (acquired just prior to the acquisition of each series of spectra). After this correction, the background curve was subtracted and the value of the fluorescence intensity was calculated at the maximum of the peak (in the 670-675 nm window). This produced the fluorescence values (4 for each point in time) that we used for the graphs.

Twenty-three painted hamsters were involved in this study. During the first part of the study (September 1998), three animals received an injection of EtNBS and three one of 2I-EtNBS. Some of the results are plotted in the form of pharmacokinetics curves in the Figure A2.3. The second part of the study (October 1998) involved 9 more animals. They received an injection of 2I-EtNBS (one of them died on the way, hence there are only 9 complete curves). These results are displayed in the Figure A2.4. A final experiment was carried out with 8 animals to assess the selectivity of the dyes at lower concentrations (February 1999) with disappointing results (no selectivity was found with either dye).

Results and discussion

Figure A2.3 shows some of the results of the first part of the study. Each curve represents the measurements for one animal. The vertical scales of Fig. A2.3a and A2.3b are comparable. This means that the smaller values for 2I-EtNBS reflect the smaller fluorescence signals that we observed. This might be due to the smaller solubility of 2I-EtNBS.

Figure A2.3a shows the pharmacokinetics of the EtNBS in one hamster. Altogether, three hamsters received the same injection at the time of this study. On the second hamster, no selectivity was found at any point in time after the injection. On the third hamster, a selectivity of 2:1 after 30 minutes and 1.5:1 after around 250 minutes was observed, in good agreement with the pharmacokinetics curve given on Fig. A2.3a (data not shown).

Figure A2.3b shows the pharmacokinetics of the 2I-EtNBS in one hamster. Altogether, three hamsters received the same injection at the time of this study. On the second hamster, no selectivity was found at any point in time after the injection. On the third hamster, a selectivity of 3:1 after a time interval of around 200 to 400 minutes was observed, in good agreement with the pharmacokinetics curve given in Fig. A2.3b (data not shown).

In both cases, these results appear promising as there seems to be some selectivity of the dyes for early cancerous lesions in this model. However, since this seems to be more marked in the case

of the 2I-EtNBS, it was decided that the second part of the study would take place with this fluorophore only as a start.

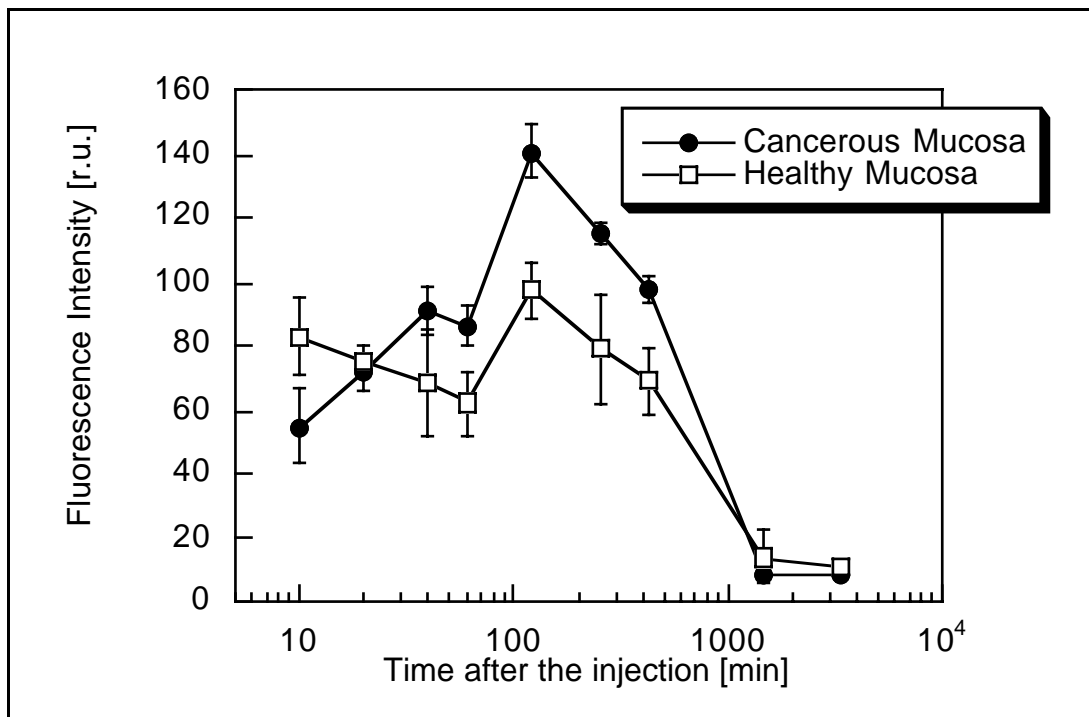


Figure A2.3a: Relative fluorescence signal of EtNBS on the healthy and cancerous cheek pouch of one hamster as a function of the time interval after the injection of 2.5 mg/kg. The excitation wavelength is 600 nm and the detection is above 645 nm.

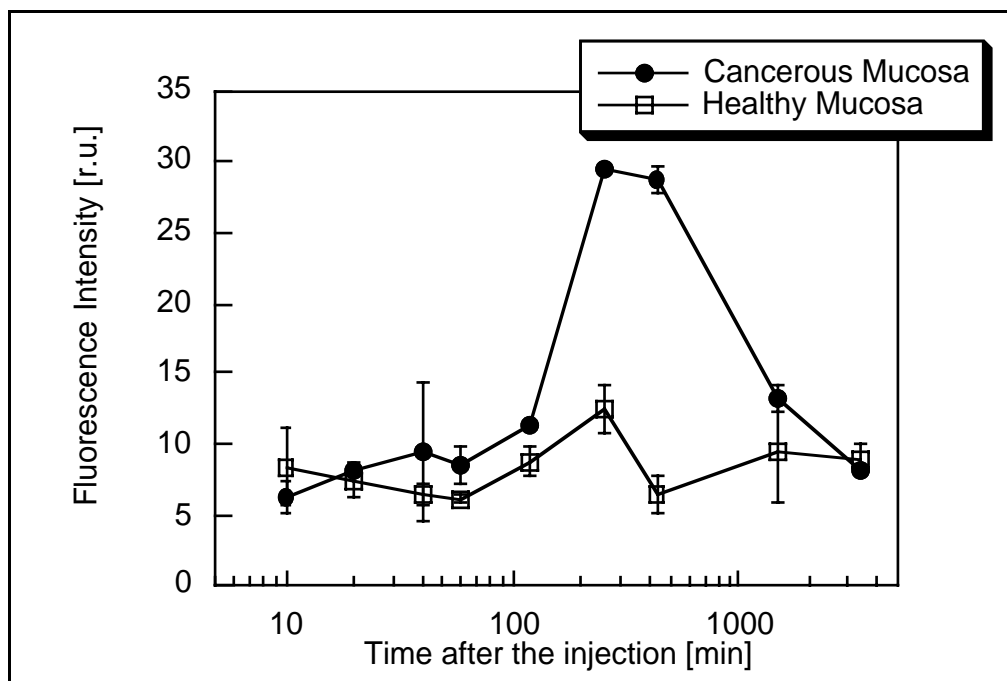


Figure A2.3b: Relative fluorescence signal of 2I-EtNBS on the healthy and cancerous cheek pouch of one hamster as a function of the time interval after the injection of 2.5 mg/kg. The excitation wavelength is 600 nm and the detection is above 645 nm.

Figure A2.4 shows the results of the first and the second part of the study. This curve represents the measurements for all the 13 animals that received 2.5 mg/kg of 2I-EtNBS. The surprising feature of Fig. A2.4 is that there is hardly a trace of the selectivity we observed in the first part of the study.

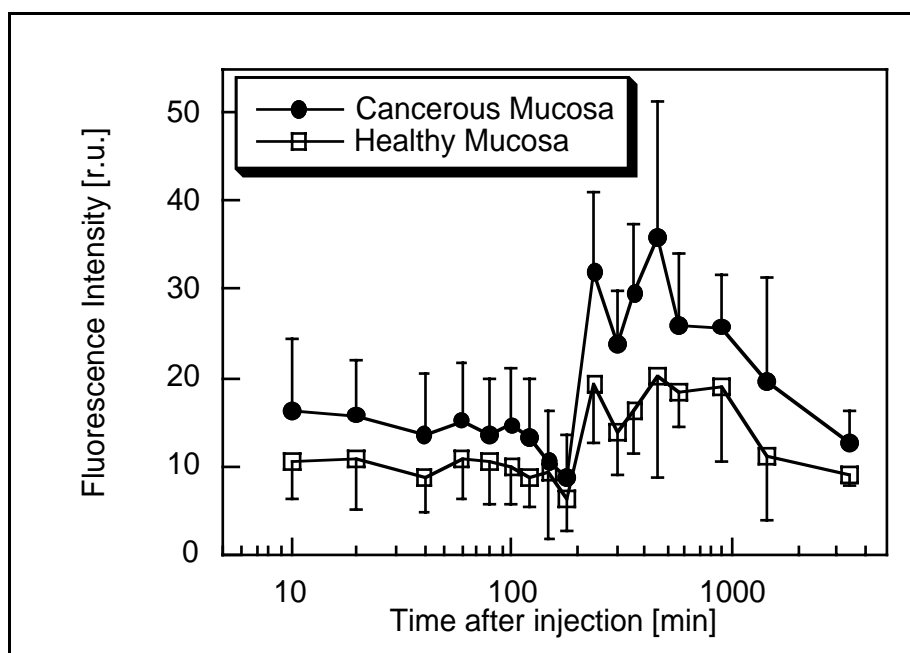


Figure A2.4: Relative fluorescence signal of 2I-EtNBS on the healthy and cancerous cheek pouch of thirteen hamsters as a function of the time interval after the injection of 2.5 mg/kg. The excitation wavelength is 600 nm and the detection is above 645 nm.

It is a rather difficult to gather much relevant information from these results. Some selectivity has definitely been observed in the first part of the study and this looks like it is consistent with other results obtained with these dyes (a 3:1 selectivity has been observed between tumor and healthy tissue in mice after the extraction of the dye [2]). Moreover, this selectivity could be lost at higher drug concentrations. If we use the first fluorescence measurement at 10 min after the 2I-EtNBS injection as an indication of the drug dose that the animals received, we notice that the animals in the second part of the study received 3 times as much as the animals in the first part of the study (although the data are not shown, this is the case on all curves). However, it should be noted that all the animals received the same injection. Hence, it is hard to believe that a factor 3 in the dose received can be observed due to injection problems alone (although due to the intrinsic color of the solution, the injection is indeed a tricky part of the experiments).

This observation might be linked to solubility problems as the 2I-EtNBS seemed to be less soluble than the EtNBS. A more plausible explanation, though, is that the signals that we measured with 2I-EtNBS were very small. This is due to many limitations: the solubility of the dye is limited, as stated above; the volume that one is allowed to safely inject into the heart of a hamster is limited; the intracardiac injection has to be quick. All these reasons might well account for very small and hence noise-sensitive signals.

As a final remark, it should be stated that these fluorophores have shown very promising potential in animals bearing an implanted tumor. However, the extrapolation of such results to animals bearing a very early chemically-induced (hence neither grafted nor implanted) cancerous lesion is difficult. It could be that the interesting selectivity properties of these dyes are lost when dealing with such a lesion.

References

1. Wagnières, G., S. Inuma, K. Schomacker, T. Deutsch, T. Hasan, 'Invivo tissue characterization using environmentally sensitive fluorochromes', in 'Fluorescence Microscopy and Fluorescent Probes', 203-209, Edited by J. Slavík, Plenum Press, New York, 1996.
2. Louis Cincotta, Ergoscience, Charlestown, MA, USA, personal communication.
3. Haugland, 'Handbook of Fluorescent Probes and Research Chemicals, Molecular probes', sixth edition, 1996.
4. Castellano, F., J. Lakowicz, 'A water-soluble luminescence oxygen sensor', *Photochemistry and Photobiology*, 67(2), 179-183, 1998.
5. Thomas Stepinac, personal communication.
6. Thomas Glanzmann, 'Steady-state and time-resolved fluorescence spectroscopy for photodynamic therapy and photodetection of cancer', PhD thesis #1920, EPFL, 1998.
7. Andrejevic, S., J.-F. Savary, Ch. Fontolliet, Ph. Monnier, H. van den Bergh, '7,12-Dimethylbenz[a]anthracene-induced 'early' squamous cell carcinoma in the Golden Syrian hamster: evaluation of an animal model and comparison with 'early' forms of human squamous cell carcinoma in the upper aero-digestive tract', *International Journal of Experimental Pathology*, 77, 7-14, 1996.
8. Cincotta, L., J. Foley, A. Cincotta, 'Novel red absorbing benzo[a]phenoxazinium and benzo[a]phenothiazinium photosensitizers: in vitro evaluation', *Photochemistry and Photobiology*, 46(5), 751-758, 1987.
9. Lin, C.-W., J. Shulok, Y.-K. Wong, C. Schanbacher, L. Cincotta, J. Foley, 'Photosensitization, uptake and retention of phenoxazine Nile Blue derivatives in human bladder carcinoma cells', *Cancer Research*, 51, 1109-1116, February 15th, 1991.
10. Cincotta, L., J. Foley, A. Cincotta, 'Phototoxicity, redox behavior and pharmacokinetics of benzophenoxazine analogues in EMT-6 murine sarcoma cells', *Cancer Research*, 53, 2571-2580, June 1st, 1993.
11. Cincotta, L., D. Szeto, E. Lampros, T. Hasan, A. Cincotta, 'Benzophenothiazine and benzoporphyrin derivative combination phototherapy effectively eradicates large murine sarcomas', *Photochemistry and Photobiology*, 63(2), 229-237, 1996.
12. Cincotta, L., J. Foley, T. MacEachern, E. Lampros, A. Cincotta, 'Novel photodynamic effects of a benzophenothiazine on two different murine sarcomas', *Cancer Research*, 54, 1249-1258, March 1st, 1994.
13. Georgakoudi, I., Th. Foster, 'Effects of the subcellular redistribution of two Nile Blue derivatives on photodynamic oxygen consumption', *Photochemistry and Photobiology*, 68(1), 115-122, 1998.
14. Lin, C.-W., J. Shulok, S. Kirley, L. Cincotta, J. Foley, 'Lysosomal localization and mechanism of uptake of Nile Blue photosensitizers in tumor cells', *Cancer research*, 51, 2710-2719, May 15th, 1991.
15. Henderson, B., T. Dougherty, 'How does photodynamic therapy work?', *Photochemistry and Photobiology*, Vol. 55, No 1, 145-157, 1992.
16. Richter, A., E. Waterfield, A. Jain, B. Allison, E. Sternberg, D. Dolphin, J. Levy, 'Photosensitising potency of structural analogues of benzoporphyrin derivative (BPD) in a mouse tumour model', *British Journal of Cancer*, 63, 87-93, 1991.

A3.
***Additional
autofluorescence
measurements***

Although it is mentioned in the text of section 8.3 that the measurements of autofluorescence of the bronchial tissue were performed at several wavelengths and for several histopathological statuses, some graphs only are given explicitly. The aim of this appendix is to present the remaining data. We present here the autofluorescence mean spectra, both normalized (to compare the spectral shapes) and non-normalized (to compare the intensities) at all the wavelengths. Preceding the spectra, Table A3.1 gives the exact number of spectra and of patients for each spectrum. Finally, a graph shows the interpatient variations of the spectra and the interpatient stability of the measurements.

As will be seen in Table A3.1, not all patients have been measured at all wavelengths. This is due to safety reasons, as the anesthesia cannot be extended indefinitely. A typical patient has therefore been measured at 4 wavelengths.

Figures A3.1a to A3.11a give normalized spectra. The spectra consequently have their maximum in the 'green' region set at unity. It is sometimes a local maximum and sometimes the maximum of the spectrum. Figure A3.1b to A3.11b give relative spectra. The healthy spectrum is still set at unity and the other spectra are divided by the relevant factor to express their intensity relatively to the healthy spectrum. They can therefore be compared to each other within a wavelength but not from a wavelength to another. All the spectra in Figures A3.1a/A3.1b to A3.11a/A3.11b are corrected for the sensitivity of the detector. Their shape is therefore correct, but their magnitude is correct down to a certain multiplicative factor only. This multiplicative factor depends on the instrumentation that was used and has not been computed.

The spectra in Fig. A3.12 and A3.13 are not corrected for the sensitivity of the detector and should therefore only be compared between them.

Excitation Wavelength	Histopathological status	Number of patients	Number of spectra
350 nm	Healthy	9	59
	Inflammation/Metaplasia	3	60
	Dysplasia/CIS	2	21
365 nm	Healthy	15	182
	Inflammation/Metaplasia	3	60
	Dysplasia/CIS	2	20
	Invasive	2	36
380 nm	Healthy	8	80
	Inflammation/Metaplasia	3	66
	Dysplasia/CIS	2	18
395 nm	Healthy	8	75
	Inflammation/Metaplasia	3	66
	Dysplasia/CIS	2	15
405 nm	Healthy	34	435
	Inflammation/Metaplasia	14	295
	Dysplasia/CIS	5	61
	Invasive	4	90
420 nm	Healthy	23	193
	Inflammation/Metaplasia	13	167
	Dysplasia/CIS	4	33
435 nm	Healthy	21	185
	Inflammation/Metaplasia	13	150
	Dysplasia/CIS	5	41
450 nm	Healthy	26	344
	Inflammation/Metaplasia	13	162
	Dysplasia/CIS	5	67
465 nm	Healthy	14	121
	Inflammation/Metaplasia	12	149
	Dysplasia/CIS	3	24
	Invasive	3	27
480 nm	Healthy	13	132
	Inflammation/Metaplasia	8	90
	Dysplasia/CIS	3	27
	Invasive	2	24
495 nm	Healthy	11	102
	Inflammation/Metaplasia	6	72
	Dysplasia/CIS	1	6
	Invasive	2	24

Table A3.1: Number of patients and number of spectra taken into account for the calculation of the typical autofluorescence spectra given in Fig. A3.1-A3.11, sorted by excitation wavelength.

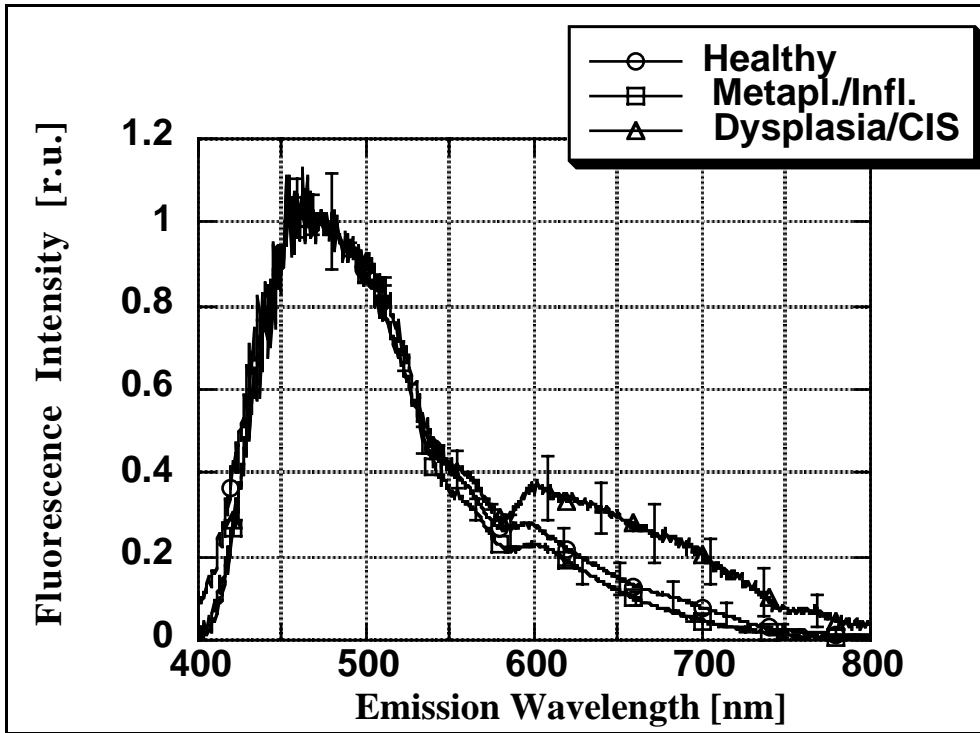


Figure A3.1a: normalized typical autofluorescence emission spectra of the lung tissue in relation to its pathological status. The excitation wavelength is 350 nm. The error bars display the 67% confidence interval. The spectra are corrected for the sensitivity of the detector.

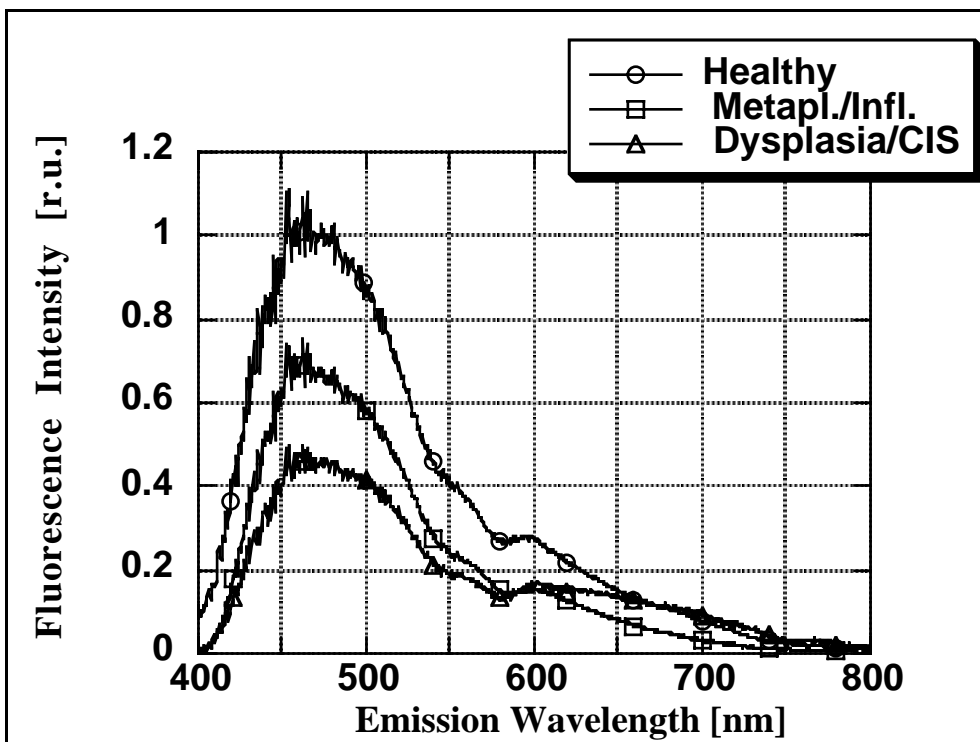


Figure A3.1b: non-normalized typical autofluorescence emission spectra of the lung tissue in relation to its pathological status. The excitation wavelength is 350 nm. The spectra are corrected for the sensitivity of the detector.

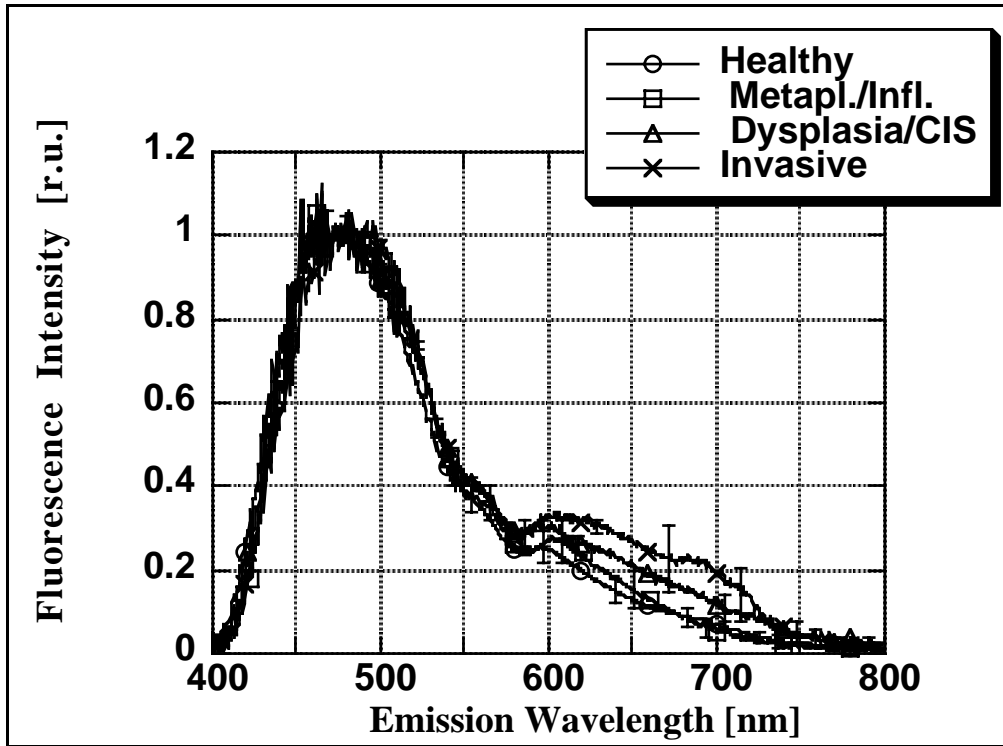


Figure A3.2a: normalized typical autofluorescence emission spectra of the lung tissue in relation to its pathological status. The excitation wavelength is 365 nm. The error bars display the 67% confidence interval. The spectra are corrected for the sensitivity of the detector.

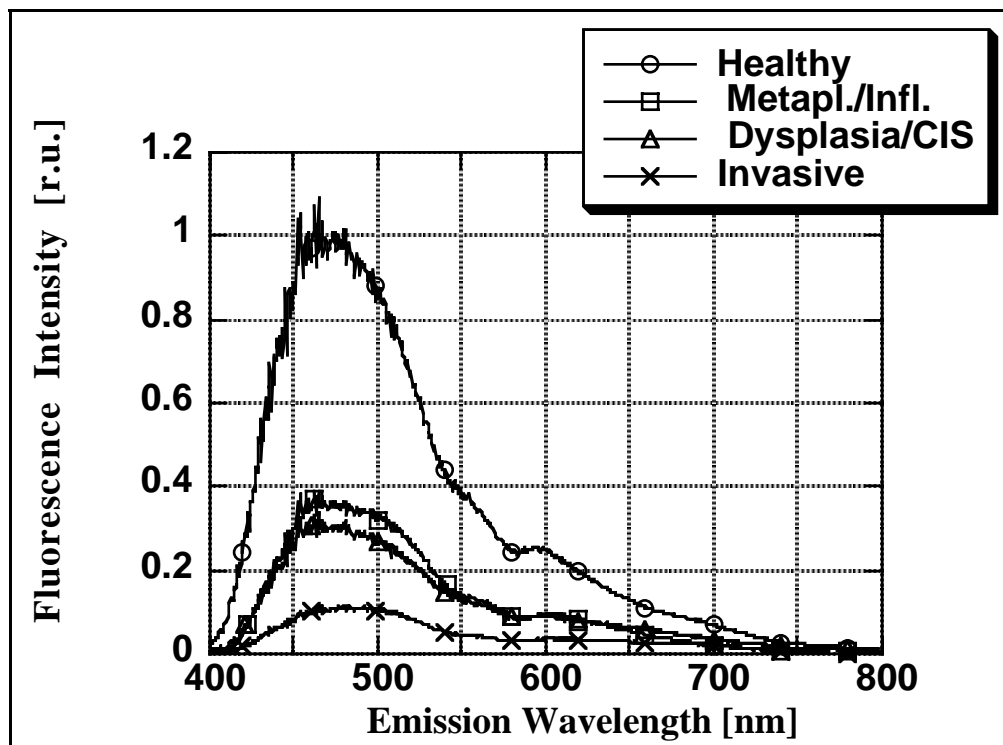


Figure A3.2b: non-normalized typical autofluorescence emission spectra of the lung tissue in relation to its pathological status. The excitation wavelength is 365 nm. The spectra are corrected for the sensitivity of the detector.

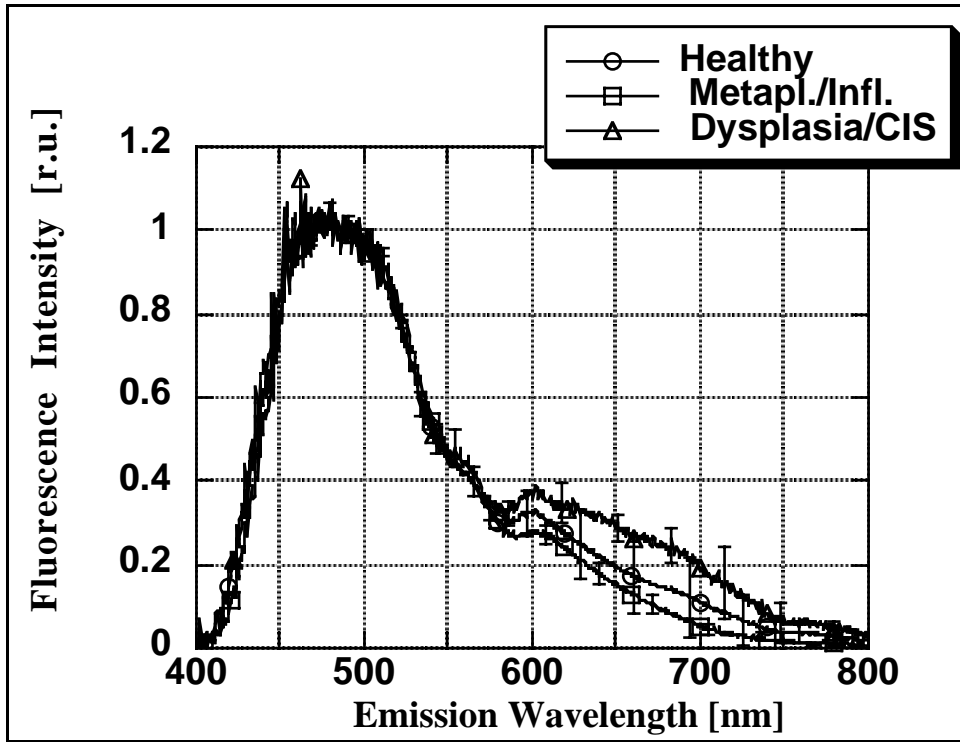


Figure A3.3a: normalized typical autofluorescence emission spectra of the lung tissue in relation to its pathological status. The excitation wavelength is 380 nm. The error bars display the 67% confidence interval. The spectra are corrected for the sensitivity of the detector.

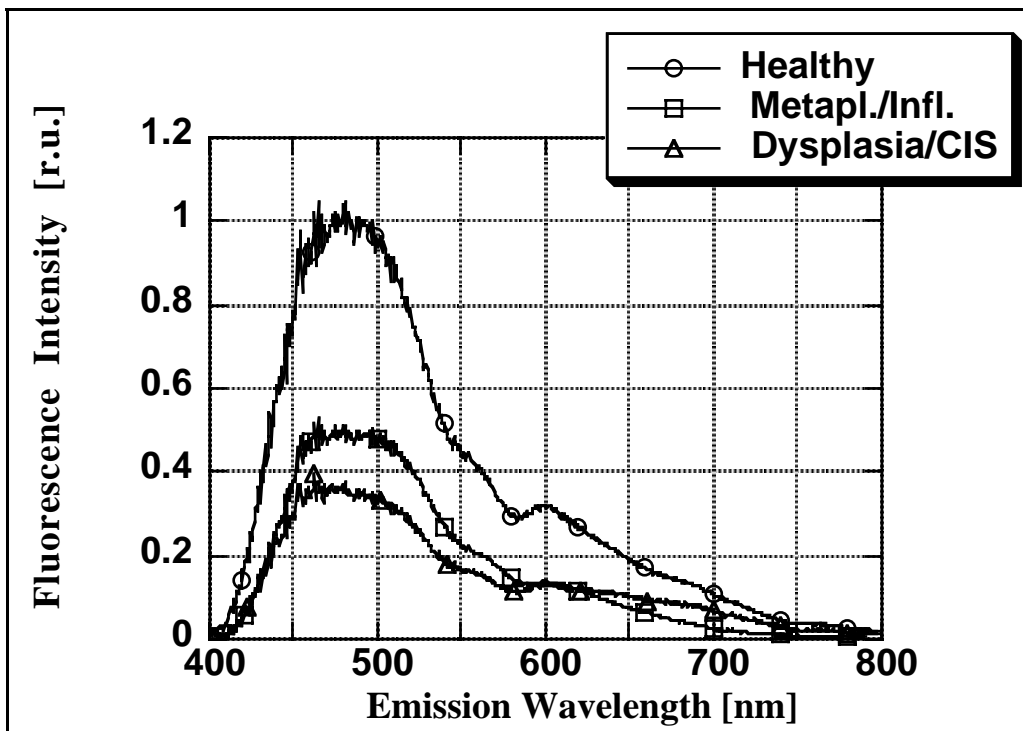


Figure A3.3b: non-normalized typical autofluorescence emission spectra of the lung tissue in relation to its pathological status. The excitation wavelength is 380 nm. The spectra are corrected for the sensitivity of the detector.

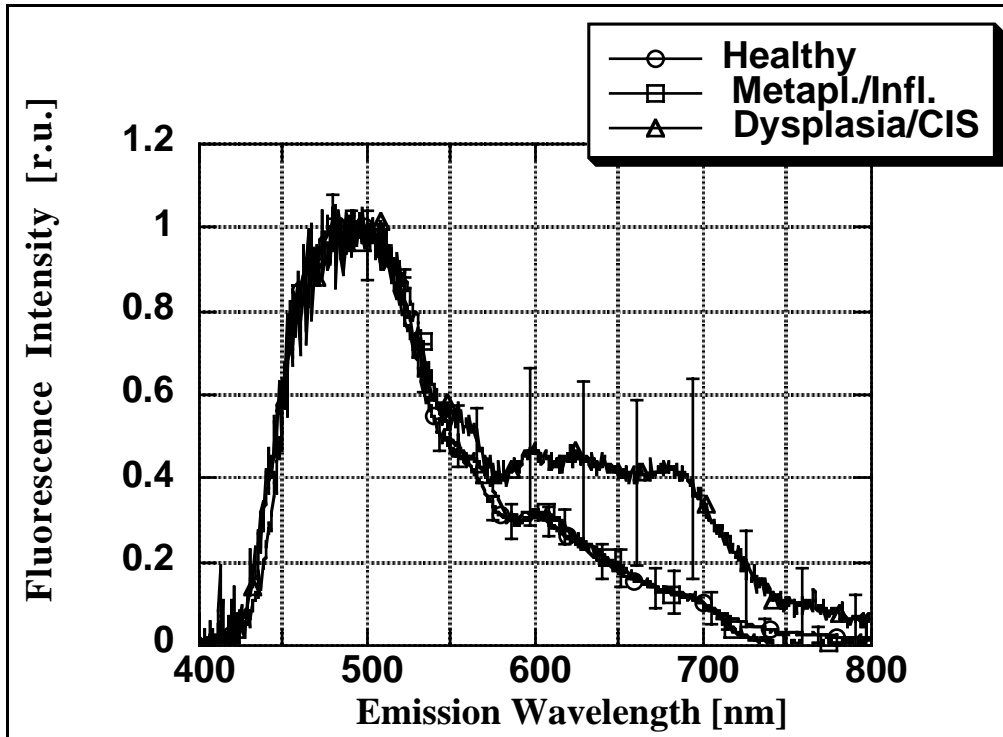


Figure A3.4a: normalized typical autofluorescence emission spectra of the lung tissue in relation to its pathological status. The excitation wavelength is 395 nm. The error bars display the 67% confidence interval. The spectra are corrected for the sensitivity of the detector.

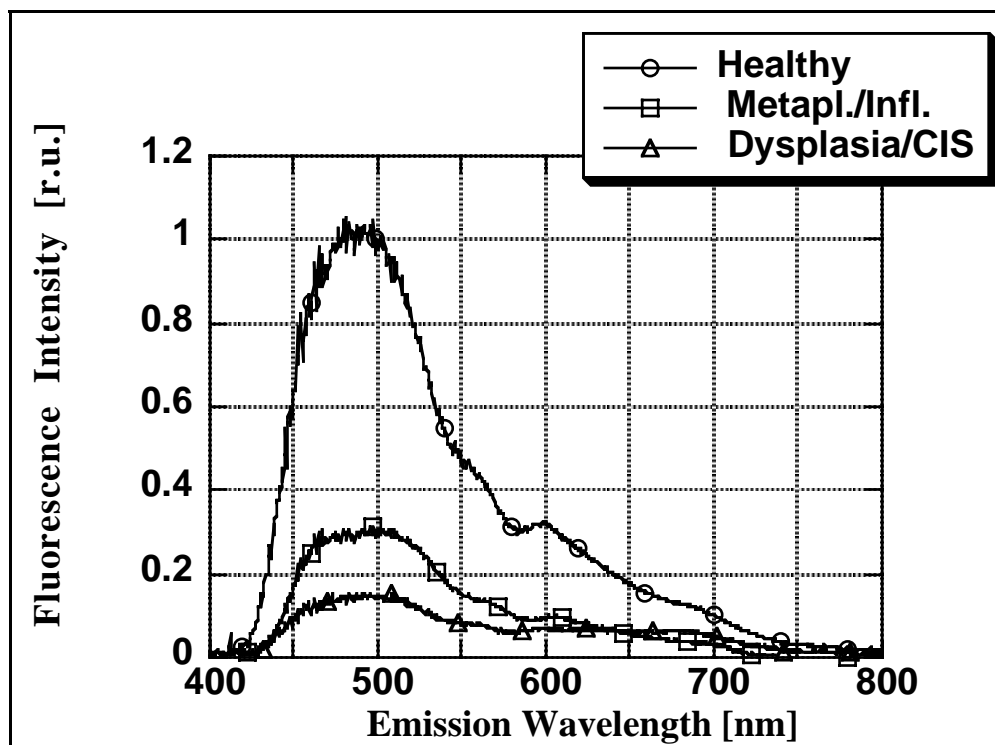


Figure A3.4b: non-normalized typical autofluorescence emission spectra of the lung tissue in relation to its pathological status. The excitation wavelength is 395 nm. The spectra are corrected for the sensitivity of the detector.

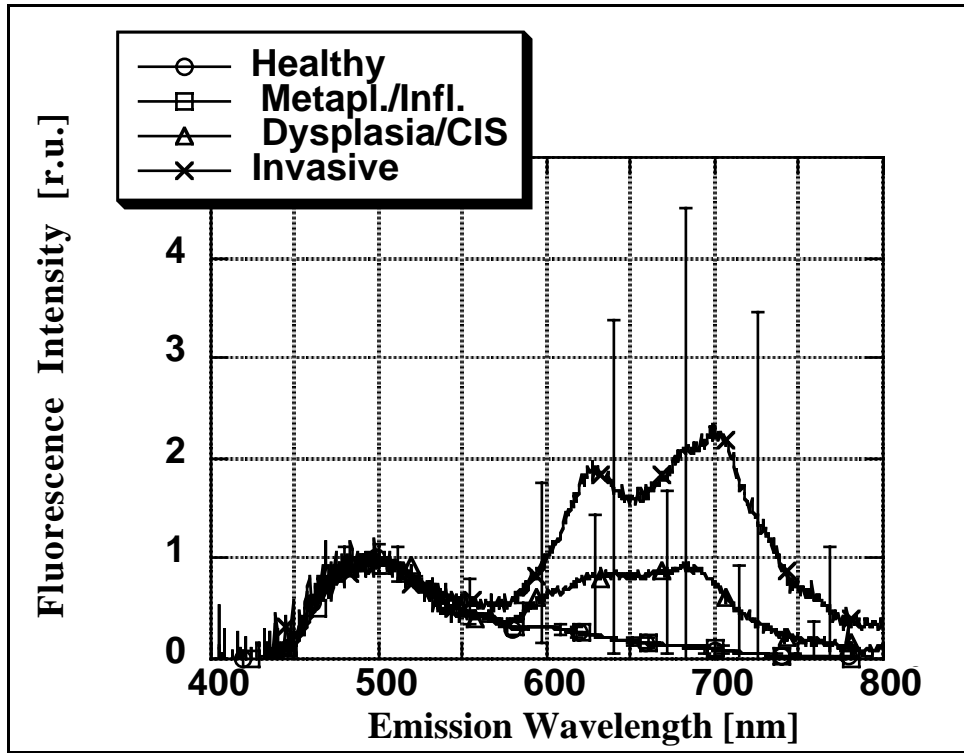


Figure A3.5a: normalized typical autofluorescence emission spectra of the lung tissue in relation to its pathological status. The excitation wavelength is 405 nm. The error bars display the 67% confidence interval. The spectra are corrected for the sensitivity of the detector.

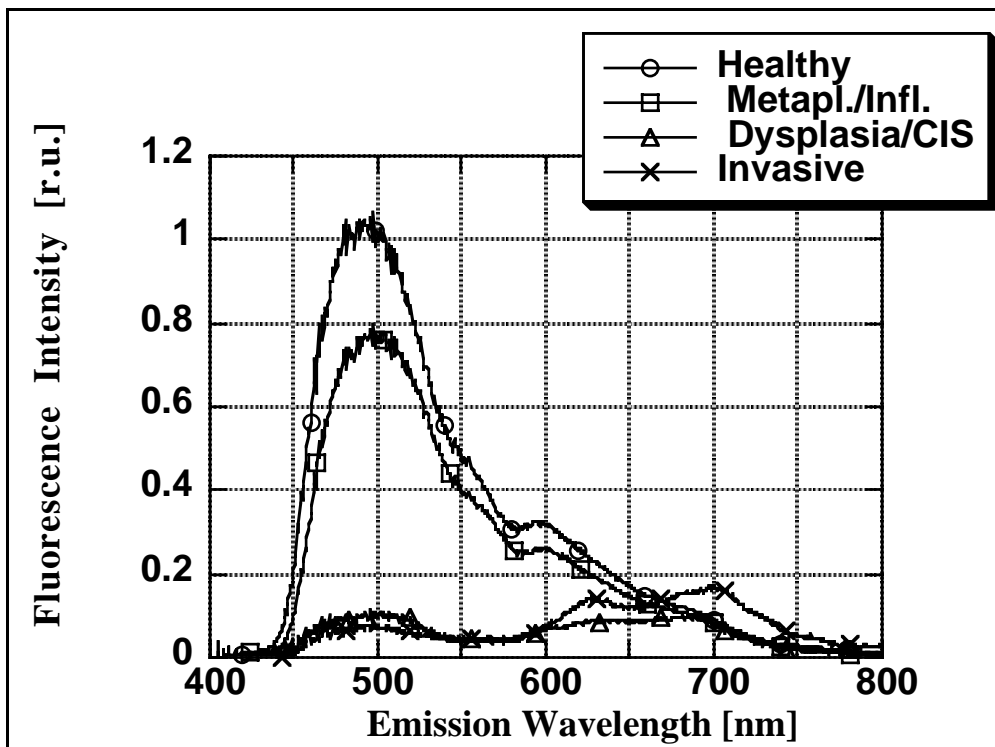


Figure A3.5b: non-normalized typical autofluorescence emission spectra of the lung tissue in relation to its pathological status. The excitation wavelength is 405 nm. The spectra are corrected for the sensitivity of the detector.

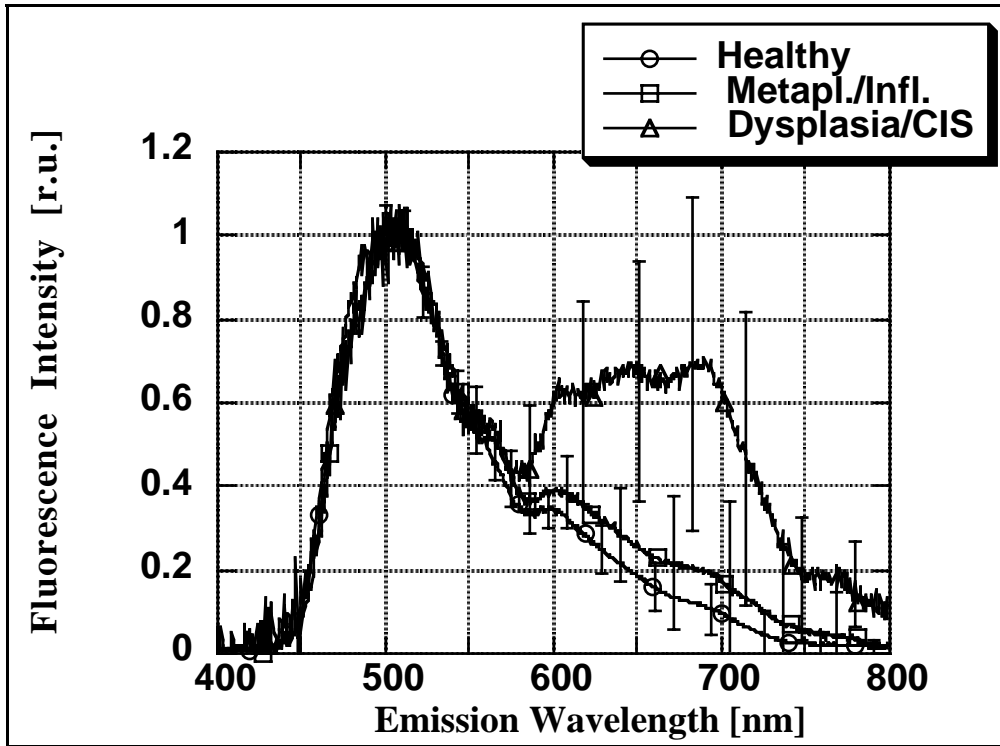


Figure A3.6a: normalized typical autofluorescence emission spectra of the lung tissue in relation to its pathological status. The excitation wavelength is 420 nm. The error bars display the 67% confidence interval. The spectra are corrected for the sensitivity of the detector.

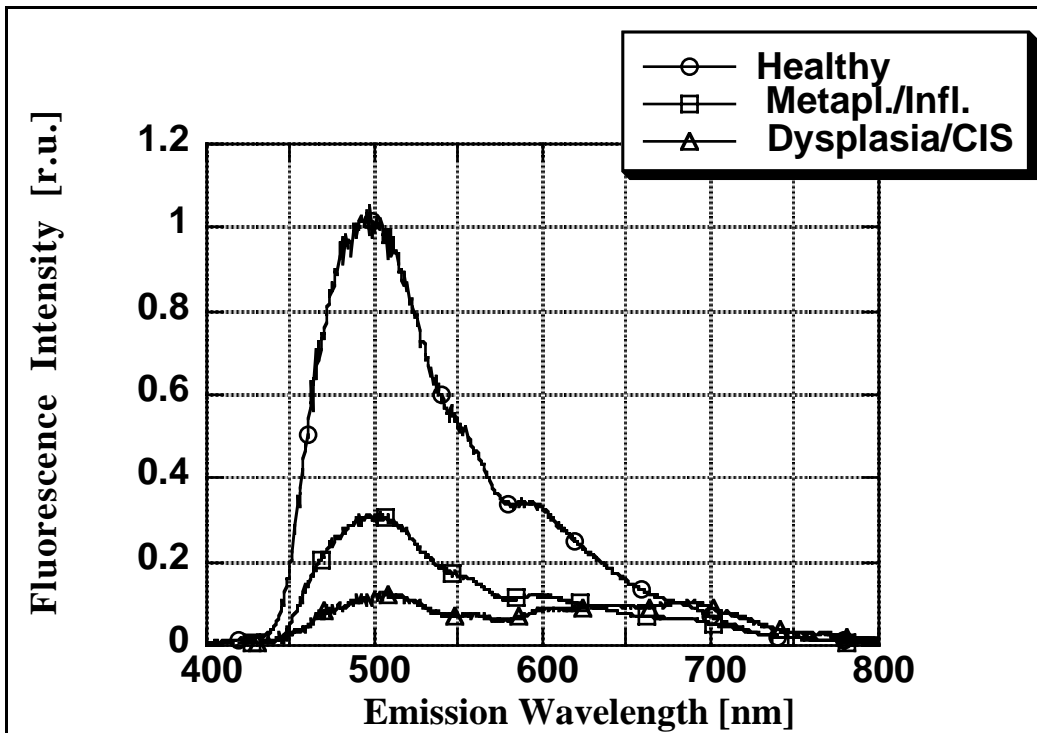


Figure A3.6b: non-normalized typical autofluorescence emission spectra of the lung tissue in relation to its pathological status. The excitation wavelength is 420 nm. The spectra are corrected for the sensitivity of the detector.

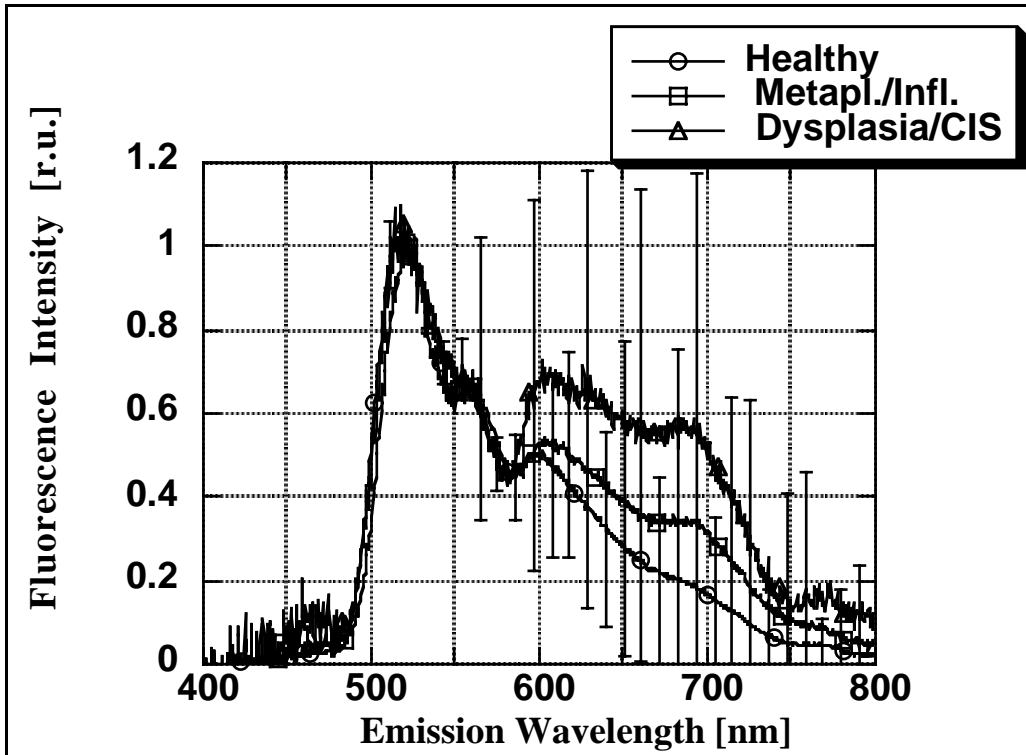


Figure A3.7a: normalized typical autofluorescence emission spectra of the lung tissue in relation to its pathological status. The excitation wavelength is 435 nm. The error bars display the 67% confidence interval. The spectra are corrected for the sensitivity of the detector.

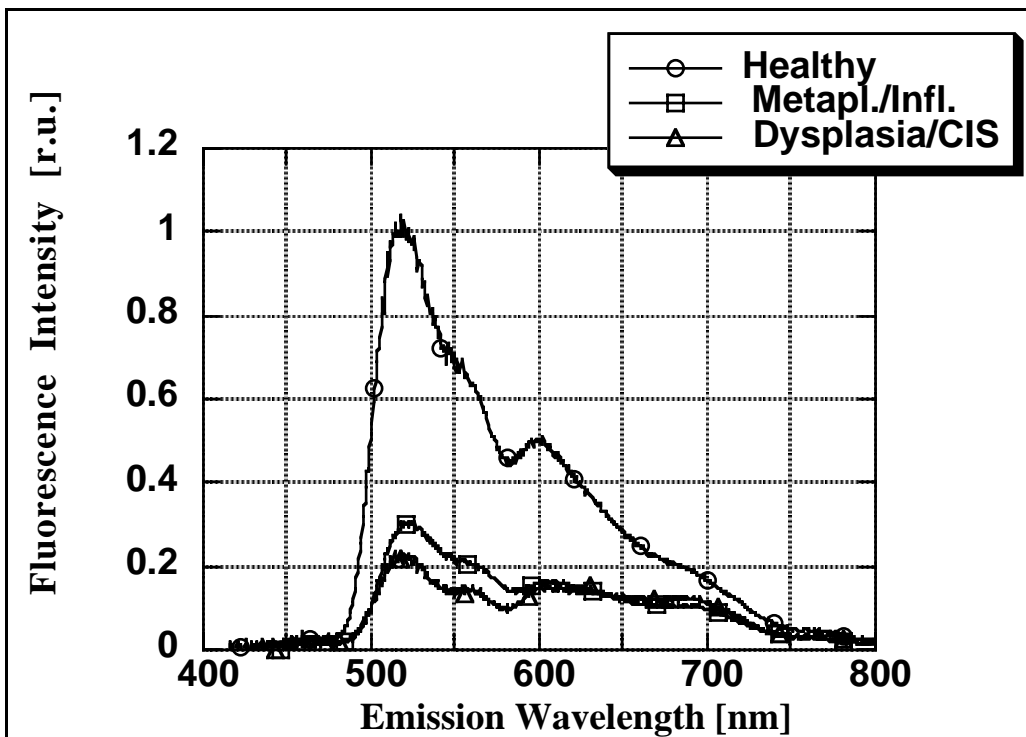


Figure A3.7b: non-normalized typical autofluorescence emission spectra of the lung tissue in relation to its pathological status. The excitation wavelength is 435 nm. The spectra are corrected for the sensitivity of the detector.

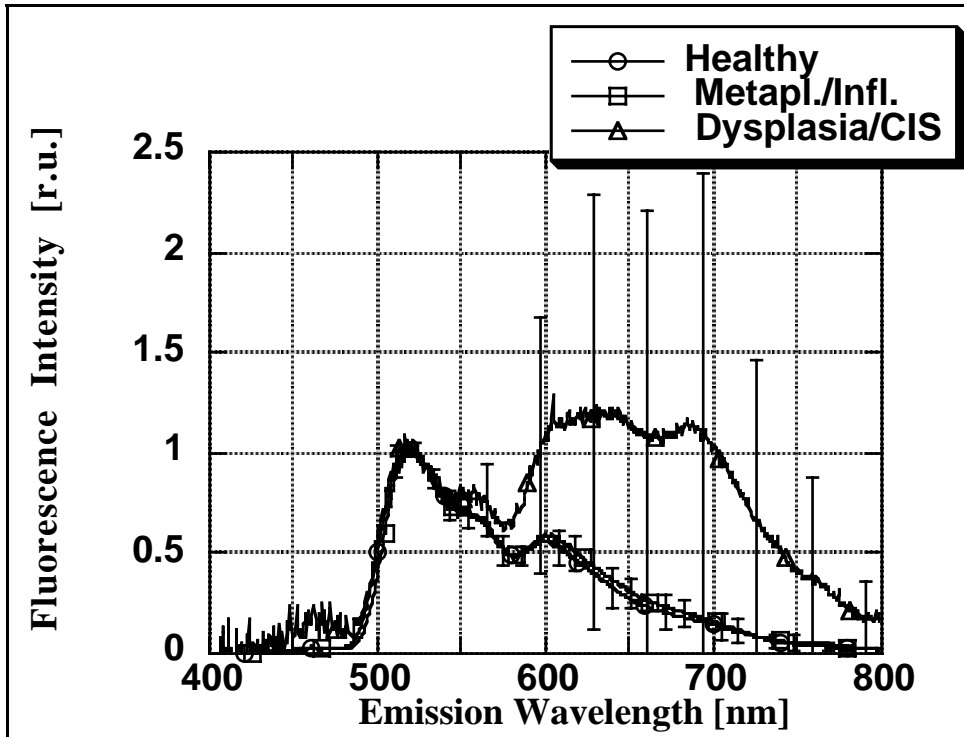


Figure A3.8a: normalized typical autofluorescence emission spectra of the lung tissue in relation to its pathological status. The excitation wavelength is 450 nm. The error bars display the 67% confidence interval. The spectra are corrected for the sensitivity of the detector.

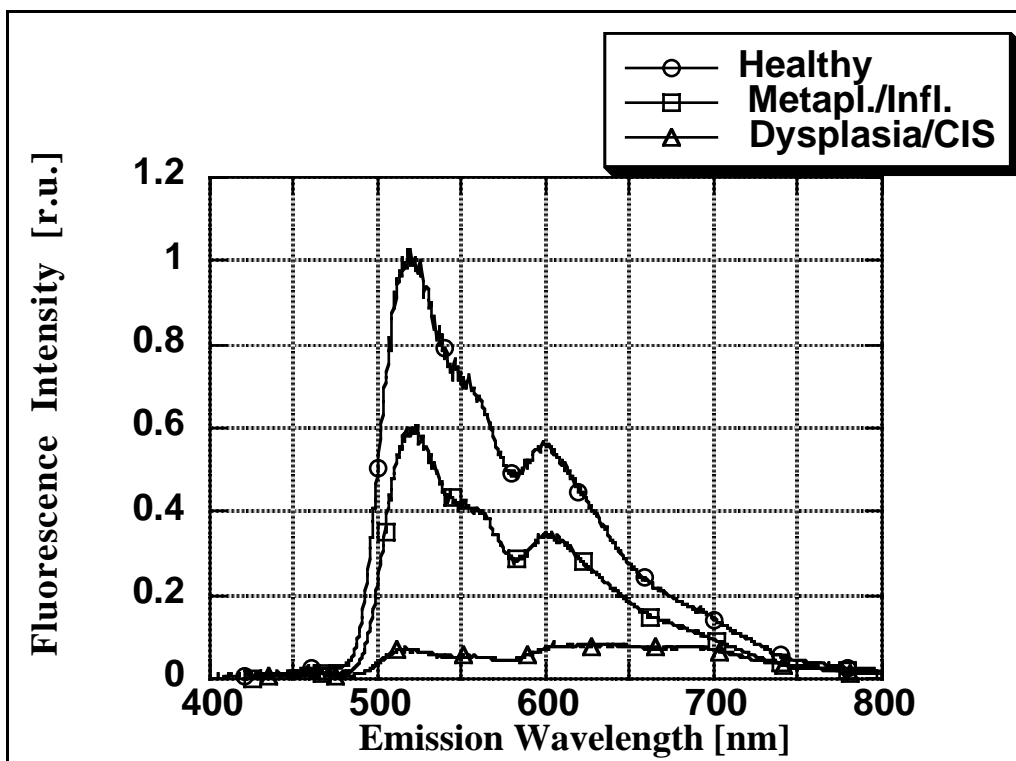


Figure A3.8b: non-normalized typical autofluorescence emission spectra of the lung tissue in relation to its pathological status. The excitation wavelength is 450 nm. The spectra are corrected for the sensitivity of the detector.

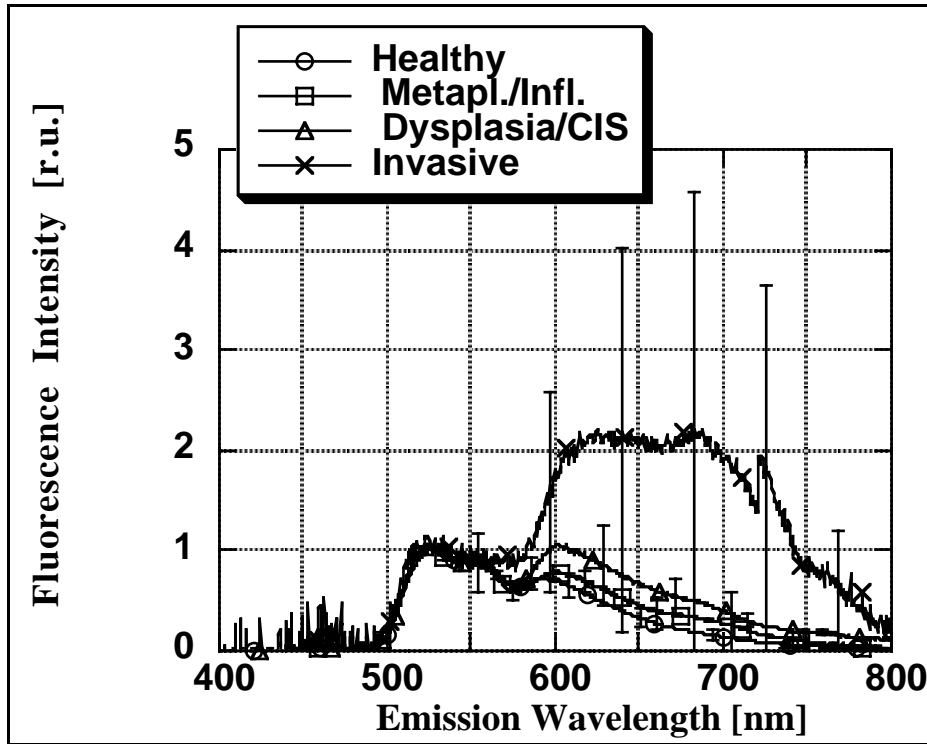


Figure A3.9a: normalized typical autofluorescence emission spectra of the lung tissue in relation to its pathological status. The excitation wavelength is 465 nm. The error bars display the 67% confidence interval. The spectra are corrected for the sensitivity of the detector.

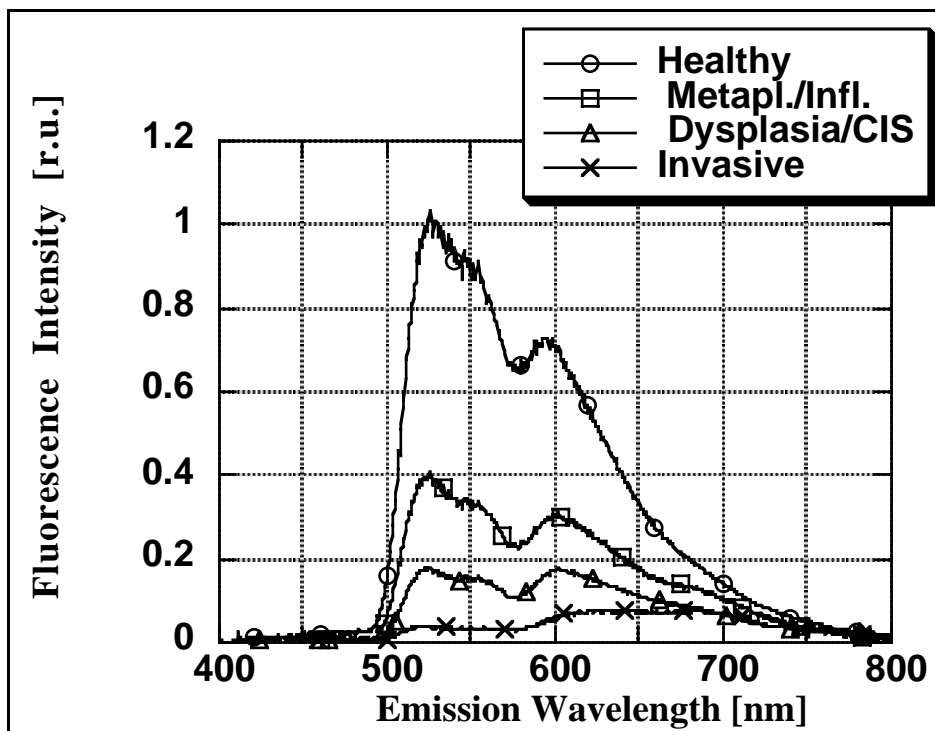


Figure A3.9b: non-normalized typical autofluorescence emission spectra of the lung tissue in relation to its pathological status. The excitation wavelength is 465 nm. The spectra are corrected for the sensitivity of the detector.

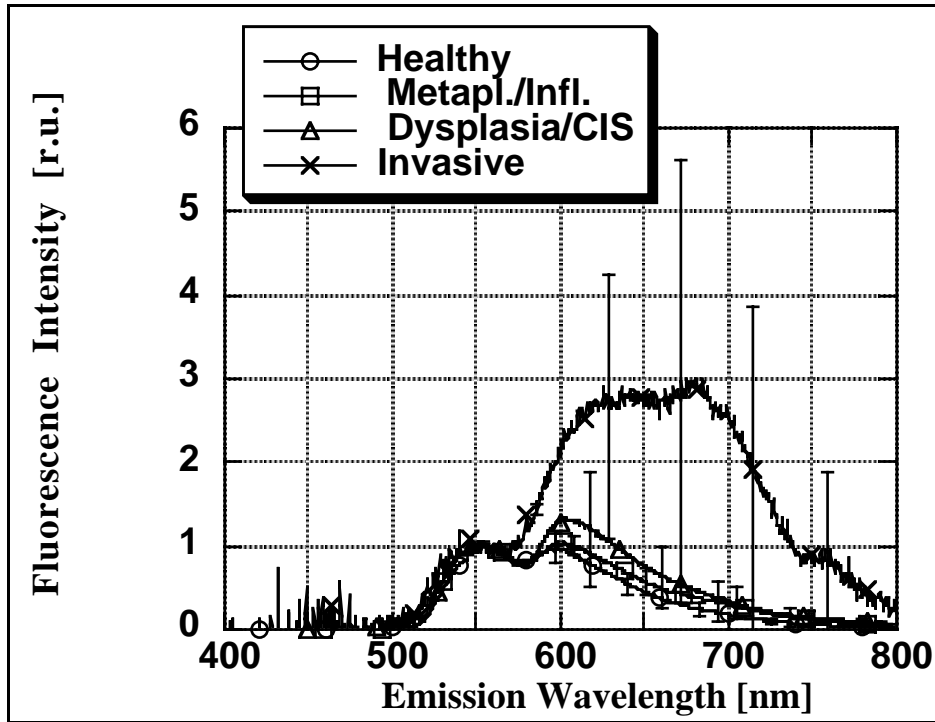


Figure A3.10a: normalized typical autofluorescence emission spectra of the lung tissue in relation to its pathological status. The excitation wavelength is 480 nm. The error bars display the 67% confidence interval. The spectra are corrected for the sensitivity of the detector.

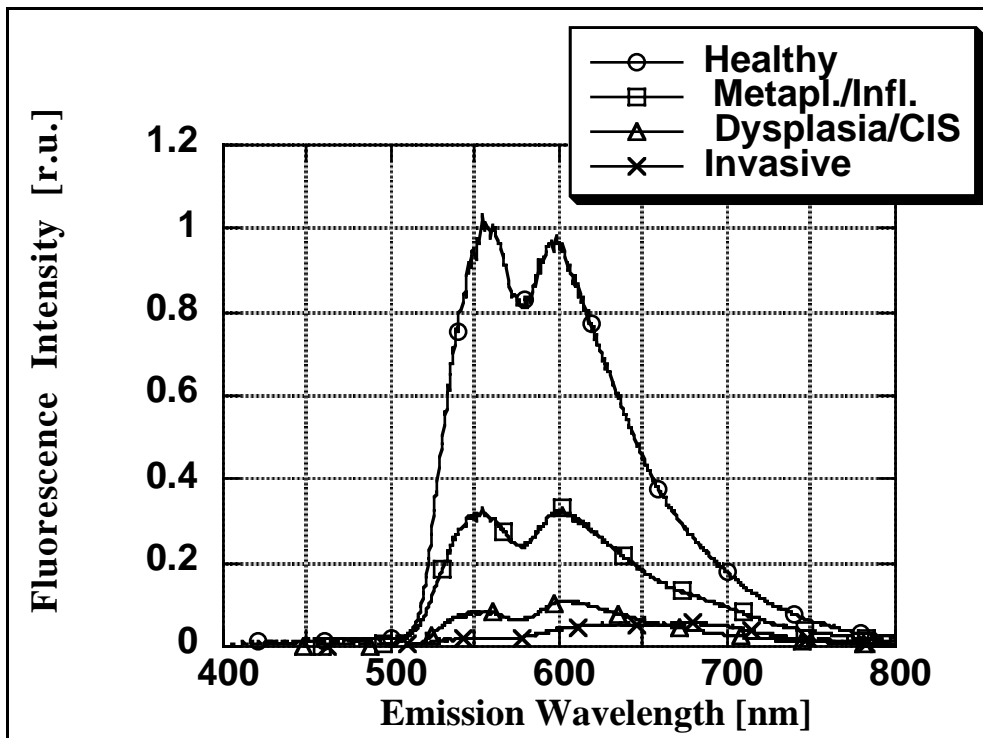


Figure A3.10b: non-normalized typical autofluorescence emission spectra of the lung tissue in relation to its pathological status. The excitation wavelength is 480 nm. The spectra are corrected for the sensitivity of the detector.

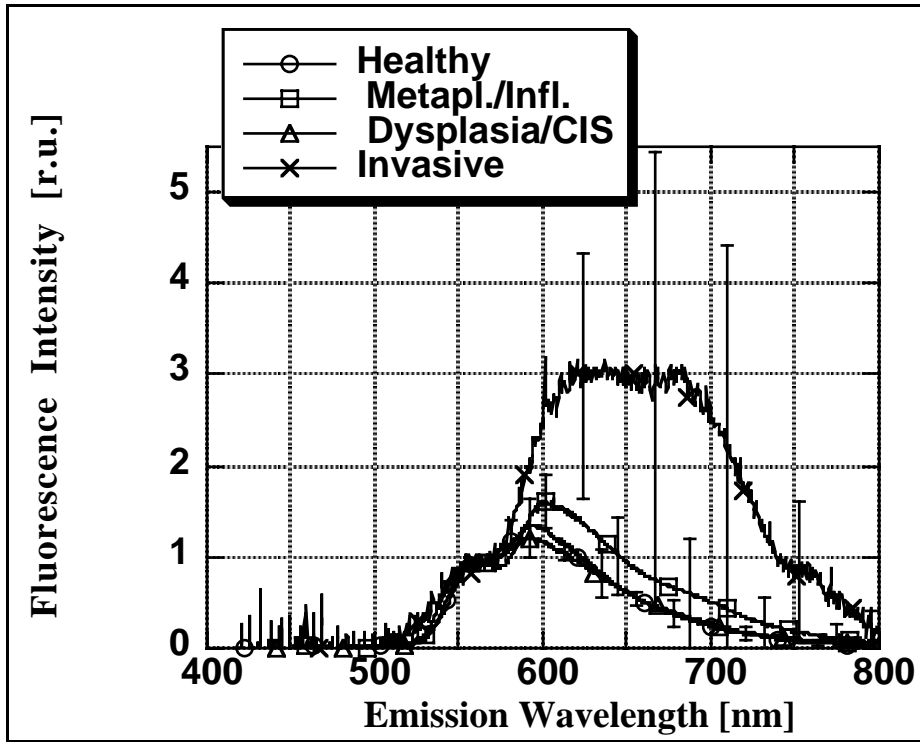


Figure A3.11a: normalized typical autofluorescence emission spectra of the lung tissue in relation to its pathological status. The excitation wavelength is 495 nm. The error bars display the 67% confidence interval. The spectra are corrected for the sensitivity of the detector.

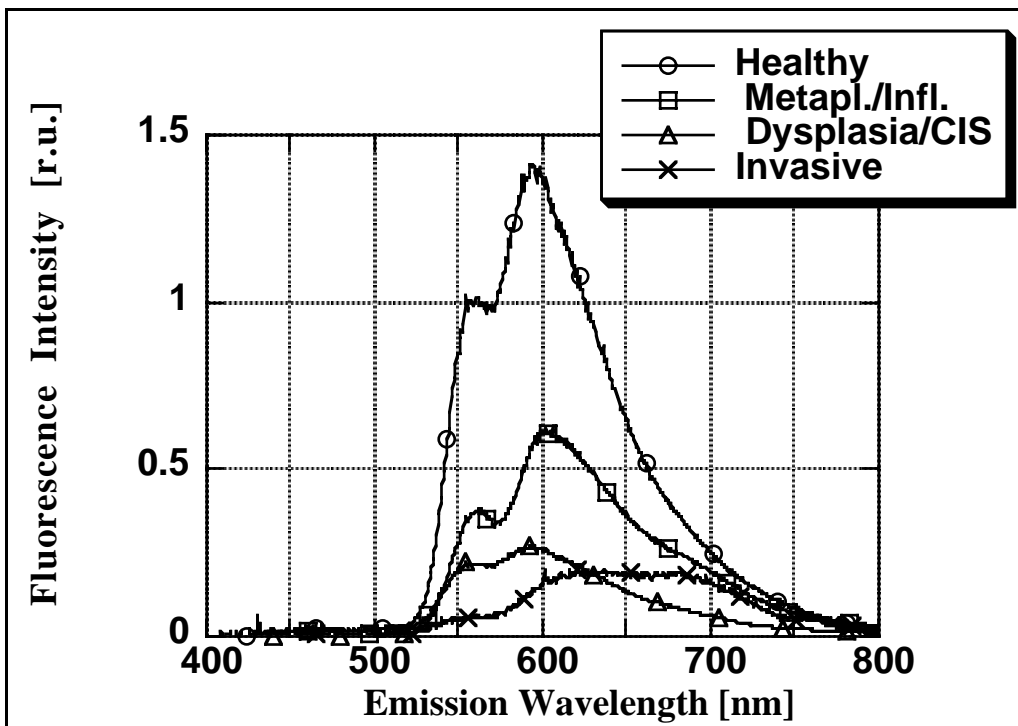


Figure A3.11b: non-normalized typical autofluorescence emission spectra of the lung tissue in relation to its pathological status. The excitation wavelength is 495 nm. The spectra are corrected for the sensitivity of the detector.

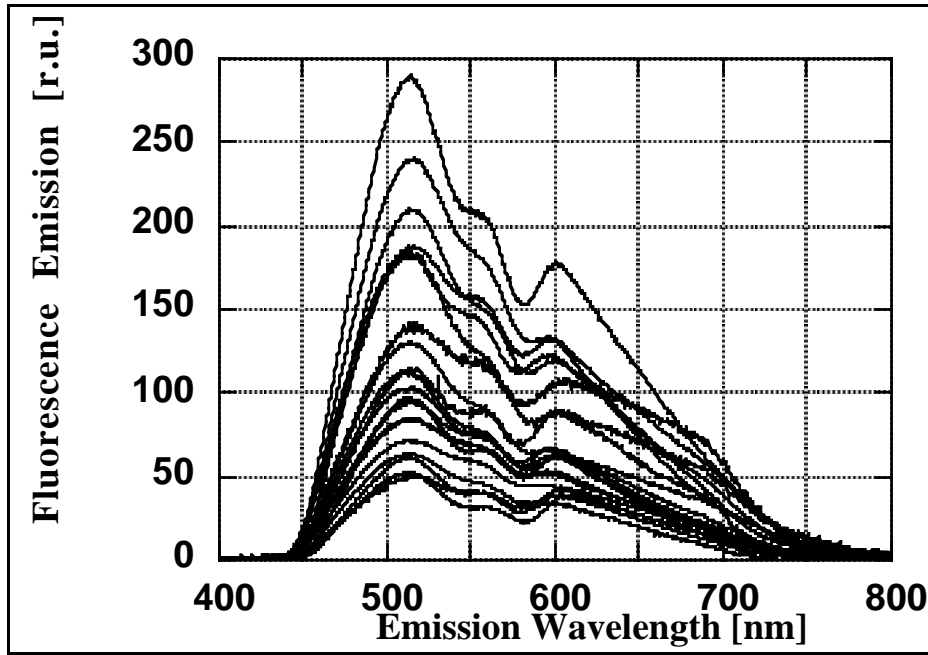


Figure A3.12: autofluorescence spectra of the bronchial tissue of 20 patients (same patients as in the Figure 19). The excitation wavelength is 405 nm.

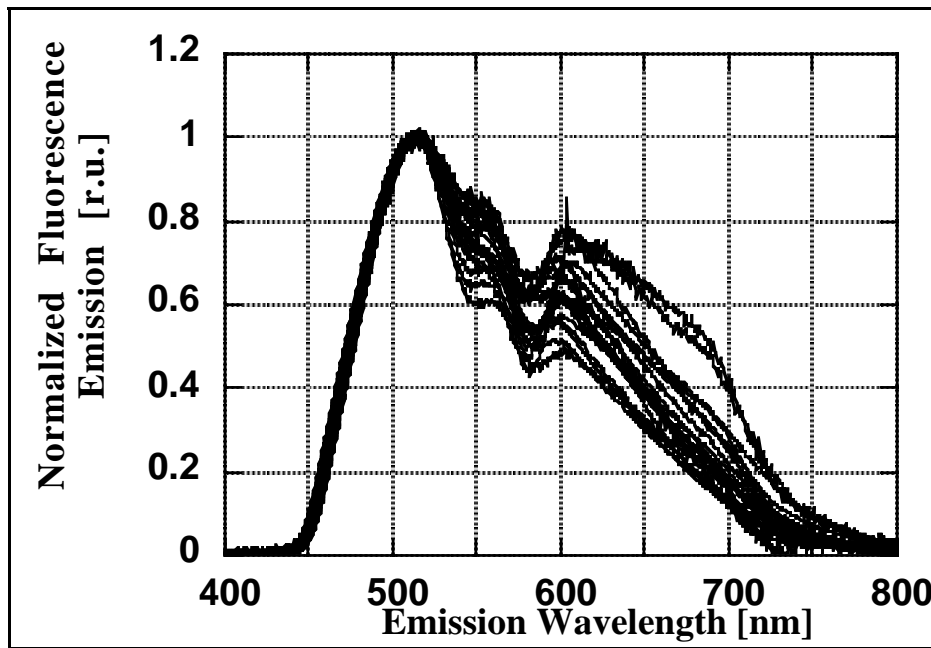


Figure A3.13: Normalized autofluorescence spectra of the bronchial tissue of 20 patients (same patients as in the Figure 18). The excitation wavelength is 405 nm.

Discussion

Figures A3.1a to A3.11a present normalized autofluorescence spectra. They were obtained with different excitation wavelengths. The first feature that can be noted is the similarity of the spectra of healthy tissue and of inflammatory/metaplastic tissue. At some excitation wavelengths, they overlap so closely that they cannot be distinguished (395, 405, 450 nm). This feature is of great importance because the inflammatory tissue is not malignant. An autofluorescence imaging system aiming at detecting early cancers should therefore assign these types of tissue to the same subgroup as healthy tissue. This goal appears achievable in the light of our results.

For the healthy and inflammatory/metaplastic tissue spectra, the error bars are small. This indicates a high reproducibility of these measurements. This fact is further corroborated by our measurements of the interpatient stability of the autofluorescence measurements (Fig. A3.13). Finally, the inpatient measurements also proved highly stable (see Section 8.3, Discussion). These observations indicate that there might well be something as a 'typical' autofluorescence spectrum for healthy bronchial tissue. This has been observed at all wavelengths (for the sake of readability, the data collected at an excitation wavelength of 405 nm only has been shown).

The typical autofluorescence spectra of the dysplasias/CIS are less stable, as expected. First of all, these spectra do not always have the same shape as the previous two spectra. Depending on the excitation wavelength, this difference is slight (350, 365, 380, 465, 480 and 495 nm) or marked (395, 405, 420, 435 and 450 nm). The error bars are also larger for the early lesions than for the healthy spectra. Several reasons can be invoked to explain this fact. Sampling error is likely to be one of them, along with the inhomogeneity of the early tumors. They are both discussed in Section 8.3, Discussion. More reasons can probably be found but this is beyond the scope of this work. On the other hand, these modifications to the spectrum of early cancerous lesions with respect to their healthy counterparts indicate that this detection method can probably produce sensitive and specific results if a relevant excitation wavelength is chosen. This is a desirable goal and the imaging systems to come will benefit from similar studies to optimize their performance.

Regardless of the excitation wavelength, the normalized spectra overlap up to a certain emission wavelength and then no longer do so. Interestingly, the wavelength region where this divergence occurs seems to be located in the same range of emission wavelengths, namely around 600 nm. This interesting feature has been discussed in detail in Section 8.3, Discussion.

Wherever available, the typical autofluorescence spectra of more invasive lesions have been included in the graphs. Again, these spectra tend to overlap the spectra of healthy tissue up to a certain point (also in the 600 nm region) and not at higher wavelengths anymore. The error bars are also larger than on healthy spectra and this probably also reflects the inhomogeneity of the lesions. It is, however, interesting to note that the relevant spectrum excited at 405 nm seems to display a structure between 600 and 700 nm that might be reminiscent of the double-peak structure of the porphyrin spectra. While this observation has not been made on each and every spectrum, it still is marked enough to be noticeable on the typical spectrum. It should also be kept in mind that several papers in the literature link invasive tumors with an increased content of endogenous porphyrins.

Figures A3.1b to A3.11b show the same typical spectra in their non-normalized form. Whereas Fig. A3.1a to A3.11a were intended to show the shape of the typical spectra, these graphs give their relative intensities. As has been reported by several authors (see Section 8.3, Discussion), a decrease in the autofluorescence is observed on the spectra of non-healthy tissues. Our data tends to confirm this observation. Moreover, regardless of the excitation wavelength, there seems to be a pattern in the evolution of the typical spectra, namely a decrease in intensity between the healthy and the inflammatory/metaplastic tissue spectra with little, if any at all, change in the shape of the spectra. The next step in the cancerization process sees a marked decrease in the intensity in most cases and is usually associated with a concomitant change of the spectral shape. This is especially marked with the excitation wavelength between 405 and 450 nm. Whenever available, the spectra

of the invasive lesions show that the decrease in intensity continues afterwards, albeit not quite as markedly.

These observations tend to show that something is happening during this process that noticeably influences the fluorescence properties of the tissue. Further studies are necessary to assess the exact reason behind this observation. As for our goal to develop an autofluorescence imaging system, this should be reassuring as to the chances of success associated with our trial.

Finally, Fig. A3.12 extends the concept of interpatient variations of the autofluorescence. Many of the molecules that are responsible for the autofluorescence are involved in the metabolism. The metabolism can vary from one patient to another and, as expected, the intensity of the autofluorescence spectrum varies accordingly. It has been found that this intensity can vary from up to one order of magnitude.

A4.
Publications and patents

Peer-reviewed publications

Georges Wagnières, Shangguan Cheng, Matthieu Zellweger, Nora Utke, Daniel Braichotte, Jean-Pierre Ballini and Hubert van den Bergh, '**An optical phantom with tissue-like properties in the visible for PDT and fluorescence spectroscopy**', *Phys. Med. Biol.*, 42, 1-12, 1997.

Thomas Glanzmann, Christophe Hadjur, Matthieu Zellweger, Pierre Grosjean, Martin Forrer, Jean-Pierre Ballini, Philippe Monnier, Hubert van den Bergh, Chang Lim and Georges Wagnières, '**Pharmacokinetics of tetra(m-hydroxyphenyl)chlorin in human plasma and individualized light dosimetry in photodynamic therapy**', *Photochemistry and Photobiology*, 67(5), 596-602, 1998.

Norbert Lange, Patrice Jichlinski, Matthieu Zellweger, Martin Forrer, Alexandre Marti, Louis Guillou, Pavel Kucera, Georges Wagnières, Hubert van den Bergh, '**Photodetection of early human bladder cancer based on the fluorescence of 5-aminolaevulinic acid hexylester-induced protoporphyrin IX: a pilot study**', *British Journal of Cancer*, 80(1/2), 185-193, 1999.

Matthieu Zellweger, Pierre Grosjean, Philippe Monnier, Hubert van den Bergh, Georges Wagnières, '**Stability of the fluorescence measurement of Foscan[®] in the normal human oral cavity as an indicator of its content in early cancers of the esophagus and the bronchi**', *Photochemistry and Photobiology*, 69(5), 605-610, 1999.

Alexandre Radu, Matthieu Zellweger, Pierre Grosjean, Philippe Monnier, '**Pulse-Oximeter as a Cause of Skin Burn during Photodynamic Therapy**', *Endoscopy* 31(9), 831-833, 1999.

Pascal Uehlinger, Matthieu Zellweger, Georges Wagnières, Lucienne Juillerat, Hubert van den Bergh and Norbert Lange, '**Determination of physical chemical properties of ALA and its derivatives and their impact on the PPIX formation in cultured cells**', *Journal of Photochemistry and Photobiology, B: Biology*, 54(1), 72-80, 2000.

Matthieu Zellweger, Alexandre Radu, Philippe Monnier, Hubert van den Bergh, Georges Wagnières, '**In vivo pharmacokinetics of Lutetium Texaphyrin in the healthy and tumoral cheek pouch mucosa. Retention and selectivity properties**', *Journal of Photochemistry and Photobiology, B: Biology*, 55(1), 56-62, 2000.

Matthieu Zellweger, Pierre Grosjean, Didier Goujon, Philippe Monnier, Hubert van den Bergh and Georges Wagnières, '**In vivo autofluorescence spectroscopy of human bronchial tissue to optimize the detection and imaging of early cancers**', accepted for publication in the '*Journal of Biomedical Optics*'.

Matthieu Zellweger, Didier Goujon, Martin Forrer, Hubert van den Bergh and Georges Wagnières, '**Absolute autofluorescence spectra of healthy bronchial tissue in vivo**', submitted to '*Applied Optics*'.

Patents

German Patent Application DE 198 00 312 '**Diagnosegerät zur bildgebenden Aufnahme fluoreszierender biologischer Gewebereiche**', filed on January 7th 1998, by G. Wagnières, M. Zellweger, N. Lange, N. Chauvin, U Zanger, A. Studzinski, H. van den Bergh

(status pending); European Patent Application EP 0 928 597 A2, filed on March 18th 1998 (status pending); United States Patent Application US 09/098 286 (status pending).

Patent Application: ER-9152 FR A1 '**Solution pour la préparation d'une substance pharmaceutique pour le diagnostic et/ou le traitement de lésions tissulaires**', H. van den Bergh, P. Jichlinski, P. Kucera, A. Marti, N. Lange, M. Zellweger, G. Wagnières, status pending.

Oral Presentations

Matthieu Zellweger, Pierre Grosjean, Georges Wagnières, Philippe Monnier, Hubert van den Bergh, '**Clinical prediction of tissular effect of mTHPC-PDT by Light Induced Fluorescence: assessment of the reliability of this method**', Regular Communication, 7th Biennial Congress of the International Photodynamic Association, Nantes, July 1998 ('Prix de Communication Scientifique' Award, July 9th 1998).

Matthieu Zellweger, Pierre Grosjean, Thomas Glanzmann, Philippe Monnier, Hubert van den Bergh, Georges Wagnières, '**Utilisation de la spectroscopie de fluorescence pour le monitoring de la dose de lumière en PDT**', Regular Communication, XVIIIth Congress of the 'Société Française des Lasers Médicaux', Les Arcs, January 1999.

Matthieu Zellweger, Pierre Grosjean, Thomas Glanzmann, Philippe Monnier, Hubert van den Bergh, Georges Wagnières, '**Prédiction du dommage tissulaire induit par une PDT de l'oesophage ou des bronches par spectroscopie de fluorescence de la mTHPC effectuée dans la cavité buccale**', Communication for the final round of the 'Prix Jeune Chercheur 1999' Award, XVIIIth Congress of the Société Française des Lasers Médicaux, Les Arcs, January 1999.

Further publications

Georges Wagnières, Shangguan Cheng, Matthieu Zellweger, Nora Utke, Daniel Braichotte, Jean-Pierre Ballini and Hubert van den Bergh, '**Design and characterization of a phantom which simultaneously simulates tissue optical properties between 400 and 650nm**', Proc. Soc. Photo-Opt. Instr. Eng., 2926, pp 94-103, 1996.

Clive Wilder-Smith, Pierre Grosjean, Georges Wagnières, Petra Wilder-Smith, Gian Dorta, Alain Woodtli, Matthieu Zellweger, Philippe Monnier, Hubert van den Bergh, '**Photoeradication of Helicobacter pylori in humans: phase 1 study**', Gastroenterology, May, 1999.

A5.
Curriculum Vitae

Curriculum Vitae

Matthieu P.E. ZELLWEGER

Fenetta 34

CH-1752 Villars-sur-Glâne

born July 26th 1971, swiss and french citizen

Education

- 1996-2000 **Swiss Federal Institute of Technology – Lausanne (EPFL)**, Ph.D. thesis in biomedical optics (Fluorescence spectroscopy of exogenous, exogenously-induced and endogenous fluorophores for the photodetection and photodynamic therapy of cancer).
- 1999 **London School of Economics**, summer session in Macroeconomics.
- 1994 **Berklee College of Music, Boston, USA**, summer session and fall semester (performance).
- 1989-1994 **University of Fribourg, University of Neuchâtel**, Chemistry studies.
- 1982-1989 **Collège St-Michel, Fribourg**, High School and Junior High School (Ancient Greek and Latin).

Working experience

- 1995 **Ciba-Geigy, Novartis, Marly, Switzerland**, Development of synthetical methods for azoic pigments and systematic investigation of a reaction.
- 1990 **Hoechst Celanese, Plast Labor, Bulle, Switzerland**, Tuning of an analytical method to measure the water content of polymers.

Publications and Awards

Author or co-author of 11 publications and 2 patents.

Scientific Communication Award, 7th Biennial Congress of the International Photodynamic Association, Nantes, France, July 1998.

Freetime

Music (Big Band of the Conservatory of Fribourg, since September 1996).

Travel (8 months around the world, Jan-Aug 1995, 8 countries).

Scuba Diving (PADI Dive Master).

Member of Mensa International since January 1999.